A CW-EPR investigation on the formation, stability and reactivity of oxygen centred radicals on TiO_2.

A thesis submitted in candidature for the degree of Doctor of Philosophy

by

Jason Green

School of Chemistry

Cardiff University

2010

ProQuest LLC
789 East Eisenhower Parkway
P.O. Box 1346
Ann Arbor, MI 48106-1346

DECLARATION

This work has not previously been accepted in substance for any degree and is not concurrently submitted in candidature for any degree.

Signed ..... (candidate)
Date .....3/12/10.....

STATEMENT 1

This thesis is being submitted in partial fulfillment of the requirements for the degree of PhD.

Signed ..... (candidate)
Date .....3/12/10.....

STATEMENT 2

This thesis is the result of my own independent work/investigation, except where otherwise stated. Other sources are acknowledged by explicit references.

Signed ..... (candidate)
Date .....3/12/10.....

STATEMENT 3

I hereby give consent for my thesis, if accepted, to be available for photocopying and for inter-library loan, and for the title and summary to be made available to outside organisations.

Signed ..... (candidate)
Date .....3/12/10.....

This work is dedicated to my family for all the love and support they give.

Acknowledgements

I would like to thank Dr Damien Murphy for giving me the opportunity to study for a PhD and for his advice and encouragement throughout my time in Cardiff.

My thanks must go to the following:
To Dr Emma Carter, for all her constant willingness to offer help and advice.

To my colleagues in the EPR labs that made the lab work so enjoyable and always picked me up on 'one of those days'. Special thanks must go to Lucia whose humour and friendship has made my past three years so enjoyable.

To Laura, who has always been there with words of encouragement and support and has made life fun whilst writing the Thesis.

Thanks must go to all the members of the Cardiff University Korfball Club and Chemsoc who have made my time outside the lab in Cardiff so enjoyable and memorable.

Finally, my love goes to my family, for the continuous love and support they give me.

Abstract

Electron Paramagnetic Resonance (EPR) spectroscopy has been used to study and identify a number of defects (eg., Ti^{3+}, O^-) and transient oxygen centred radicals (eg., $HO_2^\bullet$, $ROO^\bullet$, etc) formed under different co-adsorption conditions over the surface of polycrystalline TiO_2 (P25).

Paramagnetic surface Ti^{3+} centres were formed by thermal treatment of TiO_2 under vacuum. This system provides a good model for probing electron transfer (ET) sites at the surface of TiO_2 that may be involved in catalysis. Upon O_2 addition to the reduced surface, superoxide (O_2^-) anions are formed and stabilised. Different sites for O_2^- stabilisation have been identified; notably at oxygen vacancy sites and at a non-vacancy, high co-ordinated Ti^{4+} sites. ET from the precursor Ti^{3+} centres to O_2 (forming O_2^-) was prevented at each respective site through selective blocking using specific probe molecules (CO_2 or Ar). Carbon dioxide specifically adsorbed at the non-vacancy sites, whereas Ar preferentially adsorbed at vacancy sites, thereby preventing ET.

The decomposition of acetonitrile, methanol and toluene occurs under dark conditions over TiO_2 (P25) containing adsorbed O_2^- radicals. The reaction of the organic substrates with O_2^- resulted in the production of thermally unstable [O_2^-...substrate] associated surface complexes which decayed at T > 240K. Under photochemical conditions, a series of thermally unstable alkylperoxy radicals were identified following UV irradiation of a series of co-adsorbed organic: O_2 mixtures.

The formation of oxygen centred radicals (O_2^- and $ROO^\bullet$) and defects (O^-) on the dehydrated, partially and fully hydrated TiO_2 surface under photochemical conditions was investigated. The O_2^- radicals were formed on the dehydrated and partially hydrated surfaces. At low temperatures O_2^- radicals were accompanied by O^- defects. These O^- species were thermally unstable and decayed at T > 200K, whereas O_2^- was stable at room temperature. The population of O_2^- and O^- on the partially hydrated surface decreased as the water pressure increased; this was caused by site blocking *via* adsorbed H_2O and OH groups. On fully hydrated surfaces, no O_2^- radicals were observed. The peroxy type radical, $ROO^\bullet$, was also formed on the TiO_2 surface under all of the investigated hydration conditions.

Contents

Chapter 3

An introduction to the theory of EPR applied to polycrystalline metal oxides.

Chapter 4

Experimental details

Chapter 5

Site specific blocking of oxygen vacancies on reduced TiO_2 by probe molecules

Chapter 6

The identification of transient oxygen centred radicals on the TiO_2 surface formed under radiative and non-radiative conditions

Chapter 7

The role of water in the formation of transient oxygen radicals on the titanium dioxide surface

Chapter 1

An introduction to the properties, structure and uses of titanium dioxide

1.1 Introduction

In the current global climate, the use of renewable energy sources such as sunlight to provide energy *via* solar cells or to drive photocatalytic processes over the surface of a photoactive catalyst is highly desirable. Many metal oxides are being researched and investigated to fulfil such roles. One such metal oxide is titanium dioxide which operates efficiently for many different applications; such as air and water remediation[1-3], self cleaning[4-7], solar cells[8] and self sterilizing surfaces[9]. However in order, to make further technological advances in the performance of TiO_2 in each application, a greater understanding of the fundamental processes that take place at the semiconductor surface is needed.

A wealth of research aimed at understanding these processes currently exists, covering both single crystal samples as well as polycrystalline powder samples. Titanium dioxide has become the typical model of choice in the study of single crystal metal oxide systems *via* UHV methods, due to its suitability for study *via* a number of surface science techniques. For a comprehensive introduction to the study of metal oxides see Heinrich and Cox[10] and for surface studies of TiO_2 in particular see the review by Diebold.[11]

The study of TiO_2 as a polycrystalline powder is important, as many industrial applications of titanium dioxide utilise it in this form. However, many aspects of its performance are still poorly understood, posing a challenge in studying and understanding its reactivity. During the course of this thesis, the formation of surface stabilised oxygen radicals at specific surface sites will be studied. Further, the reactivity of these surface stabilised oxygen centred radicals with adsorbed organic substrates will be investigated to help further understand the reaction mechanisms that take place at the TiO_2 surface.

The photocatalytic reactions that take place on the TiO_2 surface in industrial processes occur in the presence of several other substrates; one unavoidable factor is the presence of water. Water plays an important role as it has been shown to both poison and promote reactions. Therefore, the behaviour of oxygen centred radicals formed *via*

photochemical reactions has been studied on a hydrated TiO_2 surface in order to investigate the possible role of surface hydroxyl radicals.

1.2 General overview of TiO_2

1.2.1 Occurrence

Titanium dioxide is often found as an impurity in 'mixed substances'; it was first discovered in 1791 by William Gregor, who isolated a white metallic solid from black sand. The titanium dioxide can be extracted from ores such as ilmenite and leuoxocene. The most commonly used ore commercially is ilmenite ($FeTiO_3$) which is found as black sand and typically contains about 45-65% TiO_2. Other sands which can contain up to 95% TiO_2 can also be used to produce TiO_2. The first commercially produced TiO_2 was made available in small quantities in 1912, as an impure anatase polymorph with other metal oxides as a composite powder. Since 1912, the titanium dioxide industry has grown, with over 4 million tons produced per annum *via* the two main commercial processes: the sulphate process and chloride process, both of which will be described in detail in 1.2.2.

1.2.2 Manufacture of TiO_2

The first commercially viable method used to produce titanium dioxide was the sulphate process. This treatment produces both the anatase and rutile polymorphs of TiO_2. The process uses the mineral ilmenite ($FeTiO_3$), a black sandy material found and mined in Canada, USA, Australia, Scandinavia and Malaysia. The ore is dried, ground down and then undergoes sulphation *via* careful addition of concentrated sulphuric acid in a batch or continuous exothermic digestion reaction. The conditions of this step are carefully controlled to ensure maximum conversion of the ore to titanyl sulphate using the minimum amount of acid (eq 1.1).

$$FeTiO_3 + 2\,H_2SO_4 \longrightarrow TiOSO_4 + FeSO_4 + 2\,H_2O \quad (1.1)$$

$$TiOSO_4 \xrightarrow{OH^-} TiO_2nH_2O + H_2SO_4 \quad (1.2)$$

$$TiO_2nH_2O \xrightarrow{HEAT} TiO_2 + nH_2O \quad (1.3)$$

The resultant dry green brown cake mixture is dissolved in water or weak acid followed by treatment to ensure that only ferrous-state iron is present. The solution is

reduced resulting in a clear solution which is cooled to crystallize coarse ferrous sulphate heptahedra.

The insoluble products, including the titanyl sulphate liquor, are washed to remove the remaining impurities. The solution is then evaporated to a precise composition and hydrolyzed to make a pulp containing clusters of colloidal hydrous titanium dioxide (eq 1.2). The hydrous titanium dioxide is then calcined to evaporate the water and decompose any sulphuric acid left in the solid (eq 1.3). Once dried, seed crystals are formed and the TiO_2 is milled to produce the necessary particle size. The resulting mixture is then treated with chemicals to adjust its physical texture. The sulphate process is a simple process (Figure 1.1), which uses lower grade cheaper ores. However the operating costs are high due to the use of acid treatments, with the drawback that the TiO_2 may be contaminated with sulphate-based impurities, which may alter its chemical and photochemical properties.

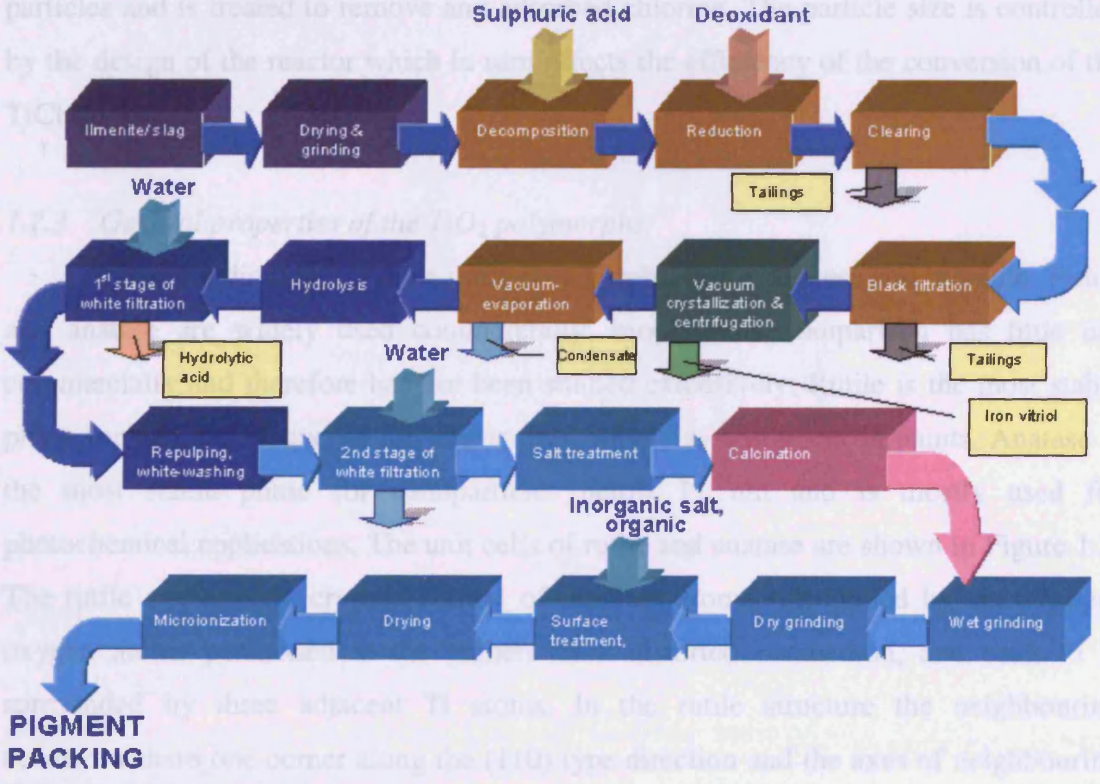

Figure 1.1 Schematic illustration of the sulphate process.

An alternative to the sulphate process is the chloride process. This is a relatively new process, with the advantage of cheaper operating costs compared to the sulphate process, as it avoids the iron sulphate waste problem. The process requires synthetic or mineral rutile ores with a TiO_2 content of over 90%. The impure ores are mixed with a source of carbon and then reacted over a fluidized bed with chlorine at 900°C (eq 1.4).

Titanium tetrachloride is the main product of this reaction along with some impurities present in the form of chlorides. The $TiCl_4$ production means the process has many advantages as the mixed chlorides can be cooled and the impurities can be separated by condensation and removed from the gas phase.

$$TiO_{2\,(impure)} + 2\,Cl_2 + C \rightarrow TiCl_4 + CO_2 \qquad (1.4)$$

$$TiCl_4 + O_2 \rightarrow TiO_{2\,(pure)} + 2\,Cl_2 \qquad (1.5)$$

The second vital stage of the process is the oxidation of the $TiCl_4$ to TiO_2. The pure titanium tetrachloride is reacted with oxygen to form TiO_2 and chlorine (eq 1.5). The chlorine from this stage is reused in the chlorination stage. Due to the high temperature at which the oxidation process is carried out, only the rutile polymorph is produced. Once cooled the gas stream passes through a separator to collect the pigment particles and is treated to remove any adsorbed chlorine. The particle size is controlled by the design of the reactor which in turn affects the efficiency of the conversion of the $TiCl_4$ to TiO_2.

1.2.3 General properties of the TiO_2 polymorphs

Titanium dioxide has three main polymorphs; rutile, anatase and brookite. Rutile and anatase are widely used commercially; brookite by comparison has little use commercially and therefore has not been studied extensively. Rutile is the most stable phase for particles above 35 nm and is used widely as a pigment in paints. Anatase is the most stable phase for nanoparticles below 11 nm and is mostly used for photochemical applications. The unit cells of rutile and anatase are shown in Figure 1.2. The rutile and anatase crystals consist of titanium atoms surrounded by six adjacent oxygen atoms positioned at the corners of a distorted octahedron, and each Ti is surrounded by three adjacent Ti atoms. In the rutile structure the neighbouring octahedra share one corner along the (110) type direction and the axes of neighbouring octahedral pairs alternate by 90°. In anatase, the octahedral pairs are connected with their edges.[11]

The diverse range of applications for which TiO_2 is used take advantage of the slight differences in structure and reactivity each of the polymorphs possess. The rutile polymorph structure is closer packed than anatase which gives rise to a greater refractive index and chemical stability with a high melting point of 2098 K. The anatase

polymorph has no specific melting point; as it undergoes a process know as rutilisation in the temperature region of 973 K to 1473 K depending on conditions, where it transforms from the anatase polymorph into the rutile polymorph.

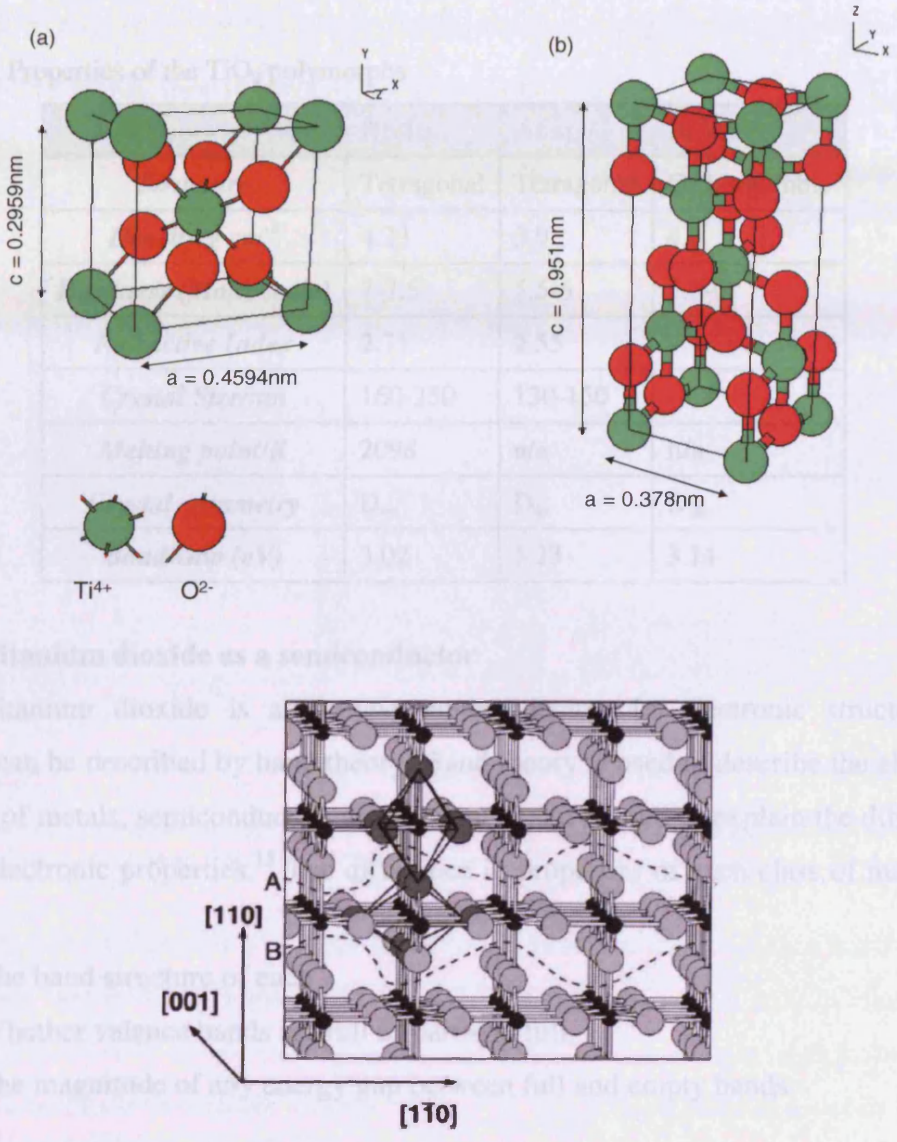

Figure 1.2 Crystal structures of the (a) rutile and (b) anatase forms of TiO_2. In (c) open channels along the [001] direction of the rutile lattice are visible.[11]

Both TiO_2 polymorphs are intrinsic photoactive *n-type* semiconductors with wide band gaps (as discussed later in section 1.3). There is growing evidence that suggests that anatase is more photoactive for a number of reactions such as O_2 photooxidation and therefore is more suitable for certain applications.[12]

The studies of mixed phased TiO_2 catalysts have recently increased with their commercial use on the rise. The mixed phase catalysts have been shown to have enhanced photoactivity compared to the individual phases which will be discussed in Chapter 2.[13,14] One such mixed phase catalyst is Degussa P25, which is a mixture of

anatase and rutile in an approximate 80%:20% ratio. Clearly the physical and chemical properties of the TiO_2 affect the photoactivity of the sample. The physical and structural properties of the three polymorphs are displayed in Table 1.1.

Table 1.1 Properties of the TiO_2 polymorphs

Property	**Rutile**	**Anatase**	**Brookite**
Structure	Tetragonal	Tetragonal	Orthorhombic
Density/g cm^{-3}	4.23	3.9	4.0
Hardness (Mohs scale)	7-7.5	5.5-6	5.5-6
Refractive Index	2.71	2.55	-
Crystal Size/nm	160-250	130-150	-
Melting point/K	2098	n/a	n/a
Crystal symmetry	D_{4h}	D_{4a}	D_{2h}
Band Gap (eV)	3.02	3.23	3.14

1.3 Titanium dioxide as a semiconductor

Titanium dioxide is an *n-type* semiconductor. Its electronic structure and bonding can be described by band theory. Band theory is used to describe the electronic structure of metals, semiconductors and insulators and is used to explain the differences in their electronic properties.[15] The difference in properties of each class of material is due to:

- The band structure of each
- Whether valence bands are full or partially full,
- The magnitude of any energy gap between full and empty bands

The band theory of solids is well supported by X-ray spectroscopic data and by two independent theoretical approaches; the *chemical approach*, which extends the concepts of molecular orbital theory to infinitely sized molecules, and the *physical approach*, where the concepts first described in the free electron theory are extended to include quantum mechanics and Fermi-Dirac statistics.[15]

In the discussion of TiO_2 as a semiconductor, the difference between each approach will not be discussed in detail here. However both approaches are explained in more detail in a number of excellent textbooks.[10,15,16] The theoretical approaches reach the same conclusion: that energy bands can be broadly split into the valence band, which is the lowest in energy and fully occupied by valence electrons, and the

conduction band, which is higher in energy and is empty or partially full with electrons (as shown in Figure 1.3a-c). In some materials, an overlap of different bands occurs; in others a forbidden gap exists between bands. The highest occupied energy level at 0 K is defined as the Fermi level with the corresponding energy called the Fermi Energy (E_F).

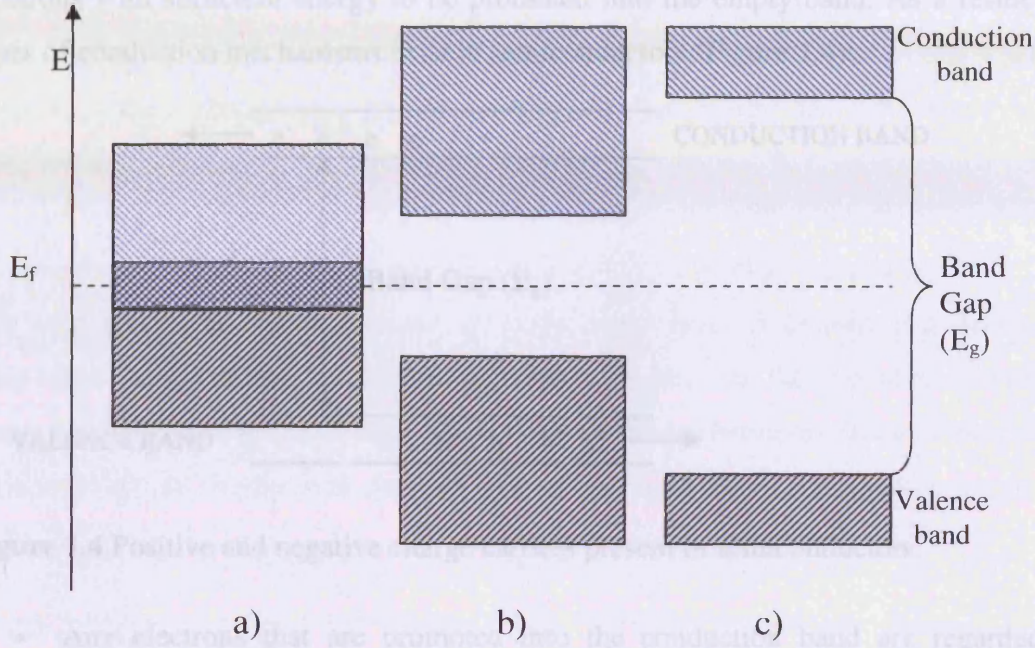

Figure 1.3 Diagram showing the band structure of a (a) metal, (b) semiconductor, (c) insulator. The grey shading indicates filled energy levels whereas blue indicates the empty energy levels.

As seen in Figure 1.3, Metals have only a partially filled valence band with no energy gap between the highest occupied orbital (HOMO) and lowest unoccupied orbital (LUMO). For conduction to occur the electrons must have enough energy to move to a vacancy in another energy level. The conduction does not occur in filled bands as the electrons have nowhere to move to. Some energy levels lying just below the Fermi level are vacant whereas some above the Fermi level are occupied (Figure 1.3a). The electrons in singly occupied states close to the Fermi level are able to move thus causing the high conductivity in metals.

The valence band for insulators is full and the conduction band empty, with the two separated by a large forbidden gap (band gap) E_g (Figure 1.3c). The Fermi level is situated between the valence and conduction bands and very few electrons from the valence band have sufficient thermal energy to be promoted into the empty conduction band above as the band gap is large (e.g. Diamond $E_g \sim 6$ eV). Therefore conductivity is negligibly small.

The band structure of semiconductors is similar to that of insulators, but the band gap is not large. The TiO_2 polymorphs have a relatively wide band gap of ~ 3 eV (anatase has a band gap of 3.2 eV and rutile 3.0 eV). The Fermi level in the semiconductor is situated in the band gap; however, its exact position must be derived as it can vary. The smaller band gap in a semiconductor (Figure 1.3b) allows some electrons with sufficient energy to be promoted into the empty band. As a result two types of conduction mechanisms exist in semiconductors (Figure 1.4):

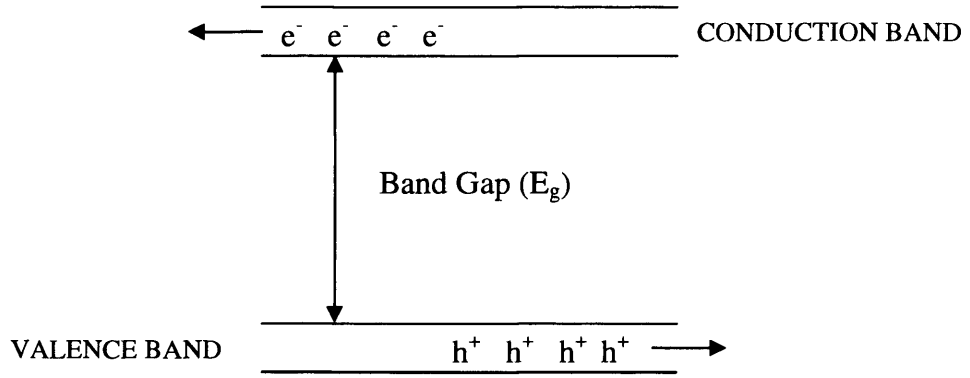

Figure 1.4 Positive and negative charge carriers present in semiconductors.

- Any electrons that are promoted into the conduction band are regarded as negative carriers moving towards a positive electrode when placed under an applied potential.
- The vacant electron levels left behind in the valence band can be regarded as positive holes. These positive holes move when an adjacent electron enters them, leaving its own position vacant as a fresh hole; holes effectively move in the opposite direction to the electrons.

Semiconductors can be broadly classified into two types; *intrinsic* or *extrinsic*; an *intrinsic* semiconductor is one that is in its "pure" state (i.e. undoped) where holes and electrons are created by thermal or by photoexcitation across the band gap. The Fermi level is essentially situated between the valence and conduction band. The number of holes and electrons present in each band is controlled in two ways; either by the magnitude of the band gap present in the material or by temperature.[15]

Elements that are not semiconductors in the pure state can be made semiconducting by doping the element with charged impurities; this is referred to as an *extrinsic* semiconductor. The doping is performed by removing a small amount of the lattice element and replacing it with the doping atom. The doped atom can either be

electron rich, leading to an *n-type* semiconductor (For example, silicon doped with arsenic), or electron poor leading to a *p-type* semiconductor (silicon doped with gallium).

The addition of a dopant results in the change in position of the Fermi level in the semiconductor. In the *p-type* semiconductor the addition of the dopant atom results in an acceptor level formed just above the valence band with the Fermi level shifted to a point halfway between the two (Figure 1.5a). Due to a change in the Fermi level the electron in the valence band may then have sufficient energy to be promoted to the acceptor level. However, the electron can not then participate in conduction, rather the positive holes that have been created in the valence band will conduct, as long as an electron moves into it leaving its original site vacant as a fresh positive hole.[15-17]

In the *n-type* semiconductor an extra donor level is created just below the conduction band with the Fermi level adjusted to be between the conduction band and donor level (Figure 1.5b). These levels acts as donor levels as the electrons have sufficient thermal energy to be elevated into the conduction band where they are free to move.[15-17]

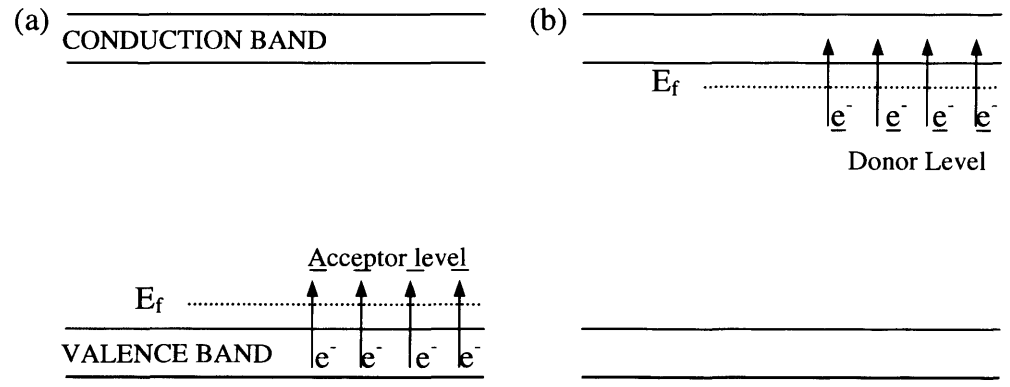

Figure 1.5 Representation of the two types of semiconductors. (a) a *p-type* semiconductor (b) an *n-type* semiconductor.[15]

TiO_2 is an inorganic material and can be classed as a *n-type* semiconductor. It is more complex structurally than a metal or semiconducting element but its properties can still be understood by utilising band theory.

The basic energy level diagram for a transition metal oxide has a valence band of oxygen 2*p* character and a conduction band of metal character. The lowest metal orbitals are normally *d*, rather than *s* as in pre-transition elements. The *d* orbitals of the transition metal ions have five-fold degeneracy in the free ions. These different directional properties produce different bonding interactions with nearby atoms. This is

known as crystal field or ligand field splitting and is important in all transition metal oxides

The *d* orbitals of a transition metal ion are split in energy as a result of the interaction of the metal orbitals with the surrounding ligand orbitals. Those *d* orbitals which point directly towards the ligands (forming σ combinations) have a larger degree of overlap than orbitals which point between the ligands (that form π combinations), and therefore form the major contribution to the ligand field splitting. The order of the d orbitals energy levels is dependent on the geometry of the ligands surrounding the transition metal atom; for TiO_2 the geometry around each Ti^{4+} cation is octahedral with the corresponding ligand field splitting shown in Figure 1.6.

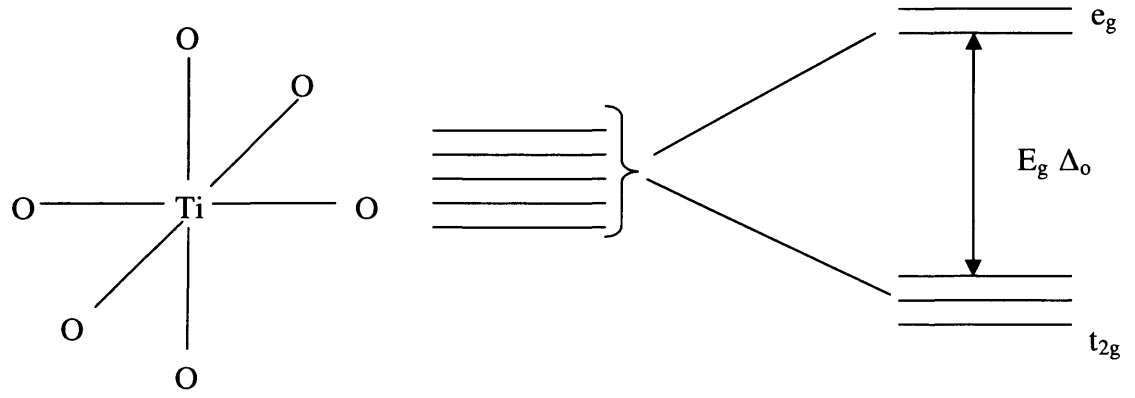

Figure 1.6 Octahedral geometry around the Ti^{4+} cation in TiO_2 and the corresponding crystal field splitting.

The wide range of electronic behaviour of the metal oxides creates difficulties, not just in the understanding and interpretation, but also of classification. d^0 insulators are stoichiometric oxides and are good insulators, also showing other properties expected of insulators: they have no optical absorptions at photon energies less than the band gap, and are diamagnetic with no unpaired electrons.[18]

The d^0 configuration is associated with the Ti^{4+} of TiO_2, therefore there are no electrons in the d band.[19] This compound has a filled valence band of predominately oxygen 2p character and a gap between this and the conduction band as shown in Figure 1.6. The observed gap of 3.1eV is fairly small and does suggest an appreciable covalent mixing between the atomic orbitals and metal orbitals. Thus the metal '*d*' orbital acts as an antibonding combination. The d^0 can be made into semiconductors by reduction *via* the loss of oxygen creating the defect sites Ti^{3+}. These have a d^1 configuration resulting in the partial occupation of the d state. This leads to conduction as shown in Figure 1.7.

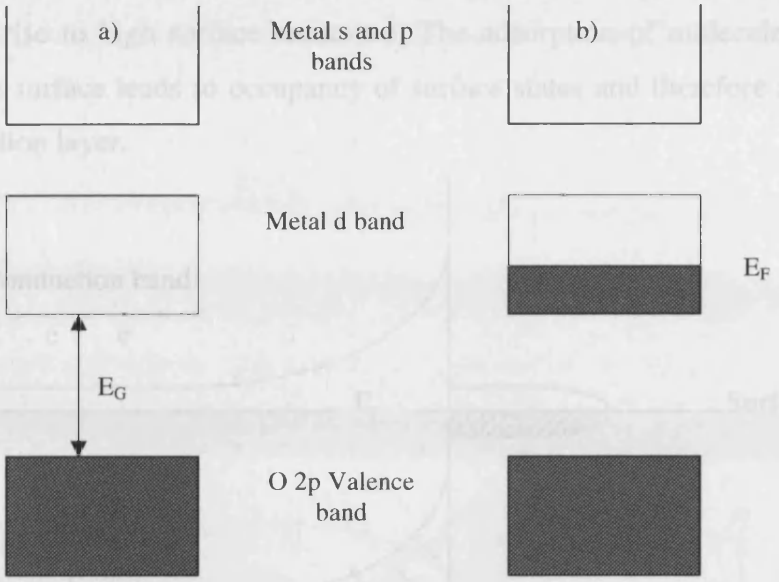

Figure 1.7 Energy bands of a transition metal oxide with a) an unoccupied d band and b) a partially filled d band.[19]

The relationship between the chemistry that takes place on the surface of a semiconductor is complex, with defect structures playing a key role. These defect sites can be introduced thermally. The generation of electron and holes in the semiconductor does not purely occur from thermal energy alone; this process can also be initiated by UV irradiation as explained in Section 1.3.2. The ability of TiO_2 to convert photons into chemical energy is the fundamental reason behind the use of TiO_2 for many different applications. For this to occur band bending must occur. As previously discussed for *n-type* and *p-type* semiconductors the position of the Fermi level in the bulk of a solid is controlled by the energy levels introduced as a result of doping. At the surface, the same energy levels associated with surface adsorbate or defects have more importance, possibly resulting in a different position of the Fermi level relative to the band edges as compared to the bulk. However, for a solid in equilibrium the Fermi level must be at the same energy throughout the solid. Therefore to achieve this equilibrium the band edges at the surface must bend.

For TiO_2, when there are surface states located in the bandgap there is transfer of electrons from the donor levels of the surface region in the surface states. This results in a depletion layer where there is an electrostatic field from the unbalanced positive charge of the ionized donors, causing the shift of the band energies. This is displayed in Figure 1.8.

The depletion layer formed as a result of diffusion of charge carriers through the solid gives rise to high surface resistance. The adsorption of molecules from the gas phase at the surface leads to occupancy of surface states and therefore alters the width of the depletion layer.

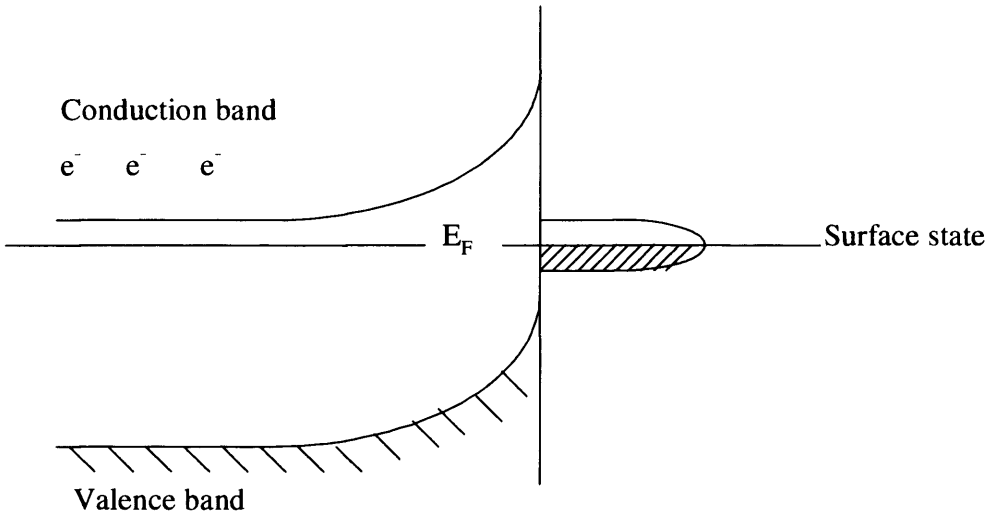

Figure 1.8 Band bending due to a surface state on an *n-type* semiconductor such as TiO_2.

This phenomenon is utilised in some solid-state sensors, where the presence of different gases alters the conductivity. For example, on adsorption of oxygen at the surface on an *n-type* semiconductor such as TiO_2, charge transfer occurs removing electrons from the surface and forming superoxide (O_2^-) anions and producing a depletion layer. Molecules that can be catalytically oxidized on the surface then liberate electrons, hence reducing the band bending and increasing the surface conductance.

1.3.1 Photocatalysis

A photocatalytic reaction is initiated when the energy of the absorbed photon *hv* exceeds or equals the band gap of the semiconductor. This causes excitation of an electron (e^-) from the valence band to the conduction band which results in an excited electron (e^-) - positive hole pair (h^+) as seen in Figure 1.9. The lifetime of the e^-/ h^+ pair can be sufficiently long in a semi-conductor, in the nanosecond regime, for migration of the e^-/h^+ pair to the surface of the TiO_2.[20] The e^-/h^+ pair can undergo surface recombination (Pathway A) or radiation-less recombination in the bulk of the semiconductor resulting in the release of heat (Pathway B). Once at the surface the photogenerated charge carrier can participate in interfacial electron transfer with surface adsorbed species. The trapped electron can reduce a surface adsorbed electron acceptor

(Pathway C) and a surface adsorbed electron donor can be oxidised by transfer of an electron to a surface photogenerated hole (pathway D) as described by the following:[21]

$$A + e^- \rightarrow A^- \quad (1.6)$$

$$D + h^+ \rightarrow D^+ \quad (1.7)$$

The processes of back reaction between the oxidised donor and electron, or reduced acceptor and hole, can occur after the initial transfer, especially when the species are strongly adsorbed on the semiconductor surface.[22]

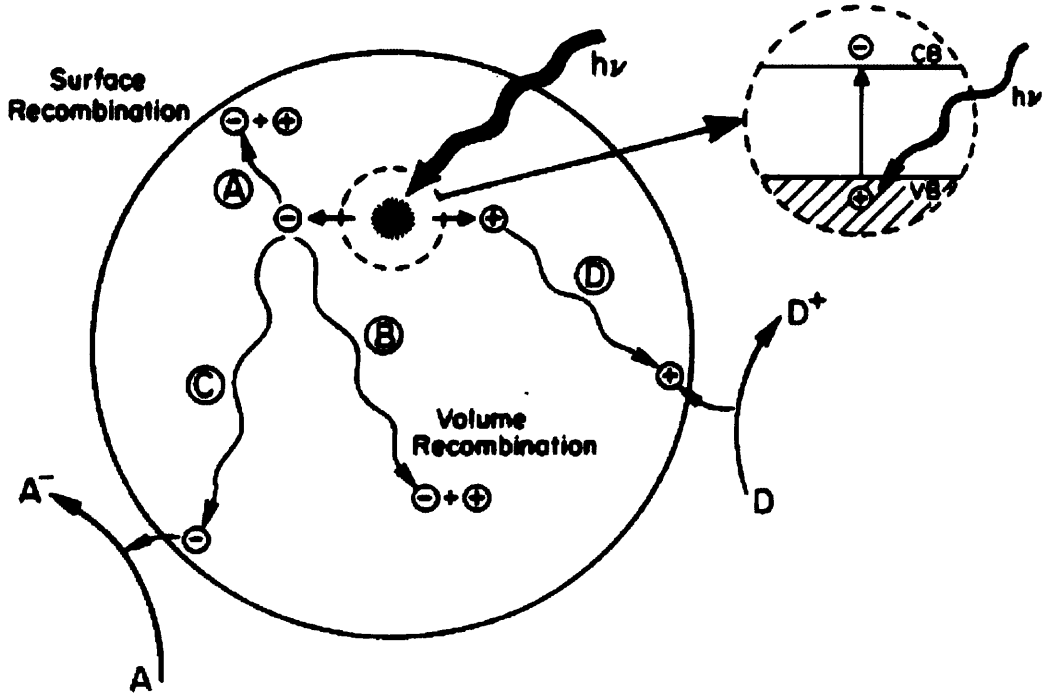

Figure 1.9 Schematic representation of photoexcitation in a semiconductor, followed by de-excitation events (including recombination and surface reaction).[21]

The efficiency of photoinduced transfer of electrons to surface adsorbed species on semiconductor photocatalysts depends on the band edge positions of the semiconductor and the redox potentials of the adsorbates. If the oxidation potential of the reacting species lies above the band gap oxidation potential an oxidation reaction occurs, whereas if the reduction potential of the reacting species lies below that of the band gap edge a reduction occurs.

1.3.2 Titanium dioxide based photocatalysis

The photooxidation of organic molecules over semiconductors proceeds *via* the following general equation:

$$\text{Organic contaminant} + O_2 \xrightarrow{h\nu, TiO_2} x\ CO_2 + y\ H_2O \qquad (1.8)$$

The desire is to eliminate the pollutant or pollutant precursor, by conversion to the mineralised products, carbon dioxide and water. The products can then be safely disposed of. An ideal photocatalyst for photooxidation possesses the following attributes:[23]

- Photostability,
- Chemically and biologically inert nature,
- Availability and low cost,
- Capability to adsorb reactants under efficient photonic activation ($h\nu >$ band gap).

TiO_2 fulfils the majority of the requirements, displaying high photoactivity, high corrosive resistance, low toxicity and is readily available at low cost. The biggest hurdle to the use of TiO_2 is the accessibility of the band gap. Although relatively small, the band gap is only accessible to predominantly UV light. This has led to much research into trying to reduce this energy gap so that it is easily accessible to the visible light region; this has focussed on doping the TiO_2 with metal impurities,[24] or coupling TiO_2 with narrow band gap semiconductors and doping with non-metal atoms.[25]

Despite much research into discovering an ideal photocatalyst, titania in its anatase polymorph form has remained the bench mark against which any emerging candidate material is tested. The anatase form is reported to give the best photoactivity and stability, and also has a higher surface adsorptive capacity towards many organic compounds.[26] The rutile phase is generally less active because of higher rates of recombination of the photogenerated charge carriers.[26] The ability of the photogenerated charge carriers to remain spatially separated in the photoexcited solid until they are able to undergo further reaction with surface adsorbates is an important factor in photocatalysis. If the spatial separation of the charge carriers is insufficient, charge carrier recombination leads to the dissipation of photon energy into heat. The study of charge carrier generation and recombination is therefore key to the development of efficient photocatalysts.

The photocatalytic process proceeds in the following manner on the TiO_2. Irradiation of the TiO_2 results in the generation of electron and holes (eq 1.9)

$$TiO_2 + h\nu \rightarrow e^-_{cb} + h^+_{vb} \quad (1.9)$$

$$O^{2-} + h^+_{vb} \rightarrow O^- \quad (1.10)$$

$$Ti^{4+} + e^-_{cb} \rightarrow Ti^{3+} \quad (1.11)$$

The positive holes are trapped at bulk or surface O^{2-} ions giving paramagnetic O^- species (eq 1.10). The electrons are trapped on local Ti^{4+} ions located in the bulk, or at the surface,[27] giving EPR active Ti^{3+} species (eq 1.11). In mixed phase system, it is also possible for e^- to be trapped at the anatase-rutile interface.[13,14] The formation of O^- and Ti^{3+} on irradiation makes TiO_2 attractive to study *via* EPR as O^- and Ti^{3+} are paramagnetic, so their formation can be used as an indirect probe of the photogenerated electrons and holes.

There are a number of other processes that can take place at the TiO_2 surface. If the surface of TiO_2 is populated with surface hydroxyls a number of titanol moieties Ti_{surf}-OH are present at the surface.[28] These can act as trapping centres for photo-induced electron vacancies (h^+) arising within the bulk of the crystal (eq 1.12),[28] The photo induced electron can also be trapped at surface Ti-OH groups (eq 1.13).[29]

$$Ti^{4+}_{surf}\text{-}OH + h^+_{vb} \rightarrow Ti^{4+}_{surf}\text{-}OH^{\bullet} \quad (1.12)$$

$$Ti^{4+}_{surf}\text{-}OH + e^-_{cb} \rightarrow Ti^{3+}\text{-}OH \quad (1.13)$$

Direct hole transfer from the TiO_2 to surface adsorbed organic species is also possible however this will be discussed in detail in Chapter 2.

1.3.3 Photoelectrochemistry

The band bending that occurs at the surface of a semiconductor can be utilised by photoelectron chemistry, at the semiconductor- electrolyte interface. In an *n-type* semiconductor, the photogenerated electrons (e^-) can migrate into the bulk of the solid whereas the holes (h^+) migrate to the surface where they can participate in surface reactions, hence acting as a photoanode.

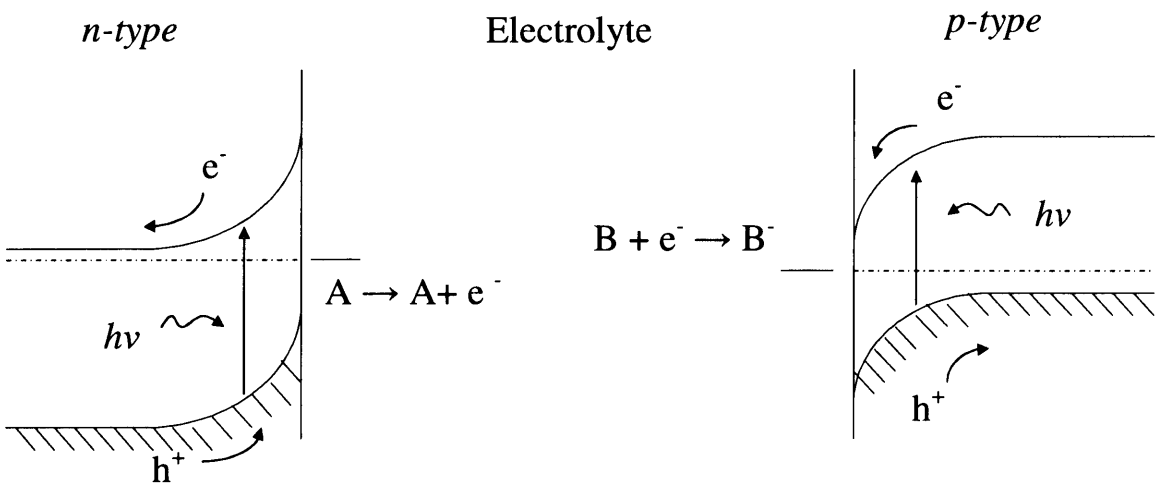

Figure 1.10 Semiconductor photoelectrodes separated by an electrolyte. Electrons and holes produced by light absorption are separated by band bending at the surface of the semiconductors.

In a *p-type* semiconductor the opposite occurs - the electrons migrate to the surface and act as a photocathode. Figure 1.10 shows a cell made up of the two types of semiconductors separated by an electrolyte; opposite redox reactions occur at the two electrodes resulting in a potential difference between them.

1.4 General applications of TiO_2

Since the isolation of titanium dioxide, it has been used for a diverse range of applications (Table 1.2). The most common commercial use is as a pigment in paint due to its high refractive index and opacity. The famous experiment, performed by Fujishima and Honda, demonstrated that water could be split by the use of sunlight over a TiO_2 photoanode and Pt Electrode into hydrogen and oxygen (eq 1.14).[30]

$$H_2O \xrightarrow{UV} H_2 + \tfrac{1}{2} O_2 \qquad (1.14)$$

Since this discovery, extensive work focussing on the production on hydrogen (as a combustible fuel) from water as a means of solar energy conversion has been performed. This has led to a growth of interest in the use of metal oxide semiconductors and their applications as photoactive catalysts. A number of the individual uses are listed in Table 1.2. Inoue *et al.*,[31] showed that CO_2 could undergo photocatalytic reduction over TiO_2, which attracted more interest in TiO_2 as a photocatalyst. It's main use though is as a heterogeneous photocatalyst in both aqueous and gaseous systems in the degradation of both inorganic and organic compounds.[32-36]

Table 1.2 Selected applications of TiO_2

Category	Properties	Uses
Pigment	High refractive index and opacity	Plastics, paper, paint, cosmetics, food.
Self Sterilising	The photocatalytic activity of titania results in thin films of the material showing self cleaning and disinfecting properties	Building tiles, cement, textiles, medical devices, food preparation surfaces.
Water Purification	Photocatalytic removal of contaminants	Used for the removal of organic pollutants
Air Purification	Relies on TiO_2 photocatalytic properties	Used to deodorize, decontaminate and disinfect air, and as a road surface to decompose NO
Gas Sensors	Electrical resistivity changes in the presence of adsorbed gases	Monitoring exhaust fumes
Solar Cells	Adsorbed dye molecules extend UV absorption into solar spectrum	Dye sensitized nanocrystalline solar cells
Superhydrophilicity	Adsorbed OH groups lowers the contact angle for water to ~ 0	Anti fogging mirrors, self cleaning windows

1.4.1 Water purification

The use of TiO_2 as a photocatalyst to purify water has many different applications ranging from water disinfection and remediation of metal contamination to the removal of chemicals ranging from VOC's to endocrine disruptor chemicals (EDC's).[21,33,37] The earliest reports of water purification were by Bard *et al.*,[38,39] who found that suspensions of TiO_2 powder could photocatalyze the conversion of cyanide to cyanate, thus detoxifying the water. The advantage of TiO_2 photocatalysis for water decontamination is that the key components are: TiO_2 in a powdered or immobilized form, and UV light, either from sunlight or artificial sources. This significantly reduces the cost compared to other advanced oxidation techniques (UV/O_3, UV/H_2O_2, photofenton).[1,3] Additionally, no toxic intermediates are generated in the decontamination process which makes it attractive for cleaning the water environment.[1]

One problem with TiO_2 photocatalysis is that it is only feasible for the treatment of wastewater that contains contaminants at low to medium pollutant concentrations, because of its relatively low efficiency and the limited flux of UV photons.[9] However, the advantages outweigh any potential limitations. For example it been shown to be particularly useful for the removal of endocrine disruptor chemicals in an aqueous environment (these include natural hormones, dioxins, bisphenol- A etc).[37,40-42] These chemicals disrupt endocrine functions in both humans and wildlife and have been implicated as a health hazard. The use of TiO_2 provides the advantage of removing the chemicals at a faster rate compared to conventional biological methods. It is also more economical than chemical oxidation methods as the EDC are often at low concentrations.[41]

1.4.2 Air purification

The purification of air is one of the many uses of gas phase heterogeneous catalysts over the TiO_2 surface; the advantage of TiO_2 in the removal of gaseous pollutants is its suitability for use in many different environments for different applications. These can range from the removal of volatile organic compounds (VOCs) from the atmosphere to removal of NO_x and SO_x on roads covered in TiO_2.

VOCs are a particularly important topic as they occur widely in industry and domestically. They have been shown to have long term health effects, as many are toxic, with some considered as carcinogenic, mutagenic or teratogenic.[43-45] The problem with the emission of VOC's which can be emitted from interior furnishings and building materials. The VOC's can form photochemical smog in large built up areas or be the cause of sick building syndrome and other diseases in the workplace.

Titanium dioxide is used widely in photocatalytic air cleaning filters, where the ability to decompose the organic substances *in-situ* on exposure to the TiO_2 surface, rather than accumulate them in a filter which then needs further cleaning, is a major advantage. TiO_2 also exhibits an antibacterial quality which makes it ideal for cleaning air in the workplace; Figure 1.11 is an example of TiO_2 used in an air filter system. The TiO_2 nanoparticles are coated onto the body of the filter with active co-absorbents. The co-absorbents facilitate the adsorption of VOCs on the filter, and ensure that no intermediate gaseous compounds are released. The absorbed substrates diffuse on the surface of the absorbent until they reach the TiO_2, and then undergo photodecomposition.

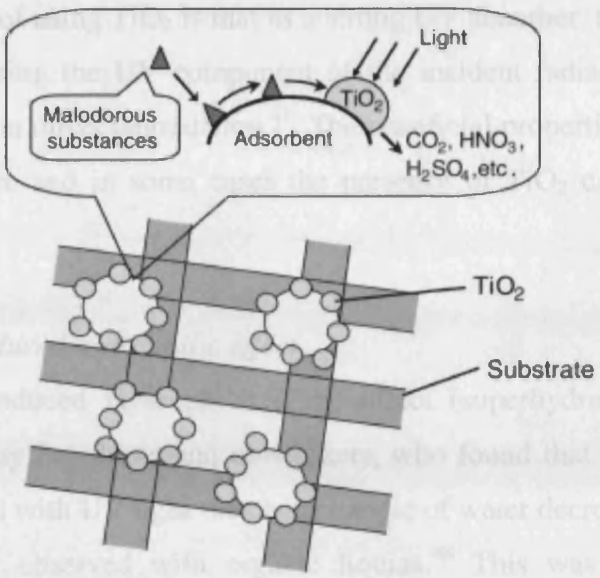

Figure 1.11 Schematic diagram of an air cleaning filter; the substrate materials (ceramics, paper, fabrics) are coated with a composite of TiO_2 and absorbents.[25]

The ability of TiO_2 to survive corrosive environments is demonstrated in its use for the removal of NO emitted from car exhausts. The removal of NO is important as it is thought to be responsible for air pollution in urban areas. The NO in the air is oxidized when the catalyst is exposed to light. Through the intermediate stage of nitrogen dioxide (NO_2) it is converted to nitric acid, which must be stored.[25,46] The ability to degrade NO has seen TiO_2 used in Italy and Japan, where the TiO_2 has been incorporated into road surfaces to convert NO_x and SO_x to more environmentally benign forms i.e. NO_3^- and SO_4^{2-}.

1.4.3 Pigments

TiO_2 is used as a pigment in paints due to its high refractive index and opacity. The powder is also used as an opacifier to provide whiteness to a number of products such as paints, plastics, toothpaste, food and cosmetics with up to 4 million tons of TiO_2 used for this purpose annually worldwide.

The use of TiO_2 as a pigment in paint has its advantages and disadvantages. The biggest disadvantage is that under UV light the paint can degrade by two independent processes. Firstly the binder can be degraded by the UV light, which can cause homolytic bond fission to occur within the organic binders. The resulting free radicals species are released in the polymer matrix and the structural integrity is eventually compromised. The binder can also be degraded by the photoactivity of the TiO_2 where its high photactivity can produce undesirable effects, as it is a UV activated oxidation

catalyst. The upside of using TiO_2 is that as a strong UV absorber, the TiO_2 protects the paint film by absorbing the UV component of the incident radiation and shields the binder molecules from direct degradation.[47] The beneficial properties of TiO_2 outweigh the destructive nature and in some cases the presence of TiO_2 can almost treble the lifetime of the resin.

1.4.4 The photo induced hydrophilic effect

The Photo Induced Hydrophilic (PIH) effect (superhydrophilicity), was first discovered in 1995 by Fujishima and co-workers, who found that when the surface of TiO_2 was illuminated with UV light the contact angle of water decreased to near 0° with the same behaviour observed with organic liquids.[48] This was as a result of the formation of two areas, one with hydrophobic properties, and the other with hydrophilic properties. This has led to several applications using this effect, such as antifogging mirrors and self cleaning surfaces. The mechanism of the PIH effect is still not fully understood with a number of possibilities for the mechanism suggested.[25] It is believed that the electron and holes are still produced, but upon irradiation that they subsequently react in a different way. The electrons tend to reduce the Ti^{4+} cations to the Ti^{3+} state and the holes oxidize the O^{2-} anion. In this process oxygen atoms are ejected, creating oxygen vacancies. Water molecules then occupy these oxygen vacancies producing adsorbed OH groups, which tend to make the surface hydrophilic. The TiO_2 coatings can maintain their hydrophilic properties indefinitely as long as they are illuminated. It is these properties that have led to many new applications of TiO_2.[25]

1.4.5 Self cleaning surfaces

The use of TiO_2 as a self cleaning surface arises due to the ability of the surface to decompose organic contamination with the aid of UV light.[25,49] This application of TiO_2 as a self cleaning substance was first demonstrated by Fujishima *et al.*,[49,50] using a titania-coated tile in 1992. The surface when coated with TiO_2 was found to maintain its cleanliness under UV irradiation as shown in Figure 1.12. The presence of water was found to enhance the cleaning properties when applied to the surface.[50] The enhancement was attributed to the Photo Induced Hydrophilic property of the TiO_2 surface explained in 1.4.4.[49,51] The PIH effect removes the limitation of the self cleaning function set by the number of incident photons. The best use of these self cleaning

surfaces was found to be in construction materials such as glass, tiles, aluminium and tent materials and has been in use in Japan since the 1990s.

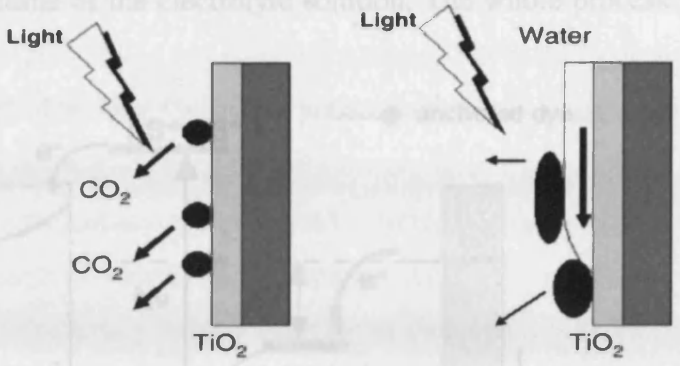

Figure 1.12 Schematic diagram of the decontamination process occurring on the superhydrophilic self-cleaning surface.[49]

1.4.6 Solar cells

The total incident solar energy that is available on a typical sunny day in Great Britain is 2.4×10^{11} kW/hr, with Great Britain's annual electricity consumption in the region of 2.8×10^{7} kW/hr.[52] If a small fraction of the incident solar energy could be utilised then the need to produce energy from other non-renewable sources would be reduced. The problem with using TiO_2 is that it is not particularly good at converting light into electricity. The visible light output doesn't fit into the correct frequency for solar conversion (i.e. visible light is not equal to the band gap) and some modifications need to be made to the TiO_2 to make it accessible to the visible light. The most effective cells are dye sensitized solar cells (DNSC).[12] In these cells the colloidal TiO_2 particles are coated in a light sensitive dye, typically ruthenium based to help improve the quantum yield of conversion. The cells differ from conventional semiconductor devices in that they separate the function of light absorption from charge carrier transport. The cells are constructed using a high surface area film of nanocrystalline TiO_2 coated onto a conducting glass. The ruthenium complex is then adsorbed onto the TiO_2. The role of the ruthenium complex is to absorb the sunlight and exploit the light energy to induce a vectorial electron transfer reaction. After excitation of the dye by solar photons, an electron is injected into the conduction band of the TiO_2 where subsequently, by band bending occurring at the interface between the semiconductor and the SnO_2 glass substrate, the electron is extracted to flow around an external circuit. After passing through a load, the electron is returned to the cell *via* the counter electrode, where it is accepted by a redox electrolyte solution which fills the cell. Electron transfer then occurs between the reduced electrolyte and the dye to return the dye to its original form,

effectively closing the circuit. The presence of the electrolyte ensures that the whole process is continuous and regenerative, resulting in solar cells that have a working life as long as the lifetime of the electrolyte solution. The whole process is summarised in Figure 1.13

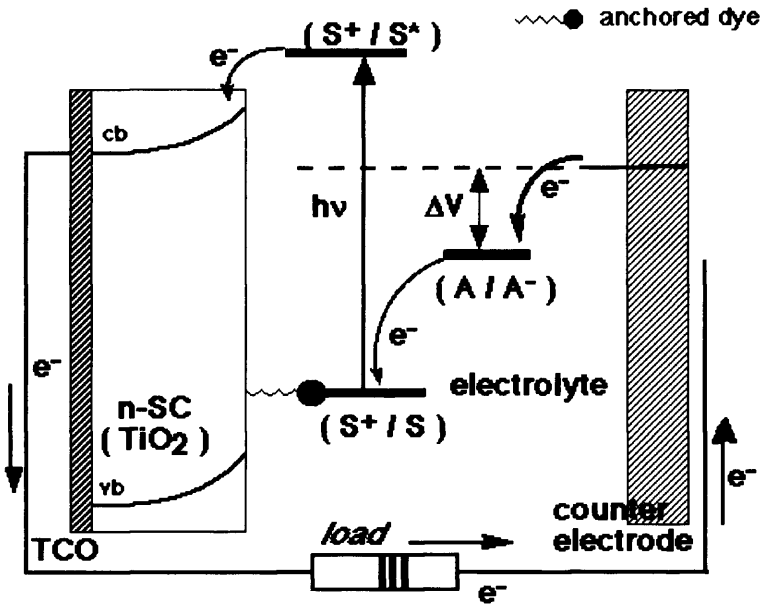

Figure 1.13 Principles of operation of a dye sensitized nanocrystalline solar cell (DSNC). (A/A^-) represents the redox couple, S represents the sensitizer (S* excited state, S^+ oxidised state).[12]

The advantage of this type of solar cell is that they have the potential to allow the conversion of a high proportion of the incident solar energy (46%) to electrical current at an exceptional efficiency (80%). The overall light to energy conversion yield is 7.1-7.9% in simulated solar light and 12% in diffuse daylight. The cells display exceptional stability (sustaining at least five million turnovers without decomposition) which coupled with the low cost make practical applications based on these more readily feasible.

1.5 Summary

In this chapter, the general physical and chemical properties of TiO_2 have been highlighted. These properties have led to TiO_2 being utilised for a wide range of industrial and commercial applications. One of the most important properties is the photocatalytic activity of TiO_2. Photoirradiation of TiO_2 by a photon with energy equal to or greater than that of the band gap results in the creation of electron (e^-)/ hole (h^+) pairs in the bulk of TiO_2. The e^-/ h^+ pairs can migrate to the surface and participate in reactions with surface adsorbates.

A major area of research is focussed on the surface species formed after reaction with these photogenerated pairs and the role they play in the reaction mechanism of the degradation of organic substrates. However, the activity of the photocatalysis does not purely depend on the charge carriers themselves but how they are utilised at the interface since certain surface planes are known to be more active than others. The most fundamental steps in the photocatalytic process are the electron transfer (ET) events that take place between the surface and adsorbed substrate. In the case of the photogenerated electron, it can become localised at Ti^{3+} centres. The Ti^{3+} centres are important as they have been shown to be catalytic hotspots. One of the aims of this thesis is to probe these Ti^{3+} centres indirectly using a surface probe (O_2^-), to investigate how the presence of co-adsorbed gases may prevent important electron transfer events from occurring (Chapter 5).

The nature of the paramagnetic species on the TiO_2 surface will be investigated by Electron Paramagnetic Resonance (EPR) spectroscopy. This technique has the advantage that it can characterise thermally unstable paramagnetic oxygen species stabilised on the TiO_2 surface. The reactivity of surface oxygen species stabilised at the Ti^{3+} sites will be investigated as they have been shown to react with adsorbed organic substrates. A series of thermally unstable intermediates formed over TiO_2 under dark conditions has therefore been investigated along with thermally unstable species produced under UV irradiation (Chapter 6). The photocatalytic reactions on the surface of TiO_2 often take place in the presence of water vapour as it is an unavoidable component, and its role in the photocatalytic processes on TiO_2 is poorly understood. The EPR technique will also be used in the identification of oxygen species on both dehydrated and hydrated surface and the differences in behaviour of the radicals between the two surfaces will be explored (Chapter 7).

1.6 References

(1) Bahnemann, D. *Solar Energy* **2004**, *77*, 445.

(2) Jo, W.-K.; Park, K.-H. *Chemosphere* **2004**, *57*, 555.

(3) Ollis, D. F.; Pelizzetti, E.; Serpone, N. *Environmental Science and Technology* **1991**, *25*, 1523.

(4) Minabe, T.; Tryk, D. A.; Sawunyama, P.; Kikuchi, Y.; Hashimoto, K.; Fujishima, A. *Journal of Photochemistry and Photobiology A-Chemistry* **2000**, *137*, 53.

(5) Nakajima, A.; Hashimoto, K.; Watanabe, T.; Takai, K.; Yamauchi, G.; Fujishima, A. *Langmuir* **2000**, *16*, 7044.

(6) Heller, A. *Accounts of Chemical Research* **1995**, *28*, 503.

(7) Paz, Y.; Luo, Z.; Rabenberg, L.; Heller, A. *Journal of Materials Research* **1995**, *10*, 2842.

(8) Gratzel, M. *Nature* **2001**, *414*, 338.

(9) Roa, T. N., Fujishima, A. Tryk, D.A. Semiconductors Electrodes and Photoelectrochemistry. In *Encyclopedia of Electrochemistry*; Bard, A. J., Ed.; Weinheim, **2002**; Vol. 6.

(10) Cox, P. A., Henrich, V.A. , *The Surface Science of Metal Oxides* Cambridge University Press, **1994**.

(11) Diebold, U. *Surface Science Reports* **2003**, *48*, 53.

(12) Oregan, B.; Gratzel, M. *Nature* **1991**, *353*, 737.

(13) Hurum, D.; Agrios, A. G.; Gray, K. A.; Rajh, T.; Thurnauer, M. C. *Abstracts of Papers of the American Chemical Society* **2001**, *222*, U427.

(14) Hurum, D. C.; Agrios, A. G.; Crist, S. E.; Gray, K. A.; Rajh, T.; Thurnauer, M. C. *Journal of Electron Spectroscopy and Related Phenomena* **2006**, *150*, 155.

(15) West, A. *Basic Solid State Chemistry*, Second ed.; Wiley, **1999**.

(16) Smart, L., Moore, E., *Solid State Chemistry. An Introduction*, Second ed.; Chapman and Hall, **1996**.

(17) McCash, E. *Surface Chemistry*; Oxford: Oxford, **2001**.

(18) Cox, P. A. *Transition Metal Oxides, An introduction to the electronic structure* **1995**; Vol. 27.

(19) Cox, P. A. *The Electronic Structure and Chemistry of Solids* Oxford Science Publications **1987**.

(20) Nosaka, Y.; Fox, M. A. *Journal of Physical Chemistry* **1988**, *92*, 1893.

(21) Linsebigler, A. L.; Lu, G. Q.; Yates, J. T. *Chemical Reviews* **1995**, *95*, 735.

(22) Fox, M. A.; Dulay, M. T. *Chemical Reviews* **1993**, *93*, 341.

(23) Carp, O.; Huisman, C. L.; Reller, A. *Progress in Solid State Chemistry* **2004**, *32*, 33.

(24) Borgarello, E.; Kiwi, J.; Gratzel, M.; Pelizzetti, E.; Visca, M. *Journal of the American Chemical Society* **1982**, *104*, 2996.

(25) Fujishima, A.; Zhang, X. T.; Tryk, D. A. *Surface Science Reports* **2008**, *63*, 515.

(26) Riegel, G.; Bolton, J. R. *Journal of Physical Chemistry* **1995**, *99*, 4215.

(27) Howe, R. F.; Gratzel, M. *Journal of Physical Chemistry* **1985**, *89*, 4495.

(28) Primet, M.; Pichat, P.; Mathieu, M. V. *Journal of Physical Chemistry* **1971**, *75*, 1216.

(29) Szczepankiewicz, S. H.; Colussi, A. J.; Hoffmann, M. R. *Journal of Physical Chemistry B* **2000**, *104*, 9842.

(30) Fujishima, A.; Honda, K. *Nature* **1972**, *238*, 37.

(31) Ishitani, O.; Inoue, C.; Suzuki, Y.; Ibusuki, T. *Journal of Photochemistry and Photobiology A-Chemistry* **1993**, *72*, 269.

(32) Addamo, M.; Augugliaro, V.; Coluccia, S.; Faga, M. G.; Garcia-Lopez, E.; Loddo, V.; Marci, G.; Martra, G.; Palmisano, L. *Journal of Catalysis* **2005**, *235*, 209.

(33) Alberici, R. M.; Jardim, W. E. *Applied Catalysis B-Environmental* **1997**, *14*, 55.

(34) Berger, T.; Diwald, O.; Knozinger, E.; Napoli, F.; Chiesa, M.; Giamello, E. *Chemical Physics* **2007**, *339*, 138.

(35) Cermenati, L.; Albini, A.; Pichat, P.; Guillard, C. *Research on Chemical Intermediates* **2000**, *26*, 221.

(36) Dai, W. X.; Chen, X.; Zheng, X. P.; Ding, Z. X.; Wang, X. X.; Liu, P.; Fu, X. Z. *Chemphyschem* **2009**, *10*, 411.

(37) Nakashima, T.; Ohko, Y.; Tryk, D. A.; Fujishima, A. *Journal of Photochemistry and Photobiology A-Chemistry* **2002**, *151*, 207.

(38) Frank, S. N.; Bard, A. J. *Journal of the American Chemical Society* **1977**, *99*, 303.

(39) Frank, S. N.; Bard, A. J. *Journal of Physical Chemistry* **1977**, *81*, 1484.

(40) Ohko, Y.; Ando, I.; Niwa, C.; Tatsuma, T.; Yamamura, T.; Nakashima, T.; Kubota, Y.; Fujishima, A. *Environmental Science & Technology* **2001**, *35*, 2365.

(41) Nakashima, T.; Ohko, Y.; Kubota, Y.; Fujishima, A. *Journal of Photochemistry and Photobiology A-Chemistry* **2003**, *160*, 115.

(42) Ohko, Y.; Iuchi, K. I.; Niwa, C.; Tatsuma, T.; Nakashima, T.; Iguchi, T.; Kubota, Y.; Fujishima, A. *Environmental Science & Technology* **2002**, *36*, 4175.

(43) Augugliaro, V.; Coluccia, S.; Loddo, V.; Marchese, L.; Martra, C.; Palmisano, L.; Pantaleone, M.; Schiavello, M. *3rd World Congress on Oxidation Catalysis* **1997**, *110*, 663.

(44) Demeestere, K.; Dewulf, J.; Van Langenhove, H.; Sercu, B. *Chemical Engineering Science* **2003**, *58*, 2255.

(45) Kim, S. B.; Hwang, H. T.; Hong, S. C. *Chemosphere* **2002**, *48*, 437.

(46) Ichiura, H.; Kitaoka, T.; Tanaka, H. *Chemosphere* **2003**, *51*, 855.

(47) Scott, G. *Pure and Applied Chemistry* **1980**, *52*, 365.

(48) Wang, R.; Hashimoto, K.; Fujishima, A.; Chikuni, M.; Kojima, E.; Kitamura, A.; Shimohigoshi, M.; Watanabe, T. *Nature* **1997**, *388*, 431.

(49) Fujishima, A.; Zhang, X. T. *Comptes Rendus Chimie* **2006**, *9*, 750.

(50) Wang, R.; Hashimoto, K.; Fujishima, A.; Chikuni, M.; Kojima, E.; Kitamura, A.; Shimohigoshi, M.; Watanabe, T. *Advanced Materials* **1998**, *10*, 135.

(51) Fujishima, A.; Zhang, X.; Tryk, D. A. *International Journal of Hydrogen Energy* **2007**, *32*, 2664.

(52) Boyle, S. A., J. *The Greenhouse Effect*; N.E.L.: London, **1989**; Vol. 214.

Chapter 2

The role of reactive oxygen intermediates in heterogeneous TiO_2 based photocatalysis.

2.1 Introduction

Titanium dioxide has played an important part in heterogeneous catalysis in recent years. The scope of the research is vast, focusing on many different aspects of the TiO_2 such as its surface structure, the nature of reactive species and the photocatalytic processes which take place at its surface. In the following chapter, the surface structure of both TiO_2 polymorphs (rutile and anatase) will be discussed along with mixed phase TiO_2 formulations. At the surface of titanium dioxide a number of surface oxygen species have been identified to play a key role in the photocatalytic degradation of organics. The formation of these surface species however can be affected by a number of different factors, such as surface morphology, particle size and the presence of water.[1-4]

The TiO_2 surface is complex with major differences arising between the two main polymorphs. The co-ordination of the titanium and oxygen atoms can result in different surface structures which can lead to differing behaviour under specific surface treatments such as thermal annealing or UV irradiation. Surface Ti^{4+} centres can be reduced to surface Ti^{3+} centres, by trapping of photogenerated electrons or through surface reduction. This leads to the removal of O^{2-} which results in the formation of Ti^{3+} centres and associated oxygen vacancies. These vacancies have been shown to be reactive and can act as 'catalytic hotspots' by providing a conduit for electron transfer. The catalytic hotspots have been shown to be essential to govern the adsorption of O_2. At the Ti^{3+} centres, O_2 molecules can be adsorbed non-dissociatively to form O_2^- species. The EPR technique has been used to characterise this O_2^- species since they have been used to indirectly probe the TiO_2 surface.[5] The EPR technique has also been used to study a number of oxygen centred radicals on the reduced or stoichiometric surface on TiO_2 and their identity and EPR characteristics will be discussed in this chapter.

A number of surface oxygen species have been shown to participate in catalytic reactions at the TiO_2 surface and are also used to study the remote gas phase oxidation of organic species. Many studies have focussed on studying these reactions and surface

intermediates under model conditions, i.e., clean fully dehydrated stoichiometric surfaces. However, the behaviour under standard catalytic conditions must be considered compared to non-standard 'model' conditions. The presence of water vapour is unavoidable on the TiO_2 surface catalysts under standard catalytic conditions, therefore much research into the role of water has been performed, often focussing on how the H_2O is adsorbed at the TiO_2 surface (either as water or hydroxyl groups). The surface hydroxyl groups are believed to become hydroxyl radicals *via* trapping of a photogenerated hole and are believed to play an important role in the oxidation of organic species.

The following discussion is by no means a complete review of the available literature. For a more comprehensive review on single crystal studies of TiO_2 see the review by Diebold,[6] or for a comprehensive discussion on the TiO_2 surface see the recent review by Fujishima.[7-9]

2.2 The titanium dioxide surface

In any metal oxide system, the surface structure has a strong influence on the local surface chemistry due to the mixture of ionic and covalent bonding present.[10] The TiO_2 surface has been studied extensively and this has led to an unprecedented level of understanding. However there are still many questions left to answer, including what governs the difference in reactivity between pure phase TiO_2 and mixed phase TiO_2. The difference in reactivity can be related to surface geometry and surface defects which have been shown to play an important role in catalysis.

2.2.1 Surface structure of the rutile polymorph

The surface structure of the TiO_2 rutile polymorph has been extensively studied as rutile single crystals are widely available. A number of crystal faces have been studied for rutile, focussing typically on the (110), (001) and (100) faces.

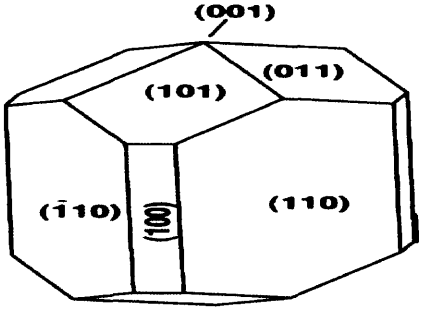

Figure 2.1 The equilibrium shape of a TiO_2 crystal using the Wulff construction based on the surface energies calculated in ref 11.[11]

Theoretical calculations have shown the (110) crystal face to have the lowest surface energy and the (001) surface to have the highest surface energy. Ramamoorthy *et al.*,[11] used these results to construct the Wulff plot shown in Figure 2.1. The Wulff construction gives the equilibrium crystal shape of a macroscopic crystal. Experimental results have been found to match and confirm these calculations.

Due to its relative stability much of the work has therefore focussed on the (110) surface, which has been well characterised using a number of different techniques.[6] The rutile (110) surface contains 6-fold and 5-fold co-ordinated titanium atoms and 3-fold and 2-fold oxygen atoms. The surface has rows of bridging oxygen atoms which are connected to the two 6-fold co-ordinated Ti atoms. The 5-fold co-ordinated Ti atoms run parallel to and alternate with the rows of bridging oxygens (Figure 2.2).

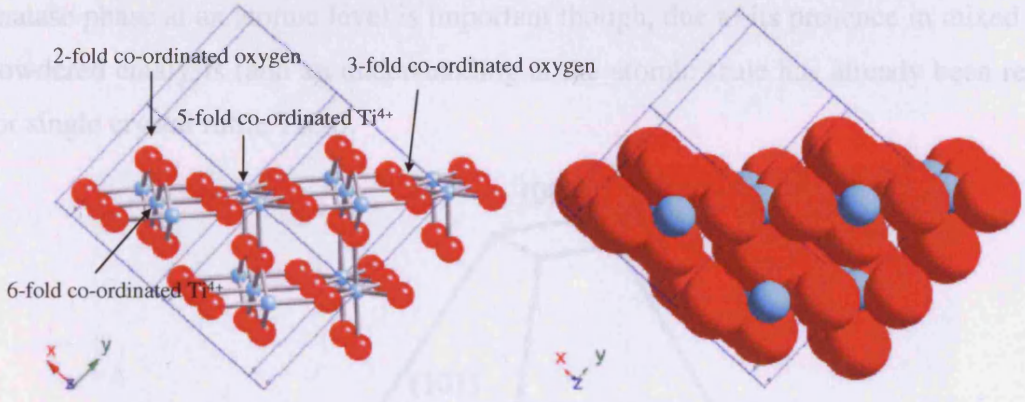

Figure 2.2 Surface structure of the rutile (110) surface.[7]

The bridging oxygens have attracted much debate as they are believed to be removed relatively easily by thermal annealing resulting in point defects; these in turn have been shown to affect the overall chemistry at the surface. Two types of defects have been identified on the TiO_2 surface: The first type is formed after the loss of a bridging oxygen, resulting in the reduction of two 6-fold co-ordinated Ti^{4+} cations to 5-fold co-ordinated Ti^{3+} centres. The second type is formed on the main surface plane, when the two 5-fold co-ordinated Ti^{4+} cations become 4-fold co-ordinated Ti^{3+} centres upon removal of oxygen (Figure 2.3). The result of this reduction in co-ordination number is accompanied by an increase in chemical reactivity with the general view that low co-ordination surface sites are more reactive than high co-ordination surface sites. A review of the surface chemistry at these point defects is discussed in section 2.2.3

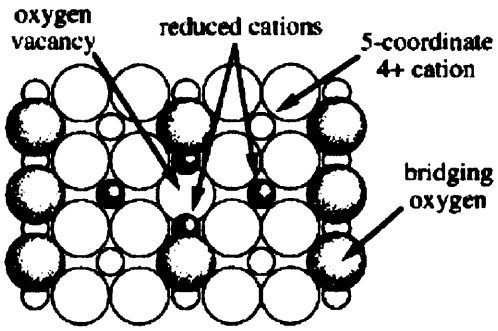

Figure 2.3 Schematic model showing the top view of an oxygen vacancy along the bridging oxygen row on TiO_2 (110).[12]

2.2.2 *Surface structure of the anatase polymorph*

The anatase phase of titanium dioxide has received less attention as it is difficult to grow single crystals of sufficient size for UHV studies. The understanding of the anatase phase at an atomic level is important though, due to its presence in mixed phase powdered catalysts (and an understanding at the atomic scale has already been reached for single crystal rutile TiO_2).

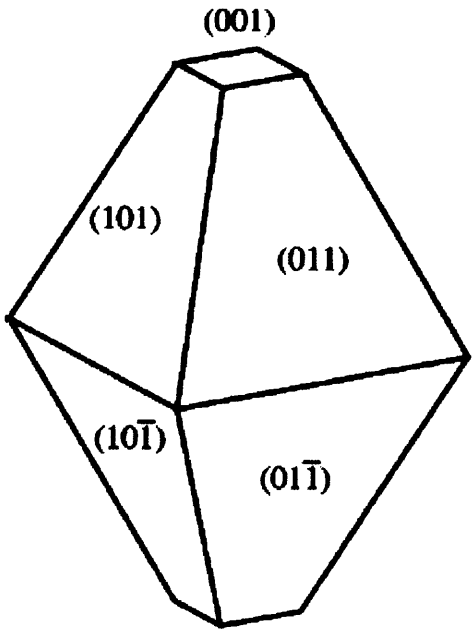

Figure 2.4 The equilibrium shape of the TiO_2 anatase crystal according to surface energy calculations.[13]

When anatase TiO_2 crystals are synthesised they are typically dominated by the thermodynamically stable (101) face (more than 94%), according to the Wulff construction for anatase (Figure 2.4).[13] This was demonstrated by theoretical calculations which confirmed the relative stability of each crystal face.

STM studies by Hebenstreit *et al*,.[14] at the (101) surface identified titanium cations in a number of different co-ordination environments. Two types of Ti atoms

were situated at terraces with 5-fold and 6-fold co-ordination; at the step edges the Ti atoms had 4-fold co-ordination and were found to be preferential active sites for gas adsorption (Figure 2.5). On the (101) anatase surface the authors found that, unlike the rutile surface, the removal of oxygen to create surface defects was difficult.[14] The 2-fold co-ordinated oxygens at the saw tooth edges were expected to be removed by annealing under UHV conditions. Several imperfections were observed, but no definitive proof for point defects was found. The authors believed this could be due to the inability of STM to image the defects or purely that the (101) anatase surface is very stable against the loss of two fold co-ordinated oxygen atoms.[14]

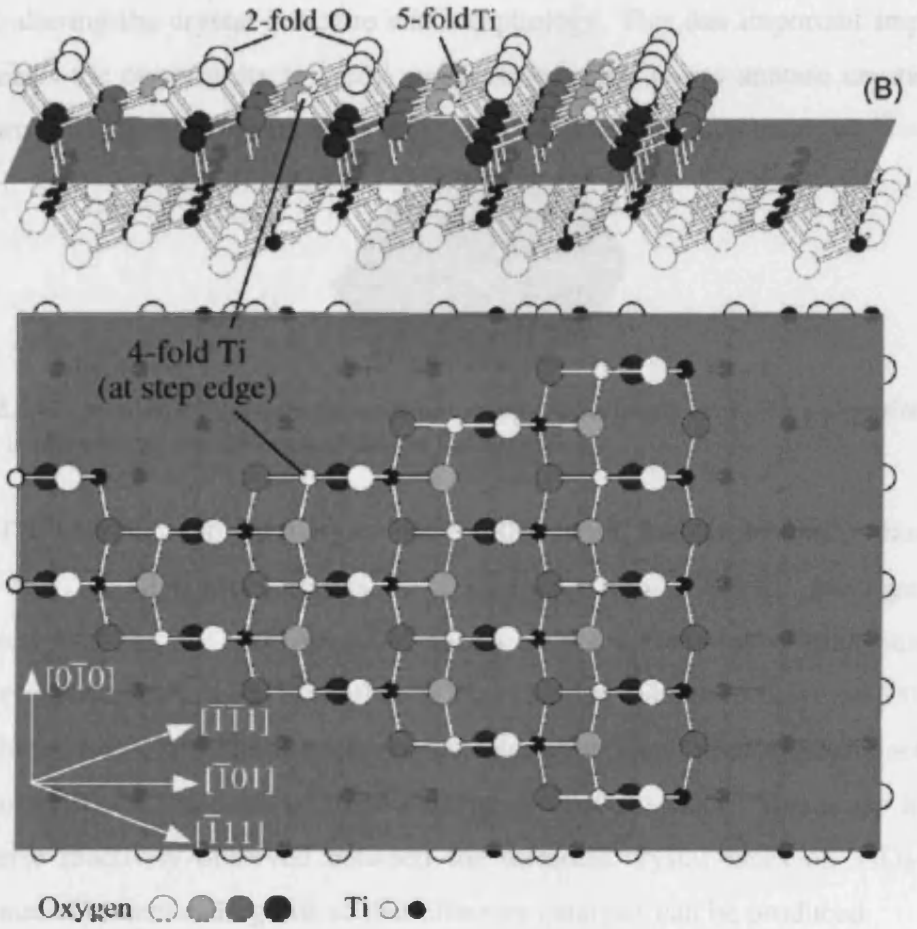

Figure 2.5 Atomic model of the anatase (101) (1×1) surface, with top and side view. The two possible terminations for step edges along [010] are indicated by A and B.[14]

The stable (001) surface was shown to contain exclusively 5-fold co-ordinated Ti atoms, as well as 2-fold and 3-fold co-ordinated oxygen atoms. Until recently the more reactive (001) face of anatase was little studied due to difficulties in synthesising this facet. Surfaces with high reactivity usually diminish rapidly during the crystal growth process as a result of the minimization of surface energy. A significant paper

was published by Yang *et al.*,[15] who used theoretical calculations to explore whether different non-metal adsorbate atoms terminated at the Ti surface would lower the surface energy and subsequent aid in the formation of the more reactive (001) surface. For the fluorine terminated surface, the relative stability of the facets is reversed such that (001) surface is energetically preferable to the (101) surface. Using hydrofluoric acid as a morphology controlling agent, the authors were able to synthesis uniform anatase TiO_2 single crystals with a high percentage (47%) of (001) facets (Figure 2.6). The authors also showed that the surface could easily be cleaned of the fluorine atoms terminated at the surface by using heat treatment, to produce a fluorine free surface without altering the crystal structure and morphology. This has important implications as it creates the opportunity to study well defined, high purity anatase crystals which could have promising applications in solar cells, sensors and photocatalysis.[15]

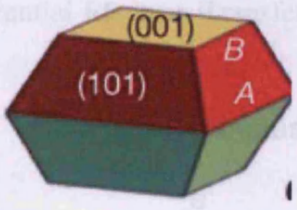

Figure 2.6 Calculation of the crystal formed in using hydrofluoric acid. The proportion of (001) surfaces is increased compared to that shown in Figure 2.4.

The photocatalytic activity of these (001) facets has already been shown to be greater than mixed phase catalysts. In a study by Han *et al.*,[16,17] rectangular TiO_2 nanosheets with highly reactive (001) facets at the surface were synthesized by a hydrothermal treatment with hydrofluoric acid solution. The percentage of (001) facets in the sheets was 89%. The nanosheets were found to show photocatalytic activity far exceeding that of P25 due to the high percentage of (001) facets. This study highlights the diverse reactivity observed between the different crystal faces on TiO_2 and the importance of understanding this so that effective catalysts can be produced.

2.2.3 Structure of mixed phase TiO_2

Mixed phase TiO_2 has been shown to display enhanced photocatalytic activity compared to naturally occurring single phase TiO_2. One such mixed phase sample is P25 TiO_2 (~ 20% rutile, 80% anatase) which is the most studied mixed phased catalyst. It is therefore often used as a benchmark to compare the photoactivity of new TiO_2 formulations.

Initially the dominant theory behind the enhanced photoactivity of the mixed-phase materials relative to the pure phase was thought to be due to the transfer of photogenerated electrons from the anatase phase into the lower energy trapping sites in the rutile phase (Figure 2.7a), thus improving the efficiency of electron hole separation and thereby yielding greater catalytic activity. The model gained support based on the fact that the conduction band of rutile is lower in energy than that of anatase.[18] The group of Komaguchi *et al.*,[19] studied the photoresponse of the Ti^{3+} signal in partially reduced P25 material using visible light. Using EPR the authors found that the Ti^{3+}_{latt} signal is slightly different for anatase compared to rutile; therefore in the mixed phase material the relative response of the $Ti^{3+}_{anatase}$ centres versus Ti^{3+}_{rutile} centres could be monitored. The authors demonstrated that the observed photo-response was due to the excitation of the trapped electron and not by generation of electron-hole pairs.[19] These important results indicated preferential Electron Transfer (ET) from anatase to rutile in TiO_2 by photoexcitation.

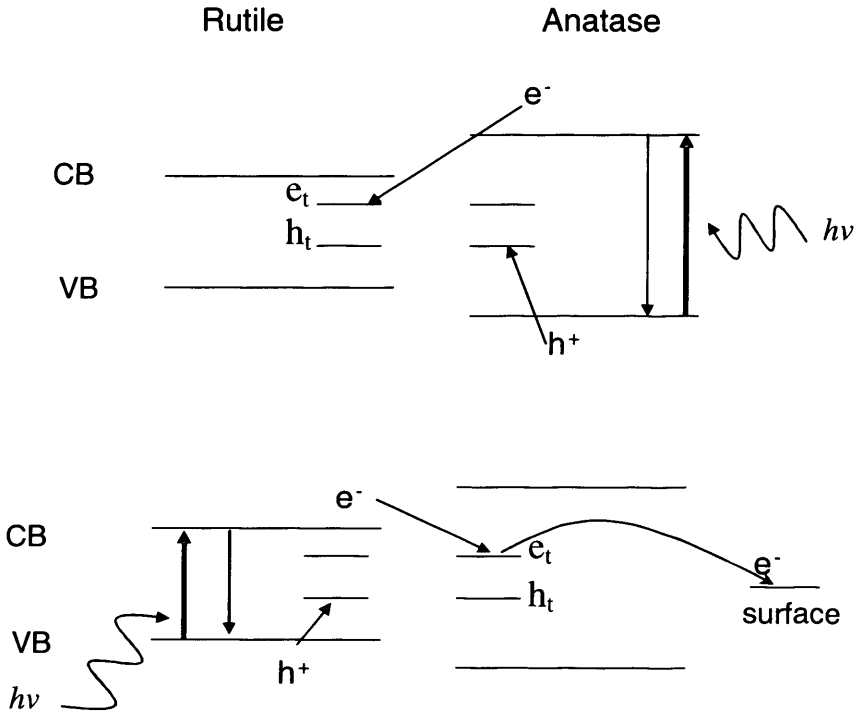

Figure 2.7 (a) Proposed model of P25 activity where charge separation occurs on the anatase polymorph and rutile acts as an electron sink. (b) Model proposed of a rutile antenna and subsequent charge separation.[20,21]

However Hurum *et al.*,[22] argued that an alternative picture of the charge separation is possible (shown in Figure 2.7b). Using the EPR technique (which is suited to study the dynamics of charge separation) to study colloidal P25, they found that the photoactivity of the mixed phase material is enhanced due to three factors; (1) the

smaller band gap of rutile extends the useful range of photoactivity into the visible region; (2) the stabilization of charge separation by electron transfer from rutile to anatase slows recombination; (3) the small size of the rutile crystallites facilitates this transfer, making catalytic hotspots at the rutile-anatase interface. The process was found to be dependant on the interface between the TiO_2 planes and also on particle size. The most important finding was that the rutile-anatase interface facilitates the charge transfer from rutile to lower energy anatase lattice trapping sites. The transfer of the photogenerated electron to anatase trapping sites then allows a hole (h^+) to reach the surface which would otherwise have been trapped by recombination. Subsequent electron transfer moves the electron from anatase trapping sites to surface trapping sites (Figure 2.7b). This describes the reverse energy transfer indicating that the electrons migrate from rutile to anatase. Energetically this is possible if the transfer is from rutile to lower anatase trapping sites, as the anatase trapping site was shown to be 0.8 eV lower in energy that the anatase conduction band, placing it well below the rutile conduction band.

In a further study Hurum *et al.*,[21,22] used EPR to study a series of colloidal P25 suspensions using a modified sonication/centrifugation method. They found a link between the size of the aggregates and its charge trapping properties. As the size of the aggregates increased, the population of the rutile trapping sites increased. In other words, as the size increased the trapped charges remained on rutile and less transfer to anatase occurred.

The EPR technique was then used study charge transfer processes between tri chlorophenol (TCP) and the P25 TiO_2 surface.[20,21] The authors attributed the high activity of the mixed phase TiO_2 for TCP oxidation to a distorted 4-fold co-ordinated defect site located at the phase interfaces where a charge transfer complex is likely. They believed that such a site would occur at the interface of the anatase and rutile particles where other processes, such as phase transformation and chemical reactions due to electron transfer are know to be enhanced. Hurum *et al.*,[21,22] described these interfacial sites act as "catalytic hotspots".

2.2.4 Role of surface defects

Surface $Ti^{3+}_{surface}$ centres have been shown to act as electron conduits in photocatalysis. The Ti^{3+} centres can be formed by trapping of photogenerated electrons (e^-) at Ti^{4+} centres after UV irradiation of TiO_2. If electron accepting species are at the

surface of TiO_2, the electron can be transferred. A typical route for producing these surface Ti^{3+} centres, in both single crystal and powder samples, is by thermal annealing which results in the removal of surface O^{2-} anions and subsequent Ti^{3+} formation. Additionally, these centres can be created on single crystals under UHV conditions by electron bombardment or spluttering.[6] The characterisation of these surface defects has been carried out by Temperature Programmed Desorption (TPD) [23-25], Electron Paramagnetic Resonance (EPR), [5,26] X-ray Photoelectron Spectroscopy (XPS)[24,27] and Ultraviolet Photoelectron spectroscopy (UPS)[6].

After annealing at high temperatures and under UHV conditions, Ti^{3+} centres can be created on the rutile (110) surface. These are recognized as point defects and are believed to exist at oxygen vacancy sites located within the bridging oxygen rows of the TiO_2- (1x1) surface. The TPD technique has been used by many groups to probe the presence of thermally created defect sites on a rutile (110) surface. CO_2 was used as the probe molecule on the reduced and fully oxidized TiO_2 surfaces as it was found to adsorb non-dissociatively. Henderson *et al.*,[12] showed that CO_2 was adsorbed at two different sites on the TiO_2 surface as two peaks were observed in the TPD data. The CO_2 was found to be linearly bound at 5-fold co-ordinated Ti^{4+} sites, which desorbed in the TPD at 137K, and also at a second site assigned to vacancy Ti^{3+} sites which desorbed at 166K.

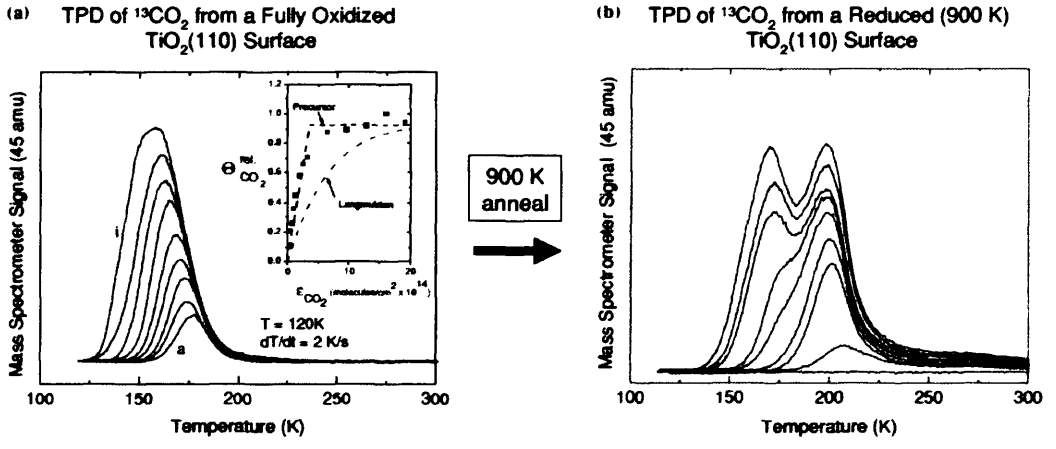

Figure 2.8 CO_2 TPD from oxidized (left) and reduced (right) TiO_2 (110) surfaces. [23,24]

Thompson *et al.*,[23] used CO_2 to probe the effect of thermal annealing on the defect density at the surface using reduced and fully oxidised TiO_2. On the fully oxidized surface only one peak due to CO_2 adsorbed at Ti^{4+} sites was observed (Figure 2.8a), whereas on the reduced surface two peaks could be seen in the TPD plots (Figure 2.8b) belonging to CO_2 adsorbed at the 5-fold co-ordinated Ti^{4+} site and the vacancy

Ti^{3+} site. The results indicate that CO_2 chemisorbs at defect sites on the TiO_2 surface with a higher binding energy (54 kJ/mol) than on regular sites (48.5 kJ/mol).[23]

The surface Ti^{3+} sites have been shown to react with surface adsorbed molecules.[25] Lu *et al.*,[25] showed that adsorbed D_2O, $^{13}CH_2O$ and ^{15}NO can interact with the Ti^{3+} centres and react reductively at these sites to produce D_2, $^{13}C_2H_4$ and $^{15}N_2O$ respectively. The Ti^{3+} sites were found to have abstracted the oxygen from the adsorbates with oxidation of the surface Ti^{3+} sites observed. Clearly the chemistry at these Ti^{3+} sites is complex with molecules adsorbed both dissociatively and non-dissociatively.

Oxygen is frequently used as a molecular probe of these surface defects. Oxygen has been shown to be adsorbed dissociatively at the Ti^{3+} centres to form O^{2-}, resulting in stoichiometric surface, or non-dissociatively with electron transfer from Ti^{3+} to molecular oxygen to form O_2^- species. The adsorption of oxygen at these Ti^{3+} sites is not always straightforward as shown by Henderson *et al.*[12] The authors found that after adsorption of CO_2 on purely vacancy sites, followed by exposure of oxygen, no displacement of the CO_2 from the vacancy site occurs. Further, on heating the sample to desorb the CO_2 from the vacancy sites, the adsorbed O_2 does not move into the vacancy sites to reoxidize the surface. The formation of surface species such as O_2^- will also be hindered if the adsorption of the O_2 is blocked. The O_2^- has been shown to play an important role in many oxidation reactions. For example, Linsebigler *et al.*,[28] have reported that O_2^- radicals located at surface defects were responsible for determining the photocatalytic oxidation of CO on the TiO_2 surface.

The importance of understanding the role of each co-adsorbate in the photocatalytic oxidation of CO was highlighted by Dai *et al.*[29] The authors investigated the effect that chemisorption of O_2, CO and H_2 had on the photocatalytic oxidation of CO over the vacuum treated TiO_2 surface. The authors found that the CO would adsorb at oxygen vacancies and would subsequently react with adjacent lattice oxygen to produce CO_2 and H_2O, accompanied by the formation of new surface oxygen vacancies. This process was found to be enhanced by the introduction of H_2. The chemisorption of H_2 at surface oxygen vacancies was found to result in dissociation to H atoms which were then observed to react with lattice oxygen to form OHO species. In contrast, the addition of oxygen was found to 'heal' the surface oxygen vacancies.[29]

Dai *et al.*,[29] found the order of adsorption to be important. For example, the introduction of oxygen to the surface prior to CO admission was found to promote the

photooxidation of CO. The presence of hydrogen was not found to be a benefit in most of the systems studied.[29] However, in the $CO/H_2/O_2$ system, the presence of H_2 was found to promote the oxidation of CO due to its promoting affect on the formation of new oxygen vacancies.[29]

The chemistry at the TiO_2 surface is rich, with the Ti^{3+} surface centres responsible for acting as electron transfer sites. The literature contains many studies detailing the addition of individual gases onto the surface to probe the nature of the vacancy site. However, little work has been performed on investigating the competition for the surface Ti^{3+} sites by co-adsorbed gases. In this Thesis, it is intended to use the superoxide radical O_2^- (discussed in section 2.3.1) to indirectly probe the Ti^{3+} centres at the surface of P25 TiO_2.

2.3 Characterisation of oxygen species at the surface of metal oxides

Surface oxygen species are postulated to play an important part in reactions over metal oxide surfaces. In the course of this Thesis a number of oxygen centred radicals will be identified and discussed, therefore the following section contains a brief introduction to several oxygen centred radicals which have previously been identified by EPR. A review of the literature, discussing the important role Reactive Oxygen Species (ROS) play in catalysis will follow hereafter. The most commonly used oxidising agent is gaseous O_2, but it is generally thought that this oxygen must be converted to either O^-, O_2^- or O^{2-} on the surface (Scheme 1). The paramagnetic oxygen species involved in these processes will be discussed in the following section.

Scheme 1

2.3.1 The O_2^- ion

The superoxide radical is the most common oxygen centred radical formed on metal oxide surfaces and has been well characterized. It is formed when an electron is transferred to molecular oxygen:

$$O_2 + e^- \rightarrow O_2^- , \Delta H = -42.47 \text{ kJ/mol}^{-1} \qquad (2.1)$$

The decrease in energy when the molecular oxygen accepts the electron is the reason for the ease of formation. The O_2^- can be classified using either an ionic or

covalent model. In the following the ionic model will be discussed; for further information on the covalent model see Che and Tench.[30]

In the ionic model the O_2^- radical is classified as a 13-electron diatomic radical with three electrons in the two π^* antibonding orbitals therefore, creating a paramagnetic (S = 1/2) state as shown in Figure 2.9.

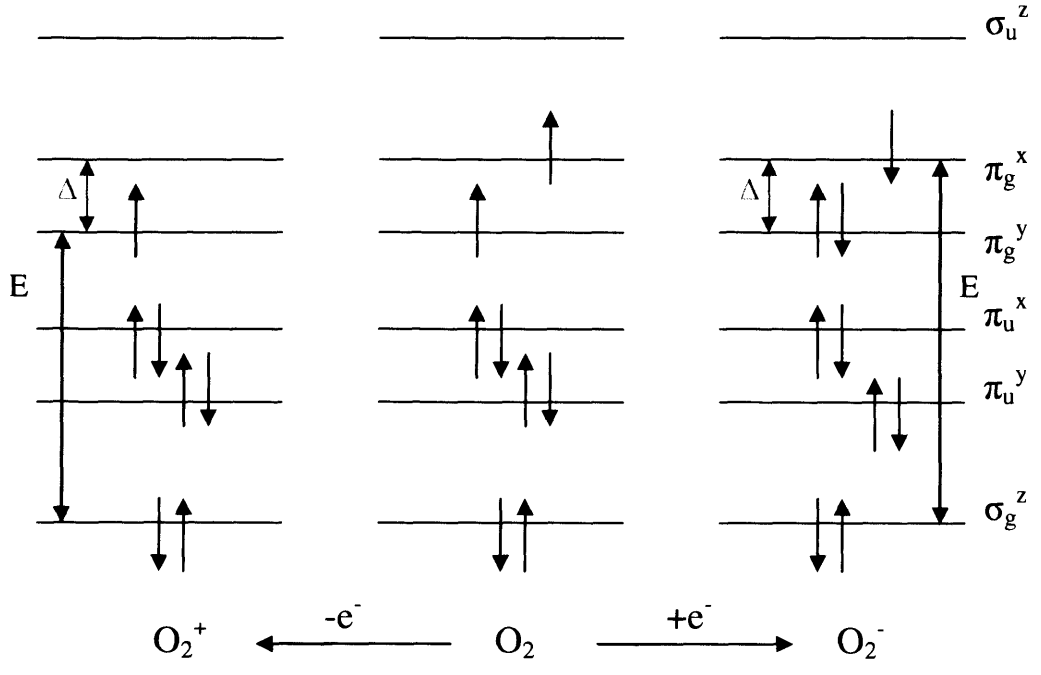

Figure 2.9 The simplified energy level diagram for the O_2^+, O_2 and O_2^- species in their ground states. When a crystal field is present, the π_g and π_u levels are not degenerate.

However, the π_g^* orbitals are degenerate and this degeneracy must be removed by an external perturbation before an EPR spectrum is observable. On formation of the O_2^- at a cationic surface site (M^{n+}), the electrostatic field from the M^{n+} lifts the degeneracy of the two π_g^* orbitals. The resulting EPR spectrum is orthorhombic, meaning that all three axes of the molecule are magnetically inequivalent ($g_{xx} \neq g_{yy} \neq g_{zz}$). The z direction is specified as along the internuclear axis, with the x and y directions perpendicular to the adsorption site (see Chapter 5 (Figure 5.16))

The expected principal values of the ***g*** tensor for O_2^- were first derived by Känzig and Cohen[31] and are given by:

$$g_{xx} = g_e \qquad (2.2)$$

$$g_{yy} = g_e + 2\lambda/E \qquad (2.3)$$

$$g_{zz} = g_e + 2\lambda/\Delta \qquad (2.4)$$

where λ is the spin orbit coupling constant for the oxygen atom, g_e is the free electron g value (2.0023), Δ is the energy splitting between the two anti-bonding orbitals ($2p\pi_y^*$

and $2p\pi_x^*$) and E is the difference between the $2p\sigma$ and $2p\pi_x^*$ orbitals, as shown in Figure 2.9. The sensitivity of the g_{zz} region to the magnitude of the local crystal field of the metal oxide provides a way to probe the surface, as it can be used to probe the nature of the adsorption site. Howe and Leith have shown that the value of g_{zz} can be used to distinguish between Mo^{6+} and Al^{3+} sites in a mixed oxide MoO_3/Al_2O_3.[32] It has also been shown that the magnitude of g_{zz} can be used to distinguish between sites of the same nominal charge, but different co-ordination environments, (this is discussed in detail in chapter 5) as observed on TiO_2[5,33,34] and MgO[35,36].

2.3.2 *The O_2^+ ion*

The O_2^+ ion has only a single electron in the π_g orbitals, compared to the three for the O_2^-, as shown in Figure 2.9, and is isoelectronic with NO. The presence of the surface will break the degeneracy of the π_g orbitals in the same way as for O_2^-, but in this case an unoccupied molecular orbital is formed slightly higher in energy than the π_g orbital since this must now contain the unpaired electron and the resulting EPR spectrum is observed to have a negative g-shift.

2.3.3 *The O_2^{2-} ion*

The O_2^{2-} ion is normally referred to as the peroxide ion, which should be distinguished from the covalent peroxy radical ($ROO^\bullet$). It has previously been treated as a dimer O^- species by other authors.[37] The ion is difficult to characterise on the surface because it is diamagnetic. Studies of metal-dioxygen complexes show that the peroxide-like complexes have an infra red band ν_∞ in the range of 800 - 932 cm^{-1}. Conductivity and chemical methods of measuring the charge on the oxygen do not distinguish between $2O^-$ and the O_2^{2-}. It is therefore not possible to obtain direct evidence on the nature of the oxygen species.

2.3.4 *Triplet oxygen*

Triplet oxygen is accepted as the form in which gaseous oxygen is physisorbed.[38] It's ground state is the triplet $^3\Sigma_g^-$ state containing two unpaired electrons. At higher energies two low lying electronically excited states exist; the singlet $^1\Delta_g$ and $^1\Sigma_g^+$ levels, as shown in Figure 2.10. In the gaseous state, the coupling of the spin angular momentum with the molecular rotation angular momentum gives rise to a spectrum that is spread over 1000 mT.[39]

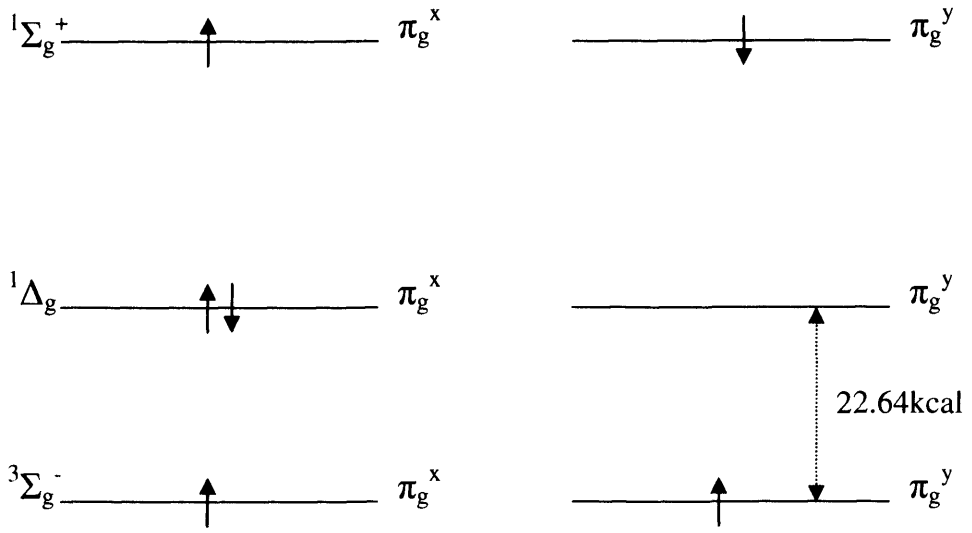

Figure 2.10 π_g orbital occupancy and energies of singlet and triplet dioxygen

2.3.5 Singlet oxygen

It was believed to be highly unlikely for singlet oxygen to take part in any reaction at the surface of metal oxides as its energy level is too high at around 22.64 kcal above the ground state of triplet oxygen. However it has been shown to be an important reactive intermediate in atmospheric, biological and therapeutic processes and as a reagent in organic synthesis. The formation of singlet oxygen ($^1O_2$) has been detected by Nosaka *et al.*,[40] who generated $^1O_2$ on an irradiated TiO_2 surface. Detection of the near infra-red phosphorescence at 1270nm gave direct evidence for the presence of $^1O_2$. Singlet oxygen was also believed to form by oxidation of O_2^- with holes on the TiO_2 surface. The lifetime of the singlet oxygen is 2μs which is short compared to those of $^\bullet$OH radicals (*ca.* 10μs) and trapped holes.[40]

2.3.6 The O^{2-} ion

The O^{2-} ion is often neglected in discussions about oxygen species at surfaces, yet there is much evidence indicating that they can be formed as the final stage of some adsorption processes. The O^{2-} ion is diamagnetic and it can't be studied by EPR. However, the presence of O^{2-} on the surface and the effect on surface properties should always be considered even though it cannot be directly observed.

2.3.7 *The O^- ion*

The O^- species has received considerable attention as it is believed to play an important role in oxidative reactions at the surface of metal oxides. Che and Tench describe much of the early work on mononuclear oxygen species on metal oxide surfaces in their excellent review.[37] The O^- trapped hole species has been identified over a number of different surfaces by EPR.[37] Theoretical calculations have shown that the spectrum is dependant on the O_{2p} energy levels. The energy level diagrams for tetragonal and octahedral symmetry are shown in Figure 2.11.

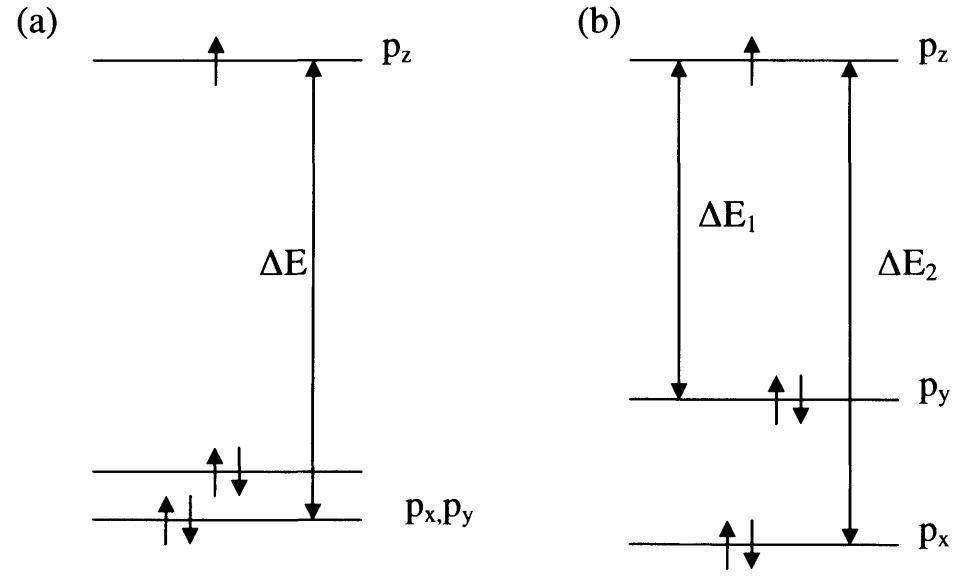

Figure 2.11 The energy-level diagram for the O^- radical in (a) an axial crystal field and (b) an orthorhombic crystal field.

The two different symmetries observed have different principal ***g*** tensors, which have been calculated theoretically to first order. For orthorhombic symmetry the g components of the tensor for the O^- species have been calculated as:

$$g_{zz} = g_e \tag{2.5}$$

$$g_{xx} = g_e + 2\lambda/\Delta E_1 \tag{2.6}$$

$$g_{yy} = g_e + 2\lambda/\Delta E_2 \tag{2.7}$$

where ($\lambda > 0$) is the spin orbit coupling constant of oxygen.

For the axial case (tetragonal symmetry) the p_x and p_y orbitals are degenerate, hence the ***g*** tensor components are calculated as:

$$g_{\parallel} (= g_{zz}) \approx g_e \tag{2.8}$$

$$g_{\perp} (= g_{xx} = g_{yy} =) g_e + (2\lambda/\Delta E) \tag{2.9}$$

where λ is the oxygen spin-orbit coupling constant (0.0014eV) and ΔE is the energy separation between the p_z orbital and p_x and p_y. The O^- species is sensitive to the surface crystal field as $g_\perp$ includes ΔE. If the O^- species is formed close to a more positively charged ion a larger splitting of the p orbitals is observed leading to a lower $g_\perp$ value. This sensitivity to the local surface crystal field was used by Scotti *et al.*,[41] to identify a number of different stabilisation sites on the surface of TiO_2 and to distinguish between O^- stabilised on rutile and anatase polymorphs.

The formation of O^- can occur in a number of different ways. Lunsford *et al.*,[42] discovered that O^- could be generated by addition of N_2O to an MgO surface containing surface F centres at 298K, as described by;

$$N_2O + e^- \rightarrow N_2 + O^- \qquad (2.10)$$

This treatment resulted in an EPR signal with g values of $g_1 = 2.047$, $g_2 = 2.019$ and $g_3 = 2.002$.

Table 2.1, Reported g values for the O^- ion in the bulk or surface of metal oxides

Oxide	Comments	g_1	g_2	g_3	Reference
MgO	Single Crystal	2.0385	2.0385	2.0032	43
ZnO	Single Crystal	2.0193	2.0193	2.0024	44
TiO_2	Hydrated P25	2.028	2.016	2.004	41
TiO_2	Sol gel rutile	2.0229(I)	2.0049	2.0049	41
TiO_2	Sol gel Anatase	2.017 2.0123	2.0024	2.0024	41
TiO_2	P25	2.016	2.002	2.002	45
MgO	Axial	2.042	2.042	2.0013	45

The trapped hole species has also been identified over the surface of TiO_2. UV irradiation of TiO_2 results in the formation of photogenerated hole and electrons. These charges can migrate to the surface where they are trapped by Ti^{4+} (in the e^- case (eq 2.11) or at surface or bulk anions (in the h^+ case) (eq 2.12)

$$Ti^{4+} + e^- \rightarrow Ti^{3+} \qquad (2.11)$$

$$Ti^{4+}\text{-}O^{2-} + h^+ \rightarrow Ti^{4+}\text{-}O^- \qquad (2.12)$$

More recent studies on the surface of TiO_2 have shown that O^- can be formed on the dehydrated and fully hydrated surfaces with the O^- formed on both the rutile and anatase polymorphs.

2.3.8 The O_3^- ion

The ozonide (O_3^-) ion is the only well studied species that contains more than two oxygen nuclei. It is a 19-electron radical and is isoelectronic with the AB_2^- type radicals such as SO_2^- and NO_2^{2-} which have been observed on surfaces.[30] Due to the large separation in the energy levels of these ions (Figure 2.12), they are not perturbed by the surface crystal field and are therefore crystal field insensitive. The ***g*** tensor can therefore be used to fingerprint the species.[30]

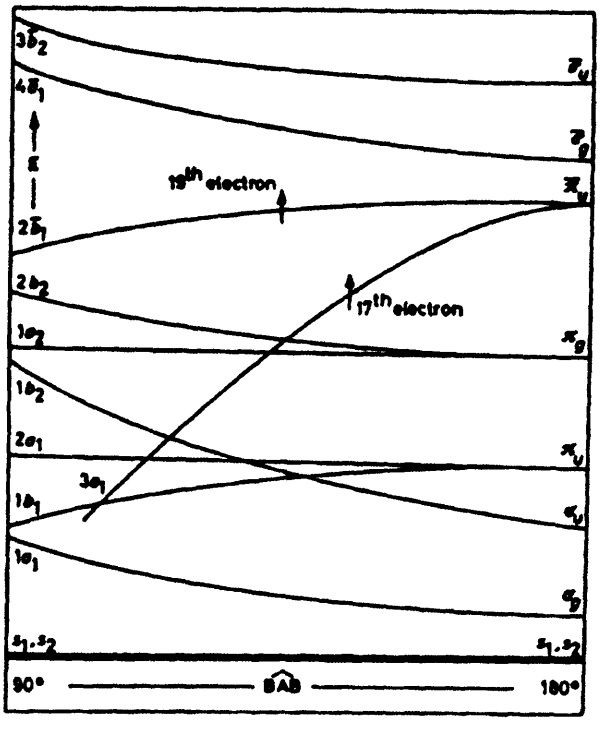

Figure 2.12 Correlation diagram for AB_2 molecules. [46]

The O_3^- ion on MgO was first reported by Tench and Lawson [42], with a ***g*** tensor in agreement with the theoretical arguments and this was later confirmed by Williamson *et al.*[47] The O_3^- was formed by reaction of a trapped hole with molecular oxygen as described by (eq 2.13):

$$O^- + O_2 \rightarrow O_3^- \qquad (2.13)$$

To obtain further information on the identity of the radical measurements were performed using the ^{17}O isotope, which provided further details from the hyperfine

pattern.[48] The ion can be labelled in two ways; in the first instance the reaction of $^{17}O^-$ with $^{16}O_2$ gives a new spectrum of six lines with a hyperfine splitting of 2.6 mT centred on $g_{xx} = 2.0014$. In the second instance, the $^{16}O^-$ ion reacts with ^{17}O enriched molecular oxygen ($^{17}O_2$) to give a spectrum with three sets of six lines centred on $g_{xx} = 2.0014$ with the hyperfine splitting of 2.6 mT, 8.2 mT and 6.5 mT respectively. No hyperfine interaction was detected in the other two directions and it is estimated to be less than 0.5 mT. The O_3^- ion is thermally unstable and on warming to room temperature decomposes to form O_2^-.[48] The ozonide radical prepared from $^{17}O^-$ and $^{16}O_2$ decomposes to form O_2^-, which does not contain ^{17}O. The O_3^- ions prepared from $^{16}O^-$ and $^{17}O_2$ decompose to form $^{17}O_2^-$. The two oxygen atoms are equivalent and display a hyperfine pattern of 11 lines separated by 77 mT. The evidence indicates that in the O_3^- ion, the three oxygen atoms are in different environments as shown by Figure 2.13.

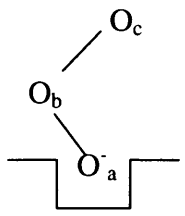

Figure 2.13 Schematic representation of the orientation of the ozonide radical on the surface of metal oxides.

2.3.9 The $HO_2^\bullet$ radical

The hydroperoxy radical is expected to be a more stable radical than the hydroxyl radical. Early EPR spectra thought to be due to $HO_2^\bullet$ radicals showed a broad asymmetric single line with no hyperfine splitting detected. The unpaired electron is expected to be in the π_x^* level, which is split from the π_y level by the proton (the x direction is taken to be perpendicular to the plane of the radical, and the z direction is taken along the O-O bond). The unpaired electron is mostly localised on the unprotonated oxygen, hence the proton hyperfine coupling should be negative and small.

The g values of the hydroperoxy radical are similar to the superoxide radicals discussed in section 2.3.1 but the values of Δg are much smaller because of the greater effect of the proton. This results in the trend of g values described by:

$$g_{zz} >> g_{yy} \sim g_{xx} \sim 2.0023 \qquad (2.14)$$

The g values from signals attributed to the hydroperoxy radical are listed in Table 2.2. The values of the hyperfine splittings are more difficult to analyse because of the possibility that the g and A axes are not coincident.

Table 2.2 g values for the $HO_2^{\bullet}$ radical

Medium	g tensor				Reference
	g_{xx}	g_{yy}	g_{zz}	g_{av}	
H_2O_2 glass	2.0023	2.0065	2.0350	2.015	46
H_2O or H_2O_2	2.0085	2.0085	2.027	2.015	46

2.3.10 Characterisation of oxygen species in heterogeneous catalysis

Maria *et al.*,[49] used EPR spectroscopy to monitor and characterise the changes in oxygen centred radicals formed by the UV irradiation of oxygen adsorbed on the TiO_2 particles of different sizes. A number of oxygen species were identified to form by the trapping of photogenerated holes and electrons. The photogenerated species were trapped at the surface by electron donors and acceptors. The spin Hamiltonian parameters of the oxygen species formed on the TiO_2 catalysts of differing particle size (P6 and P11) are shown in Table 2.3.

Table 2.3 Identification of radicals formed on various TiO_2 samples after the UV irradiation of oxygen.[2]

Sample	Species	g_1	g_2	g_3	Radical
P6	A	2.003	2.014	2.022	Ti^{4+}-O^--Ti^{4+}- OH
	B	2.003	2.008	2.034	$HO_2^{\bullet}$
	C	2.002	2.009	2.026	O_2^-
P11	D	2.003	2.016	2.029	Ti^{4+}-O^{2-}-Ti^{4+}-O^-
	E	2.002	2.008	2.011	O_3^- (O_2-O^-)

As the particle size was increased, the authors observed a decrease in the signal arising from the subsurface Ti^{4+}-O^--Ti^{4+}-OH species (Species A). This was accompanied by an increase in the surface O^- species, Ti^{4+}- O^{2-} - Ti^{4+} -O^- (Species D), as the particle size increases. These observations indicate that under irradiation of the smaller TiO_2 particles the photogenerated holes were trapped at subsurface sites (Species A), whereas on larger particles the photogenerated holes were trapped at surface sites (Species D).

Berger *et al.*,[3] studied the interaction of these photogenerated charge carries with oxygen on TiO_2 nanocrystals by EPR spectroscopy. The photogenerated electrons were found to be trapped at the surface by molecular oxygen to form O_2^- (eq 2.17).

$$TiO_2 + h\nu \rightarrow e^-_{cb} + h^+_{vb} \quad (2.15)$$

$$h^+_{vb} + O^{2-} \rightarrow O^- \quad (2.16)$$

$$Ti^{3+} + O_2 \rightarrow Ti^{4+}\ldots O_2^- \quad (2.17)$$

$$Ti^{4+} + O_2 + e^-_{cb} \rightarrow Ti^{4+}\ldots O_2^- \quad (2.18)$$

$$O_3^- \rightarrow O_2 + O^- \quad (2.19)$$

The photogenerated holes were trapped at the surface by the O^{2-} to form O^- (eq 2.16). At 90K, the O^- species could react with molecular oxygen to produce the ozonide species O_3^- (eq 2.13). The ozonide species was found to be thermally unstable and decomposed at T = 120K into the O^- species and molecular oxygen (2.19). Berger *et al.*,[3] summarised the charge trapping by oxygen in the schematic shown in Figure 2.14:

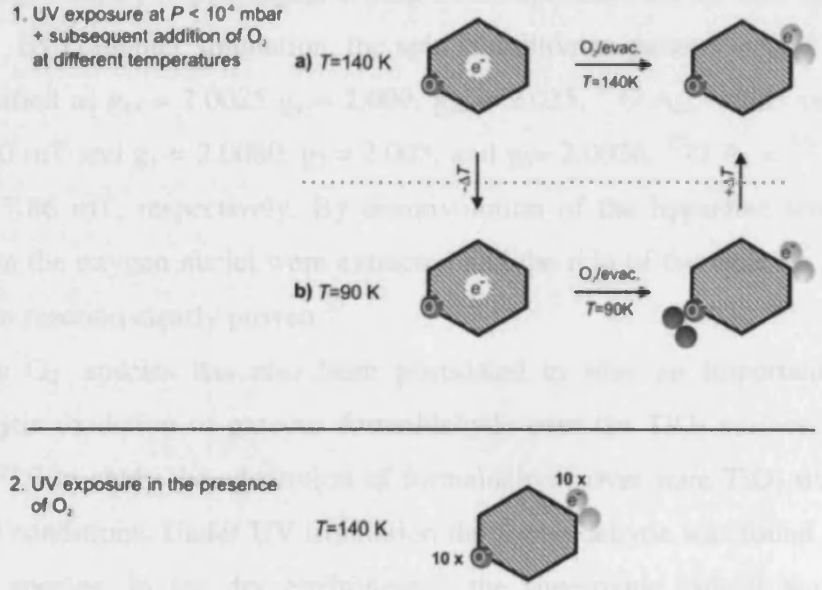

Figure 2.14 Schematic representation of the interaction between trapped charges on TiO_2 nanocrystals with molecular O_2

In step 1, at T = 140K, a photogenerated electron/hole pair (e^-/h^+) is created; the hole is trapped at the surface O^{2-} to form the surface O^- species, the trapped electrons are readily transferred to gas phase oxygen to produce adsorbed O_2^- ions (1a). If the experiment was performed at 90K (1b) an ozonide type adduct is formed between the surface O^- species and O_2 which is unstable at 140K; this is accompanied by the O_2^-

species. In the presence of oxygen the concentration of trapped electron and hole centres were found to be enhanced by a factor of ten as the oxygen (an efficient electron scavenger) traps the e^- to form the O_2^- species (step 2). The trapping of the electrons prevents recombination of the photogenerated charges. The work by Berger *et al.*,[3] demonstrates the radical species that can be formed in the presence of oxygen, after trapping of photogenerated e^- and h^+. The O_3^- and O^- species have been detected at low temperatures but they are unobserved in the EPR spectrum after annealing to higher temperatures ($T > 120K$ for O_3^- and $T > 200K$ for O^-) due to their thermal instability.

Although the O_3^- ozonide surface oxygen radical is thermally unstable it has been shown to participate in photooxidation reactions. A recent study by Murata *et al.*,[50] provided evidence that the O_3^- species can be formed on highly dispersed TiO_2. The O_3^- species was found to be the active oxidation species for the epoxidation of propene. The work was extended to a number of other light alkenes, such as ethene and butene, whereby the authors confirmed *via* EPR the electronic structure of the O_3^- and the reaction mechanism of the insertion of molecular oxygen into the C=C bond of the olefin. Using $^{17}O_2$, a complex signal arising from superimposed O_2^- and O_3^- species was identified. By computer simulation, the spin Hamiltonian parameters for both radicals were identified as $g_{xx} = 2.0025$ $g_{yy} = 2.009$, $g_{zz} = 2.025$, ^{17}O $A_{xx} = 7.51$ mT, ^{17}O $A_{yy} = {}^{17}O$ $A_{zz} = 0$ mT and $g_1 = 2.0080$, $g_2 = 2.003$, and $g_3 = 2.0026$, ^{17}O $A_1 = {}^{17}O$ $A_2 \sim 0$ mT, ^{17}O $A_3 = 7.86$ mT, respectively. By deconvolution of the hyperfine tensor, the spin densities on the oxygen nuclei were extracted and the role of the ozonide radical in the epoxidation reaction clearly proven.[50]

The O_2^- species has also been postulated to play an important role in the photocatalytic oxidation of gaseous formaldehyde over the TiO_2 surface. Sun *et al.*,[51] used DRIFTS to study the adsorption of formaldehyde over pure TiO_2 under both dry and humid conditions. Under UV irradiation the formaldehyde was found to convert to a formate species. In the dry environment, the superoxide radical was formed by reaction of adsorbed oxygen with photogenerated electrons which was then available for further reaction as shown in Figure 2.15a. Alternatively under hydrated conditions the hydroxyl radical was believed to act as the oxidant (Figure 2.15b). Clearly surface conditions can be an important factor, in determining the type of oxygen species formed.

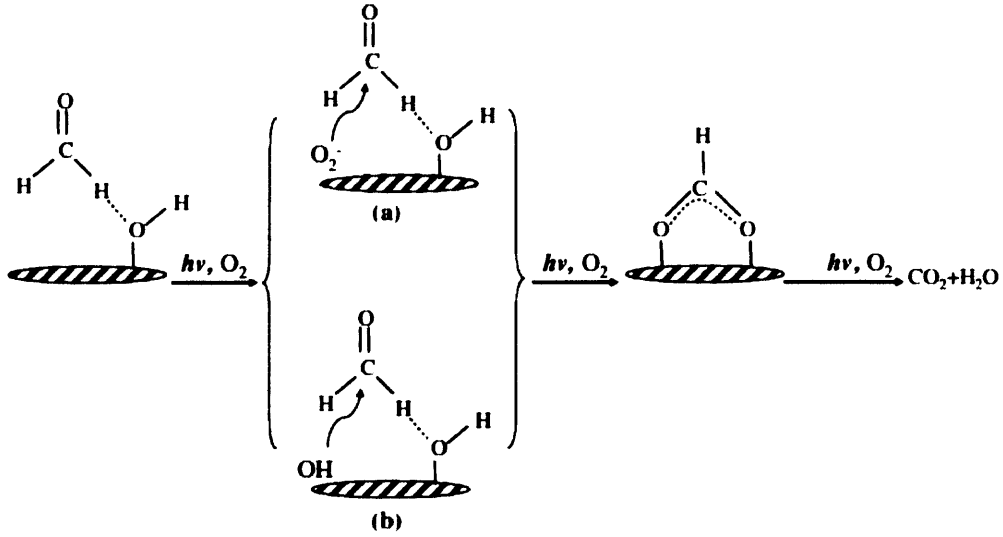

Figure 2.15 Proposed reaction scheme for the photocatalytic oxidation of formaldehyde over the TiO_2 surface. (a) Superoxide radical anion O_2^- as the oxidant (b) hydroxyl radical $^{\bullet}OH$ as an oxidant. [51]

One of the most relevant studies on the oxidation of organic compounds was a study by Tatsuma *et al.*,[52] who investigated the remote oxidation of an organic substrate *via* the gas phase. The authors UV irradiated a TiO_2 coated glass plate which was separated from an organic film separated by a small gap (50μm to 2.2mm). Aliphatic and aromatic substances were shown to be oxygenated and decomposed to generate CO_2 by the active oxygen species that were generated at the TiO_2 surface and transported into the gas phase (Figure 2.16). Tatsuma *et al.*,[52] believed the most likely candidate responsible for the oxidation of the organic substrate was $^{\bullet}OH$.

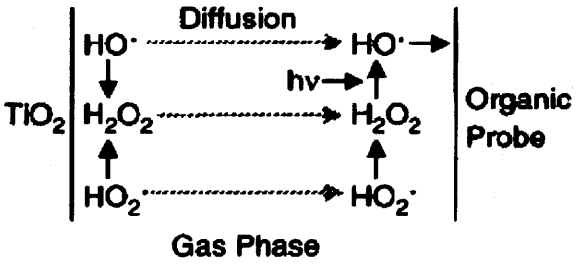

Figure 2.16 Remote oxidation of an organic probe by UV irradiation of TiO_2.[52]

A recent study by Carter *et al.*,[1] showed that a series of thermally unstable organoperoxy intermediates could be generated on the P25 TiO_2 surface. The authors found the intermediates to form both on the activated and reduced TiO_2 surface. The type of radical species formed are summarised in Figure 2.17. In pathway I, the Ti^{3+} centres were formed *via* UV irradiation or thermal annealing. Addition of oxygen to Ti^{3+} centres formed O_2^- which subsequently reacted with adsorbed acetone to form an

$[CH_3COCH_3....O_2^-]$ type adduct (Pathway III). This adduct was observed to be thermally unstable and decayed on annealing to room temperature.

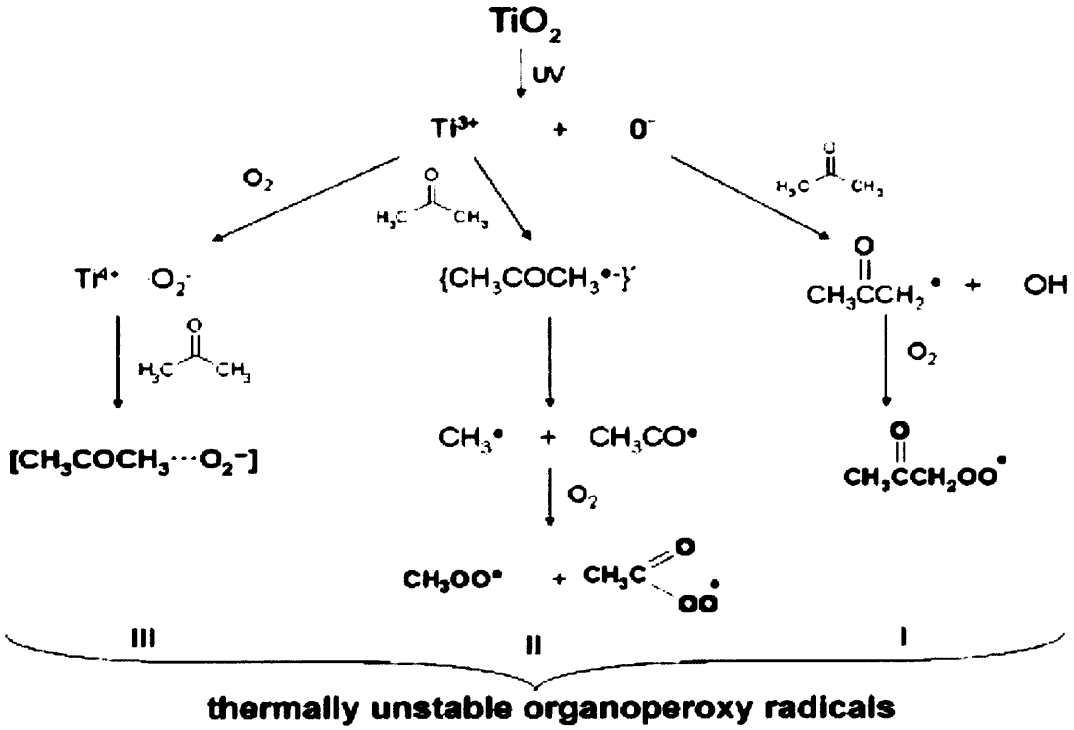

Figure 2.17 Competing reaction pathways in the decomposition of acetone.[1]

Under an acetone rich atmosphere, the Ti^{3+} centres could react directly with acetone to produce the $\{CH_3COCH_3^{\bullet-}\}^*$ species which underwent a disproportionate reaction to give ($CH_3^\bullet$) and ($CH_3CO^\bullet$) (Pathway II). These species were indirectly indentified through their reactions with molecular oxygen to form the organoperoxy radicals $CH_3OO^\bullet$ and $CH_3CO_3^\bullet$ respectively. The acetone was also found to react with the O^- species to give the $CH_3COCH_2^\bullet$ species which, in the presence of O_2, formed the $CH_3COCH_2OO^\bullet$ organoperoxy species (Pathway I).

The identification of these organoperoxy intermediates is important as very little work exists on what role the $^\bullet OH$, $^\bullet OOH$, O^-, O_2^- and $ROO^\bullet$ species have in the degradation of organic compounds. Furthermore it is necessary to perform the work at low temperature to study the thermally unstable intermediates. The decomposition of a variety of organics with different functional groups is explored in detail in Chapter 6.

2.4 Interaction of the TiO_2 surface with water

The interaction between the titanium dioxide surface and water has been widely studied in the literature.[6,53-56] The potential for water to play an important role in photocatalysis must be considered as it will almost always be present (in vapour or liquid form) under real operating conditions. The research of the role of water on the TiO_2 surface is focussed on two main questions; firstly, how is the water adsorbed at the titanium dioxide surface and secondly is it adsorbed molecularly as chemisorbed and physisorbed water or dissociatively as hydroxyl groups? Secondly, what role does the water play in photochemical reactions? Does it act as an inhibitor or promoter in the reactions occurring at the TiO_2 surface? The surface hydroxyl groups formed are believed to play a key role in the photooxidation process where they can either participate directly in the reaction mechanism by trapping of photogenerated holes that reach the catalyst surface producing very reactive $^{\bullet}OH$ radicals. The surface hydroxyl groups may also change the surface properties and have been shown to assist the adsorption of reactant molecules at the surface and can act as active sites for pollutant adsorption. The hydroxyl groups have also been shown to cover the sites (exposed titanium cations with unsaturated co-ordination) where electron trapping by adsorbed oxygen takes place[2,57,58]. The following section will deal with two questions separately.

2.4.1 Dissociative or molecular adsorption

The question of whether water adsorbs at the TiO_2 surface dissociatively or in a molecular form has been studied extensively over the last decade with much of the work carried out on single crystals TiO_2 samples under UHV conditions. Henderson *et al.*,[54] used High-Resolution Electron Energy Loss Spectroscopy (HREELS) and Temperature-Programmed Desorption (TPD) to study this. The authors concluded that the adsorption of water on the rutile (110) TiO_2 surface is molecular on the stoichiometric surface but dissociative on the reduced surface. In the HREELS data, a small peak at 3690 cm^{-1} was observed which implied a small amount of dissociation on the surface at an adsorption temperature of 135 K. The 3690 cm^{-1} feature was assigned to terminal –OH groups (situated at 5-fold co-ordinate Ti^{4+} sites) that are not hydrogen bonded.

There is not much doubt that H_2O dissociates at reduced Ti^{3+} centres. However debate still exists as to whether the same process occurs at the non reduced (stoichiometric surface). Some groups have found that mixed molecular-dissociative adsorption can occur. For example, dissociative adsorption occurs at low coverages of

water but on increasing the surface coverage a mixed layer of molecular and dissociated water is present.[59] A schematic diagram showing the arrangement of these mixed monolayers is shown in Figure 2.18. The cases for purely dissociative and molecular adsorption are shown in Figure 2.18a, and 2.18b respectively. In the situation where a mixed monolayer is formed, hydrogen bonding occurs between a water molecule adsorbed at a 5-fold co-ordinate Ti^{4+} site and -OH groups adsorbed at an adjacent 5-fold co-ordinate Ti^{4+} site. There is also a weak interaction of the water molecules with the bridging oxygen.

The hydroxyl groups can occur at bridging and terminal positions. In some studies using HREELS, fine structure is observed; this is due to the existence of different crystal faces, with slightly different geometries for adsorption.

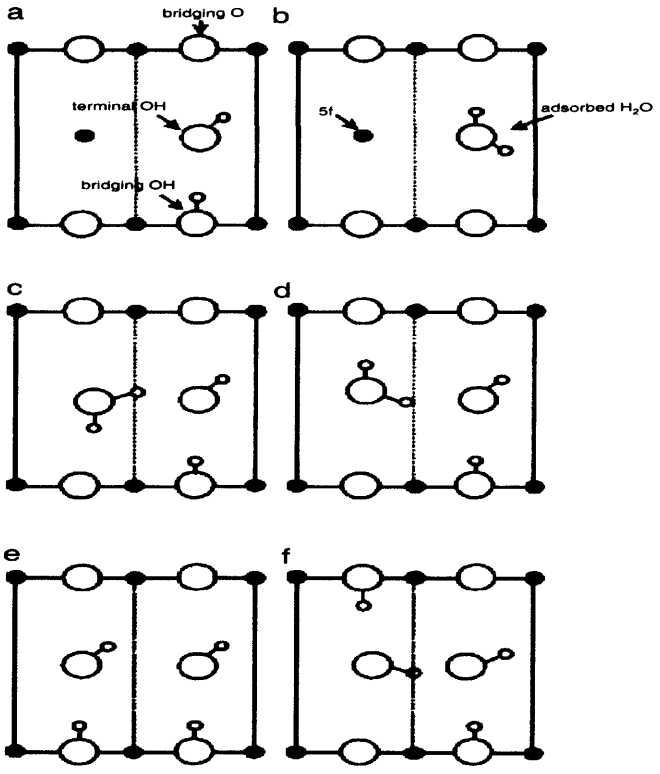

Figure 2.18 Schematic diagram of a mixed molecular water- dissociated water on the rutile (110) surface.[59]

Henderson *et al.*,[60] have shown that differences exist between the (110) and (100) rutile surfaces. The latter was found to support dissociative adsorption of water while the former was found to support molecular adsorption. This is an important finding, especially when applied to powder systems as used in many applications. The powder systems contain a variety of crystal faces where distinct situations for water dissociation may be found. Although no detailed studies have been performed on the

adsorption of water at different crystal faces contained within the powder samples, Marta *et al.*,[61] have shown that a variety of hydroxyl groups can be present. The authors performed an infrared study of the polycrystalline P25 TiO_2 surface. After outgassing at room temperature, the powder surface was covered in an almost complete monolayer of hydroxyls and water molecules co-ordinated to surface cations persisted. The infrared spectra of the P25 was characterised by a number of narrow components in the 3800 - 3600 cm^{-1} indicating the heterogeneity of surface adsorbed hydroxyl groups.

It is important to mention the advances in the use of STM to study the interactions of water with oxygen vacancies and hydroxyl groups. This technique provides a way to track individual hydroxyl groups on the surface and their interaction with water. The early work using STM has been discussed by Diebold in a thorough review.[6] Initially the study of hydroxyl groups at the surface of TiO_2 was problematic due to the difficulty in distinguishing between oxygen vacancies and hydroxyl groups formed as a result of a water molecule reacting with an oxygen vacancy. Diebold *et al.*,[6] showed that two types of defects were present on the rutile (110) surface which were termed 'A' and 'B'. The rows of 5- co-ordinate Ti atoms appeared bright in the STM image due to their high electron density, while the bridging oxygens where found to be darker.The Type 'A' defects were identified to be quite mobile and significantly brighter than the 'B' type and were proposed to be oxygen vacancies.

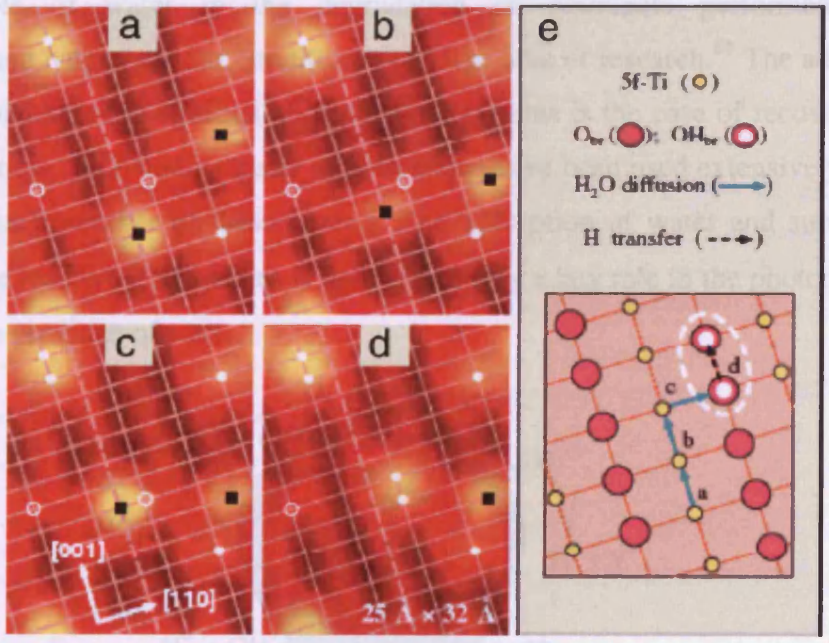

Figure 2.19 STM images of rutile (110) showing the dissociation of a water molecule at an oxygen vacancy.[62]

Work by Wendt *et al.*,[62] showed that a water molecule could migrate along a row of 5-fold coordinated Ti sites and subsequently react with a vacancy site to produce a pair of hydroxyl groups on neighbouring bridging oxygens. A second water molecule could then further catalyze the splitting of the hydroxyl pair in an energetic reaction that resulted in the protons 'jumping' several rows away.[62] This initial process is shown in Figure 2.19.

Zhang *et al.*,[56,63] highlighted the importance of the presence of hydroxyl groups on the surface in a number of studies. The authors used STM, TPD and Electron-Stimulated Desorption (ESD) to show that oxygen adatoms (O_a), hydroperoxyls and terminal hydroxyls are all observed as reaction intermediates on both the partially and fully hydroxylated rutile (110) TiO_2 surface. On the partially hydroxylated surface they found water to be involved in the reaction cycle that leading to the consumption of O_a and vacancy (V_0) sites. From these studies, water has been observed to participate in many ways, e.g., as a reactant, product and catalyst. On the fully hydroxylated TiO_2 surface, water is found to mediate the diffusion of surface species such as OH that would otherwise be stationary and thus brings reactants together catalyzing the reactions with O_2.

2.4.2 *Photocatalysis in the presence of pollutants*

The role of water in the degradation of pollutants performed under homogeneous and heterogeneous conditions is a large area of research.[64] The advantage of solid semiconductors in aqueous photocatalytic systems is the ease of recovery, low cost and robustness. TiO_2 and its many modifications have been used extensively due to its suitability for a number of these criteria. The adsorption of water and subsequent formation of the reactive $^{\bullet}OH$ species is believed to play a key role in the photocatalytic processes in the presence of water.

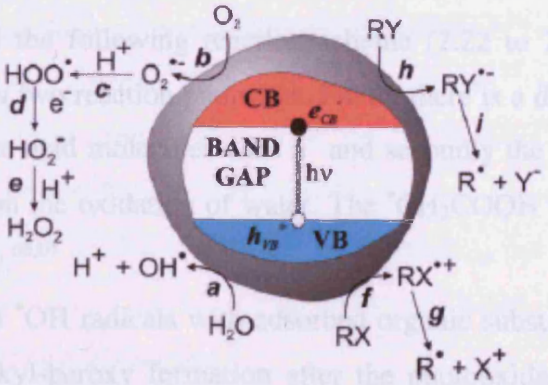

Figure 2.20 Photocatalytic processes for the elimination of pollutants.[65]

The main processes involved during photocatalysis in the presence of water and oxygen, are summarised in Figure 2.20. The photogenerated holes are scavenged by surface adsorbed water to give hydroxyl radicals (eq 2.20, Figure 2.20, pathway a):

$$h^+ + H_2O \rightarrow H^+ + {}^\bullet OH \qquad (2.20)$$

$$O_2^- + H^+ \rightarrow HO_2^\bullet \qquad (2.21)$$

The $^\bullet OH$ radical has been reported to be the most active species in the photodegradation process. The photogenerated electrons give superoxide after reaction with oxygen (eq 2.17, pathway b). Protonation of the superoxide yields the hydroperoxy radical (eq 2.21, c) that is further reduced to the hydroperoxy anion (d) and hydrogen peroxide (e) (see Figure 2.20). The pollutants which are strongly adsorbed on the catalyst surface may undergo direct ET, either oxidation to give a radical cation (f) or reduction to a radical anion (h) according to their redox potential further fragmentation processes of these species may ensue (g, i).

The formation of $^\bullet OH$ radicals was believed to play an important part in the photocatalytic decomposition of acetic acid over platinised TiO_2 powder under deoxygenated conditions.[66,67] The photocatalytic reaction was monitored by *in-situ* EPR, whereby a number of species were identified; namely a quartet with the hyperfine splitting of 0.349 mT arising from the $^\bullet CH_3$ radical, and a triplet arising from $^\bullet CH_2COOH$ radicals[66,67].

$$CH_3COOH + h^+ \rightarrow {}^\bullet CH_3 + CO_2 + H^+ \qquad (2.22)$$

$$CH_3COOH + {}^\bullet OH \rightarrow {}^\bullet CH_3 + CO_2 + H_2O \qquad (2.23)$$

$$CH_3COOH + {}^\bullet OH \rightarrow {}^\bullet CH_2COOH + H_2O \qquad (2.24)$$

The authors proposed the following reaction scheme (2.22 to 2.24) where the $^\bullet CH_3$ radicals are formed *via* two reaction pathways. Firstly there is a direct reaction between surface adsorbed acetic acid molecules with h^+ and secondly the indirect oxidation *via* $^\bullet OH$ radicals formed on the oxidation of water. The $^\bullet CH_2COOH$ is formed *via* reaction with $^\bullet OH$ radicals only.[66,67]

The reaction of $^\bullet OH$ radicals with adsorbed organic substrates was proposed as the mechanism for alkyl-peroxy formation after the photooxidation of ethylene over TiO_2.[68] The alkyl-peroxy intermediate was found to have the spin Hamiltonian

parameters of $g_1 = 2.035$, $g_2 = 2.008$, and $g_3 = 2.001$, it was also observed to be unstable on annealing to 260K. The identity of the radical was confirmed by monitoring the changes in the EPR spectrum when the isotopically labelled C_2D_4 and $^{13}C_2H_4$ analogues were used. Further proof on the identity of the radicals was provided by carrying out the photooxidation using ^{17}O enriched O_2. Two sets of six hyperfine lines were resolved, centred on g_3, with the splittings of A_3 (I) = 9.5 mT and A_3 (II) 3.5 mT; no splitting could be resolved in either of the other two directions. The signal was assigned to a peroxy radical ($ROO^{\bullet}$), with the largest hyperfine interaction due to the terminal oxygen.[68]

The proposed mechanism for the formation alkyl-peroxy intermediate is shown below. The $^{\bullet}OH$ radicals are generated as discussed in (eq 2.20) above by trapping of a photogenerated hole (h^+) at a surface OH group. The reactive $^{\bullet}OH$ radical reacts with the ethylene to form an alkyl radical (eq 2.25) which in turn reacts with oxygen to form the observed alkyl peroxy radical (eq 2.26).

$$^{\bullet}OH + C_2H_4 \rightarrow HOCH_2CH_2^{\bullet} \qquad (2.25)$$

$$HOCH_2CH_2^{\bullet} + O_2 \rightarrow HOCH_2CH_2OO^{\bullet} \qquad (2.26)$$

The review of the literature thus far clearly provides examples of the positive use of the reactive $^{\bullet}OH$ radical in photocatalysis. However, there also exists many examples whereby the formation of hydroxyl groups and the presence of physisorbed water have been shown to have an inhibitive effect on the photocatalytic activity of TiO_2 as described further below.

In a study of the photooxidation of C_2H_4, Park *et al.*,[4] found that the addition of water vapour (< 5 Torr) onto the TiO_2 catalyst led to an enhancement of the photoinduced uptake of oxygen, and subsequently an increase in the reactivity. However, when the amount of water vapour exceeded 5 Torr the reactivity and photoinduced uptake of oxygen decreased. The authors[4] believed that at low concentrations of adsorbed water, the water could react with adsorbed O_2 to form reactive $^{\bullet}OH$ radicals on irradiation, which are themselves precursors of radicals that participate in the complete oxidation of C_2H_4. On increasing the water vapour content, the number of adsorption sites available for O_2 uptake decreased, thereby decreasing the number of reactive $^{\bullet}OH$ radicals formed.[4]

Henderson *et al.*,[69] used TPD to study the effect of water on the photodecomposition of acetone on a TiO_2 (110) rutile surface. The study demonstrated that water has an inhibiting influence on the photodecomposition under UHV conditions. They found that at low water and acetone coverage, the inhibiting influence was low as sufficient sites were available to accommodate both reaction intermediates and products and allow O_2 access to the surface. However, as the first layer saturation was reached, they observed a decrease in reaction rate which continued until a 3 ML coverage when virtually no photodecomposition was observed. The authors attributed this to the fact that the water can displace acetone from the first layer and that the blocking of O_2 access to the surface occurs.

At these higher water coverages the surface is becoming more akin to an aqueous system. The aqueous systems have attracted much attention as this is relevant for improving the removal of pollutants in industrial wastewaters. The reactive nature of $^{\bullet}OH$ radicals and many other short lived radicals at the gas-solid or liquid-solid interfaces sometimes makes detection difficult. However these radicals can be transformed into more stable, and thus longer-lived, paramagnetic species by spin trapping experiments.

Recently the photocatalytic mineralization of phenol over both pure and mixed phase hydrothermal TiO_2 was studied.[70] The authors studied the photoactivity of anatase, rutile and mixed phase TiO_2 in an aqueous solution employing different oxidative agents, including H_2O_2 and O_2. They found that when employing H_2O_2, the rutile particles with the larger dimensions and high aspect ratio (size 30-70nm) x (150-350nm) displayed the highest catalytic activity due to their low tendency to recombine electrons and holes generated by UV irradiation. When O_2 was used as the oxidising agent the authors found that oxygen preferentially chemisorbed at the surface of nanosized particles of anatase and acted as an effective electron scavenger inhibiting the electron-hole recombination. By studying the different powders with EPR and identifying a number of paramagnetic species,(O^- and Ti^{3+}) and by studying the rate of formation of $OH^{\bullet}$ radicals, the authors made a correlation between charge carrier centres, the rate of formation of $OH^{\bullet}$ radicals and catalyst photoactivity.

Micic *et al.*,[71] studied the photoinduced hole transfer from TiO_2 to methanol molecules in the aqueous phase using EPR. The type of radicals formed under different conditions was studied. Initially the formation of radicals after irradiation of the aqueous alkoxide TiO_2 colloids in the presence of methanol was studied (after laser

irradiation at different pulse intensities and temperatures). At the highest laser intensities (20mJ/pulse), three EPR signals were observed at 6K which were centred at around g = 2. The radical signals were composed of a quartet with a ratio of 1:3:3:1 (accompanied by an underlying signal) and a doublet, which were assigned to the methyl ($CH_3^{\bullet}$) and formyl ($CHO^{\bullet}$) radicals respectively. The methyl radical was found to be thermally unstable and when the temperature was raised to 60K, the signal due to the methyl radicals disappeared. In contrast, the signal due to the formyl radical and the underlying signal (which was assigned to the methanol radical (CH_2O (H)) remained. The formyl radical was believed to be formed by a two photon process. It was not observed when laser intensities below 5mJ/pulse were used. At lower intensities only the methanol was observed around g = 2. The following reactions are believed to be the possible pathways for radical formation:

$$Ti^{4+}\text{-}O\text{-}Ti^{4+}\text{-}OCH_3 + e^- \rightarrow Ti^{4+}\text{-}O\text{-}Ti^{4+}\text{-}O^- + {}^{\bullet}CH_3 \quad (2.27)$$

$$Ti^{4+}\text{-}O\text{-}Ti^{4+}\text{-}OCH_3 + h^+ \rightarrow Ti^{4+}\text{-}O\text{-}Ti^{4+}\text{-}O{}^{\bullet}CH_2 + H^+ \quad (2.28)$$

$$Ti^{4+}\text{-}O\text{-}Ti^{4+}\text{-}OCH_2 + H_2O \rightarrow CHO + H_2 + Ti^{4+}\text{-}O\text{-}Ti^{4+}\text{-}OH \quad (2.29)$$

A second set of hydrated colloids were prepared, with the surface completely saturated in bound hydroxide ions and water molecules.[71] The hydroxide ions on the surface act as hole traps for the photogenerated holes, resulting in an EPR signal with resonances at g = 2.014 and 2.007 with the signal assigned to an O^- species. After irradiation at 2K in the presence of methanol, an EPR signal assigned to the methanol radical and Ti^{3+} centres was observed. Stepwise charge transfer is unlikely at these temperatures therefore the charge transfer must occur *via* the following reaction;

$$h^+ + CH_3OH \rightarrow {}^{\bullet}CH_2OH + TiO_2 + H^+ \quad (2.30)$$

At 1.9K, diffusion of the adsorbed methanol is not possible and the distance of charge transfer cannot exceed 10Å. Therefore, the methanol molecules must be located within a few monolayers of the surface of the TiO_2 particles.

The result displayed by Micic *et al.*,[71] clearly show that different radical products are observed when the methanol is added to aqueous TiO_2 solutions compared to when methanol is chemisorbed. In aqueous systems they found that only $^{\bullet}CH_2OH$

and Ti^{3+} was present while when methanol was chemisorbed on TiO_2 the $^{\bullet}CH_3$, $^{\bullet}CH_2OH$, $^{\bullet}CHO$ and Ti^{3+} species were formed.

The presence of water on the surface of TiO_2 is an important factor in photocatalysis. Some debate still exists as to what form the water is adsorbed on the surface, either as physisorbed water or surface hydroxyl groups. Once at the surface the hydroxyl groups have been shown to play an important role in the formation of radical species on the TiO_2 surface. In Chapter 7 the presence of water and its effect on the formation of O_2^-, O^- and the $ROO^{\bullet}$ species will be explored further.

2.5 Summary

The use of TiO_2 for heterogeneous photocatalysis is driven by the diverse chemistry that can occur at it's surface. Consequently the surface chemistry of TiO_2 has been well researched in the literature, particularly for single crystal systems. The surface consists of Ti^{4+} - O^{2-} pairs, which after photogeneration of charge carriers (e^-/h^+) can be reduced to Ti^{3+} centres by trapping of the electron at Ti^{4+} centres with the O^{2-} site trapping h^+ to give O^-. These Ti^{3+} centres have been shown to be conduits for electron transfer and therefore responsible for driving the catalytic reactions. The adsorption of probe gases at these sites has been used to gain information on their identity and the chemistry they can participate in. However, little information is available about there behaviour under co-adsorption conditions.

Surface oxygen species can be formed on TiO_2 and have been shown to play an important role in catalytic reactions. Many of these oxygen species can be studied by EPR spectroscopy. The O_2, O^- and O_3^- species have been studied extensively in the literature and there is plenty of information about their structure and stability. However, little work exists on their role in the photodegradation of organic compounds with studies suggesting that a family of thermally unstable organoperoxy intermediates may play an important role.

The presence of water is unavoidable under standard photocatalytic conditions. While much debate still exists about how water adsorbs on the surface and what role the surface hydroxyls have in photocatalytic reactions, it is clear it plays a major role and understanding this will aid the development of TiO_2 photocatalysis.

2.7 References

(1) Carter, E.; Carley, A. F.; Murphy, D. M. *Chemphyschem* **2007**, *8*, 113.

(2) Maira, A. J.; Yeung, K. L.; Lee, C. Y.; Yue, P. L.; Chan, C. K. *Journal of Catalysis* **2000**, *192*, 185.

(3) Berger, T.; Sterrer, M.; Diwald, O.; Knozinger, E. *Chemphyschem* **2005**, *6*, 2104.

(4) Park, D. R.; Zhang, J. L.; Ikeue, K.; Yamashita, H.; Anpo, M. *Journal of Catalysis* **1999**, *185*, 114.

(5) Carter, E.; Carley, A. F.; Murphy, D. M. *Journal of Physical Chemistry C* **2007**, *111*, 10630.

(6) Diebold, U. *Surface Science Reports* **2003**, *48*, 53.

(7) Fujishima, A.; Zhang, X. T.; Tryk, D. A. *Surface Science Reports* **2008**, *63*, 515.

(8) Fujishima, A.; Zhang, X. T. *Comptes Rendus Chimie* **2006**, *9*, 750.

(9) Fujishima, A.; Zhang, X.; Tryk, D. A. *International Journal of Hydrogen Energy* **2007**, *32*, 2664.

(10) Barteau, M. A. *Journal of Vacuum Science & Technology A* **1993**, *11*, 2162.

(11) Ramamoorthy, M.; Vanderbilt, D.; Kingsmith, R. D. *Physical Review B* **1994**, *49*, 16721.

(12) Henderson, M. A.; Epling, W. S.; Perkins, C. L.; Peden, C. H. F.; Diebold, U. *Journal of Physical Chemistry B* **1999**, *103*, 5328.

(13) Lazzeri, M.; Vittadini, A.; Selloni, A. *Physical Review B* **2001**, *63*.

(14) Hebenstreit, W.; Ruzycki, N.; Herman, G. S.; Gao, Y.; Diebold, U. *Physical Review B* **2000**, *62*, R16334.

(15) Yang, H. G.; Sun, C. H.; Qiao, S. Z.; Zou, J.; Liu, G.; Smith, S. C.; Cheng, H. M.; Lu, G. Q. *Nature* **2008**, *453*, 638.

(16) Yang, H. G.; Liu, G.; Qiao, S. Z.; Sun, C. H.; Jin, Y. G.; Smith, S. C.; Zou, J.; Cheng, H. M.; Lu, G. Q. *Journal of the American Chemical Society* **2009**, *131*, 4078.

(17) Han, X. G.; Kuang, Q.; Jin, M. S.; Xie, Z. X.; Zheng, L. S. *Journal of the American Chemical Society* **2009**, *131*, 3152.

(18) Bickley, R. I.; Gonzalezcarreno, T.; Lees, J. S.; Palmisano, L.; Tilley, R. J. D. *Journal of Solid State Chemistry* **1991**, *92*, 178.

(19) Komaguchi, K.; Nakano, H.; Araki, A.; Harima, Y. *Chemical Physics Letters* **2006**, *428*, 338.

(20) Hurum, D.; Agrios, A. G.; Gray, K. A.; Rajh, T.; Thurnauer, M. C. *Abstracts of Papers of the American Chemical Society* **2001**, *222*, U427.

(21) Hurum, D. C.; Agrios, A. G.; Crist, S. E.; Gray, K. A.; Rajh, T.; Thurnauer, M. C. *Journal of Electron Spectroscopy and Related Phenomena* **2006**, *150*, 155.

(22) Hurum, D. C.; Agrios, A. G.; Gray, K. A.; Rajh, T.; Thurnauer, M. C. *Journal of Physical Chemistry B* **2003**, *107*, 4545.

(23) Thompson, T. L.; Diwald, O.; Yates, J. T. *Journal of Physical Chemistry B* **2003**, *107*, 11700.

(24) Thompson, T. L.; Yates, J. T. *Topics in Catalysis* **2005**, *35*, 197.

(25) Lu, G. Q.; Linsebigler, A.; Yates, J. T. *Journal of Physical Chemistry* **1994**, *98*, 11733.

(26) Komaguchi, K.; Maruoka, T.; Nakano, H.; Imae, I.; Ooyama, Y.; Harima, Y. *Journal of Physical Chemistry C* **2009**, *113*, 1160.

(27) Idriss, H.; Kim, K. S.; Barteau, M. A. *Surface Science* **1992**, *262*, 113.

(28) Linsebigler, A.; Lu, G. Q.; Yates, J. T. *Journal of Physical Chemistry* **1996**, *100*, 6631.

(29) Dai, W. X.; Chen, X.; Zheng, X. P.; Ding, Z. X.; Wang, X. X.; Liu, P.; Fu, X. Z. *Chemphyschem* **2009**, *10*, 411.

(30) Che, M. T., A.J. *Advances in Catalysis* **1983**, *32*, 1.

(31) Kanzig, W., Cohen,M. H. *Physical review letters* **1959**, *3*, 509.

(32) Howe, R. F.; Leith, I. R. *Journal of the Chemical Society-Faraday Transactions I* **1973**, *69*, 1967.

(33) Anpo, M.; Che, M.; Fubini, B.; Garrone, E.; Giamello, E.; Paganini, M. C. *Topics in Catalysis* **1999**, *8*, 189.

(34) Attwood, A. L.; Murphy, D. M.; Edwards, J. L.; Egerton, T. A.; Harrison, R. W. *Research on Chemical Intermediates* **2003**, *29*, 449.

(35) Giamello, E.; Ugliengo, P.; Garrone, E. *Journal of the Chemical Society-Faraday Transactions I* **1989**, *85*, 1373.

(36) Chiesa, M.; Giamello, E.; Paganini, M. C.; Sojka, Z.; Murphy, D. M. *Journal of Chemical Physics* **2002**, *116*, 4266.

(37) Che, M.; Tench, A. J. *Advances in Catalysis* **1982**, *31*, 77.

(38) Farle, M., Zomack, M., Baberschke, K. *Surface Science* **1985**, *160*, 205.

(39) Tinkham, M.; Strandberg, M. W. P. *Physical Review* **1955**, *97*, 951.

(40) Nosaka, Y.; Daimon, T.; Nosaka, A. Y.; Murakami, Y. *Physical Chemistry Chemical Physics* **2004**, *6*, 2917.

(41) Scotti, R.; Bellobono, I. R.; Canevali, C.; Cannas, C.; Catti, M.; D'Arienzo, M.; Musinu, A.; Polizzi, S.; Sommariva, M.; Testino, A.; Morazzoni, F. *Chemistry of Materials* **2008**, *20*, 4051.

(42) Tench, A. J.; Lawson, T. *Chemical Physics Letters* **1970**, *7*, 459.

(43) Wertz, J. E.; Auzins, P.; Griffiths, J. H. E.; Orton, J. W. *Discussions of the Faraday Society* **1959**, 136.

(44) Galland, D.; Herve, A. *Physics Letters A* **1970**, *A 33*, 1.

(45) Tench, A. J.; Lawson, T.; Kibblewhite, J. *Journal of the Chemical Society-Faraday Transactions I* **1972**, *68*, 1169.

(46) Atkins, P. W., Symons, M. C. R. *Structure of Inorganic Radicals : An Application of Electron Spin Resonance to the study of Molecular Structure*; Elsevier: London, 1967.

(47) Williamson, W. B.; Lunsford, J. H.; Naccache, Z. *Chemical Physics Letters* **1971**, *9*, 33.

(48) Wong, N. B.; Lunsford, J. H. *Journal of Chemical Physics* **1972**, *56*, 2664.

(49) Maira, A. J.; Yeung, K. L.; Soria, J.; Coronado, J. M.; Belver, C.; Lee, C. Y. *Applied Catalysis B-Environmental* **2001**, *29*, 327.

(50) Murata, C.; Hattori, T.; Yoshida, H. *Journal of Catalysis* **2005**, *231*, 292.

(51) Sun, S.; Ding, J. J.; Bao, J.; Gao, C.; Qi, Z. M.; Li, C. X. *Catalysis Letters* **2010**, *137*, 239.

(52) Tatsuma, T.; Tachibana, S.; Fujishima, A. *Journal of Physical Chemistry B* **2001**, *105*, 6987.

(53) Henderson, M. A. *Abstracts of Papers of the American Chemical Society* **1994**, *207*, 131.

(54) Henderson, M. A. *Surface Science* **1996**, *355*, 151.

(55) Henderson, M. A. *Surface Science Reports* **2002**, *46*, 5.

(56) Zhang, Z.; Du, Y.; Petrik, N. G.; Kimmel, G. A.; Lyubinetsky, I.; Dohnalek, Z. *Journal of Physical Chemistry C* **2009**, *113*, 1908.

(57) Panayotov, D.; Yates, J. T. *Journal of Physical Chemistry B* **2004**, *108*, 2998.

(58) Thompson, T. L.; Panayotov, D. A.; Yates, J. T. *Journal of Physical Chemistry B* **2004**, *108*, 16825.

(59) Zhang, C. J.; Lindan, P. J. D. *Journal of Chemical Physics* **2003**, *118*, 4620.

(60) Henderson, M. A. *Langmuir* **1996**, *12*, 5093.

(61) Davit, P.; Martra, G.; Coluccia, S. *Journal of the Japan Petroleum Institute* **2004**, *47*, 359.

(62) Wendt, S.; Matthiesen, J.; Schaub, R.; Vestergaard, E. K.; Laegsgaard, E.; Besenbacher, F.; Hammer, B. *Physical Review Letters* **2006**, *96*.

(63) Du, Y. G.; Deskins, N. A.; Zhang, Z. R.; Dohnalek, Z.; Dupuis, M.; Lyubinetsky, I. *Journal of Physical Chemistry C* **2009**, *113*, 666.

(64) Abdullah, U. I. G. A. H. *Journal of photochemistry and Photobiology C - Photochemistry Reviews* **2008**, *9*, 12.

(65) Ravelli, D.; Dondi, D.; Fagnoni, M.; Albini, A. *Chemical Society Reviews* **2009**, *38*, 1999.

(66) Nosaka, Y.; Kishimoto, M.; Nishino, J. *Journal of Physical Chemistry B* **1998**, *102*, 10279.

(67) Nosaka, Y.; Koenuma, K.; Ushida, K.; Kira, A. *Langmuir* **1996**, *12*, 736.

(68) Gonzalezelipe, A. R.; Che, M. *Journal De Chimie Physique Et De Physico-Chimie Biologique* **1982**, *79*, 355.

(69) Henderson, M. A. *Journal of Catalysis* **2008**, *256*, 287.

(70) Scotti, R.; D'Arienzo, M.; Testino, A.; Morazzoni, F. *Applied Catalysis B-Environmental* **2009**, *88*, 497.

(71) Micic, O. I.; Zhang, Y. N.; Cromack, K. R.; Trifunac, A. D.; Thurnauer, M. C. *Journal of Physical Chemistry* **1993**, *97*, 13284.

Chapter 3

An introduction to the theory of EPR applied to polycrystalline metal oxides

3.1 Introduction

Electron paramagnetic resonance (EPR) spectroscopy allows the study of paramagnetism in solids, liquids and gases. It is this versatility that has led to it being used in a variety of disciplines such as chemistry, biology, medical science, physics and geology.[1,2] EPR is a highly sensitive method and can detect concentrations down to 10^{-7}M compared to NMR which can only detect concentrations down to 10^{-3}M. This ability to study low concentrations of paramagnetic entities makes EPR an excellent technique in the study of polycrystalline metal oxides, as the number of paramagnetic centres on metal oxide surfaces is often low. Although EPR can only detect paramagnetic species, it can be used to study diamagnetic oxide materials by using suitable paramagnetic probes, including nitroxides and transition metal ions. The paramagnetic centres studied can range from surface defects, inorganic or organic radicals to metal cations or supported metal complexes and centres.[3-6] The paramagnetic centres will produce characteristic EPR profiles with well defined spin Hamiltonian parameters. The paramagnetic centres themselves can be affected by a number of different variables, such as pretreament condition or nature of the support and local environment; these differences can be evidenced by changes in the EPR spectra. The literature has focussed on the study of surface paramagnetic centres in heterogeneous catalysis and material science where EPR is recognised as a powerful tool for the catalytic chemist. A number of review articles and monographs have appeared over the years specifically on EPR in catalysis, notably by Lunsford[7], Howe[8], Che[9], Giamello[10], Sojka[11] and Dyrek[12].

3.2 Historical perspective

The EPR technique at its simplest level is an extension of the famed Stern Gerlach experiment which showed that a beam of silver atoms directed through an inhomogeneous magnetic field is split into two, thus proving that an electron magnetic moment in an atom can only take discrete orientations in a magnetic field.[13] This concept was linked to the electron spin angular momentum by Uhlenbeck and Goudsmit,[14] who suggested that the electron has an intrinsic angular momentum called its 'spin', which was therefore confirmed by the Stern-Gerlach experiment.

The earliest recorded EPR spectrum was by Zavoisky,[15] who detected a radio frequency absorption line from a $CuCl_2.H_2O$ sample at a magnetic field of 4.76 mT and a frequency of 133 MHz. The results were interpreted by Frenkel as resulting from paramagnetic resonance.[13,16]

The rapid growth in the use of EPR from 1946 onwards was fuelled by the availability of low cost microwave components following the end of World War II, which had been used for radar equipment that operated in the 9 GHz region. Much of the early work was performed in the USA by Cummerow and Haliday[17] and in England by Bagguley and Griffiths.[18]

It is important to note that EPR has advanced from its early origins of continuous wave (*cw*)-EPR at X-band (~ 9.5 GHz). Within the last two decades a multitude of commercially available spectrometers have been developed that offer multi-frequency EPR (1-600GHz) (See Table 3.1) and pulsed EPR techniques. The advent of multi-frequency EPR enhances the information gained from a sample in which the principle g values may only differ slightly, offering increased resolution of g-values and also enhanced sensitivity. These attributes make it particularly useful for systems where the concentration of paramagnetic species is low.

Table 3.1 Characteristics of the microwave frequencies employed in EPR experiments

	L-band	**S-band**	**X-band**	**K-band**	**Q- band**	**W-band**
Frequency, ν/ GHz	1	3	9	24	34	94
Wavelength, λ/ cm	30	10	3	1.25	0.88	0.32
Energy, E/kJmol^{-1}	4×10^{-4}	1.2×10^{-3}	3.9×10^{-3}	9.5×10^{-3}	1.35×10^{-2}	3.74×10^{-2}

Pulsed EPR gives the user the ability to obtain information on the local environment of paramagnetic centres and their interaction with nuclear spins, electron-electron distances in biological systems and dynamical information from systems such as membranes. One technique which is commonly used is ESEEM (Electron Spin Echo Envelope Modulation), which provides the ability to obtain information regarding interactions of electron spins with the surrounding nuclei. This yields important structural information for samples such a metalloproteins for which single crystals are difficult to obtain.

EPR has grown into a vast field, therefore the following section is a concise introduction to the basic principles of EPR and how it can be used to study polycrystalline powder systems, as all the samples studied in this thesis are polycrystalline metal oxide powders. For a more in-depth review of EPR theory and its applications there are a number of excellent modern textbooks.[19,20,21,22]

3.3 Basic principles of EPR

The electron has the fundamental properties of mass, charge and intrinsic angular momentum, or spin, (a vector donated by symbol **S**). From the Heisenberg uncertainty principle, only the square of the intrinsic angular momentum (S^2), and one component in a given direction (for example z), can be measured with certainty. The total spin quantum number can only assume integer or half integer values (0, 1/2, 1....) and for a single unpaired electron S = 1/2. The allowed values of the component of S along an arbitrary direction are restricted to the quantum numbers M_S which have 2S+1 possible components. Two values of M_S are therefore allowed for S = 1/2 (2 S+1 are the only allowed values) i.e. $S_z = 1/2\hbar$ (sometimes referred to as ↑ or α state, where $M_s = 1/2$) and $S_z = -1/2\hbar$ (sometimes referred to as ↓ or β state, where $M_s = -1/2$). The symbol ħ represents the unit of angular momentum ($\hbar = h/2\pi$ where h is Planck's constant $h = 6.626 \times 10^{-34}$ Js). S^2 in general is $s(s+1)\hbar$ and becomes, for an electron, $S^2 = 3/4\hbar^2$ with $S = (\sqrt{3}/2)\hbar$ (Figure 3.1)

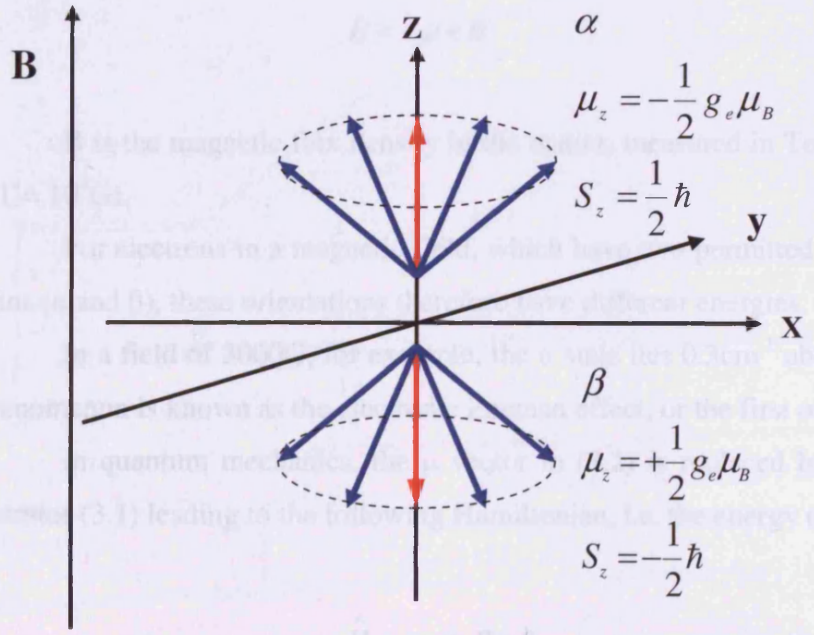

Figure 3.1 Figure showing the two different energy states of an electron in a magnetic field.

An electron has associated with it a magnetic moment due to its intrinsic spin. The magnetic moment μ_s has colinear and antiparallel components to the spin itself and is given by:

$$\mu_s = -g_e \mu_B S \qquad (3.1)$$

where g_e is the free electron g value ($g_e = 2.0023$), μ_B is the Bohr magneton with $\mu_B = \frac{eh}{4\pi mc}$ ($\mu_B = 9.27 \times 10^{-24}$ JT^{-1}) (e and m being the electron charge and mass respectively) and c the velocity of light.

When no magnetic field is present the spin vectors S (and the corresponding magnetic moments) of an assembly of free electrons are randomly aligned, but in the presence of an external magnetic field magnetic moments tend to align and define the axis of orientation of the S_z component, as shown in Figure 3.1. Due to the uncertainty with respect to the S_x and S_y components the vectors representing the spin of the electrons can lie on the surface of one of the two cones whose axes coincide with the z axis. In this way all electrons assume one of the two permitted S_z values ($+1/2\hbar$,$-1/2\hbar$). From classical physics it is known that the energy of interaction between the magnetic field and magnetic dipoles (which have a given magnetic moment μ), is itself given by the scalar product:

$$E = -\mu \bullet B \qquad (3.2)$$

B is the magnetic flux density in the matter, measured in Tesla (T) or Gauss (G) ($1T = 10^4 G$).

For electrons in a magnetic field, which have two permitted orientations of their spins (α and β), these orientations therefore have different energies.

In a field of 3000G, for example, the α state lies $0.3cm^{-1}$ above the β state. This phenomenon is known as the electronic Zeeman effect, or the first order Zeeman effect.

In quantum mechanics, the μ vector in (3.2) is replaced by the corresponding operator (3.1) leading to the following Hamiltonian, i.e. the energy operator:

$$\hat{H} = g_e \mu_B B \bullet S \qquad (3.3)$$

As **B** lies along the z-axis ($B_x = B_y = 0$, $B = B_z$) then the following equations can be written:

$$\hat{H} = g_e \mu_B B \hat{S}_z \qquad (3.4)$$

This is the simplest example of a spin Hamiltonian, i.e. the energy operator acting on the spin components of the whole electron wave function. $\hat{S}_z$ acts on the spin functions α and β according to: $\hat{S}_z |\alpha\rangle = 1/2|\alpha\rangle$ and $\hat{S}_z |\beta\rangle = -1/2|\beta\rangle$.

The permitted energy levels of the system (i.e., the energies corresponding to the two allowed orientations of the spin) are therefore:

$$E = (\pm 1/2)\, g_e \mu_B \mathbf{B} \qquad (3.5)$$

The lower energy state occurs when the magnetic moment of an electron is aligned with the applied magnetic field ($M_s = -1/2, \beta$). A higher energy state occurs when μ_s is aligned in opposition to the magnetic field ($M_s = +1/2, \alpha$). The energy between these two states is:

$$\Delta E = g_e \mu_B B = h\nu \qquad (3.6)$$

where ν is the frequency.

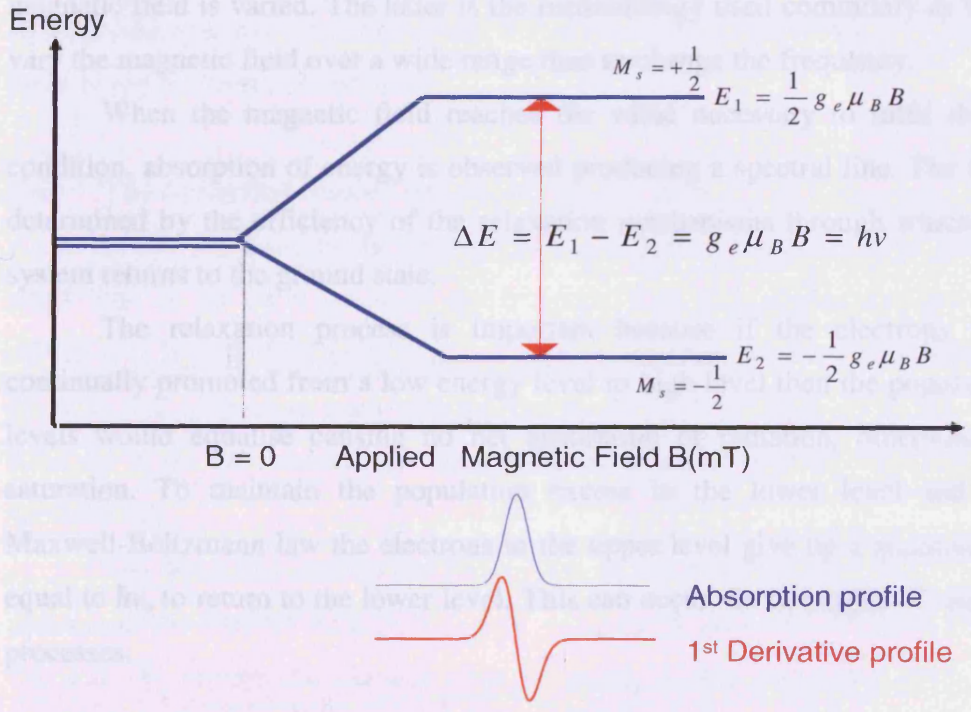

Fig 3.2 The electronic Zeeman effect. The energy difference between the α and β spin states is proportional to the value of the applied magnetic field.

In this system under thermal equilibrium and the influence of the external applied magnetic field, the spin population is split between the two levels according to the Maxwell Boltzmann law;

$$\frac{n_1}{n_2} = e^{\frac{-\Delta E}{kT}} \qquad (3.7)$$

where k is the Boltzmann constant, T is the absolute temperature, n_1 and n_2 are the spin population characterised by the M_s values of +1/2 and -1/2 respectively. At 298K in a field of about 3000G the ratio n_1:n_2 is calculated as:

$$\frac{n_1}{n_2} = 0.9986 \qquad (3.8)$$

Therefore the population of the two Zeeman levels are almost equal, but the slight excess in the lower level gives rise to net absorption, resulting in an EPR signal.

To induce transitions between the two Zeeman levels the paramagnetic system needs electromagnetic radiation that matches the frequency ν of the resonance condition $h\nu$ in equation (3.6).

The existence of these two levels and the possibility of inducing transitions from the lower energy level to the higher one is the basis of EPR spectroscopy. The experiments can be performed in two ways; either the magnetic field is kept constant and the applied frequency varied, or the applied frequency is held constant and the magnetic field is varied. The latter is the methodology used commonly as it is easier to vary the magnetic field over a wide range than to change the frequency.

When the magnetic field reaches the value necessary to fulfil the resonance condition, absorption of energy is observed producing a spectral line. The line width is determined by the efficiency of the relaxation mechanisms through which the excited system returns to the ground state.

The relaxation process is important because if the electrons were to be continually promoted from a low energy level to high level then the population of both levels would equalise causing no net absorption of radiation, otherwise known as saturation. To maintain the population excess in the lower level and satisfy the Maxwell-Boltzmann law the electrons in the upper level give up a quantum of energy, equal to $h\nu$, to return to the lower level. This can occur via two types of spin relaxation processes:

3.3.1 Spin-lattice relaxation (T_{1e}):

The magnetic energy absorbed by the paramagnetic system is dissipated in phonons, i.e. vibrational, rotational and translational energy. The mechanism by which this dissipation occurs is known as the spin lattice relaxation, which is characterised by an exponential decay of energy as a function of time. The exponential time constant is denoted T_{1e} or spin lattice relaxation time. The spins relax back towards their thermal equilibrium positions.

The value of T_{1e} is sensitive to:

(i) Temperature: a decrease in temperature decreases the population of phonons and leads to a longer relaxation time and correspondingly narrower lines.

(ii) The presence of nearby electronic excited states: when these are close ($\approx$ $100cm^{-1}$) to the ground state, the relaxation time will be very short and linewidth very large (even unobservable).

3.3.2 Spin-spin relaxation (T_{2e}):

The excess spin energy can be exchanged between the paramagnetic centres either through dipolar or exchange coupling from one molecule to another. This mode of relaxation is important when the concentration of paramagnetic species is high. If the relaxation time is too fast then the electrons will only remain in the upper state for a short period and give rise to a broadening of the spectral linewidth as a consequence of Heisenberg's uncertainty principle.

3.4 The hyperfine tensor: origin and significance.

In the presence of an applied magnetic field a single electron gives rise to a single line in the EPR spectrum and contains very little useful information. This of course is a hypothetical system and is not representative of a real system where the electron will interact at least with its associated nucleus. This gives rise to hyperfine structure in the EPR spectrum, which is the most useful source of information in EPR spectroscopy.

The hyperfine interaction (A) is due to the interaction between the magnetic moment of the electron with the magnetic moment of a nearby $I > 0$ nucleus. As a result the field (**B**) around the electron changes owing to this additional magnetic moment

coming from the nucleus creating a perturbed local field ($\mathbf{B}_{local}$) which must be added to the **B**. Hence:

$$h\nu = g\mu_B(B + B_{local}) \qquad (3.9)$$

The nuclear spin quantum number (I) has an associated magnetic moment (μ_N) written as:

$$\mu_N = g_n \mu_N \mathrm{I} \qquad (3.10)$$

where g_n is the nuclear g factor for a proton and μ_N = nuclear magneton value (μ_N is smaller than μ_B by a factor of 1838, i.e. the ratio of the mass of a proton to that of an electron).

The contribution from the magnetic field and the orbitals, as well as the contribution from the magnetic field of the nucleus, are considered in the complete spin Hamiltonian as shown:

$$\hat{H} = g_e\mu_B \mathbf{B}\,\hat{\mathbf{S}} - g_n\mu_N\,\hat{\mathbf{I}} + \hat{\mathbf{I}}\,\mathbf{A}\,\hat{\mathbf{S}} \qquad (3.11)$$

where $\hat{\mathbf{I}}$ = spin operator for the nuclear spin, **A** = hyperfine coupling, $\hat{\mathbf{S}}$ = spin operator for the electron spin.

The interaction between the unpaired electron and a spin active nucleus gives rise to further splitting of the lines, producing the hyperfine pattern in the EPR spectrum.

Two types of electron spin-nuclear spin interactions can occur. These are called the isotropic interaction (A_0) and the anisotropic interaction (B_0), which will be discussed in the following section.

For a solid state paramagnetic species where the unpaired electron is localised upon a magnetic nucleus, each of the principal g tensor components will be split into (2nI + 1) lines, where I is the spin quantum number of the nucleus involved. For each g tensor component, the set of lines (determined by 2nI + 1) will be spaced by a splitting constant, which corresponds to the appropriate component of the anisotropic coupling. For example, g_1 is split by A_1, g_2 split by A_2 etc. In powder samples, the EPR spectra often have large line widths. Consequently some hyperfine detail may not be resolved and the precise splitting can remain unknown.[23]

3.4.1 The isotropic interaction

The isotropic interaction deals with s type orbitals or orbitals with partial s character because these orbitals have finite probability density at the nucleus. This interaction is termed the Fermi contact interaction. The corresponding isotropic coupling constant a_{iso} is given by

$$a_{iso} = (8\pi / 3g_e g_n \mu_B \mu_N) |\Psi(0)|^2 \qquad (3.12)$$

where g_n and μ_N are the nuclear analogues of g_e and μ_B respectively, and $|\Psi(0)|^2$ is the square of the absolute value of the wavefunction of the unpaired electron evaluated at the nucleus.

Since s orbitals have a high electron density at the nucleus, the hyperfine coupling constant will be large and since s orbitals are also spherically symmetrical it will be independent of direction.

The following section discusses the energy level diagram arising for an unpaired electron due to its interaction with an associated nucleus with I = 1/2.

The energy of an electron with magnetic quantum number M_S interacting with a nucleus of quantum number M_I is given by 3.13:

$$E(M_s, M_I) = g\,\mu_B\,B\,M_s - g_N\,\mu_N\,B\,M_I + h\,a_{iso}\,M_s\,M_I \qquad (3.13)$$

For the interaction of an unpaired electron ($M_S = \pm 1/2$) with a single proton ($M_I = \pm 1/2$) the above equation gives rise to 4 energy levels

	M_s	M_I	
$E_1 = +1/2 g\mu_B B + 1/2 g_N\mu_N B - 1/4 h a_{iso}$	+1/2	-1/2	(3.14)
$E_2 = +1/2\, g\mu_B B - 1/2\, g_N\mu_N B + 1/4 h a_{iso}$	+1/2	+1/2	(3.15)
$E_3 = -1/2\, g\mu_B B + 1/2\, g_N\mu_N B + 1/4 h a_{iso}$	-1/2	-1/2	(3.16)
$E_4 = -1/2\, g\mu_B B - 1/2\, g_N\mu_N B - 1/4 h a_{iso}$	-1/2	+1/2	(3.17)

The transitions between energy levels are restricted by selection rules, which state that for a transition to be allowed $\Delta M_S = \pm 1$ and $\Delta M_I = 0$. It is found that two possible resonance transitions can occur, namely ΔE_1 and ΔE_2, as shown in Figure 3.3 below:

$$\Delta E_1 = E_3 - E_1 = g\mu_B B - \tfrac{1}{2} h a_{iso} \qquad (3.18)$$

$$\Delta E_2 = E_4 - E_2 = g\mu_B B + \tfrac{1}{2} h a_{iso} \qquad (3.19)$$

The two transitions give rise to two absorptions of equal intensity separated by the hyperfine coupling constant a_{iso} , the isotopic hyperfine coupling.

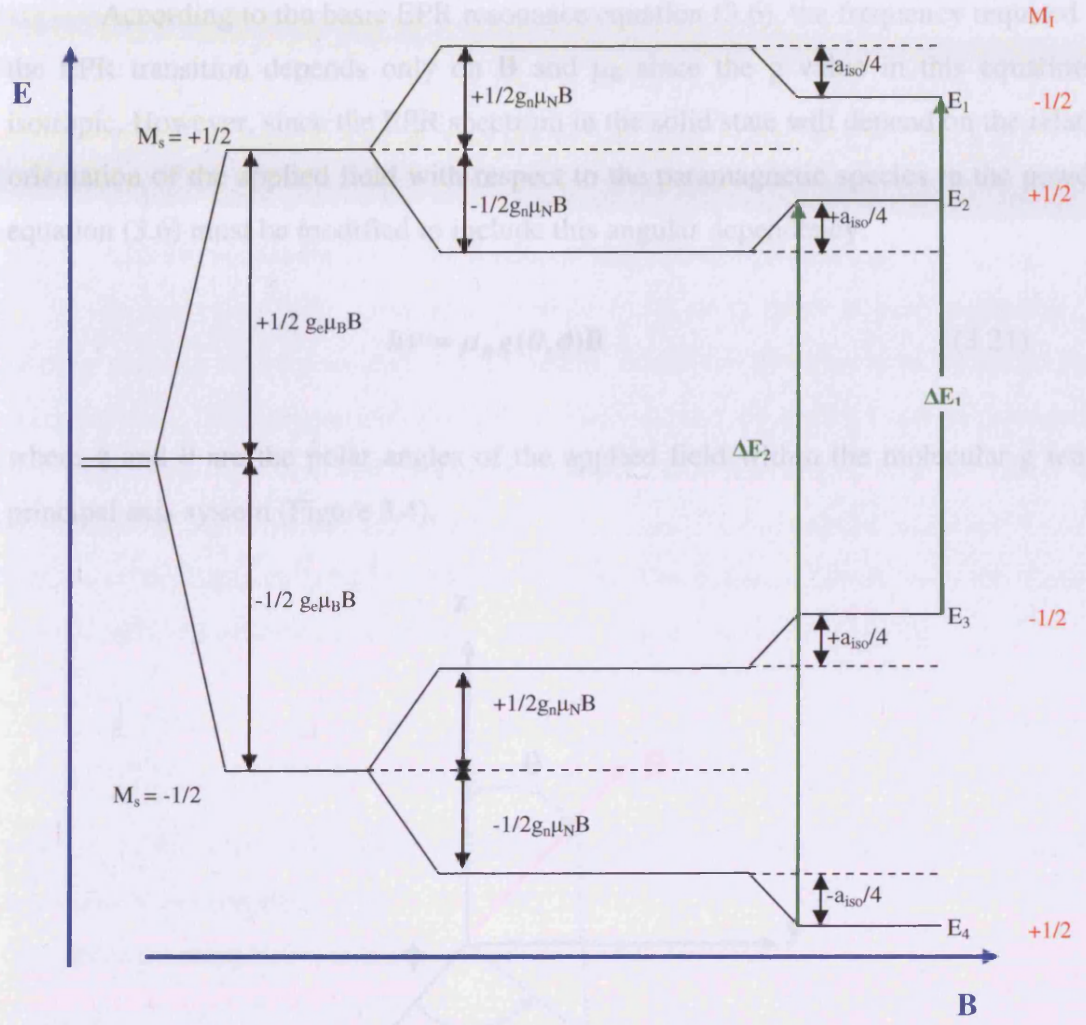

Figure 3.3 Energy level diagram for the interaction of a proton (I = 1/2) with an unpaired electron (S = ½) in an applied magnetic field.

3.4.2 The g tensor: origin and significance

The theory and analysis of the spectrum in the solid state, such as that arising from a heterogeneous catalyst, is more complex due to anisotropies in the simple spin Hamiltonian introduced earlier in equation (3.11) which only considered isotropic or average contributions from g and a. A more appropriate Hamiltonian for the solid state, which takes into account these anisotropies, is given by:

$$\hat{H} = \mu_B \mathbf{S} \cdot \mathbf{g} \cdot \mathbf{B} + \sum (g_N \mu_N \mathbf{I} \cdot \mathbf{B} + \mathbf{I} \cdot \mathbf{A} \cdot \mathbf{S}) \qquad (3.20)$$

The isotropic g and A values are now replaced by two 3 x 3 matrices representing the g and A tensors which arise from the anisotropic electron Zeeman and hyperfine interaction. Other energy terms may also be included in the spin Hamiltonian, including the anisotropic fine term D for electron-electron interactions.

According to the basic EPR resonance equation (3.6), the frequency required for the EPR transition depends only on **B** and μ_B since the g value in this equation is isotropic. However, since the EPR spectrum in the solid state will depend on the relative orientation of the applied field with respect to the paramagnetic species in the powder, equation (3.6) must be modified to include this angular dependency:

$$h\nu = \mu_B g(\theta,\phi)\mathbf{B} \qquad (3.21)$$

where ϕ and θ are the polar angles of the applied field within the molecular g tensor principal axis system (Figure 3.4).

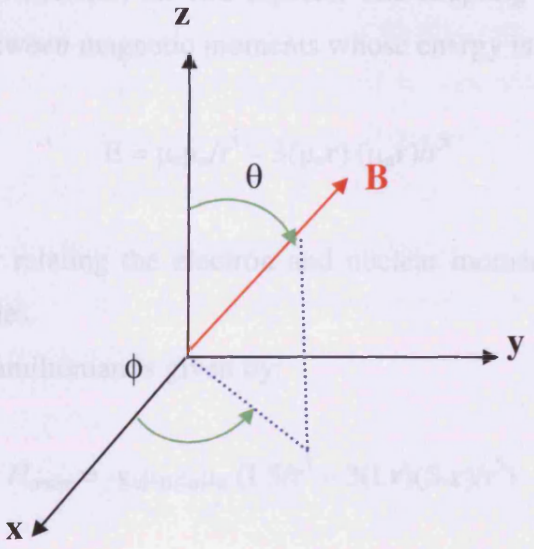

Fig. 3.4 Orientation of the magnetic field with respect to the **g** tensor principal axis system denoted X, Y, Z.[17]

Because g now depends on the angles (θ,ϕ) it should be described using the following Zeeman Hamiltonian:

$$\hat{H} = \mu_B \cdot \mathbf{S} \cdot \mathbf{g} \cdot \mathbf{B} \qquad (3.22)$$

where g is now no longer written as a simple scalar quantity. An explicit expression for $g(\theta,\phi)$ can be found by writing the components of the field in the g tensor frame *via* the

polar angles defined in Figure 3.4. For example one must define the g value in terms of B in all three principal directions, then sum all terms to represent the anisotropic powder profile. This treatment is beyond the scope of this chapter, and can be found in any EPR textbook. However, it is sufficient to note here that the effective g value can finally be expressed in a form to encompass the angular terms from equation (3.23) such that:

$$g(\theta,\phi) = \sqrt{\sin^2\theta\cdot\cos^2\phi\cdot g_1^2 + \sin^2\theta\cdot\sin^2\phi\cdot g_2^2 + \cos^2\theta\cdot g_3^2} \qquad (3.23)$$

3.4.3 Anisotropic interaction (The A tensor; origin and significance)

In non-spherically symmetric orbitals (p, d or f) there is zero probability of finding electron density located at the nucleus; rather the electron is to be found some distance away. The interaction between the electron and the nucleus can be regarded as the interaction between two magnetic dipoles. The interaction will be small and dependent on the direction of the orbital with respect to the applied magnetic field, as well as to the distance between the two dipoles. The coupling arises from the classical dipolar interaction between magnetic moments whose energy is given by:

$$E = \mu_s\mu_n/r^3 - 3(\mu_s\mathbf{r})\,(\mu_n\mathbf{r})/r^5 \qquad (3.24)$$

where **r** is the vector relating the electron and nuclear moments and r is the distance between the two dipoles.

The corresponding Hamiltonian is given by:

$$H_{aniso} = -g_e\mu_B g_n\mu_n\,(\mathbf{I}.\mathbf{S}/r^3 - 3(\mathbf{I}.\mathbf{r})(\mathbf{S}.\mathbf{r})/r^5) \qquad (3.25)$$

H_{aniso} is averaged to zero when the electron cloud is spherical and comes to a finite value in the case of axially symmetrical orbitals. In the case of rapid tumbling of the paramagnetic species (as occurs in low viscosity solution) the anisotropic term of the hyperfine interaction is averaged to zero and the isotropic term is the only one observed.

Since the electron is not localised at one position in space, equation (3.25) must be averaged over the electron probability distribution. The magnitude of the anisotropic hyperfine interaction then depends on the orientation of the paramagnetic system with respect to the external field.

In the general case, both isotropic and anisotropic hyperfine interactions contribute to the experimental spectrum. The whole interaction is therefore dependent once again on orientation and must be expressed by a tensor. The effective spin Hamiltonian for this more realistic description of a paramagnetic species in the solid state was given earlier in (3.20). Nevertheless the A tensor may be split into its component isotropic and anisotropic parts as follows;

$$A^i = \begin{bmatrix} A_1 & 0 & 0 \\ 0 & A_2 & 0 \\ 0 & 0 & A_3 \end{bmatrix} = a_{iso} + \begin{bmatrix} T_1 & 0 & 0 \\ 0 & T_2 & 0 \\ 0 & 0 & T_3 \end{bmatrix} \qquad (3.26)$$

Where $a_{iso} = A_1 + A_2 + A_3 /3$. The anisotropic part of the A tensor corresponds to the dipolar interaction as expressed by the Hamiltonian in (3.25). In a number of cases, the second term of the matrix in (3.26) is a traceless tensor and has the form (-T,-T, 2T). For this reason, in the case of EPR spectra of paramagnetic species having both isotropic and anisotropic hyperfine couplings and undergoing rapid tumbling in a low viscosity solution, the anisotropic term is averaged to zero and the observed hyperfine coupling corresponds to the isotropic part only. Extremely useful information can be derived from the hyperfine structure of an EPR spectrum including the s and p characters of the orbitals hosting the unpaired electron (or the co-efficient of the atomic wavefunctions involved in the SOMO orbital). In simplest terms this data can be deduced from the following relations;

$$C_S^2 = \frac{a_{iso}}{A_O} \text{ and } C_P^2 = \frac{T}{B} \qquad (3.27)$$

where A_o and B are the experimental, or more frequently the theoretical, hyperfine couplings assuming pure s and p orbitals for the elements under consideration and co-efficient $C_S^2 + C_P^2 = 1$. Appropriate corrections and orbital coefficients must be included to account for the specific orbital hosting the unpaired electron, but (3.27) nevertheless illustrates simply how the spin density can be calculated to first approximation.

3.5 Symmetry of real systems: Powder EPR spectra

EPR spectroscopy is suitable for analysis of samples that are in a range of phases and physical states. Here the focus is on EPR spectra recorded in the solid state. While some advances have been made in single crystal EPR, the majority of samples studied are polycrystalline materials and many real chemical systems such as glasses, catalysts, ceramics, minerals, and micro- and nanoporous materials can be studied. The spectra recorded are referred to as 'powder' spectra, comprising of all possible orientations of the paramagnetic species with respect to the magnetic field. The profile of the powder spectrum depends on the symmetry of the system under study, with three symmetries possible: Isotropic, Axial and Orthorhombic for a system comprising solely of Zeeman interactions. These will be discussed in the following section.

Table 3.2. Relationship between the EPR Symmetry and Molecular Point Symmetry of Paramagnetic Centres

EPR Symmetry	**g and A tensors**	**Coincidence of tensor axis**	**Molecular point symmetry**
Isotropic	$g_{xx} = g_{yy} = g_{zz}$ $A_{xx} = A_{yy} = A_{zz}$	All coincident	O_h, T_d, O, T_h, T
Axial	$g_{xx} = g_{yy} \neq g_{zz}$ $A_{xx} = A_{yy} \neq A_{zz}$	All coincident	D_{4h}, C_{4v}, D_4, D_{2d}, D_{6h}, C_{6v}, D_6, D_{3h}, D_{3d}, C_{3v}, D_3
Rhombic	$g_{xx} \neq g_{yy} \neq g_{zz}$ $A_{xx} \neq A_{yy} \neq A_{zz}$	All coincident	D_{2h}, C_{2v}, D_2
Monoclinic	$g_{xx} \neq g_{yy} \neq g_{zz}$ $A_{xx} \neq A_{yy} \neq A_{zz}$	One axis of g and A coincident	C_{2h}, C_s, C_2
Triclinic	$g_{xx} \neq g_{yy} \neq g_{zz}$ $A_{xx} \neq A_{yy} \neq A_{zz}$	Complete non-coincidence	C_1, C_1
Axial non-colinear	$g_{xx} = g_{yy} \neq g_{zz}$ $A_{xx} = A_{yy} \neq A_{zz}$	Only g_{zz} and A_{zz} coincident	C_3, S_6, C_4 S_4, C_{4h}, C_6 C_{3h}, C_{6h}

The EPR tensors can be classified on the basis of their symmetry (for instance, an isotropic tensor has three equal principal components, and an axial tensor has two

equal components differing from the third), which in turn depends on the point symmetry of the paramagnetic centre. Radicals, and in general paramagnetic species located at solid surfaces are subject to some symmetry restrictions, and often radicals with much reduced symmetry are observed. In the case of the most symmetric cases (isotropic, axial and rhombic tensors) the axes of the g and A tensors coincide, while in other cases they do not. The structure of the EPR tensors and the relationship between the EPR symmetry and point symmetry of the paramagnetic centres are gathered in Table 3.2.

3.5.1 Isotropic symmetry

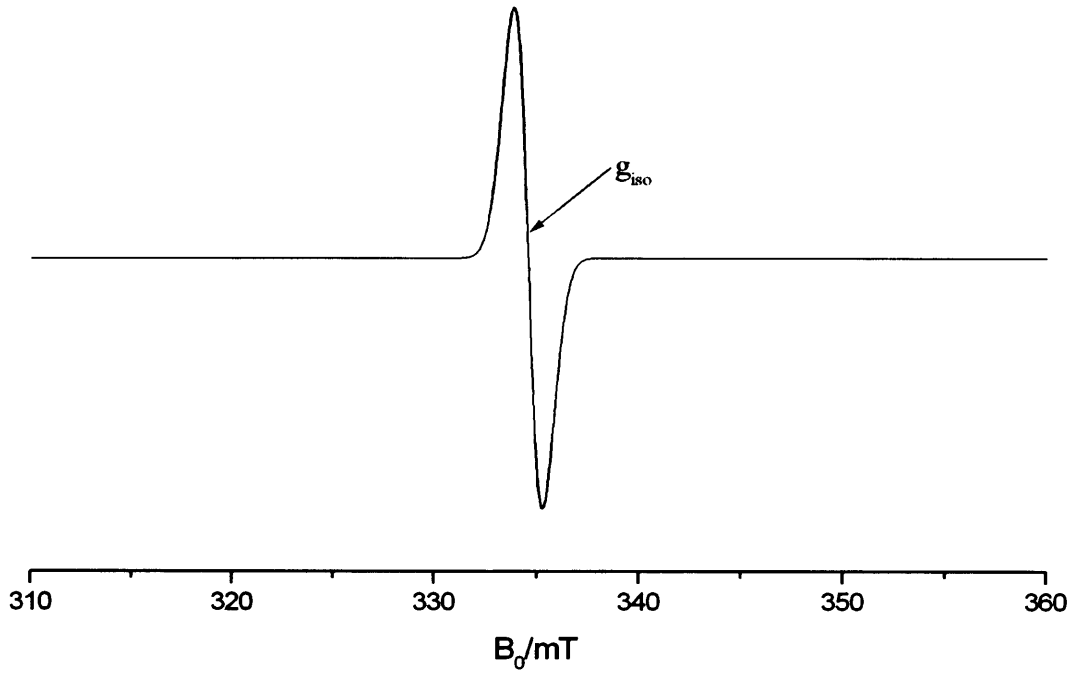

Figure 3.5 Simulated isotropic EPR spectrum for an S = 1/2, I = 0 system

Systems with perfect cubic symmetry such as octahedral (O_h) and tetrahedral (T_d) tend to give rise to a g tensor which is characterised by a single symmetrical line where $g_{zz} = g_{yy} = g_{xx}$ (see Figure 3.5). The isotropic signal is most often seen in low viscosity solutions where the g value (g_{iso}) is the result of the averaging of the three components. It is rare in solids except for solid state defects.

3.5.2 Axial symmetry

Axial symmetry will be observed when two of the principal g values, i.e. x and y, are equal. The unique value is designated as $g_{\|}$ (g_{zz}) and is referred to as "g parallel", whilst the other value is $g_{\perp}$ ($g_{xx} = g_{yy}$), "g perpendicular". When z is the unique

symmetry axis of the system and θ the angle between the z axis and the magnetic field, the x and y directions are equivalent and the angle Φ becomes meaningless.[19]
So for axial symmetry (x = y ≠ z) the resonant field can then be calculated using the equation:

$$\mathbf{B} = h\nu / \mu_B (g_\perp^2 \sin^2\theta + g_\parallel^2 \cos^2\theta)^{-1/2} \qquad (3.28)$$

The $g_\parallel = g_{zz}$ and $g_\perp = g_{xx} = g_{yy}$ are the values measured when the axis of the paramagnetic species is respectively parallel and perpendicular to the applied magnetic field. The EPR spectra in this thesis were recorded using polycrystalline materials. Since the sample is solid the anisotropy of the various magnetic interactions influences the spectra and the values are not averaged as in the solution case. Simple consideration shows that the absorption intensity (which is proportional to the number of microcrystals at resonance for a given θ value), is maximum when $\theta = \pi / 2(\mathbf{B}_\perp)$ and minimum when $\theta = 0$ ($\mathbf{B}_\parallel$). This allows the extraction of the g values that correspond to the turning points of the spectrum.

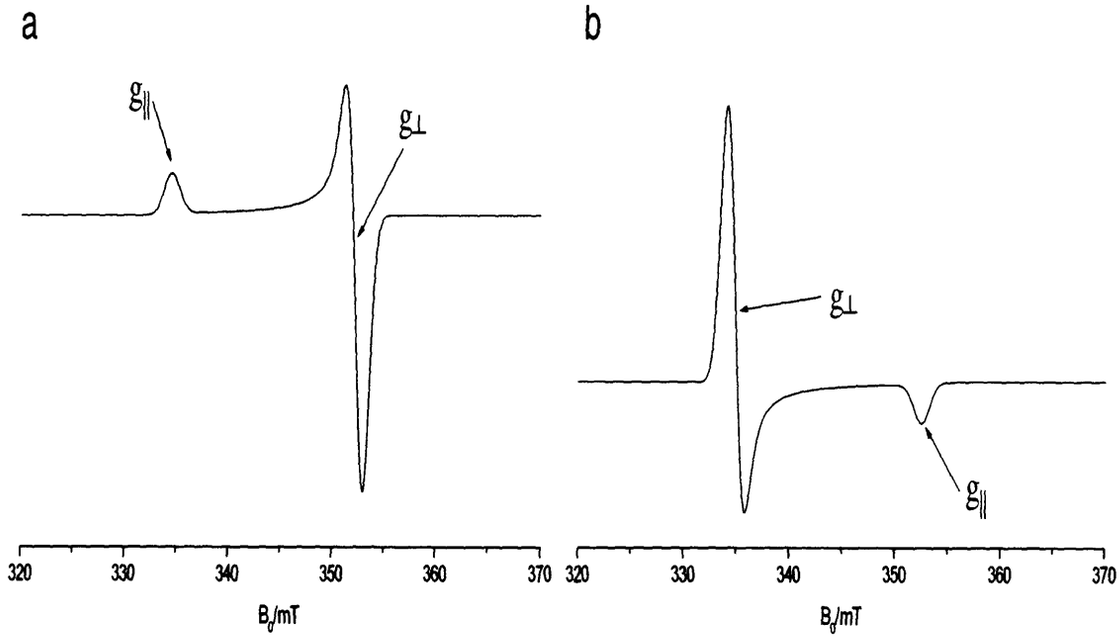

Figure 3.6 Simulated axial EPR spectra where (a) $g_\parallel > g_\perp$ and (b) $g_\perp > g_\parallel$.

3.5.3 Orthorhombic symmetry

If the system has three distinct values of g i.e. $g_{xx} \neq g_{yy} \neq g_{zz}$ it is designated orthorhombic. The axes are designated g_1, g_2, and g_3 with the g_{xx}, g_{yy}, g_{zz} notation only used when the orientation of the principal axes of the system with respect to the

magnetic field has been determined from studies of the paramagnetic crystal in a single crystal sample. In all other cases g_1, g_2 and g_3 should be used.

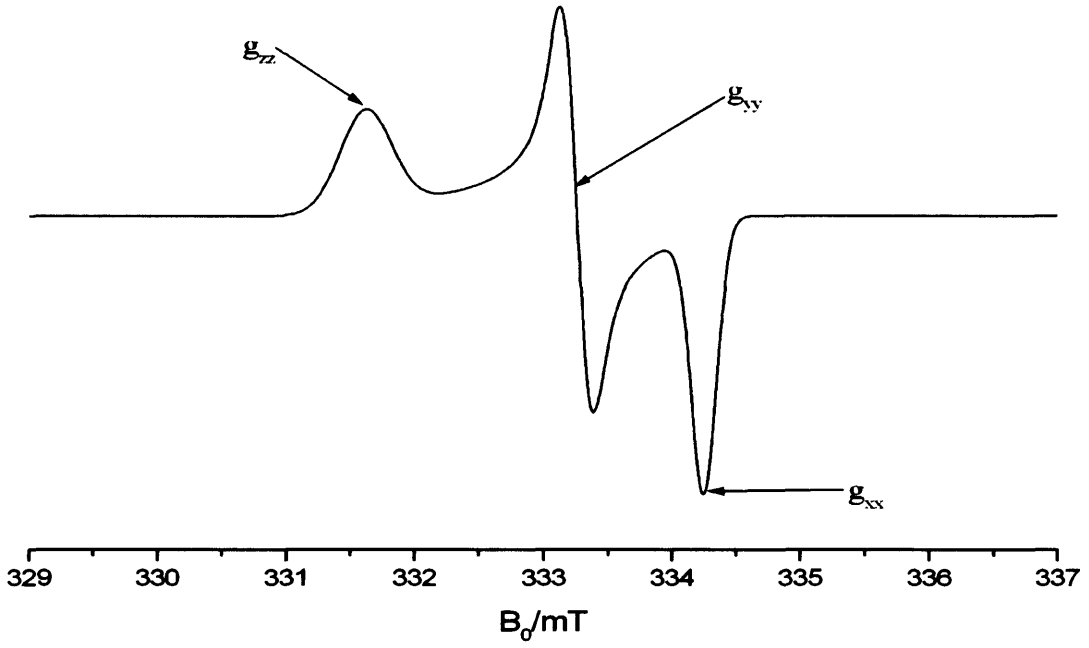

Figure 3.7 Simulated orthorhombic EPR spectrum where $g_{xx} \neq g_{yy} \neq g_{zz}$.

3.6 Interpreting powder EPR spectra

In the following chapters many powder EPR spectra will be presented; these spectra are often complex and the overall spectrum is a combination of many different factors including:

- The presence of several species in the system that have different EPR parameters, including nuclei with different nuclear spins.
- Broadening of the lines as a result of dipolar spin-spin interactions or due to motional phenomena, leading to loss of resolution.

Throughout this thesis the strategy to interpret the complex EPR spectra was to first extract the g and A values, by computer simulation, of all the components present in the spectrum and then to make an informed assignment of a suitable paramagnetic species. The confirmation of this assignment is then aided by a number of different methods to gain additional information on the species such as behaviour at elevated temperatures and reactivity. The following section will briefly discuss the rationale behind the experiments, all of which have been used throughout the course of the thesis.

3.6.1 *Measurement of g values*

The absolute determination of the g values may be performed by measuring B and ν independently and simultaneously, using a Gauss meter and a frequency meter respectively. The g value can be determined by comparing field values at resonance for the sample investigated and that of a reference sample (e.g. diphenyl-picryl-hydrazyl (DPPH), $g_{ref} = 2.0036$), which can be written as;

$$h\nu = g_{ref}\mu_B B_{ref} = g\mu_B \mathbf{B} \qquad (3.29)$$

Provided ν is invariant during the whole experiment, g is given by:

$$g = g_{ref}\frac{B_{ref}}{B} \qquad (3.30)$$

3.6.2 *Simulation of spectra*

The spin Hamiltonian parameters obtained from the experimental data can be extracted by computer simulation. Simulations lead to accurate values of the g and A tensors for each species contributing to the spectrum and can also provide information on their relative populations through peak deconvolution. For example, Figure 3.8a shows an orthorhombic spectrum with three signals in the g_1 component. Following in Figures 3.8b, c and d are shown the individual orthorhombic signals which result in the spectrum shown in Figure 3.8a when added together in a linear combination.

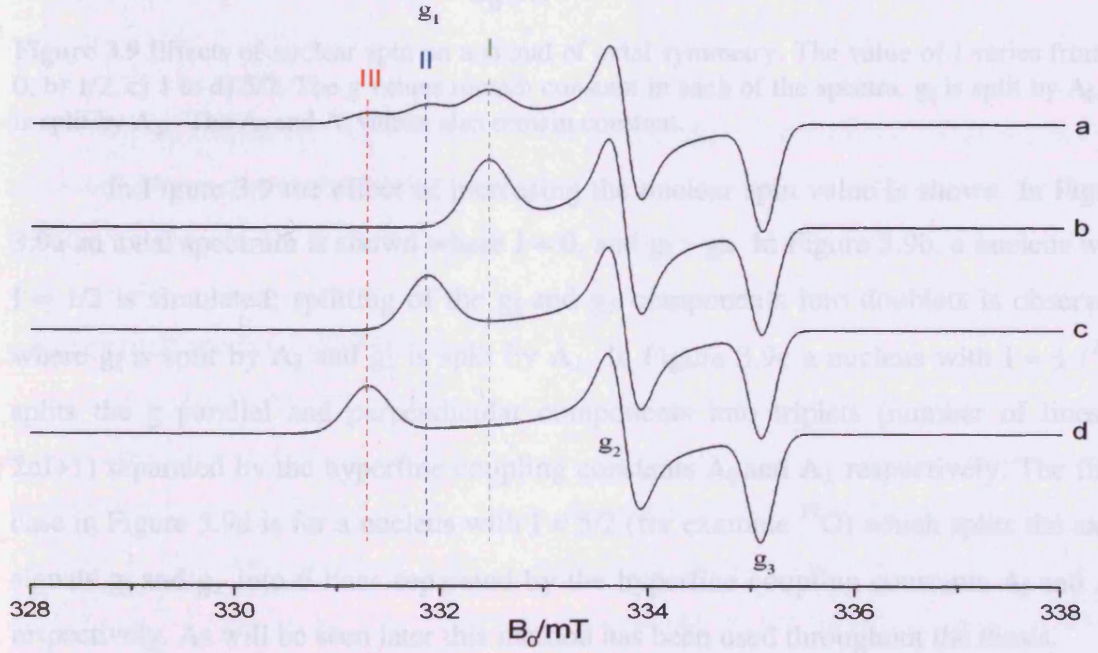

Figure 3.8 A simulated EPR spectra of three superimposed orthorhombic signals (ratio 1:1:1) possessing equivalent g_2 and g_3 values but different g_1 values. The individual signals from the three species are shown in (b), (c) and (d).

3.6.3 *Isotopic labelling*

Paramagnetic species with nuclear spin I = 0 can be substituted with isotopes of I > 0. The presence of hyperfine structure in a spectrum can be beneficial when determining the nature of atoms interacting with the unpaired electron, and the nature of this interaction. The value of the nuclear spin determines the overall number of hyperfine lines and the hyperfine patterns produced will be strongly dependent on the relative abundance of the I ≠ 0 component.

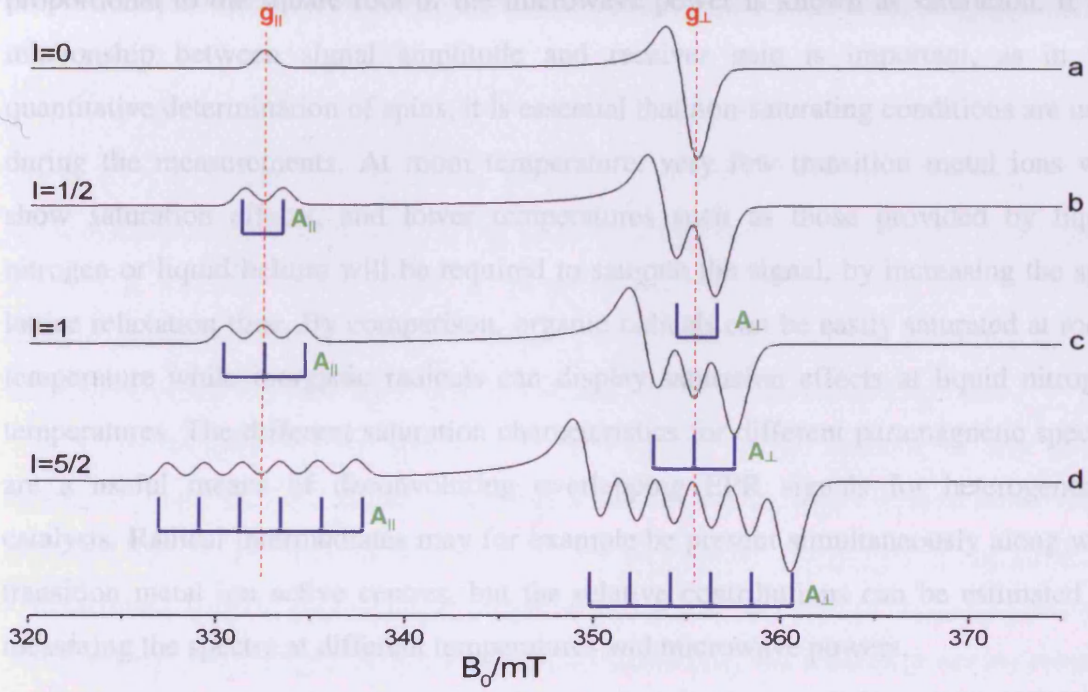

Figure 3.9 Effects of nuclear spin on a signal of axial symmetry. The value of I varies from a) 0, b) 1/2, c) 1 to d) 5/2. The g values remain constant in each of the spectra. $g_{\|}$ is split by $A_{\|}$, $g_{\perp}$ is split by $A_{\perp}$. The $A_{\|}$ and $A_{\perp}$ values also remain constant.

In Figure 3.9 the effect of increasing the nuclear spin value is shown. In Figure 3.9a an axial spectrum is shown where I = 0, and $g_{\|} > g_{\perp}$. In Figure 3.9b, a nucleus with I = 1/2 is simulated; splitting of the $g_{\|}$ and $g_{\perp}$ components into doublets is observed, where $g_{\|}$ is split by $A_{\|}$ and $g_{\perp}$ is split by $A_{\perp}$. In Figure 3.9c a nucleus with I = 1 (^{2}H) splits the g parallel and perpendicular components into triplets (number of lines = 2nI+1) separated by the hyperfine coupling constants $A_{\|}$ and $A_{\perp}$ respectively. The final case in Figure 3.9d is for a nucleus with I = 5/2 (for example ^{17}O) which splits the axial signals $g_{\|}$ and $g_{\perp}$ into 6 lines separated by the hyperfine coupling constants $A_{\|}$ and $A_{\perp}$ respectively. As will be seen later this method has been used throughout the thesis.

3.6.4 Variable power and temperature

The applied microwave power is a very important consideration in EPR. At low values the signal amplitude will increase in direct proportion to the square root of the microwave power received by the sample in the cavity ($I \propto \sqrt{P}$). This relationship only occurs up to a certain level, beyond which the signal amplitude increases less rapidly than required by this equation, and in some cases may even start to decrease. The phenomenon whereby the rate of increase of signal amplitude is less than directly proportional to the square root of the microwave power is known as saturation. If the relationship between signal amplitude and receiver gain is important, as in the quantitative determination of spins, it is essential that non-saturating conditions are used during the measurements. At room temperature, very few transition metal ions will show saturation effects, and lower temperatures such as those provided by liquid nitrogen or liquid helium will be required to saturate the signal, by increasing the spin lattice relaxation time. By comparison, organic radicals can be easily saturated at room temperature while inorganic radicals can display saturation effects at liquid nitrogen temperatures. The different saturation characteristics for different paramagnetic species are a useful means of deconvoluting overlapping EPR signals for heterogeneous catalysts. Radical intermediates may for example be present simultaneously along with transition metal ion active centres, but the relative contributions can be estimated by measuring the spectra at different temperatures and microwave powers.

3.6.5 Surface probes

Probe molecules can be used to test different features of the oxide surface by monitoring changes in the EPR spectrum upon adsorption. The addition of the probe molecule may result in changes in line shape, linewidth and g values of the paramagnetic species present, depending on the strength of the interaction between the paramagnetic species and probe molecules.

Charge transfer may occur between the surface and the probe molecule, giving rise to new EPR signals, or alternatively the spectrum may simply be affected by line broadening in the presence of the probe molecule which vanishes upon evacuation. Oxygen is commonly used as a probe molecule, and has been used successfully to distinguish between the species situated in the bulk and on the surface of metal oxides[24].

3.6.6 *Quantification of the number of spins*

The intensity of the EPR signal can of course be related to the concentration of the paramagnetic species present in the catalyst. However, although this quantitative analysis is frequently used in the literature to estimate the number of spins, it is inherently difficult to obtain absolute concentrations accurately. The relationship between signal intensity and sample concentration is given by;

$$C = \frac{KI}{GP_{ij}} \tag{3.31}$$

where K is a simple proportionality constant, I is the EPR signal intensity, G the spectrometer receiver gain, and P_{ij} the EPR transition probability. The proportionality constant K depends on the sample in question, and will be influenced by a variety of factors including (i) the properties of the cavity, with the sample included, (ii) the microwave power incident upon the sample, and (iii) the modulation amplitude.

The intensity of the signal must be obtained in the absence of any power saturation. Since the EPR signal consists of a first derivative, rather than an absorbance, this must also be factored into the analysis. Usually double integration of the spectrum is performed over a defined scan range (after careful adjustment to the base line). Alternatively, for a single symmetric first derivative line, the following simple relation may be used;

$$I = A(p - p)w^2 \tag{3.32}$$

Where A(p-p) is the peak to peak amplitude of the first derivative line and w is the linewidth parameter for the Lorentzian or Gaussian lineshape.

To compare the intensities of two signals (for example, between a known standard and a sample of unknown concentration), one must therefore ensure that K and P_{ij} in equation 3.31 are identical for both sample and reference standard, in other words, factors (i-iii) must be identical. This is surprisingly difficult to achieve in practise since the sample cell, sample volume, position in cavity, dielectric properties of the sample and reference standard must be identical if factor (i) is to be realised. In other words, the standard should ideally have identical EPR properties to that of the unknown, and must be recorded under identical instrumental conditions. Thus for example, it would be

completely inappropriate to use a DPPH reference sample as a standard to determine the absolute concentration for a Cu(II) containing catalyst.

3.6.7 Physical state of the sample

In EPR spectroscopy, it is possible to measure spectra of paramagnetic samples in a variety of forms, including fluid solution, frozen solution, powdered solid or single crystal. Clearly, for heterogeneous polycrystalline systems, such as oxides, the problems of solvent choice, lossy samples, poor quality glass conditions when frozen, *etc*, are all eliminated and this facilitates the greater case in analysing such heterogeneous systems. Polycrystalline samples do not usually present problems with respect to dielectric loss, unless they are of ionic compounds with large ionic charges or alternatively if too large a sample is placed in the cavity. When using powdered solids it is important to grind the sample sufficiently to avoid any preferential orientation of the crystallites. The occurrence of preferential orientation of paramagnets in either powders or glasses may be examined by re-recording the spectrum after rotating the sample tube to give a different orientation with respect to the magnetic field. If the spectrum changes then there is some preferential orientation of the paramagnet and care must then be exercised in the interpretation of the spectrum.

3.7 Summary

The EPR technique although limited to the study of paramagnetic species is an important technique in the study of heterogeneous catalysts. If paramagnetic centres, such as defects, radicals and transition metal ions are present, the technique can help provide information on the identity of the species, local environment and behaviour.

3.8 References

(1) Pilbrow, J. R., Lowrey, M.R. *Rep. Prog. Phys* **1980**, *43*, 433.

(2) Pilbrow, J. R. High Resolution EPR Applications to Metalloenzymes and Metals in Medicine INTRODUCTION. In *High Resolution EPR: Applications to Metalloenzymes and Metals in Medicine*, **2009**; pp 1.

(3) Che, M.; Giamello, E. *Spectroscopic Characterisation of Heterogeneous Catalysts,Part B*; Elsevier Science Publishers: Amsterdam, **1987**; Vol. 57.

(4) Murphy, D. M.; Chiesa, M. EPR of Paramagnetic Centres on Solid Surfaces. In *SPR- Electron Paramagnetic Resonance* C., G. B., Ed.; RSC, **2008**; Vol. 21.

(5) Murphy, D. M.; Rowlands, C. C. *Chemical Applications of EPR* Academic Press: London, **1999**.

(6) Lunsford, J. H. *EPR methods in Heteroegeneous Catalysis*; Springer-Verlag: New York, **1987**.

(7) Lunsford, J. H. *Advances in Catalysis* **1972**, *22*, 265.

(8) Howe, R. F. *Advances in Colloid and Interface Science* **1982**, *18*, 1.

(9) Che, M.; Taarit, Y. B. *Advances in Colloid and Interface Science* **1985**, *23*, 235.

(10) Che, M., Giamello, E. *Studies in Surface Science and Catalysis* **1987**, *57*, B265.

(11) Sojka, Z.; Che, M. *Applied Magnetic Resonance* **2001**, *20*, 433.

(12) Dyrek, K.; Che, M. *Chemical Reviews* **1997**, *97*, 305.

(13) Gerlach, W.; Stern, O. *Zeitschrift Fur Physik* **1922**, *9*, 353.

(14) Uhlenbeck. G.E.; Goudsmit. S. *Naturwissenschaften* **1925**, *13*, 953.

(15) Zavoisky, E. *Journal of physical Chemistry, U.S.S.R* **1945**, *9*, 211.

(16) Frenkel, J. *Journal of Physics -U.S.S.R* **1945**, *9*, 299.

(17) Cummerow, R. L.; Halliday, D. *Physical Review* **1946**, *70*, 433.

(18) Bagguley, D. M. S.; Griffiths, J. H. E. *Nature* **1947**, *160*, 532.

(19) Atherton, N. M. *ESR, Theory and Applications*; John Wiley and Sons, **1973**.

(20) Weil, J. A., Bolton, J.R., Wertz, J.E *Electron Paramagnetic Resonance: Elementary Theory and Practical Applications*; John Wiley and Sons, **1994**.

(21) Schweiger, A., Jeschke, G. *Principles of Pulse Electron Paramagnetic Resonance*; OUP: Oxford, **2001**.

(22) Giamello, E., Brustolon, M. *Electron Paramagnetic Resonance: A Practitioners Toolkit* Wiley **2009**.

(23) Mabbs, F. E., Collison.D *EPR of d Transition Metal Compounds, Studies in Inorganic Chemistry* Elsevier, **1992**; Vol. 16.

(24) Jenkins, C. A.; Murphy, D. M. *Journal of Physical Chemistry B* **1999**, *103*, 1019.

Chapter 4

Experimental details

4.1 Introduction

In this chapter details on the materials and reagents used in the thesis will be described; further experimental details on how these materials were handled will also be discussed.

4.2 TiO_2 samples

The polycrystalline TiO_2 sample used in this work is a mixed phase P25 powder (~ 80% anatase, 20% rutile) supplied by *Degussa*, which has a surface area of approximately 49 m^2g^{-1}. The morphology of P25 has been described elsewhere, and it is reported that plate like particles are present with the average particle size of ca. 40 nm.[1]

4.3 Apparatus

4.3.1 Vacuum line

The schematic representation of the vacuum line used for the treatment of powdered TiO_2 samples is shown in Figure 4.1. The line is constructed from 12 mm bore Pyrex glass tubing with Apiezon type T hydrocarbon grease used to seal all taps and non fused joints.

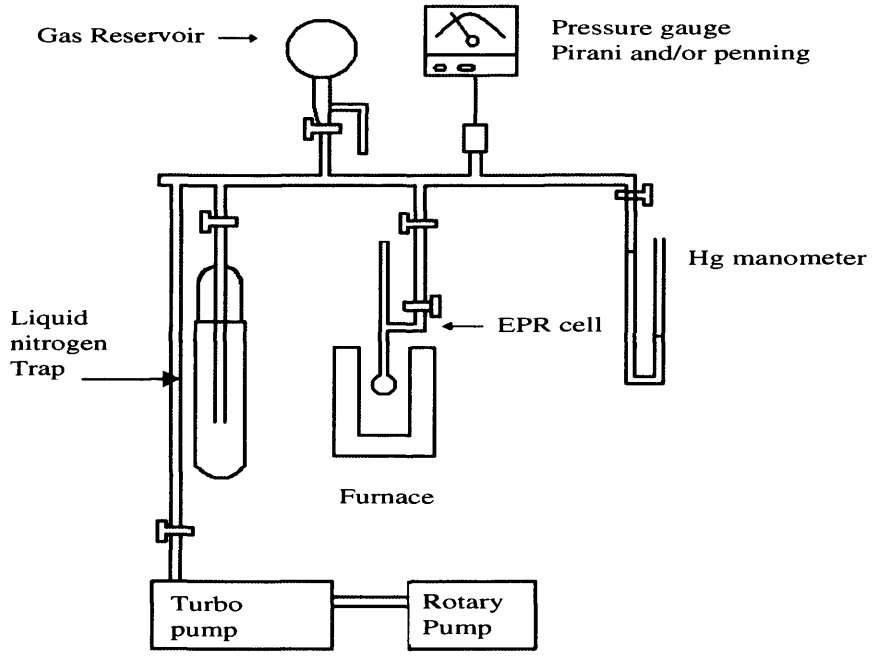

Figure 4.1 Schematic view of vacuum manifold used for sample preparation.

The line is connected to an Alcatel C1 series rotary vane pump and an Alcatel ATP80/100 turbo pump which can combine to reach base pressures of 10^{-5} Torr. The pressure measurements were made with an Alcatel ACS 100 pirani gauge. High temperature heat treatments of the samples were performed using an electric tube furnace, capable of maintaining temperatures between 323 and 1073K. Powder samples were heated in the bulb section of the EPR cell, and then transferred to the capillary section (4 mm bore) for EPR measurements. Gases can be added to the line from the reservoir and mixed in the line before exposure to the sample in the EPR cell.

4.3.2 EPR Spectrometer

All EPR spectra were recorded on a *Bruker EMX* spectrometer operating at X-band frequencies (~ 9.5 GHz), employing 100 kHz field modulation, 10 mW microwave power and fitted with a high sensitivity cavity (ER4119 HS). The spectrometer is equipped with a variable temperature unit to allow measurements to be performed at temperatures ranging from 120 to 298K. The g values were determined using a DPPH standard, and are accurate to ±0.001. EPR computer simulations were performed using the SimEPR32 program.[2]

4.3.3 Ultra Violet lamp

An *Oriel Instruments UV lamp* (model N° 66021) was used for all irradiations. The construction of the lamp is shown in Figure 4.2. The power output can be varied between 50 and 1000W.

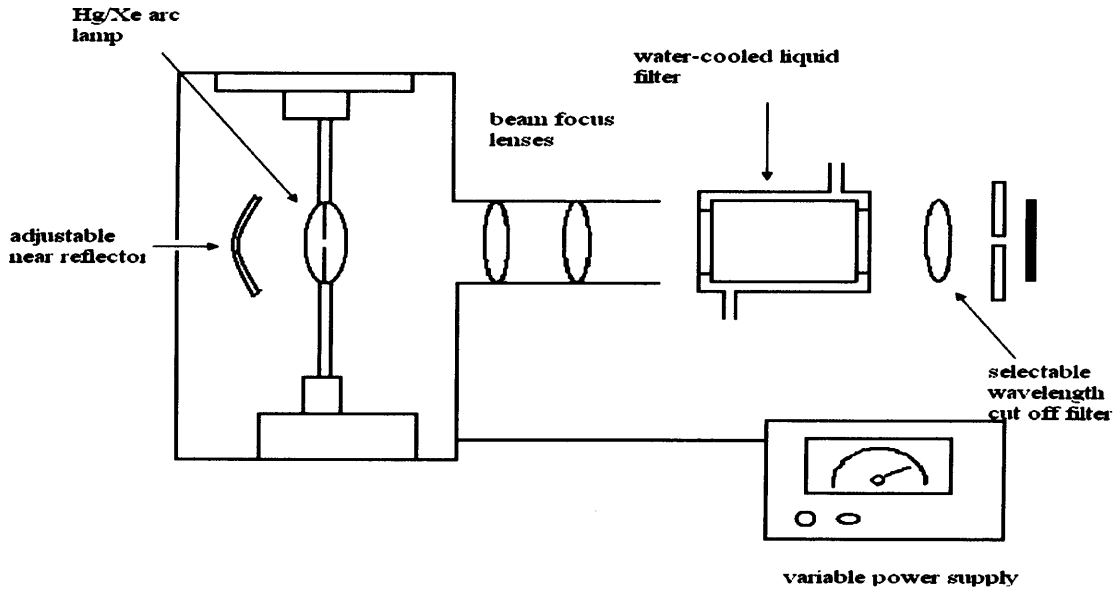

Figure 4.2 Construction of UV light source.

The Hg/Xe arc lamps used have a broad band spectral output from 250 nm to > 2500 nm; the UV output below 280 nm accounts for only 4 - 5% of the total lamp output. In all experiments, a water filter was used in order to absorb infrared frequencies and prevent sample heating by the UV beam.

Samples were treated on the vacuum line before irradiation *ex-situ* in a finger dewar at 77K to prevent sample heating. Following irradiation the samples were rapidly transferred to a precooled EPR cavity.

4.4 Methods

4.4.1 Reduction

The polycrystalline TiO_2 powder (*ca.* 10 mg) was placed in the bulb portion of the EPR cell. The bulb portion of the cell was heated to 423K under dynamic vacuum (10^{-4} Torr) and left overnight to remove any physisorbed water from the surface. The furnace temperature was raised over a period of 5 hours to a final temperature of 773K and left at this temperature for 1 hour. This produced a non-stoichiometric sample that was blue in colour due to the excess number of Ti^{3+} centres, and shall hereafter be referred to as a *reduced* sample.

4.4.2 Oxidation

A reduced sample of polycrystalline TiO_2 was prepared by repeating the method in 4.4.1 above. The sample was exposed to excess oxygen (50 Torr, *via* vacuum manifold) at 773K, and left under this pressure at the same temperature for one hour. Subsequently the sample was cooled to room temperature under the oxygen atmosphere, before evacuation of the excess oxygen at 298K. This treatment produced a clean oxidised surface, almost completely free of any surface hydroxyl groups. Oxygen exposure at 773K resulted in the formation of diamagnetic surface O^{2-} lattice anions, and therefore produced a clean reoxidised stoichiometric surface; hereafter this sample is referred to as the *activated* sample.

4.4.3 Freeze-pump thaw purification

To freeze pump thaw the desired liquid a small amount of liquid was placed into an empty quartz EPR cell. The sample tube was then frozen by placing into liquid nitrogen. Following this the cell was opened to the vacuum line until the base pressure

was achieved. The cell was then closed to the vacuum line; the sample was carefully thawed, allowing the impurities in the liquid to bubble to the surface.

The procedure was repeated (three or four times) until the liquid became deoxygenated. The deoxygenated liquid was then added to the sample by closing the vacuum line to the pump and opening both cells to the line.

4.4.4 Hydration of TiO_2

Following activation of the polycrystalline TiO_2 surface (as described in 4.4.2), the vapours of triply distilled water (10 Torr) were added to an activated sample, and left at 673K for 1 hour. The sample was subsequently cooled to 298K before evacuation for 30 minutes to remove any physisorbed water molecules. This sample hereafter will be referred to as a *fully hydrated* surface.

4.5 Addition of probe gases

4.5.1 Addition to a reduced surface

The chosen probe gas (CO_2, O_2 and Ar) was admitted to the vacuum manifold from the gas reservoir as shown in Figure 4.1. The probe gas was then exposed to the *reduced* sample at room temperature for 10 minutes, followed by evacuation for 10 minutes or addition of a second gas as explained in 4.5.2.

4.5.2 Sequential adsorption to a reduced surface

In this case, a probe gas (Ar or CO_2) was admitted to the EPR sample cell (*ca.* 10 minutes), while still under the probe gas atmosphere a dose of molecular oxygen (10 Torr) was admitted. The oxygen was allowed to react with the surface, and the cell was evacuated at RT before EPR measurements.

4.5.3 Co-adsorption of mixtures of gases to a reduced surface

The various ratios of chosen gases (CO_2/O_2, Ar/O_2) were mixed in the vacuum manifold prior to exposure to the sample (ca. 10 minutes) before subsequent treatments. In the case of CO_2/O_2 or Ar/O_2 the excess gas was evacuated at room temperature prior to EPR measurements.

4.6 Addition of Organic substrates

4.6.1 Addition of organic substrates to O_2^-

The pre-prepared samples were cooled to 77K before addition of the chosen organic (substrate) at this temperature. Thereafter the sample was annealed to a series of elevated temperatures (200-260K) for a period of 10 minutes at each temperature. The annealed sample was then fully cooled to 130K to record the EPR spectrum.

4.6.2 Addition of organic substrate: O_2 mixtures

Activated samples of P25 TiO_2 were exposed at 298K to the following organics (in a gaseous state) mixed with oxygen from the vacuum manifold: acetonitrile: O_2, methanol: O_2 and toluene: O_2. The organic to O_2 ratio (i.e., organic: O_2) was ~10:1 in all experiments. The final pressure of gas admitted to the EPR cell was dependent on the room temperature vapour pressures of the particular organic substrate (acetonitrile: O_2 = 70 Torr final pressure; methanol: O_2 = 98 Torr; toluene: O_2 = 22 Torr). Small volumes of the organics were held in the bulb section of an EPR cell and were purified *via* the freeze-pump-thaw technique before expansion into the vacuum manifold. In all cases, the organic pressure was in excess over oxygen during the photolysis experiments. The samples containing the co-adsorbed gases were then irradiated at 77K for a period of 30 minutes before rapid transfer to the pre-cooled EPR cavity, where the spectra were recorded at 130K.

4.7 Materials

4.7.1 Gases

All gases were supplied by *Argo International* (unless stated) and were of extremely high purity (which will be stated for each individual gas). The gases were added to the sample *via* the vacuum line at room temperature. The volume of gas used is stated in each case and was measured using the mercury manometer attached to the vacuum line. *Icon Services Inc.* (New Jersey) supplied the ^{17}O-labelled dioxygen gas (63% enrichment) and was used without further purification.

4.7.2 Liquids

All reagents used were of analytical grade and supplied by *Aldrich Chemical Ltd.* Further purification was not therefore employed except for the deoxygenation of liquid, performed when required by the freeze pump thaw method described in 4.4.3.

Triply distilled water was used in hydration experiments, and was also subjected to repeated freeze pump thaw steps prior to use.

4.8 References

(1) Martra, G. *Applied Catalysis A-General* **2000**, *200*, 275.

(2) Spalek, T.; Pietrzyk, P.; Sojka, Z. *Journal of Chemical Information and Modeling* **2005**, *45*, 18.

Chapter 5

Site specific blocking of oxygen vacancies on reduced TiO_2 by probe molecules

5.1 Introduction

Since the pioneering work of Fujishima and Honda on the photoassisted splitting of water over TiO_2[1], an explosion of interest and development in the applications of titania, ranging from sterilization[2] and solar energy conversion[3,4] to pollution control[4] and fuel cells[5], has occurred (Chapter 1). In most of these applications a host of possible photochemical, chemical and electrochemical reactions occur at the surface, the rates of which are often dependent on a host of other factors that are still poorly understood.[6,7]

One of the more active fields of titania research is photocatalysis. In this application light induced charge separated pairs (electrons and holes) are used to drive surface reduction and oxidation reactions as efficiently as possible. The emphasis in recent years has therefore focussed on visible light induced photocatalysis by modification (such as doping with metal and non-metal impurities, coupling with narrow band-gap semiconductors, and preparing oxygen deficient materials) or sensitisation (such as anchoring dyes of oxides on the surface) of TiO_2.[8]

Regardless of the approach adopted to improve photocatalysis, the activity will depend not only on the charge carrier formation, lifetimes and separation, but also on their utilisation at the interface, since certain surface planes are known to be more active than others.[9,10] Fundamental to this utilisation step is the electron transfer (ET) event occurring at the interface, and this too is dependent on surface morphology. Quite often the excess electrons generated in the TiO_2 semiconductor during photocatalysis can be easily delocalised through the conduction band, but they can also become readily localised at bulk and surface Ti^{4+} cations to give surface Ti^{3+} centres. These Ti^{3+}_{surf} centres in particular act as important electron conduits in photocatalysis, and the efficiency of this ET step may be intimately linked to the co-ordination and location of the Ti^{3+}. For thermally reduced TiO_2, an abundance of Ti^{3+}_{surf} centres are easily generated in tandem with surface oxygen vacancies. These reduced surfaces become ideal model systems to investigate the role of localised electron states and oxygen vacancies in the formation and stabilisation of reactive oxygen species of importance to photocatalysis.

Carter *et al.*,[11] have recently investigated the nature of various oxygen centred radicals formed over the mixed phase TiO_2 material (Degussa P25). While a series of transient organoperoxy radicals were identified in the photocatalytic oxidation of organic substrates[12-14], stable oxygen centred radicals such as O_2^- can be easily formed and conveniently studied by Electron Paramagnetic Resonance (EPR).[11] Among the many surface sites available for O_2^- stabilization on P25, one site in particular was found to be unusual in terms of its stability and reactivity compared to the radicals at other surface sites. This unusual site was assigned to an O_2^- radical adsorbed at an oxygen vacancy defect on the anatase surface, labelled [Vac...O_2^-].[11] These O_2^- radicals provide an indirect means of interrogating the Ti^{3+}_{surf} centres, which in turn provides information on the important ET sites on the TiO_2 surface. The results in this chapter will demonstrate how ET from these sites to O_2 can be selectively blocked using appropriate probe molecules (CO_2 and Ar). These findings have important implications in the field of photocatalysis, revealing not only the competitive behaviour of co-adsorbed gases for surface sites, but also how the selective blocking of these key sites may prevent important ET events from occurring under reaction conditions.

5.2 Experimental

Full experimental details are given in Chapter 4; however the key steps are briefly summarised here. The P25 was thermally reduced at 773K under vacuum to produce the reduced sample, before addition of either (i) O_2 (ii) CO_2/O_2 or (iii) Ar/O_2 at room temperature for 15 minutes, followed by evacuation at this temperature. The mixture of gases were added *via* two alternative methods namely *co-adsorption,* where both gases (either CO_2/O_2 or Ar/O_2) were premixed in the vacuum manifold before addition, or *sequential adsorption,* where CO_2 or Ar were first admitted to the sample cell followed by molecular oxygen.

5.3 Results

5.3.1 Formation of O_2^- on P25 TiO_2 by thermal treatment and photolysis.

A sample of P25 TiO_2 was annealed under vacuum at 773K producing a blue coloured sample. The corresponding EPR signal is shown in Figure 5.1a. The EPR signal is characteristic of Ti^{3+} centres which have been extensively studied and discussed in detail in the literature.[15,16] The pertinent detail to note here is that this signal contains contributions from both bulk and surface Ti^{3+} centres. The EPR signal

resulting from the Ti^{3+} is also broad due to the heterogeneous nature of the TiO_2 surface so that it is impossible to distinguish between specific Ti^{3+} co-ordination centres. The additional isotropic signal at g = 2.003 is assigned to medium polarised conduction electrons as has been described elsewhere in the literature[17,18] and so will not be discussed in detail here.

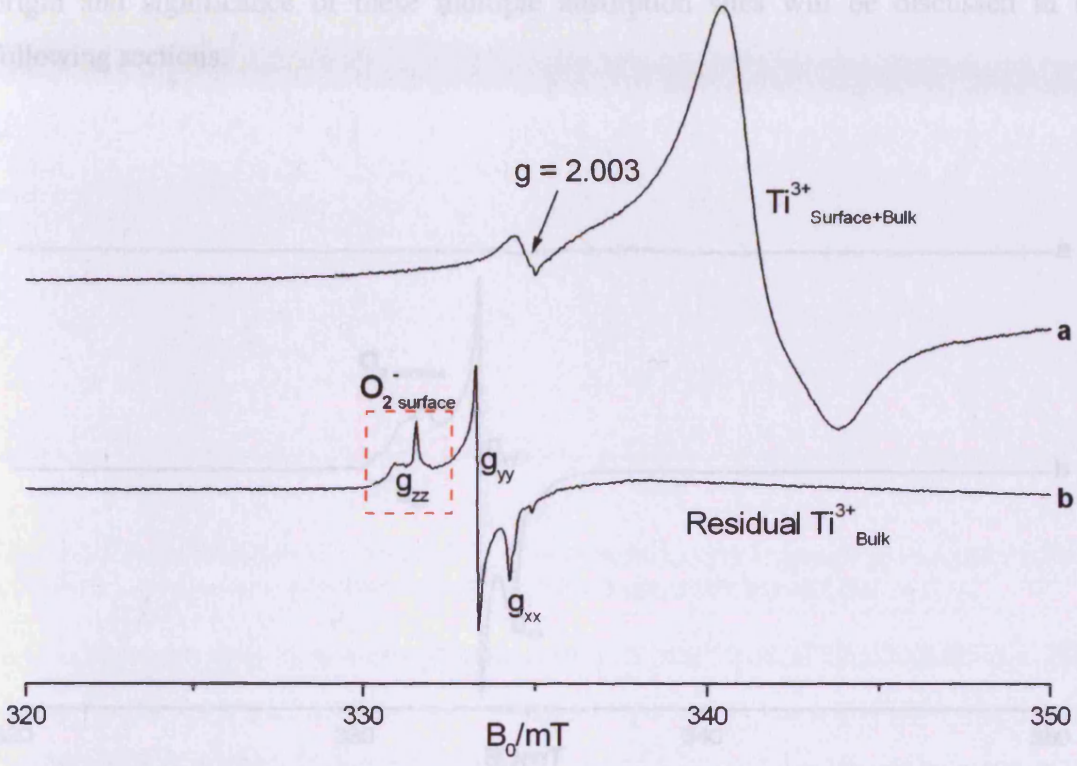

Figure 5.1 *cw*-EPR spectra (130K) of P25 TiO_2 after (a) thermal reduction at 773K for 1 hour and (b) after addition of molecular oxygen (10 Torr) at 298K.

Upon exposure of $^{16}O_2$ at 298K to the previously prepared reduced sample, the EPR signal due to the Ti^{3+} surface cations disappears immediately and a new EPR signal is observed (Figure 5.1b). A low intensity signal due to unreacted (residual) bulk Ti^{3+} is also weakly resolved. The new orthorhombic EPR signal with g values of g_{xx} = 2.005, g_{yy} = 2.011, and g_{zz} = 2.019, 2.020, 2.023 and 2.026 can be assigned to the surface stabilised superoxide radical, O_2^-.[19] In this case the O_2^- is formed *via* electron transfer from the Ti^{3+} centres, produced *via* thermal reduction, to the adsorbed O_2.

An alternative method of generating O_2^- is *via* UV irradiation of a TiO_2 surface under an oxygen atmosphere (Figure 5.2). UV irradiation of the clean oxidised TiO_2 results in the generation of electrons and holes and in the presence of oxygen the electrons are scavenged, resulting in the formation of the surface superoxide radical (Figure 5.2b).

The superoxide radicals generated under both conditions (by thermal treatment in Figure 5.1, and by photolysis, shown in Figure 5.2) are essentially the same and each shares the same g_{yy} and g_{xx} values. However they can be distinguished by slight differences in their complex g_{zz} regions which are characterised by a distribution of peaks representative of multiple adsorption sites on the titanium dioxide surface. The origin and significance of these multiple adsorption sites will be discussed in the following sections.

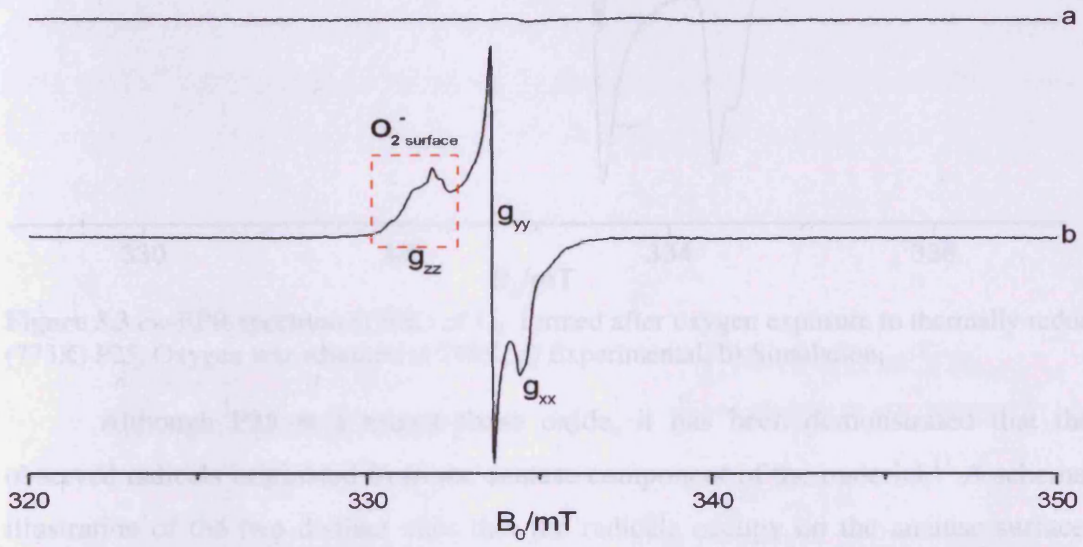

Figure 5.2 *cw*-EPR spectra (130K) of P25 TiO_2 after a) reoxidation at 773K and, b) UV irradiation under a molecular oxygen atmosphere at 77K followed by evacuation at RT.

5.3.2 Formation of O_2^- on P25 TiO_2; stabilization at vacancy and non-vacancy sites

As previously mentioned, a multitude of peaks can be observed in the g_{zz} region. For clarity these are shown in Figure 5.3a. These reflect the diversity of different adsorption sites on the TiO_2 surface; this will be thoroughly explained and discussed in section 5.4.1. The corresponding computer simulation of the experimental EPR spectrum is also given in Figure 5.3b. At least three distinct g_{zz} peaks can be clearly resolved in Figure 5.3, hereafter labelled sites I-III. Closer analysis of the spectrum, by computer simulation, reveals an additional minor site labelled II' (Table 5.1). To simplify the discussion, these sites will be broadly classified as site I type (which has been attributed to O_2^- stabilised at oxygen vacancies, labelled [Vac…O_2^-])[11] and sites II-III type (which have been attributed to O_2^- anions adsorbed at non vacancy sites on five co-ordinate Ti^{4+} centres).[11]

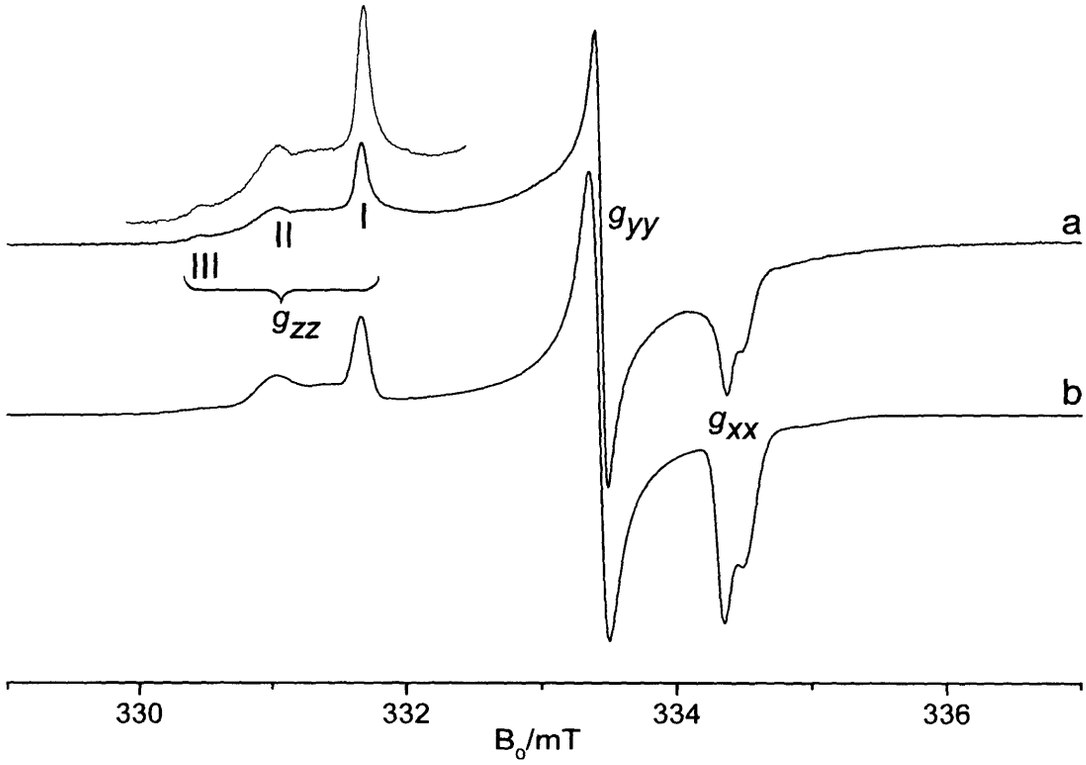

Figure 5.3 *cw*-EPR spectrum (130K) of O_2^- formed after oxygen exposure to thermally reduced (773K) P25. Oxygen was admitted at 298K. a) Experimental, b) Simulation.

Although P25 is a mixed-phase oxide, it has been demonstrated that these observed radicals originated from the anatase component of the material.[11] A schematic illustration of the two distinct sites that the radicals occupy on the anatase surface is shown in Figure 5.4.[20] The key properties of the radicals at this [Vac....O_2^-] site I were:

- Under low temperature photoirradiation, site I selectively decayed in intensity compared to sites II-III;
- Site I selectively decayed after warming to increased temperatures under dynamic vacuum;
- From studying the ^{17}O data it was found that the O_2^- at site I possessed equivalent oxygen atoms.
- displayed higher reactivity with organic substrates.[11,13]

By comparison, the O_2^- anions on five co-ordinate centres were also bound in a side-on manner, but were non photo-labile, were thermally stable, and displayed relatively poor reactivity with organic substrates.

Table 5.1; Spin Hamiltonian parameters for O_2^- radicals adsorbed on thermally reduced TiO_2 (P25). The ^{17O}A values are taken from ref [13].

Site	g_{xx}	g_{yy}	g_{zz}	A_{xx}/ mT	A_{yy}/ mT	A_{zz}/ mT	% Cont.
I	2.005	2.011	2.019	7.64	<1	<1	43
II'	2.004	2.011	2.020	7.86	<1	<1	16
II	2.004	2.011	2.023				36
III	2.001	2.011	2.026	7.97	<1	<1	5

As the physiochemical properties of these two groups of superoxide radical are so different, it is reasonable to postulate that initial electron transfer (ET) from the different Ti^{3+} centres may be prevented by blocking the sites using a suitable choice of adsorbate. As a result the following section describes how this can occur using CO_2/O_2 and Ar/O_2.

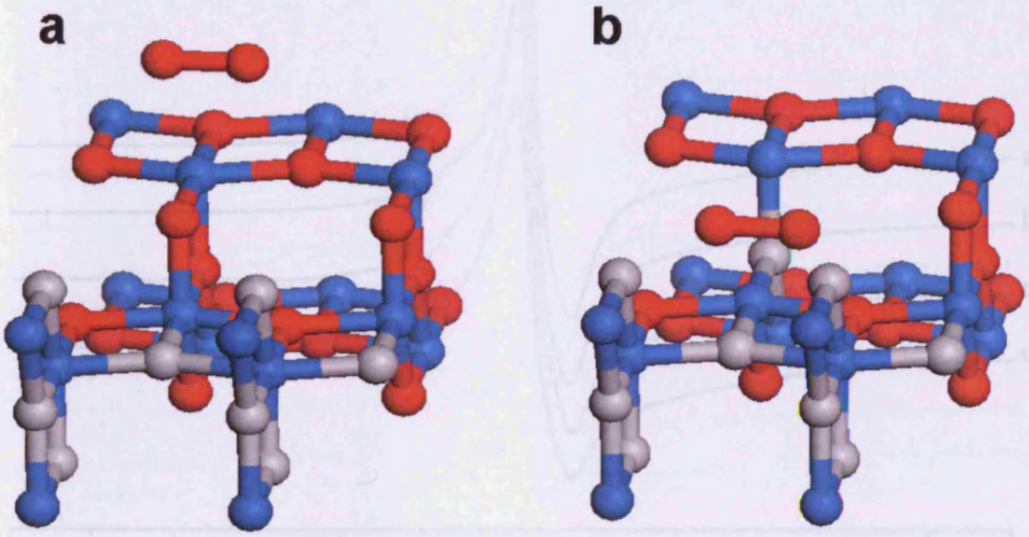

Figure 5.4: Schematic illustration of the two families of O_2^- anions on the P25 surface. (a) represents sites II – III based on non-vacancy 5-coordinate Ti centres, and (b) represents the site I type due to [Vac…O_2^-]. Atom colours: Ti: blue, O: red (O in foreground grey for clarity). Removal of the oxygen atom in a) leaves the vacancy shown in b).[20]

5.3.3 CO_2/O_2 adsorption; specific blocking of non-vacancy sites.

The competitive interaction of CO_2 and O_2 with the reduced TiO_2 surface was investigated using two methods; in the first one a co-adsorption methodology was adopted, while in the second case a sequential approach was adopted (see experimental). As will be seen later, even though the CO_2 does not react directly with Ti^{3+} surface centres, the aim of the experiment was to explore whether the CO_2 could effectively

block the Ti^{3+} centres and therefore prevent ET to O_2 forming O_2^-. If this is the situation, does the manner in which the CO_2 is admitted to the sample affect the outcome?

5.3.3.1 Interaction of CO_2 only with the reduced TiO_2 surface

To the thermally reduced surface, a chosen pressure of CO_2 (increasing in pressure from 0.5- 10 Torr as shown in Figure 5.5a-d) was added at 298K. Upon CO_2 addition no change was observed in the EPR spectrum of the Ti^{3+} centres, indicating that there is no reactivity with CO_2 (see Figure 5.5a-d). Evacuation of the CO_2 (at 298K), and subsequent addition of molecular oxygen resulted in the formation of O_2^- anions, with an identical spectral profile to that shown in Figure 5.3. In other words, all $Ti^{3+}_{surface}$ centres are available for O_2 reduction, following the removal of the weakly adsorbed CO_2 by evacuation prior to O_2 addition.

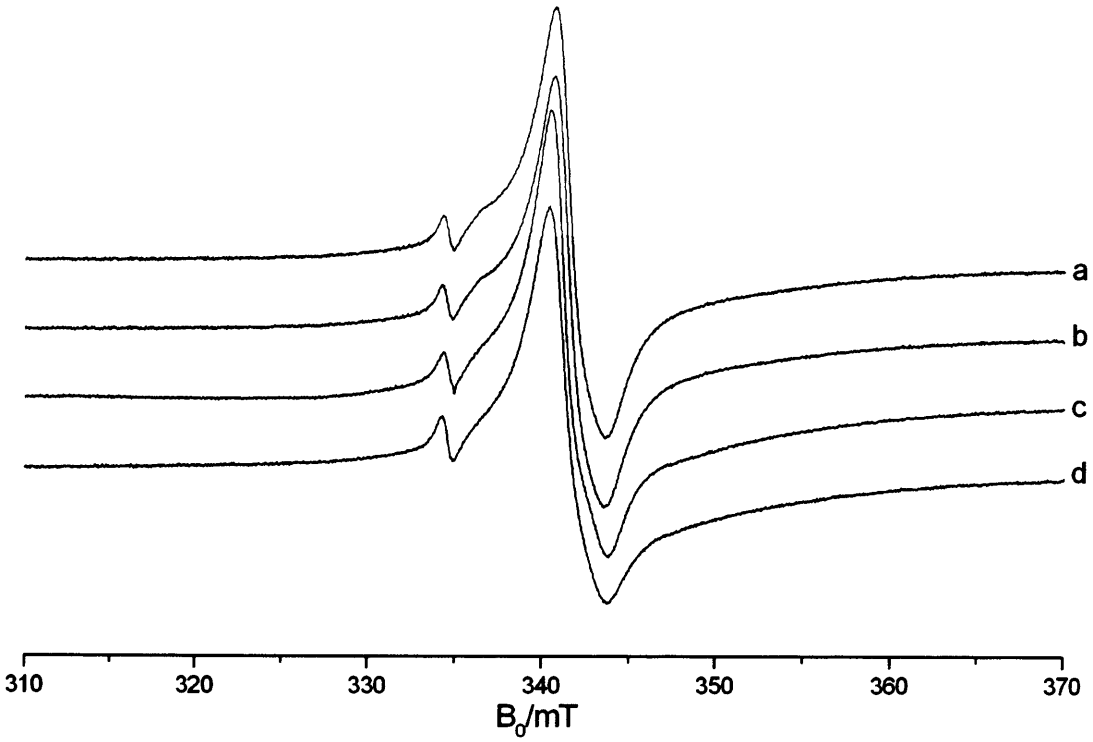

Figure 5.5: *cw*-EPR spectra (120K) of P25 TiO_2 a) after thermal reduction (773K) and after addition of b) 0.5 Torr c) 5 Torr and d) 10 Torr CO_2 at 298K.

5.3.3.2 Co-adsorption of CO_2/O_2

As shown previously in Figure 5.1, addition of molecular oxygen to a reduced surface resulted in the loss of the Ti^{3+} EPR signal, which was replaced by the characteristic EPR signal of O_2^- on P25 TiO_2 as shown in Figure 5.3. The addition of CO_2 to a reduced TiO_2 surface followed by evacuation, and subsequent addition of oxygen results in an unchanged O_2^- profile as seen in Figure 5.3.

The co-adsorption of CO_2/O_2 to the reduced surface does however result in a change to the profile of the resultant O_2^- EPR spectra (Figure 5.6). In particular a notable redistribution of the relative peak intensities in the g_{zz} region can be seen as a function of the CO_2 pressure (see Figure 5.6a-g for comparison). As the CO_2 pressure increases (i.e. the CO_2/O_2 ratio increases), the intensity of the g_{zz} peaks arising from sites II-III characterised by the g_{zz} components at g_{zz} = 2.021-2.026 decrease dramatically, until they are virtually absent in Figure 5.6g. By comparison, the g_{zz} peak at 2.019, corresponding to the vacancy site I, remains largely unperturbed. It should be noted that at high CO_2 pressures (> 2 Torr), the overall integrated signal intensity of the entire O_2^- spectrum begins to decrease, as expected with excess CO_2 on the surface. Nevertheless the loss of signal intensity at site I is substantially less compared to the loss of sites II-III in the low pressure regime (< 2 Torr).

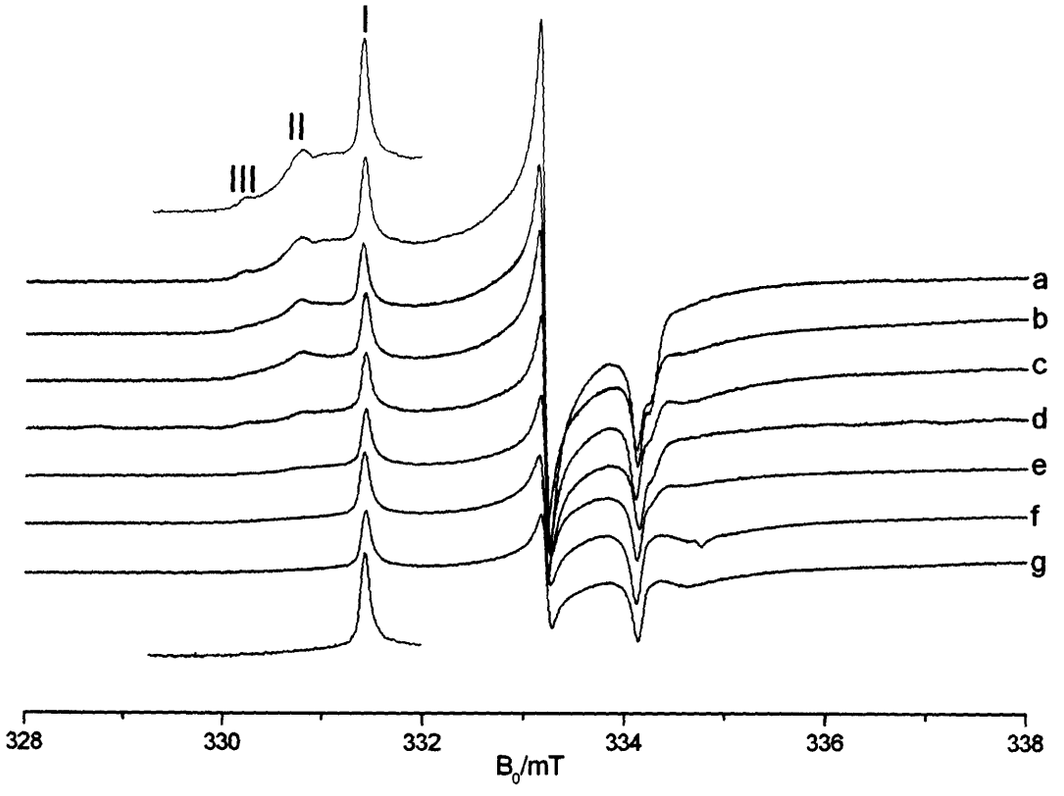

Figure 5.6: *cw*-EPR spectra (120K) of superoxide radicals (O_2^-) formed after CO_2:O_2 (co-adsorbed) exposure to thermally reduced (773K) P25, showing the effects of increasing CO_2 pressure. The ratios of CO_2:O_2 were a) 0.0:1, b) 0.006:1, c) 0.03:1, d) 0.05:1, e) 0.06:1, f) 0.33:1 and g) 0.66:1. The total pressure in the cell was maintained at 15 Torr throughout. Gases were admitted at 298K, followed by evacuation after 10 minutes of exposure.

The individual contributions of site I and sites II-III to the overall O_2^- integrated signal intensity in each individual spectrum in Figure 5.6 were determined by simulation. An example of this process is shown in Figure 5.7a-e. The experimental and

complete simulated spectra are shown in Figure 5.7a and 5.7b respectively. The complete simulation in Figure 5.7b is obtained using the summed contributions from the individual sites (I-III, Figure 5.7c-e). In the case below, Figure 5.7b consists of the summed contribution of 70% from site I, 24% from site II and 6% from site III.

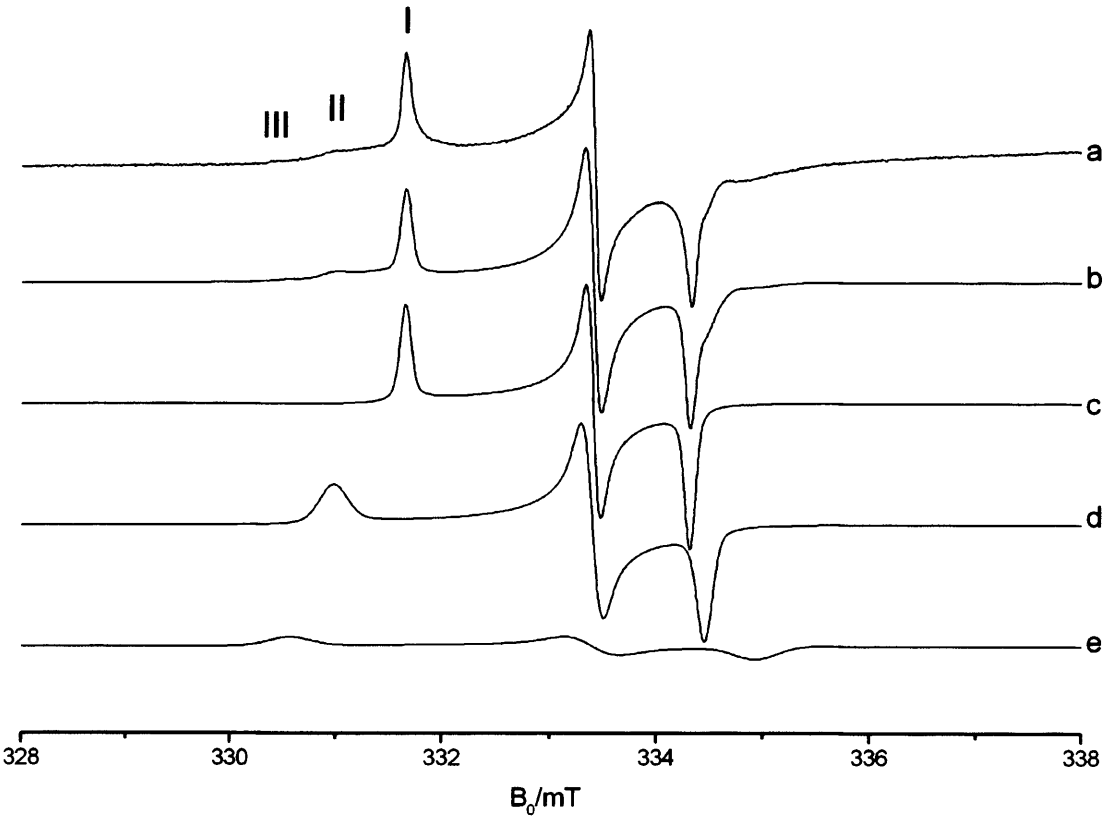

Figure 5.7 *cw*-EPR spectrum (130K) of O_2^- formed after a mixture of CO_2/O_2 was exposed to thermally reduced sample (773K) P25 TiO_2. a) Experimental, and simulations of b) complete, c) site I, d) site II, and e) site III. The complete simulation (b) was obtained using the summed contributions of 70% from Site I (c), 24% from Site II (d) and 6% from site III (e).

Extraction of the relative contribution for the sites I-III enabled the trends in Figure 5.6 to be clearly visualised. The relative signal intensities of the O_2^- species attributed to site I and sites II-III are plotted as a function of CO_2 pressure in Figure 5.8. The figure clearly shows that upon increasing CO_2 pressure the relative signal intensity of sites II-III decreases significantly, while the relative signal intensity of site I remains constant at pressures < 2 Torr. As the pressure of CO_2 gas is increased (> 2 Torr) a global decrease is observed (see inset Figure 5.8) and the relative signal intensity of all sites decreases.

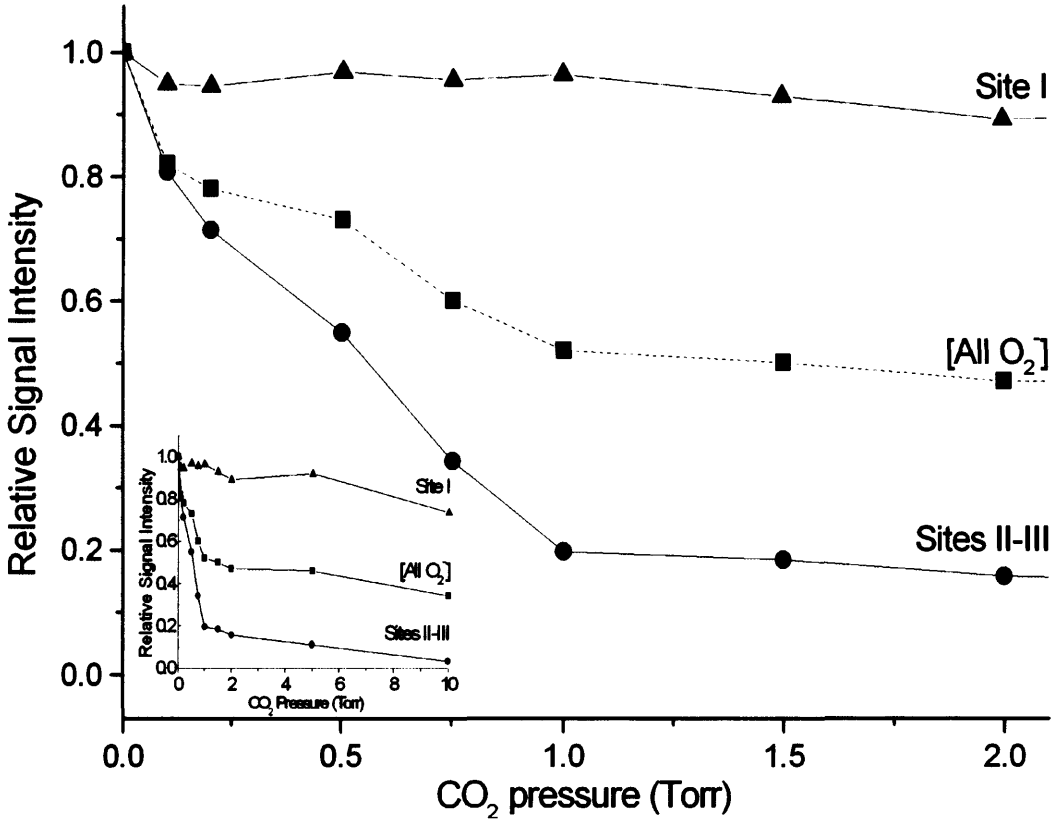

Figure 5.8: Variation in the relative EPR signal intensities of adsorbed O_2^- versus CO_2 pressure, in a CO_2:O_2 (co-adsorbed) gas mixture. The relative intensities of sites I, II & III were determined by simulation of the spectra. The relative integrated intensity of the entire superoxide spectrum (including all three contributing sites) is labelled [All O_2^-].

In summary, the EPR evidence for a co-adsorbed mix of CO_2/O_2 on thermally reduced TiO_2 demonstrates clearly the divergent perturbations caused by CO_2 on the two families of adsorbed O_2^- anions on the P25 TiO_2 surface; namely no blocking of the vacancy (site I) and selective blocking of the non-vacancy (sites II-III) adsorption sites at low pressures (< 2 Torr). On moving to higher pressures (> 2 Torr) there is a global decrease in the O_2^- signal intensity as the CO_2 begins to saturate the surface.

5.3.3.3 Sequential adsorption of CO_2/O_2

The previous experiment was repeated under sequential CO_2/O_2 adsorption conditions. In this case the CO_2 was first exposed to the reduced sample for 10 minutes, followed by subsequent admission of oxygen. The resulting EPR spectra (Figure 5.9) display identical trends to those shown in Figure 5.6. That is, on increasing the pressure of CO_2 there is a redistribution of the relative peak intensities in the g_{zz} region. On moving from Figure 5.9a-h, the relative intensity of the peaks resulting from sites II-III, decrease substantially compared to site I on increasing the pressures of CO_2 in the CO_2/O_2 ratio (where CO_2 < 2 Torr). However, at ratios where the CO_2 pressure is

greater than 2 Torr, there is a global decrease in signal intensity where all sites are blocked by CO_2. The sequential results confirm that sites II-III are blocked selectively compared to site I, indicating specific site blocking also occurs under these conditions.

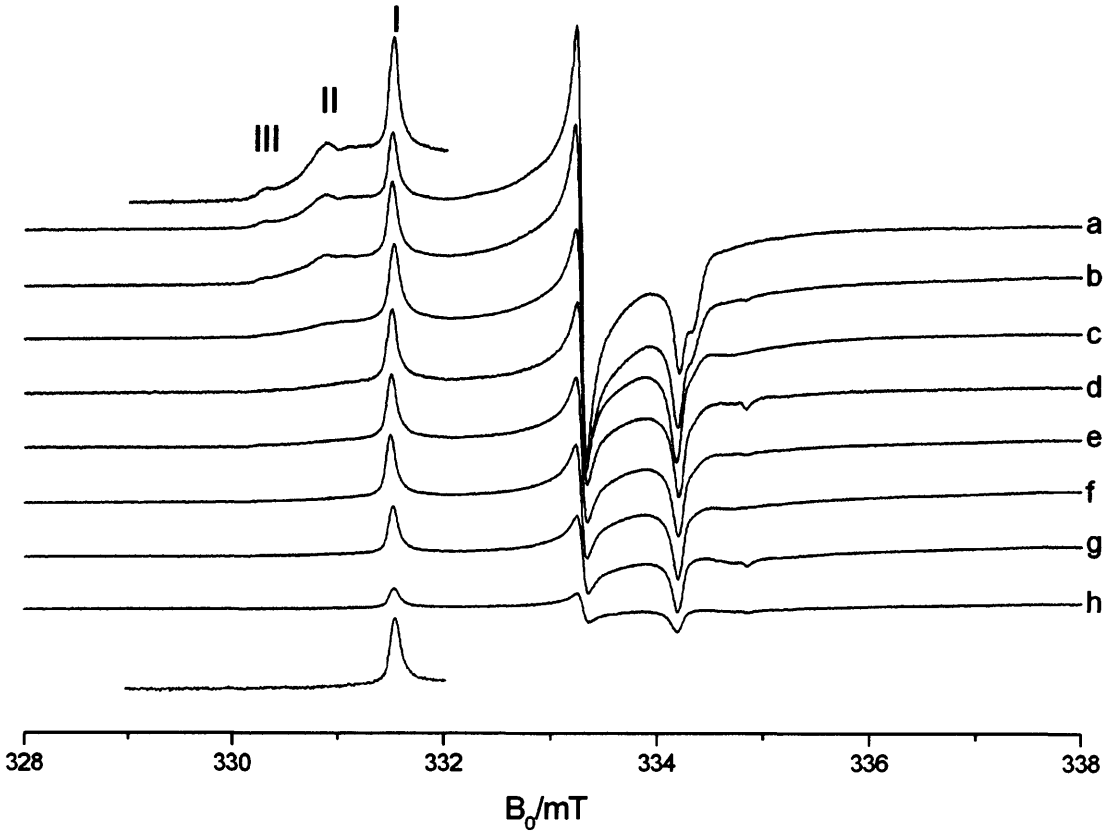

Figure 5.9: *cw*-EPR spectra (130K) of O_2^- formed after CO_2:O_2 exposure (sequential) to thermally reduced (773K) P25, showing the effects of increasing CO_2 pressure. The ratios of CO_2:O_2 were a) 0.0:1, b) 0.0006:1, c) 0.006:1, d) 0.03:1, e) 0.06:1, f) 0.33:1, g) 0.66:1 and h) 6.6:1. The total pressure in the cell was maintained at 15 Torr throughout. Gases were admitted at 298K, followed by evacuation after 10 minutes of exposure.

5.3.3.4 Behaviour of the Ti^{3+} signal on CO_2 adsorption

Further confirmation of the blocking of surface sites by CO_2 was also obtained by analysis of the Ti^{3+} signal itself, rather than the O_2^- signal. In principle the changes to the integrated signal intensity of O_2^- versus Ti^{3+} could be compared. However a direct comparison is difficult for a number of reasons: (i) the relaxation characteristics of both species are very different; (ii) the Ti^{3+} signal is actually a composite of bulk and surface centres, and (iii) the high abundance of $Ti^{3+}_{surface}$ centres leads to spin broadened signals. Nevertheless, changes in the relative trends in [Ti^{3+}] and [O_2^-] signal intensities can be compared.

As shown in Figure 5.10, upon addition of O_2 to a pre-reduced surface most of the initial Ti^{3+} signal is lost. In this case all available $Ti^{3+}_{surface}$ centres react with surface

adsorbed O_2 to form O_2^-, leaving only the residual (unreacted) bulk Ti^{3+} signal (Figure 5.10b).

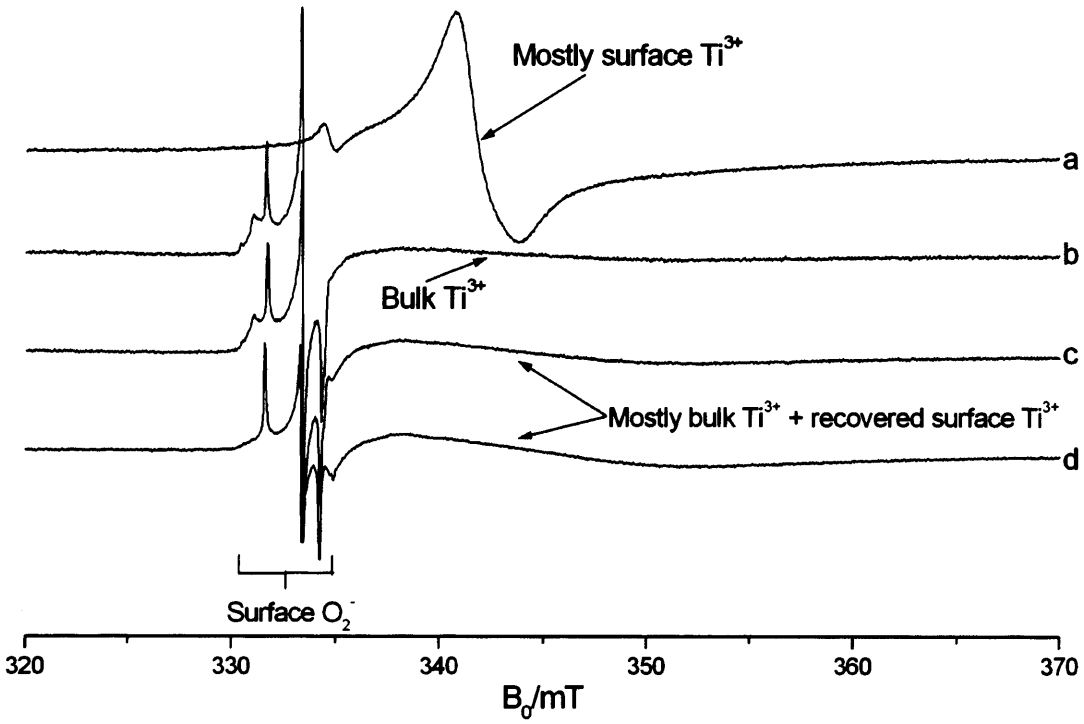

Figure 5.10 *cw*-EPR spectra (130K) of a) thermally reduced (773K) P25; and O_2^- formed after exposure of the following to the thermally reduced P25 (b) O_2, (c) CO_2:O_2 (0.033:1, co-adsorbed) and (d) CO_2:O_2 (0.33:1, co-adsorbed).

However, as the CO_2 ratio in a co-adsorbed mixture increases, the amount of residual $Ti^{3+}_{surface}$ centres also increases. This is just perceptible in the spectra 5.10c and 5.10d compared to 5.10b as shown in Figure 5.10. This confirms that the CO_2 simply blocks certain $Ti^{3+}_{surface}$ sites. Removal of CO_2 (i.e. during the evacuation procedure) should then re-expose these previously blocked Ti^{3+} surface centres, and produce more O_2^- in the presence of molecular oxygen. To confirm this, a second dose of oxygen was readmitted to the EPR cell. The O_2^- signal intensity recovered to that expected of O_2^- in the absence of CO_2, and simultaneously the Ti^{3+} surface signal diminished in intensity (Figure 5.11a-b). The values displayed in Figure 5.11 were obtained by double integration of the signal arising from the Ti^{3+} centres. In other words, the Ti^{3+} surface sites initially blocked by CO_2 are fully recovered following CO_2 evacuation. The remaining Ti^{3+} signal observed following the second dose of oxygen is due to bulk centres, which are unavailable for surface adsorption.

To conclude, on addition of a mix of CO_2/O_2 either sequentially or *via* co-adsorption, one can observe *via* EPR the divergent effects that CO_2 has on the surface of

P25 TiO_2, which in turn affects the two families of adsorbed O_2^- anions formed on the surface. As the CO_2 pressure is increased there is a selective blocking of the non-vacancy sites (Sites II-III) and no blocking of the vacancy (Site I). The effect of the variation in CO_2 pressure is also manifested in the Ti^{3+} signal that is observable by EPR.

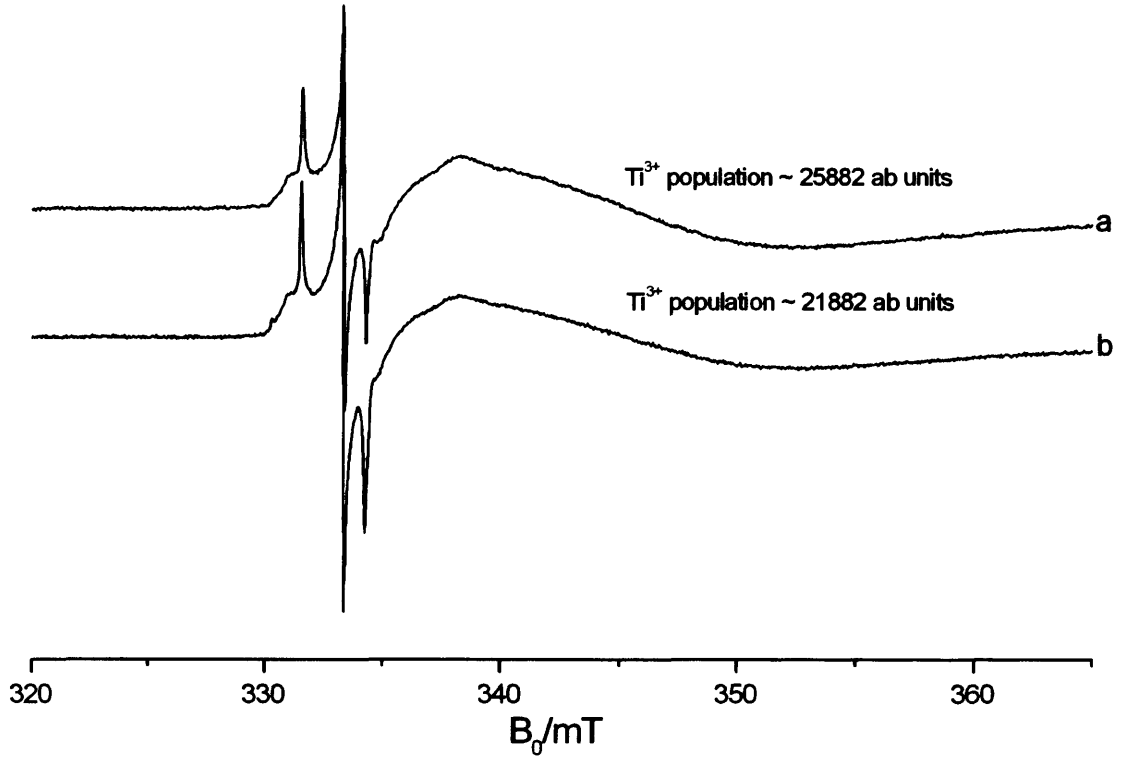

Figure 5.11: *cw*-EPR spectra of O_2^- formed after a) CO_2:O_2 (0.66:1, co-adsorbed) exposure to thermally reduced (773K) P25, and b) after the second addition of O_2 at 298K. The Ti^{3+} population is calculated by double integration of the Ti^{3+} signal.

5.3.4 *Ar/O_2 adsorption: specific blocking of the vacancy site*

5.3.4.1 Interaction of argon only with the reduced TiO_2 surface

A parallel set of experiments as described above for CO_2/O_2 were also performed using Ar/O_2. Although the interaction of Ar with TiO_2 is expected to be significantly weaker compared to CO_2, the Ar atom has approximately similar dimensions compared to that of the oxygen vacancy, and so was considered a suitable candidate to specifically probe the vacancy sites. It should be noted that the initial exposure of Ar to the reduced TiO_2 surface caused an increase in the Ti^{3+} EPR signal intensity (by a factor of 2; see Figure 5.12). It is postulated that the high charge density of the Ti^{3+} sites coupled with the strongly polarisable electron cloud of Ar causes a partial quenching of the spin-spin broadening at these sites.

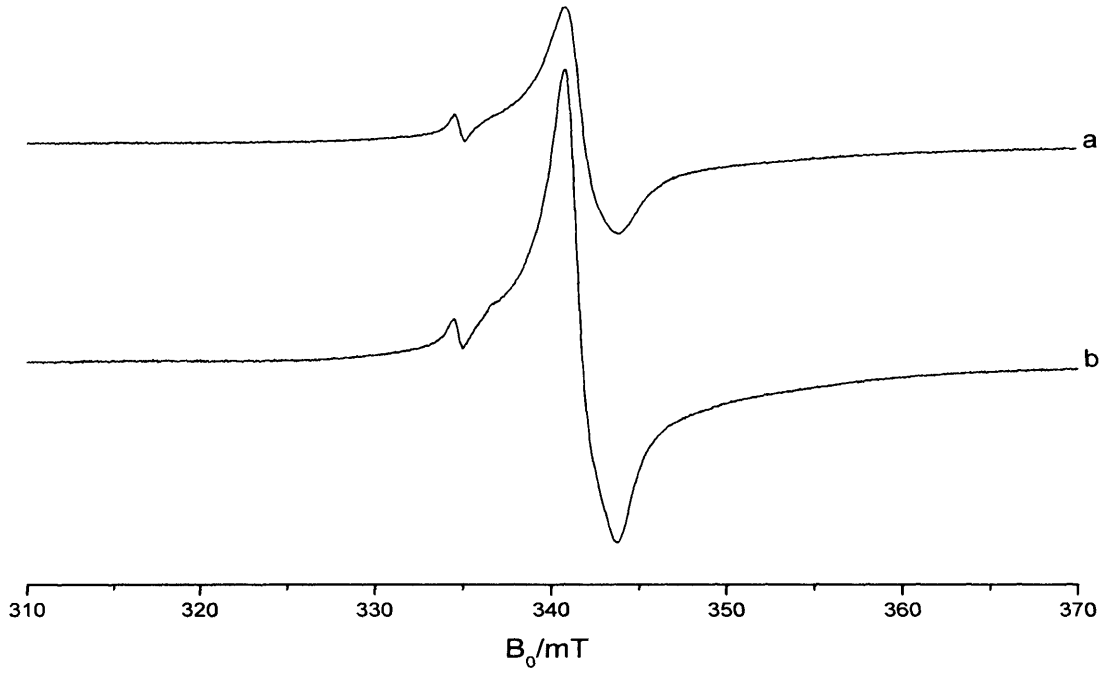

Figure 5.12: *cw*-EPR (120K) spectra of a) Ti^{3+} centres formed after thermal reduction (773K) of P25, and b) after addition of argon (10 Torr) to the Ti^{3+} centres.

5.3.4.2 Co-adsorption of Ar/O_2

The Ar/O_2 mixture was exposed to the thermally reduced TiO_2 surface at room temperature; the excess gas was evacuated prior to the EPR measurements. Unlike the results obtained with CO_2, co-adsorption of argon and oxygen did not lead to any site specific blocking as seen in Figure 5.13.

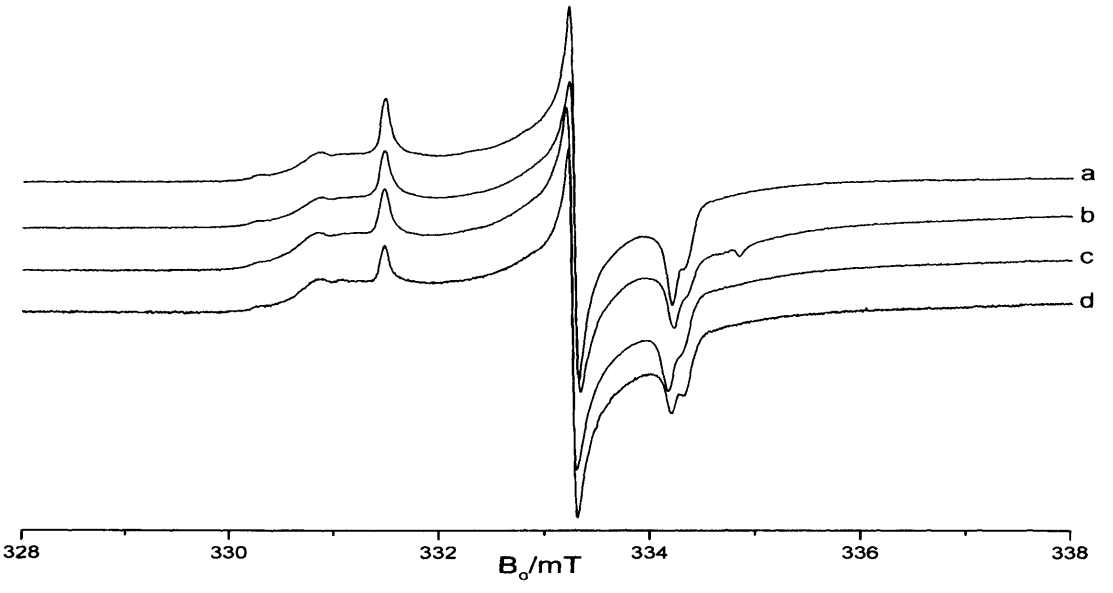

Figure 5.13: *cw*-EPR spectra (130K) of O_2^- formed after Ar/O_2 (co-adsorbed) exposure to thermally reduced (773K) P25, showing the effects of increasing Ar pressure. The ratios of Ar/O_2 were a) 0:1, b) 0.33:1, c) 0.66:1 and d) 3.33:1. The total pressure in the cell was maintained at 15 Torr throughout. Gases were admitted at 298K, followed by evacuation after 10 minutes of exposure.

On increasing the Ar pressure in the Ar/O_2 ratio no redistribution is seen in the g_{zz} region of the superoxide (Figure 5.13a-d). In other words, regardless of the Ar pressure used, the resulting O_2^- spectra all had identical profiles to that shown earlier in Figure 5.3. This implies that all $Ti^{3+}_{surface}$ sites are available for reactivity with O_2 under these conditions.

5.3.4.3 *Sequential adsorption of Ar/O_2*

A series of experiments where Ar and O_2 were sequentially adsorbed to the reduced surface (Figure 5.14) was then performed. As the Ar pressure was increased, a corresponding notable change was observed in the g_{zz} region of the spectra (Figure 5.14a-h). The intensity of the site I peak at $g_{zz} = 2.019$ selectively decreased compared to the site II-III peaks. This is most obviously seen by comparing Figure 5.14a to 5.14h, representing the two extreme cases where Ar is absent (Figure 5.14a) compared to the situation with the highest Ar pressure (Figure 5.14h).

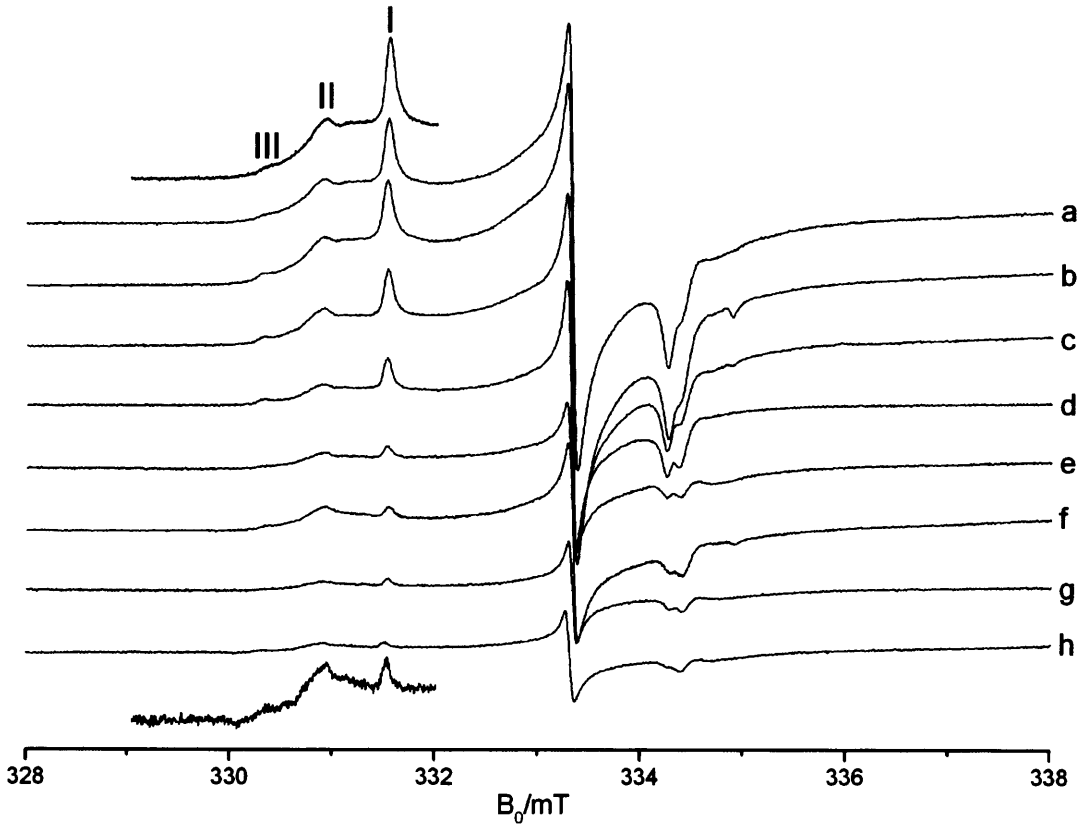

Figure 5.14 *cw*-EPR spectra of O_2^- formed after Ar/O_2 (sequential) exposure to thermally reduced (773K) P25, showing the effects of increasing Ar pressure. The ratios of Ar/O_2 were a) 0.0:1, b) 0.006:1, c) 0.03:1, d) 0.05:1, e) 0.06:1, f) 0.33:1 and g) 0.66:1 h) 1:1. The total pressure in the cell was maintained at 15 Torr throughout. Gases were admitted at 298K, followed by evacuation after 10 minutes of exposure.

The relative loss of site I signal intensity compared to sites II-III is clearly illustrated in Figure 5.14. The relative signal intensities of the O_2^- species attributed to site I and sites II-III have been plotted as a function of CO_2 pressure in Figure 5.15. Once again while the initial presence of Ar appears to disrupt the overall formation of O_2^-, the loss is more pronounced for site I. Clearly Ar must therefore block ET from the Ti^{3+} sites to oxygen, preventing formation of the [Vac....O_2^-] site I species. These results are easily understood since Ar interacts weakly with the TiO_2 surface. In the absence of competing oxygen (i.e. in this sequential experiment), the argon probe is of a suitable size to occupy the vacancy site, forming a weak interaction with the TiO_2 surface and thereby preventing subsequent formation of superoxide on addition of molecular oxygen. However when a mixture of Ar/O_2 is exposed to the surface (i.e. in the previous co-adsorbed experiment), there is a greater tendency for the oxygen to chemisorb at the vacancy site I compared to argon, thereby explaining the data in Figure 5.13. This situation is opposite to that found earlier with CO_2, where it was suggested that the CO_2 molecule was too large to sit in the vacancy site and therefore preferentially blocked the five co-ordinate sites II-III.

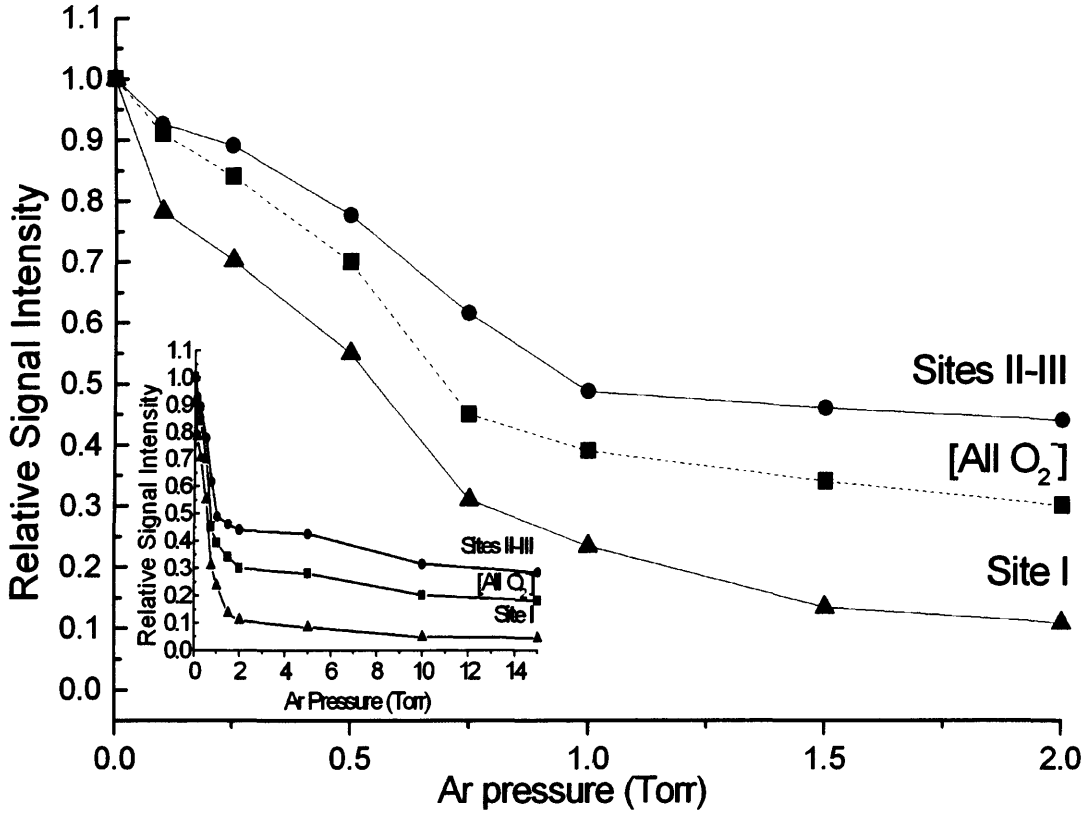

Figure 5.15: Variation in the relative signal intensities of adsorbed O_2^- versus Ar pressure, in an Ar/O_2 (sequential) gas mixture. The relative intensities of sites I, II and III were determined by simulation of the spectra. The relative integrated intensity of the entire superoxide spectrum (including all three contributing sites) is labelled [All O_2^-].

5.4 Discussion

5.4.1 Nature of the surface adsorbed superoxide radical

The superoxide radical is an important oxygen species that has been widely studied in the literature.[21,22] It has been shown that it can play a key role in many catalytic reactions and has been used as a probe at the surface of metal oxides due to its sensitivity to the electric field gradients at the surface.[11] The superoxide radical can be generated by a number of methods including: (i) direct surface–oxygen electron transfer; (ii) photoinduced electron transfer; (iii) surface intermolecular electron transfer; and (iv) decomposition of hydrogen peroxide.[21] Here we shall discuss the superoxide generated *via* the direct surface-oxygen electron transfer that occurs on a thermally reduced surface.

The thermal reduction of P25 under vacuum results in the loss of lattice oxygen, leaving behind four electrons per desorbed oxygen molecule as shown in equation 5.1. The four electrons are then trapped at the Ti^{4+} sites in, or close to, the oxygen vacancy to form Ti^{3+} centres at both vacancy and non vacancy sites (i.e. Ti^{3+}_{vac} and $Ti^{3+}_{non\text{-}vac}$ reduced centres).(Eq 5.2)

$$2\ O^{2-}_{(lattice)} \rightarrow O_{2\,(g)} + 4\ e^- \qquad (5.1)$$

$$4\ Ti^{4+} + 4\ e^- \rightarrow 4\ Ti^{3+}_{(vac\ +\ non\text{-}vac)} \qquad (5.2)$$

These Ti^{3+} centres are EPR active and give a characteristic EPR spectrum as shown previously in Figure 5.1a, and have been well studied in the literature.[15,16,23] However, owing to the broad linewidth of the Ti^{3+} signal the heterogeneity of the surface Ti^{3+} centres can not be directly observed in the corresponding EPR spectrum. The Ti^{3+} centres can react with adsorbed organics[13] and oxygen[11,24] and the heterogeneity of the TiO_2 surface is thereby indirectly manifested in the EPR signals of the resulting radicals. In the case of O_2 an electron is transferred from the Ti^{3+} centre to the molecular oxygen resulting in the formation of a surface stabilised superoxide anion (O_2^-) (Eq 5.3)

$$Ti^{3+} + O_2 \rightarrow Ti^{4+}....O_2^- \qquad (5.3)$$

The superoxide radical is a 13 electron diatomic radical with three electrons in the two π^* antibonding orbitals.[22,25] However the two π^* antibonding orbitals are degenerate and this degeneracy is only lifted when an external perturbation, such as an

electric field or surrounding ion, is present. Once this condition is satisfied, as occurs following surface adsorption, an EPR spectrum is observed. The signal is intrinsically orthorhombic as the unpaired electron is confined in a π type orbital. In this case all three axes on the molecule are inequivalent. The z direction is specified as along the internuclear axis and the x and y directions are perpendicular to the adsorption site, as shown in Figure 5.16.

The expected principal values of the ***g*** tensor were calculated by Känzig and Cohen for the case of an ionic superoxide in the bulk of alkali halides.[26] The three principal values usually exhibit three distinct g values with the trend $g_{zz} > g_{yy} > g_{xx}$. Ignoring second order terms and assuming $\lambda < \Delta << E$, the g components for the superoxide are given by:

$$g_{xx} = g_e \tag{5.4}$$

$$g_{yy} = g_e + 2\lambda/E \tag{5.5}$$

$$g_{zz} = g_e + 2\lambda/\Delta \tag{5.6}$$

where λ is the spin orbit coupling constant for the oxygen atom, g_e is the free electron g value (2.0023), Δ is the energy splitting between the two antibonding $2p\pi_y^*$ and the $2p\pi_x^*$ orbitals and E is the energy difference between the $2p\sigma$ and $2p\pi_y^*$ orbital as shown in Figure 5.16.

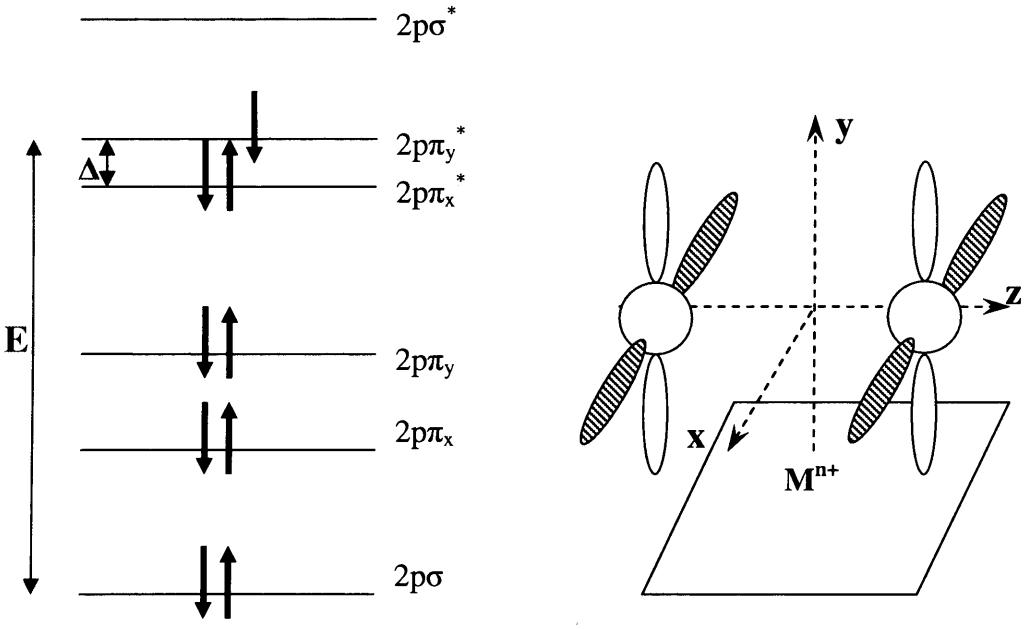

Figure 5.16 Energy level diagram for O_2^- in the ground state. When a crystal field is present the degeneracy of the $2p\pi_y^*$ and $2p\pi_x^*$ energy level is lifted. On the right is an illustration of the adsorption mode of O_2^- on a cationic surface site.

The key equation is 5.6, since this shows that the Δ term is sensitive to the local crystal field which removes the degeneracy of the two π* orbitals and hence determines the shift in the g_{zz} value with respect to the free g_e values. The g_{zz} region can therefore be used as a probe of the oxide surface and can provide information on the nature of the adsorption site such as cationic charge (M^{n+}) and of differences in local co-ordination geometry.

5.4.2 *Formation of O_2^- on P25; stabilization at vacancy and non-vacancy sites.*

The g_{zz} region of O_2^- stabilised on the P25 TiO_2 surface displays a multitude of peaks, indicating the presence of multiple adsorption sites. As mentioned earlier they can be broadly grouped into two families of sites: site I is attributed to O_2^- stabilised at oxygen vacancies labelled [Vac...O_2^-]. The remaining sites II-III were attributed to O_2^- anions adsorbed at non-vacancy sites at five co-ordinate Ti^{4+} centres.[11] Carter *et al.*,[11] assigned the two sets of sites by studying their properties and behaviour under selected conditions. They found that superoxide radicals stabilised at [Vac...O_2^-] site I, identified by the g_{zz} value 2.019, were thermally unstable at 333K compared to the O_2^- radicals stabilised at non-vacancy sites, which decayed at the higher temperature of 353K. The superoxide radicals stabilised at vacancy sites were also found to display low temperature photolability, which was not observed for the radicals stabilised at non-vacancy sites. Carter *et al.*,[11] also showed that the relative contribution to the overall signal intensity from vacancy-stabilised superoxide radicals decreased when oxygen was exposed to the reduced surface at low temperature. This was attributed to the migration of O_2^- radicals between the different stabilisation sites on the surface in the temperature regime of 120K to 298K. Their work clearly shows that the O_2^- radicals stabilised at the surface of TiO_2 can behave very differently under carefully selected conditions.

5.4.3 *Site specific blocking of the non-vacancy sites by CO_2*

The surface of P25 has been shown to be very heterogeneous in nature and the formation of O_2^- radicals provides a way of indirectly probing the surface.[11,24] These O_2^- radicals have also shown selective reactivity with organic substrates which has important implications for the field of catalysis.[13,14] The aim of this study was to probe whether ET transfer from the Ti^{3+} centres to molecular oxygen forming O_2^- can be selectively blocked using an appropriately chosen probe molecule. It has been shown

that CO_2 has differing effects on the two families of adsorbed O_2^- anions on P25; namely no blocking of the vacancy (site I) and selective blocking of the non-vacancy (Site II-III) adsorption sites.

Morterra *et al.*,[27] have shown that CO_2 chemisorption on the titanium dioxide surface at 298 K is almost completely reversible and evacuation at 298 K eliminates all chemisorbed CO_2 from the surface.[27] This agrees with our findings since the interaction between the Ti^{3+} centres and CO_2 was weak and completely reversible. In other words, following CO_2 evacuation and subsequent O_2 addition, a normal O_2^- signal is observed. This indicates the Ti^{3+} centres are not perturbed in any way by the CO_2. Although the work here was performed on a reduced surface, Rasko *et al.*,[28] have shown that there is little difference in the behaviour of CO_2 on a fully oxidised or reduced surface in its general adsorption properties. The fact that carbon dioxide chemisorbs easily on the TiO_2 surface has led to it being used widely as a probe of both the fully oxidised and partially reduced TiO_2 surfaces on both single crystal[29-32] and polycrystalline samples.[33,34]

The nature of the interaction of CO_2/O_2 (both in co- and sequential adsorption experiments) with the reduced surface was described in *5.3.3.2* and *5.3.3.3*. It was found that as the CO_2 pressure was increased, the CO_2 had differing effects on the two families of adsorbed O_2^- anions on P25.

The interaction of carbon dioxide with vacuum annealed single crystal surfaces has also been extensively studied by Temperature Programmed Desorption (TPD). Confident assignments of CO_2 being bound at a non defective site (Ti^{4+}) and an oxygen vacancy site (Ti^{3+}) on a single crystal rutile surface TiO_2 have previously been made.[29-31,35] In a study by Henderson *et al.*,[29] the authors have shown that the CO_2 binds weakly on vacuum-annealed TiO_2(110) in two states, one where the CO_2 is linearly bound at the five fold Ti^{4+} sites which desorbs in TPD at 137 K, and a second that is assigned to adsorption at vacancy sites Ti^{3+} which desorbs at 166 K.

In a further study Henderson *et al.*,[35] showed that the interaction of molecular oxygen with Ti^{3+} sites on the vacuum annealed TiO_2 (110) surface could be prevented using CO_2. Upon exposure of oxygen to the surface with CO_2 present at purely the vacancy site they found that the oxygen adsorption channels were blocked by the presence of CO_2. This preferential adsorption of CO_2 at the oxygen vacancy site is in contrast to our findings where a reversed behaviour is observed (i.e., preferential CO_2 adsorption at the five-coordinate Ti^{3+} sites as opposed to the vacancy). However it must

be noted that all the single crystal work[31,35,36] was performed on a rutile (110) surface rather that the anatase polycrystalline surface responsible for the O_2^- stabilisation in this work. The differences in the morphology of P25 and a rutile (110) surface may be responsible for the difference in behaviour.

The TPD technique has also been used to probe surface sites on anatase TiO_2 nanocrystals and it was found that at 170 K the CO_2 was removed from Ti^{4+} sites and at 200 K the CO_2 was removed from the Ti^{3+} sites. These TPD results show that CO_2 is easily chemisorbed at low temperatures. However there is also plenty of evidence to indicate that CO_2 interacts with the TiO_2 surface at room temperature. Carbon dioxide adsorption on P25 anatase was studied by Martra *et al.*,[34] using IR spectroscopy they probed Lewis acid-base sites on microcrystalline TiO_2 anatase. CO_2 was found to be adsorbed in a linear form, and as bicarbonates formed *via* reaction with Ti^{4+}-O^{2-} pairs on the surface of P25 anatase. The difference in chemical behaviour of these sites was ascribed to differences in the geometric arrangement of cations and anions on the various planes present and a number of sites were formed at defect positions (edges, steps and corners). Although the work of Martra[34] was performed on a clean defect free surface this clearly showed how the heterogeneity of the surface can be probed by differences in the chemistry that takes place on the TiO_2 surface.

It this chapter it has been shown that CO_2 can selectively block the surface $Ti^{3+}_{non\text{-}vac}$ sites preventing electron transfer from Ti^{3+} to O_2, hindering formation of O_2^- at these sites. In the literature CO_2 has been shown to weakly interact with the TiO_2 surface, which has led to it being used as a probe of TiO_2 surface sites. A number of Ti^{3+} sites have been identified by Henderson *et al.*,[35] and the subsequent adsorption of oxygen at these sites can be blocked by CO_2 on a rutile sample. It is reasonable to assume that CO_2 is acting in a similar way on P25 TiO_2 as observed and discussed in this chapter.

5.4.4 Site specific blocking of the vacancy sites by argon

It has been shown in the previous section that specific stabilisation sites for O_2^- (non-vacancy) can be blocked by CO_2. The vacancy sites however were observed to remain largely unperturbed. Having made these observations, it seemed reasonable to pursue a parallel investigation using a substrate that could potentially block the oxygen vacancy sites. The addition of argon to a thermally reduced surface resulted in an increase in EPR signal intensity arising from surface Ti^{3+} centres (Figure 5.12); this was

explained as originating from the partial quenching of the spin-spin broadening between the Ti^{3+} sites due to the high charge density of the Ti^{3+} sites interacting with strongly polarisable electron cloud of Ar. The interaction of argon and TiO_2 has been studied by Gomes *et al.*,[37] Argon is an inert noble gas with a closed shell electronic structure, therefore its interaction with the TiO_2 surface results from a balance of a Van der Waals interactions and Pauli repulsions. When the argon is in close proximity with the TiO_2 surface it has been shown to undergo significant polarization from interaction with Ti^{4+} species at the surface. This results in a large dipole moment pointing towards the surface and the consequence of this is a decrease in the charge density near the Ti^{4+} atom, suggesting a decrease in the Pauli repulsion which permits the atoms to stay closer to the surface.[37] In their study the authors were clearly dealing with Ti^{4+} centres however it would be expected that the Ti^{3+} centres formed on vacuum reduction of TiO_2 would have a stronger interaction with the polarisable Ar due to the increased e^- density.[37]

The addition of a co-adsorbed mix of Ar/O_2 to a reduced surface of TiO_2 leads to the formation of O_2^- without any site specific blocking (see Figure 5.13), unlike the case for CO_2/O_2 co-adsorption (Figure 5.6). The oxygen has a greater tendency to chemisorb at the vacancy site I compared to argon. The chemisorption of oxygen is well studied and the electron transfer step from Ti^{3+} to O_2 is an exothermic reaction (-42 kJ/mol in the gas phase)[22] and the two resulting charge states are electrostatically held together (Ti^{4+}.....O_2^-). Hence on co-adsorption, the interaction of oxygen with the surface Ti^{3+} centres is favourable compared to the interaction with argon and no change is observed in the profile of the O_2^- EPR spectrum, indicating that no blocking of the surface $Ti^{3+}_{(vac + non\ vac)}$ sites responsible for ET to O_2 has occurred.

On sequential adsorption of Ar/O_2, the increasing presence of argon disrupts the formation of O_2^- and a notable change is observed in the g_{zz} region of the superoxide spectra. The loss in intensity is more pronounced for site I (g_{zz} = 2.019) compared to the site II-III (2.024-2.028) peaks. The Ar is clearly blocking ET transfer from the Ti^{3+} sites to the oxygen, preventing formation of the [Vac...O_2^-] site I species. Clearly, in the absence of oxygen to compete with, the argon molecule is small enough to sit in the vacancy site I at g_{zz} = 2.019. Much discussion has arisen about the identity and structure of the g_{zz} site at g_{zz} = 2.019. It is the site of lowest co-ordination on the TiO_2 surface, as low co-ordinated cations exert a strong electric field hence the lower value of g_{zz}, leading to the suggestion it is a vacancy site. It is postulated that this sort of vacancy is

formed when neutral oxygen is removed through annealing under vacuum. The two extra electrons are formally shared between two Ti^{3+} neighbours for each O^{2-} ion removed. For example on the TiO_2 (110) surface both bridging and in plane oxygen exist, but owing to the lower probability of desorption of the in plane oxygen, the bridging oxygens are most likely to be lost producing the vacancies shown in Figure 5.17

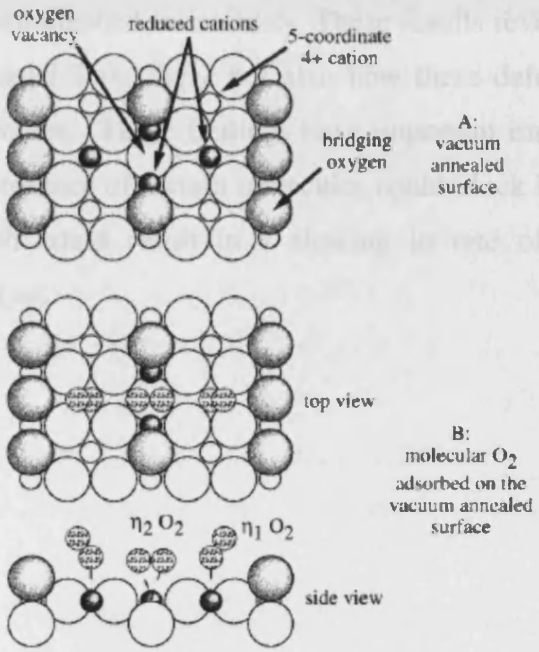

Figure 5.17 Schematic model for the bonding of O_2 to the vacuum annealed TiO_2 (110) surface. Model A shows the top view of the TiO_2 (110) surface with an oxygen vacancy site. Model B shows top and side (along the [001] direction) views of O_2 molecules bonded at vacancy and non-vacancy sites.[9]

As shown, these low co-ordinate sites have been blocked by the Ar. This observation agrees with the study by Diehl *et al.*,[38] who studied the interaction of argon with metal oxide surfaces and showed that argon prefers to interact with low co-ordination sites. It has also been proven both experimentally and theoretically that rare gases prefer sites of low co-ordination on transition metals.[38]

5.5 Conclusion

Adsorption of molecular oxygen at room temperature onto a thermally reduced titania sample (P25) leads to the formation of a heterogeneity of surface stabilized superoxide radicals (O_2^-). At least two groups of stabilization sites were previously assigned to O_2^- adsorbed at oxygen vacancies, labelled [Vac...O_2^-] or site I, and O_2^- adsorbed at other five co-ordinate Ti^{4+} centres, labelled sites II-III.[11] It has been shown for the first time that the precursor Ti^{3+} centres for electron transfer and subsequent

radical formation are found to be specifically blocked using selective probe molecules. Carbon dioxide selectively blocks the $Ti^{3+}_{non\text{-}vac}$ surface sites, preventing electron transfer from these five co-ordinate Ti^{3+} centres: this is evidenced by the absence of site II-III signals in the EPR spectrum (the Ti^{3+} sites are not affected by CO_2). On the other hand, argon selectively blocks the Ti^{3+}_{vac} surface sites, preventing ET from these lower co-ordinate Ti^{3+} centres. In this case, the EPR signal of site I [Vac...O_2^-] radicals is absent or significantly diminished in intensity. These results reveal not only the role of Ti^{3+} defects in interfacial ET on TiO_2, but also how these defects can be selectively blocked by probe molecules. These findings have important implications for catalysis as this shows that the presence of certain molecules could block ET transfer sites on the surface of TiO_2, which could result in a slowing in rate of reaction or eventual deactivation of the catalyst.

5.6 References

(1) Fujishima, A.; Honda, K. *Nature* **1972**, *238*, 37.

(2) Maness, P. C.; Smolinski, S.; Blake, D. M.; Huang, Z.; Wolfrum, E. J.; Jacoby, W. A. *Applied and Environmental Microbiology* **1999**, *65*, 4094.

(3) Gratzel, M. *Nature* **2001**, *414*, 338.

(4) Fox, M. A.; Dulay, M. T. *Chemical Reviews* **1993**, *93*, 341.

(5) Choudhary, T. V.; Goodman, D. W. *Topics in Catalysis* **2002**, *21*, 25.

(6) Linsebigler, A. L.; Lu, G. Q.; Yates, J. T. *Chemical Reviews* **1995**, *95*, 735.

(7) Hoffmann, M. R.; Martin, S. T.; Choi, W. Y.; Bahnemann, D. W. *Chemical Reviews* **1995**, *95*, 69.

(8) Fujishima, A.; Zhang, X. T.; Tryk, D. A. *Surface Science Reports* **2008**, *63*, 515.

(9) Lowekamp, J. B.; Rohrer, G. S.; Hotsenpiller, P. A. M.; Bolt, J. D.; Farneth, W. E. *Journal of Physical Chemistry B* **1998**, *102*, 7323.

(10) Hotsenpiller, P. A. M.; Bolt, J. D.; Farneth, W. E.; Lowekamp, J. B.; Rohrer, G. S. *Journal of Physical Chemistry B* **1998**, *102*, 3216.

(11) Carter, E.; Carley, A. F.; Murphy, D. M. *Journal of Physical Chemistry C* **2007**, *111*, 10630.

(12) Attwood, A. L.; Edwards, J. L.; Rowlands, C. C.; Murphy, D. M. *Journal of Physical Chemistry A* **2003**, *107*, 1779.

(13) Carter, E.; Carley, A. F.; Murphy, D. M. *Chemphyschem* **2007**, *8*, 113.

(14) Green, J.; Carter, E.; Murphy, D. M. *Research on Chemical Intermediates* **2009**, *35*, 145.

(15) Howe, R. F.; Gratzel, M. *Journal of Physical Chemistry* **1985**, *89*, 4495.

(16) Howe, R. F.; Gratzel, M. *Journal of Physical Chemistry* **1987**, *91*, 3906.

(17) Naccache, C.; Meriaude.P; Che, M.; Tench, A. J. *Transactions of the Faraday Society* **1971**, *67*, 506.

(18) Serwicka, E.; Schlierkamp, M. W.; Schindler, R. N. *Zeitschrift Fur Naturforschung Section A.* **1981**, *36*, 226.

(19) Che, M.; Tench, A. J. *Advances in Catalysis* **1982**, *31*, 77.

(20) Green, J.; Carter, E.; Murphy, D. M. *Chemical Physics Letters* **2009**, *477*, 340.

(21) Anpo, M.; Che, M.; Fubini, B.; Garrone, E.; Giamello, E.; Paganini, M. C. *Topics in Catalysis* **1999**, *8*, 189.

(22) Che, M. T., A.J. *Advances in Catalysis* **1983**, *32*, 1.

(23) Jenkins, C. A.; Murphy, D. M. *Journal of Physical Chemistry B* **1999**, *103*, 1019.

(24) Attwood, A. L.; Murphy, D. M.; Edwards, J. L.; Egerton, T. A.; Harrison, R. W. *Research on Chemical Intermediates* **2003**, *29*, 449.

(25) Atkins, P. W., Symons, M. C. R. *Structure of Inorganic Radicals : An Application of Electron Spin Resonance to the study of Molecular Structure*; Elsevier: London, 1967.

(26) Kanzig, W.; Cohen, M. H. *Physical Review Letters* **1959**, *3*, 509.

(27) Morterra, C.; Chiorino, A.; Boccuzzi, F.; Fisicaro, E. *Zeitschrift Fur Physikalische Chemie-Wiesbaden* **1981**, *124*, 211.

(28) Rasko, J.; Solymosi, F. *Journal of Physical Chemistry* **1994**, *98*, 7147.

(29) Henderson, M. A. *Surface Science* **1998**, *400*, 203.

(30) Funk, S.; Hokkanen, B.; Johnson, E.; Burghaus, U. *Chemical Physics Letters* **2006**, *422*, 461.

(31) Funk, S.; Burghaus, U. *Physical Chemistry Chemical Physics* **2006**, *8*, 4805.

(32) Thompson, T. L.; Diwald, O.; Yates, J. T. *Journal of Physical Chemistry B* **2003**, *107*, 11700.

(33) Suriye, K.; Praserthdam, P.; Jongsomjit, B. *Applied Surface Science* **2007**, *253*, 3849.

(34) Martra, G. *Applied Catalysis A-General* **2000**, *200*, 275.

(35) Henderson, M. A.; Epling, W. S.; Perkins, C. L.; Peden, C. H. F.; Diebold, U. *Journal of Physical Chemistry B* **1999**, *103*, 5328.

(36) Lu, G. Q.; Linsebigler, A.; Yates, J. T. *Journal of Chemical Physics* **1995**, *102*, 3005.

(37) Gomes, J. R. B.; Ramalho, J. P. P. *Physical Review B* **2005**, *71*.

(38) Diehl, R. D.; Seyller, T.; Caragiu, M.; Leatherman, G. S.; Ferralis, N.; Pussi, K.; Kaukasoina, P.; Lindroos, M. *Journal of Physics-Condensed Matter* **2004**, *16*, S2839.

Chapter 6

The identification of transient oxygen centred radicals on the TiO_2 surface formed under radiative and non-radiative conditions

6.1 Introduction

The use of titanium dioxide as a photocatalyst for the remediation of volatile organic compounds (VOC's) is currently a topical issue as these compounds have been shown to be harmful to human health over long term exposure and are also known to be a major contributing factor to the formation of lower-atmosphere ozone.[1] The successful application of TiO_2 in the decomposition of these VOC's relies on the catalytic reactions which occur at the oxide surface. An understanding of the interfacial chemistry at the molecular level, particularly the nature of the surface intermediates, is therefore considered central to the design of more improved catalysts with high quantum yields.

Acetonitrile, methanol and toluene are typical VOC's found in the lower atmosphere. These substances are stable yet toxic and can enter the atmosphere from automobile emissions,[2] contact with contaminated civil and industrial wastewater and burning of biomass.[3-6] Each of the organic substances has different properties providing different challenges in its degradation. Acetonitrile can undergo different oxidation routes on oxide surfaces as it possesses both an alkyl and a cyanide carbon atom. The CN^- moiety renders it a particularly interesting molecule to examine as it is representative of a number of toxic materials which are candidates for TiO_2-based oxidation processes. Methanol provides one with the chance to study how alcohols degrade on the TiO_2 surface. It has been shown to degrade by thermal and photochemical processes.[7] Toluene is widely used in the preparation of compounds such as benzaldehyde, benzyl-alcohol and chloro-derivatives which make their way into industrial waste water. It provides the chance to study how an aromatic compound behaves over the TiO_2 surface. It has been shown to degrade at both elevated temperatures[8] and under photochemical conditions.[9] However, to date only a limited number of studies have appeared on the catalytic degradation of these three substrates over TiO_2, either under dark conditions[8,10-14] or under UV irradiation.[15-24] Raskó *et al.*,[10,14] investigated the catalytic reactions of acetonitrile and acetonitrile-oxygen mixtures over TiO_2-supported rhodium and gold catalysts under dark conditions. They demonstrated that, for rhodium and gold systems, acetonitrile was adsorbed on a

number of different Lewis acid sites on the TiO_2 surface. In one possible mode of adsorption, the acetonitrile was found to be linearly co-ordinated to the metal centres (Rh and Au) *via* η^2 bonding. Dissociation of the molecule occurred at the site of the doped metal, resulting in the formation of an adsorbed $CN_{(ad)}$ moiety. This was believed to be oxidized by lattice oxygen into an NCO species, with the resulting formation of a number of other products (including CH_3NH_2, H_2, CO_2, CH_4, C_2H_4 and CO). The thermal decomposition of methanol under dark conditions was found to produce CH_4, CH_2O, $(CH_3)_2O$, CO and CO_2. The key step was adsorption of methanol at Lewis acid sites to form a surface adsorbed methoxy species, which at higher temperatures could undergo a number of different reaction routes to give the final decomposition products. Toluene however only degrades on the TiO_2 surface that has been treated at high temperatures, to produce surface Ti^{3+} centres which can then react with the adsorbed toluene.[8,13]

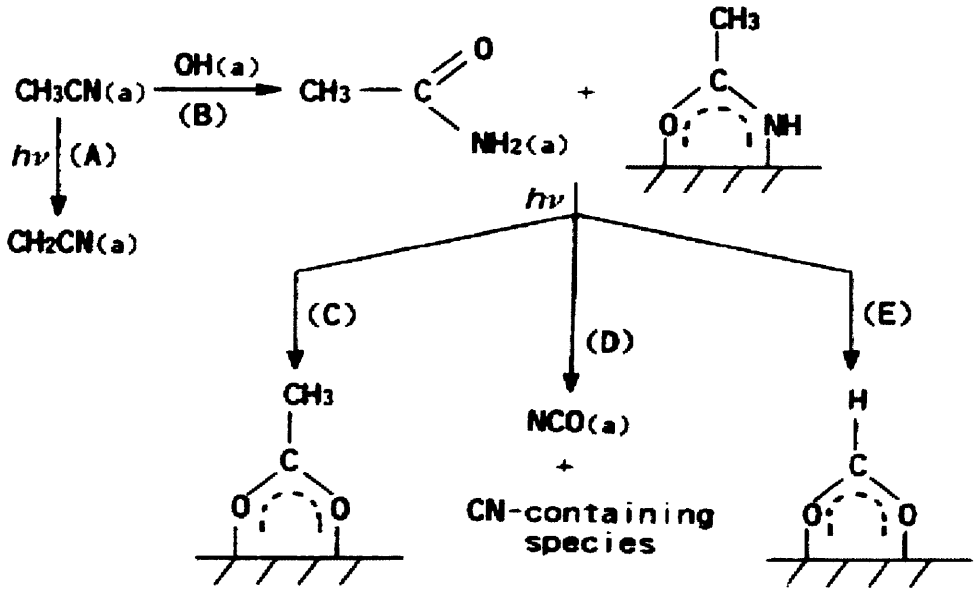

Scheme 1 Proposed reaction mechanism for the photooxidation of acetonitrile over the TiO_2 surface. (A)- (E) represent different adsorption and reaction pathways.

The VOC's chosen have all been the subject of many photocatalytic studies. The earliest study on the photocatalytic route of CH_3CN decomposition was reported by Lichtin *et al.*,[17] they identified the final products of the photooxidation over TiO_2 in a dry air stream as CO_2, H_2O and HNO_3 by gas chromatography, with NO_2 and $(CN)_2$ as the possible reaction intermediates. The observation of the cyanogen moiety was considered as proof for the existence of the $CN^{\bullet}$ radical, the latter being formed *via* a C-C bond breaking process. However, an IR study by Zhuang *et al.*,[18] later found that CH_3CN was photooxidised over TiO_2 in the presence of oxygen to form H_2O, CO_2 and

surface CO_3^{2-} with an adsorbed NCO intermediate. Additional information on the surface adsorption processes and surface products formed during photooxidation was also provided in a comprehensive study by Chaung *et al.*,[16] they showed that adsorbed CH_3CN reacted with surface OH groups, producing an acetamide (CH_3CONH_2)-type species. Upon UV irradiation of the sample, CH_3CN decomposed to $CH_2CN_{(ad)}$, whilst the acetamide species decomposed to $CH_3COO_{(ad)}$, $HCOO_{(ad)}$, $NCO_{(ad)}$ and CN^- containing species (Scheme 1).

The photooxidation of methanol was studied by Balcerski *et al.*,[25] who identified a variety of different reaction intermediates over the TiO_2 surface *via* Diffuse Reflectance Infrared Fourier Transform Spectroscopy (DRIFTS). During the initial stages both water and carbon dioxide were detected in addition to formic acid. After evacuation, the formic acid was found to persist in the DRIFTS spectra, indicating it was a surface bound species. The authors postulated a mechanism including many transient species which were not detected by DRIFTS. Similarly a number of studies have appeared on the photooxidation of toluene with the detection of multiple reaction intermediates such as benzoic acid, benzaldehyde and benzoperoxy with eventual mineralisation to CO_2.[26,27] A number of mechanistic routes have been proposed that are dependent on the reaction conditions, with many transient species believed to be present which have yet to be observed by conventional spectroscopic techniques.[26]

Most of the above reaction intermediates, formed on doped TiO_2 or on UV irradiated TiO_2 powders, were relatively stable and were studied at room temperature. However surface intermediates can also be transient (thermally unstable) in character and can therefore be difficult to detect and identify using standard spectroscopic techniques. The literature is sparse concerning the nature of the surface (and desorbed gaseous) radical intermediates produced during the oxidation process over undoped TiO_2. In many studies it has been suggested that the adsorption of molecular oxygen onto the surface of reduced TiO_2 (producing surface oxygen radicals such as O_2^-) is crucial to the photooxidation process.[1,28,29] Several Electron Paramagnetic Resonance (EPR) studies have already described the nature of the oxygen centred radicals formed in these surface reactions and their subsequent reactivity.[30-33] For example, Carter *et al.*,[30] have recently shown how a series of transient organoperoxy radicals, indirectly involving O_2^-, play a contributory role in the decomposition of acetone over polycrystalline TiO_2. Therefore, in the present chapter, the interaction of acetonitrile, methanol and toluene with superoxide radicals over polycrystalline TiO_2 will be

explored under dark conditions. Secondly a number of hole-mediated processes have been discussed for the formation of organoperoxy type radicals formed after UV irradiation of organics over the TiO_2 surface; therefore, the formation of transient radicals *via* irradiation of a co-adsorbed mix of acetonitrile, methanol and toluene with oxygen over the TiO_2 surface will be investigated.

6.2 Experimental

6.2.1 Formation of O_2^-

The TiO_2 samples were reduced as described in detail in Chapter 4. The reduced sample was then cooled to room temperature and exposed to oxygen (15 Torr) for 10 minutes before evacuation of the excess gas at 298K. This treatment results in the formation of O_2^- as described in Chapter 5.

6.2.2 Addition of organic substrates to O_2^-

The samples were precooled to 77K before addition of the chosen organic substrate (acetonitrile, methanol and toluene) at this temperature. Following this addition, the sample was annealed to a series of elevated temperatures (200-260K) for a period of 10 minutes at each specific temperature. After annealing, the sample was finally cooled to 130K prior to recording an EPR spectrum under the gas atmosphere.

6.2.3 UV irradiation of a co-adsorbed mix of an organic substrate: O_2

The co-adsorbed mix was premixed in the vacuum manifold with a ratio of 10:1 in all experiments. The gases were exposed to the activated TiO_2 sample at 298K before cooling to 77K. The sample was then UV irradiated under the organic atmosphere for 30 minutes at 77K.

6.3 Results

6.3.1 Interaction of acetonitrile with $^{16}O_2^-$

The superoxide species O_2^- were generated by room temperature addition of molecular oxygen to a thermally reduced TiO_2 powder. A typical profile for such a species is shown in Figure 6.1a and is characterised by the g values of $g_{xx} \approx 2.004$, $g_{yy} = 2.011$ and three g_{zz} values of 2.019, 2.023 and 2.026 (corresponding to three different adsorption sites, labelled I-III respectively) with an additional site II', identified by computer simulation with a g_{zz} value of 2.020 (Table 6.1).

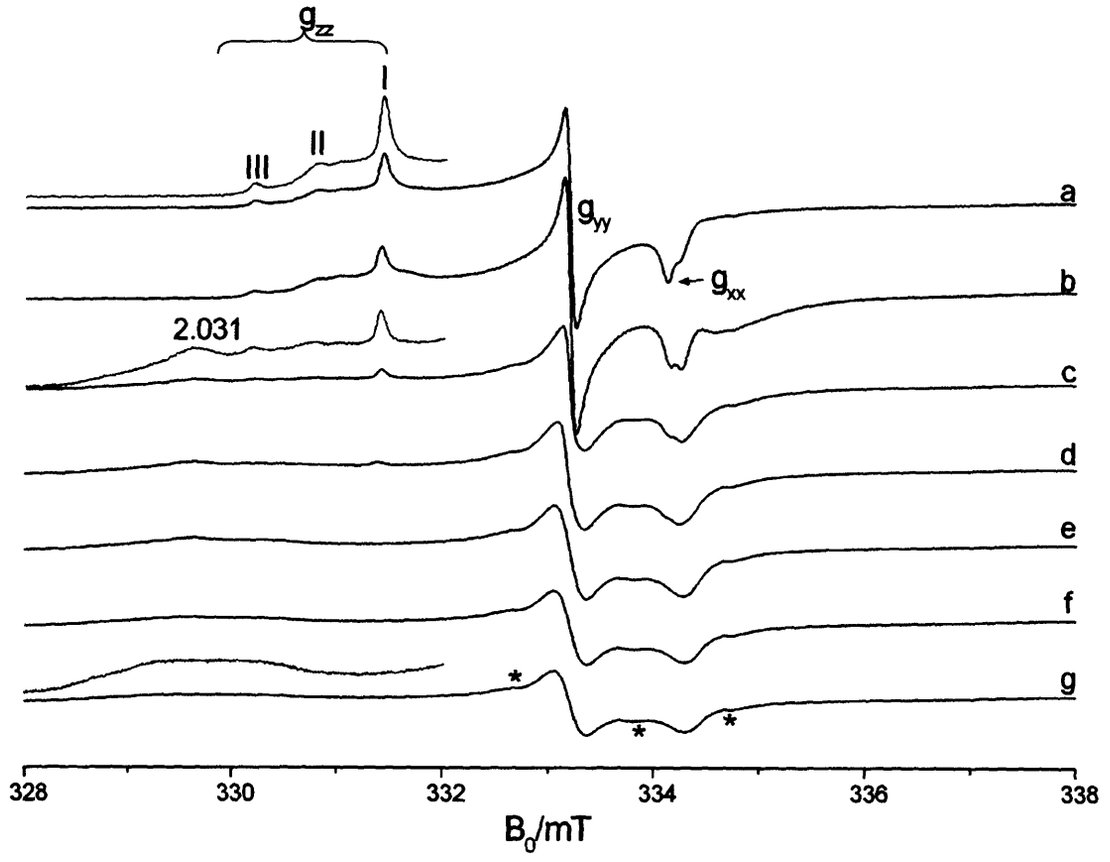

Figure 6.1 *cw*-EPR spectra (130K) of a) superoxide radicals formed by O_2 exposure to a thermally reduced TiO_2 (773K) sample. CH_3CN (7.3 Torr) was then admitted to the EPR cell at 77K, and the temperature was raised to b) 130, c) 210, d) 215, e) 220, f) 230 and g) 240K.

Exposure of acetonitrile to these O_2^- radicals at room temperature resulted in the immediate decay of the superoxide species (as evidenced by the complete loss of the O_2^- signal). By comparison, exposure of CH_3CN to O_2^- at 77K followed by subsequent annealing to temperatures in the range 200-240K resulted in a gradual decrease in O_2^- signal intensity accompanied by a redistribution of peaks in the g_{zz} region (Figure 6.1c-g).Simultaneously at temperatures of $T \approx 210K$, a new radical species (B) appears in the EPR spectrum characterised by a clearly observable peak with a g value of 2.031 (Figure 6.1c) which grows in intensity until thereafter it begins to decay irreversibly at $T > 250K$. As growth in species B is observed one sees the simultaneous loss of species A (due to O_2^-). The reactivity between CH_3CN and O_2^- appears to be site specific since the relative order of O_2^- loss follows the trend of site (I) > (II) > (III). At $T > 210K$, an additional series of peaks close to g_e were also identified in the spectra. These are labelled with asterisks (*) in Figure 6.1g and arise from the formation of the third radical species (C) which will be discussed in a later section 6.3.3.

The assignment of the new radical species B is difficult as this species is initially only identifiable by the g-value of 2.031 (presumably the remaining components of its

expected anisotropic g tensor are obscured by the g_2 (g_{yy}) and g_3 (g_{xx}) components of O_2^- and species C). To simplify the complex and overlapping g_3 (g_{xx}) and g_2 (g_{yy}) regions of the spectra (in order to extract more confidently the remaining g components of species B), oxygen was exposed to a 623K thermally reduced sample. This prevented surface speciation, producing a single group of O_2^- species characterised by g_{zz} = 2.019, g_{yy} = 2.011 and g_{xx} = 2.005 (see Figure 6.2a). This single group of O_2^- species was subsequently exposed to acetonitrile and the resulting spectra are shown in Fig 6.2b-g

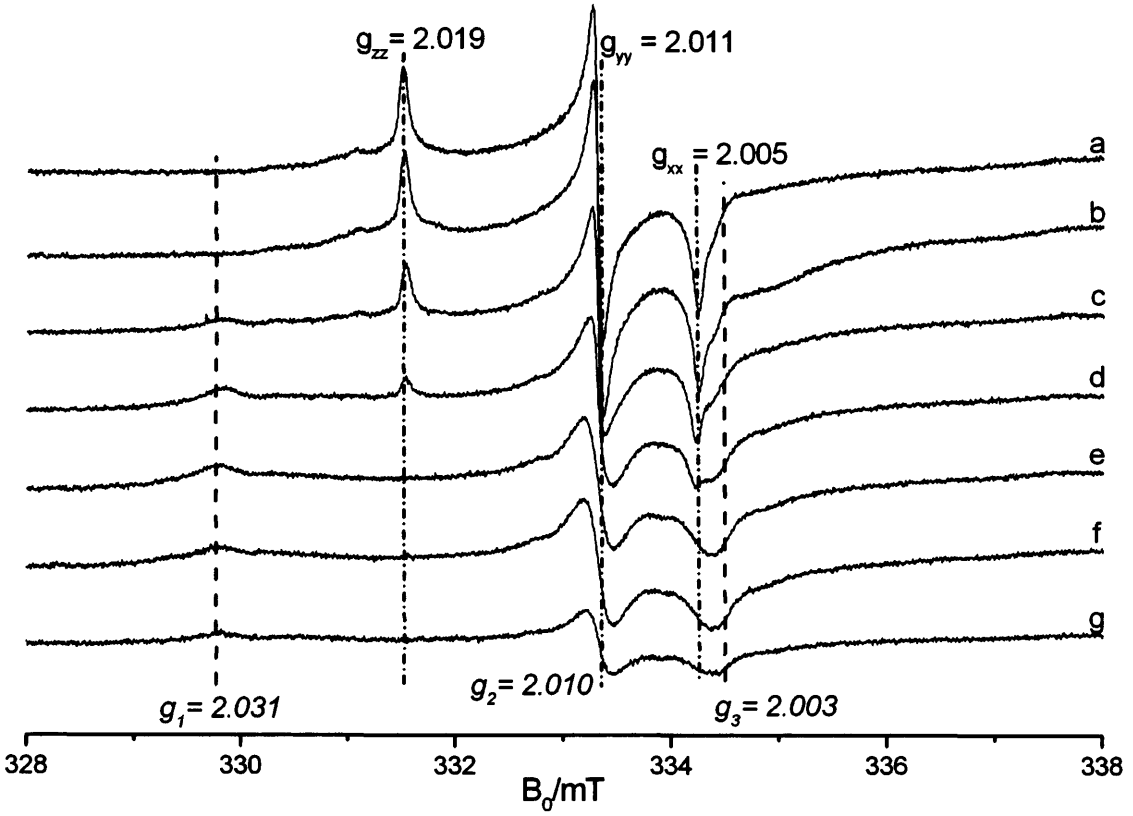

Figure 6.2 *cw*-EPR spectra (130K) of a) superoxide radicals formed by O_2 exposure to a thermally reduced TiO_2 (623K) sample. CH_3CN (7.3 Torr) was then admitted to the EPR cell at 77K, and the temperature was raised to b) 130, c) 200, d) 210, e) 215, f) 220, and g) 230K. The g values for O_2^- and species B are marked in bold and italics, respectively.

As seen in Figure 6.2, the single O_2^- peak decreases at elevated temperatures, while the peak associated with species B (characterised by g_1 = 2.031) begins to emerge. By 220K, the superoxide species is practically destroyed, leaving predominately the now easily visible signals from species B (Figure 6.2f). Owing to the improved resolution of this spectrum, computer simulation revealed that the g values for species B are g_1 = 2.031, g_2 = 2.010 and g_3 = 2.003 (with no observable hyperfine interaction).

6.3.2 *Interaction of acetonitrile with $^{17}O_2^-$*

To help further with the identification of species B, the $^{17}O_2^-$ radicals were generated by adsorption of ^{17}O-labelled dioxygen on thermally reduced TiO_2 (773K) surface. The resulting spectrum is shown in Figure 6.3 and consists of a sextet hyperfine pattern due to the singly labelled $^{16}O^{17}O^-$ radical [I (^{17}O) = 5/2], with a second 11 line hyperfine pattern from the doubly labelled $^{17}O^{17}O^-$ radical. The hyperfine pattern is easily measured to show A_{xx} = 7.7 mT which is characteristic of $^{17}O_2^-$ on TiO_2.[34] The ^{17}O hyperfine patterns of oxygen centred radicals are often unique for a given type of species (e.g. $^{17}O^-$, $^{17}O_2^-$, $^{17}O_3^-$, $RO^{17}O^\bullet$). In the latter case, owing to the unequal distribution of spin in the -$OO^\bullet$ fragment, two superimposed sextets should appear in the spectrum (due to R-$O^{17}O^\bullet$ and $R^{17}OO^\bullet$) as widely reported in the literature.[35-37] If O_2^- reacted with CH_3CN at 210K forming a peroxy entity (i.e., $NCCH_2OO^\bullet$) then the ^{17}O hyperfine pattern typical of O_2^- (Figure 6.3a) should gradually give way to a pattern typical of $RO^{17}O^\bullet/R^{17}OO^\bullet$.

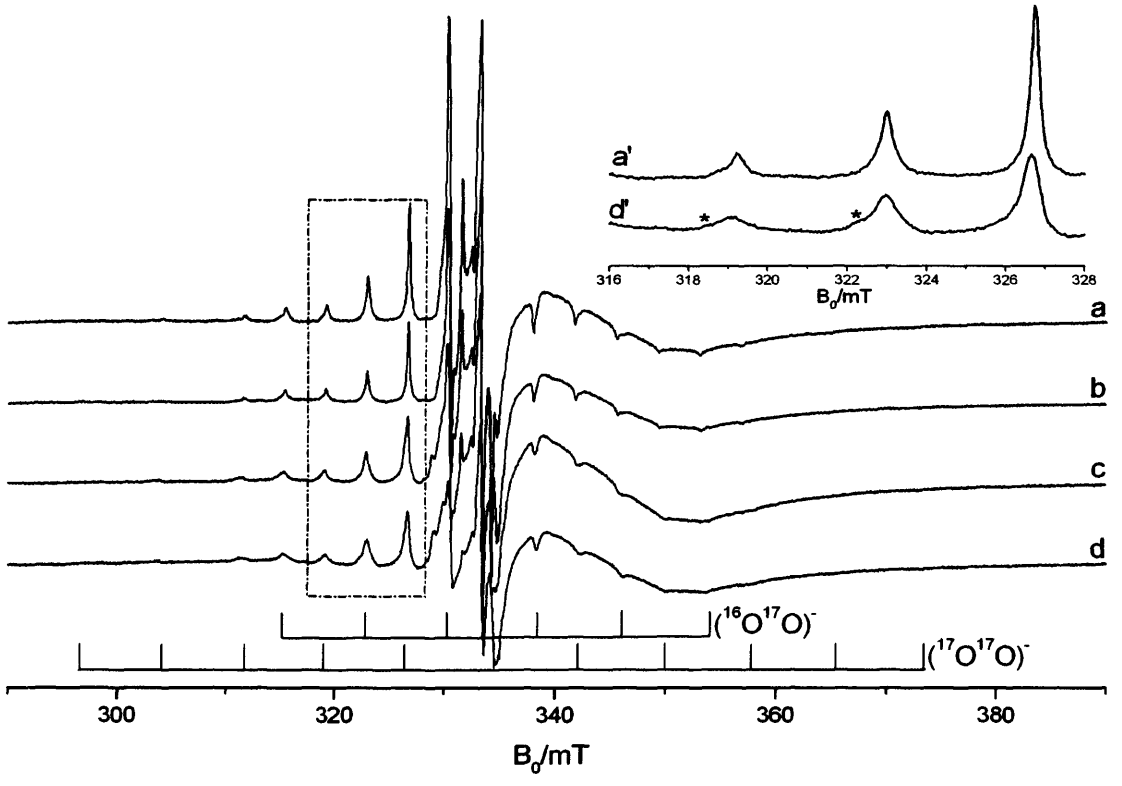

Figure 6.3 *cw*-EPR spectra (130K) of a) superoxide radicals formed by $^{17}O_2$ exposure to a thermally reduced TiO_2 (773K) sample. CH_3CN (7.3 Torr) was then admitted to the EPR cell at 77K and the temperature was raised to b) 130, c) 210, and d) 220K.

Following exposure of acetonitrile at 77K to $^{17}O_2^-$, the sample was annealed to elevated temperatures producing the spectra shown in Figure 6.3b-d. As the temperature is increased, the intensity of the $^{17}O_2^-$ signal decreases, in agreement with the previous

$^{16}O_2$ results and in addition a broadening of the hyperfine peaks occurs. On closer inspection, the origin of this 'broadening' can be ascribed to the appearance of a second overlapping ^{17}O hyperfine pattern (more clearly seen in the inset to Figure 6.3 labelled *). Since these additional peaks appear in the similar temperature region where radical B is also formed and predominates, it seems likely that this new radical B has a hyperfine pattern similar to that of $^{17}O_2^-$. More importantly this observation indicates that the molecular oxygen species associated with radical B contains equivalent oxygen atoms.

To summarise, species B is characterised by the g values of $g_1 = 2.031$, $g_2 = 2.01$ and $g_3 = 2.003$, is formed at T ~ 210K and degrades at higher temperatures. The profile of its spectrum is unaffected by deuteration. From the ^{17}O labelling of the O_2^- radical, the oxygen atoms of species B were found to be equivalent. These characteristics were similar to the paramagnetic intermediate [O_2^- ...CH_3COCH_3] identified by Carter *et al.*,[30] after the reaction of acetone with adsorbed radicals on TiO_2. It can therefore be assumed that the radical identified in this study is likely to be a similar surface complex labelled [O_2^- ....CH_3CN]; this assignment will be discussed further in section 6.4.1.

Table 6.1 Spin Hamiltonian parameters for species A, B and C identified after the interaction of CH_3CN with O_2^-.

Radical	g_1	g_2	g_3	A_1/ mT	A_2/ mT	A_3/ mT
Radical A (O_2^-)	(I) 2.019	2.011	2.005	[(a)] 7.64	<1	<1
	(II)2.023	2.011	2.004	7.86	<1	<1
	(II')2.020	2.011	2.004	7.86	<1	<1
	(III)2.026	2.011	2.001	7.97	<1	<1
Radical B [O_2^-...CH_3CN]	2.031	2.01	2.003	No resolved ^1H hfc		
Radical C ($HO_2^•$)	2.028 $g_1(g_{zz})$	2.01 $g_2(g_{yy})$	2.004 $g_3(g_{xx})$	[(b)] 1.2	1.0	1.0

(a) ^{17}O (b) ^1H

6.3.3 Identification of a hydroperoxy type species

Species C was formed after the interaction of acetonitrile with O_2^- and identifiable by the appearance of an additional set of peaks close to g_e at T ~ 210K (Figure 6.1g). The g and A values of this additional species were identified by computer simulation as $g_1 = 2.028$, $g_2 = 2.010$, $g_3 = 2.004$, $A_1 = 1.2$ mT, $A_2 = 1.0$ mT and $A_3 = 1.0$

mT (Figure 6.4a and b, Table 6.1) which were comparable to the literature values for the $HO_2^{\bullet}$ species.[38] Further confirmation for this $HO_2^{\bullet}$ assignment was obtained by repeating the experiment using fully deuterated acetonitrile (CD_3CN) (Figure 6.4c,d).

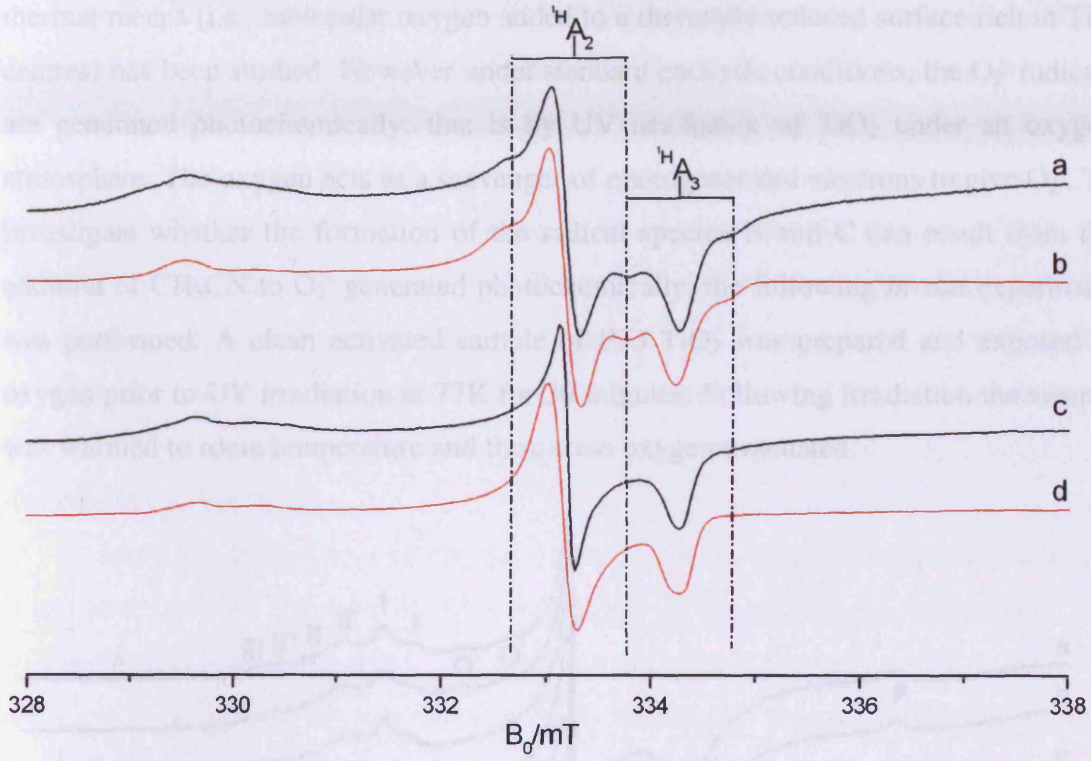

Figure 6.4 a,c) Experimental and b,d) simulated *cw*-EPR spectra (130K) of CH_3CN adsorbed at 77K onto TiO_2 containing O_2^- and following annealing to 220K; a,b) protic-CH_3CN, c,d) deuterated-CH_3CN. The A_2 and A_3 proton superhyperfine couplings are indicated.

Using deuterated acetonitrile, a barely perceptible decrease in the linewidth is observed as a direct consequence of the ratio of magnetic moments of the deuterium and hydrogen nuclei (μ_D/μ_H = 0.15). More noticeable, however, are the absence of the superhyperfine peaks associated with the smaller hyperfine couplings due to deuterium in $^2HO_2^{\bullet}$ (Figure 6.4c) which are obscured by the intrinsic linewidth of the spectrum.

The formation of this radical arises as the thermally reduced titania still contains surface basic O^{2-} anions. In the presence of these anions, the adsorbed acetonitrile can act as a Brönsted acid, leading to the formation of the CH_2CN^- anion.[15] The abstracted proton reacts with the basic surface O^{2-} anions forming hydroxyl groups, and it is proposed that these can subsequently interact with the O_2^- radical to give the hydroperoxy type radical species (Radical C)

6.3.4 *Interaction of acetonitrile with photogenerated $^{16}O_2^-$*

So far in this chapter, the formation of two transient radicals ($HO_2^\bullet$ and $[CH_3CN...O_2^-]$) formed by the reaction of acetonitrile with O_2^- radicals generated *via* thermal means (i.e., molecular oxygen added to a thermally reduced surface rich in Ti^{3+} centres) has been studied. However under standard catalytic conditions, the O_2^- radicals are generated photochemically; that is by UV irradiation of TiO_2 under an oxygen atmosphere. The oxygen acts as a scavenger of photogenerated electrons to give O_2^-. To investigate whether the formation of the radical species B and C can result from the addition of CH_3CN to O_2^- generated photochemically, the following *in-situ* experiment was performed. A clean activated sample of P25 TiO_2 was prepared and exposed to oxygen prior to UV irradiation at 77K for 30 minutes. Following irradiation the sample was warmed to room temperature and the excess oxygen evacuated.

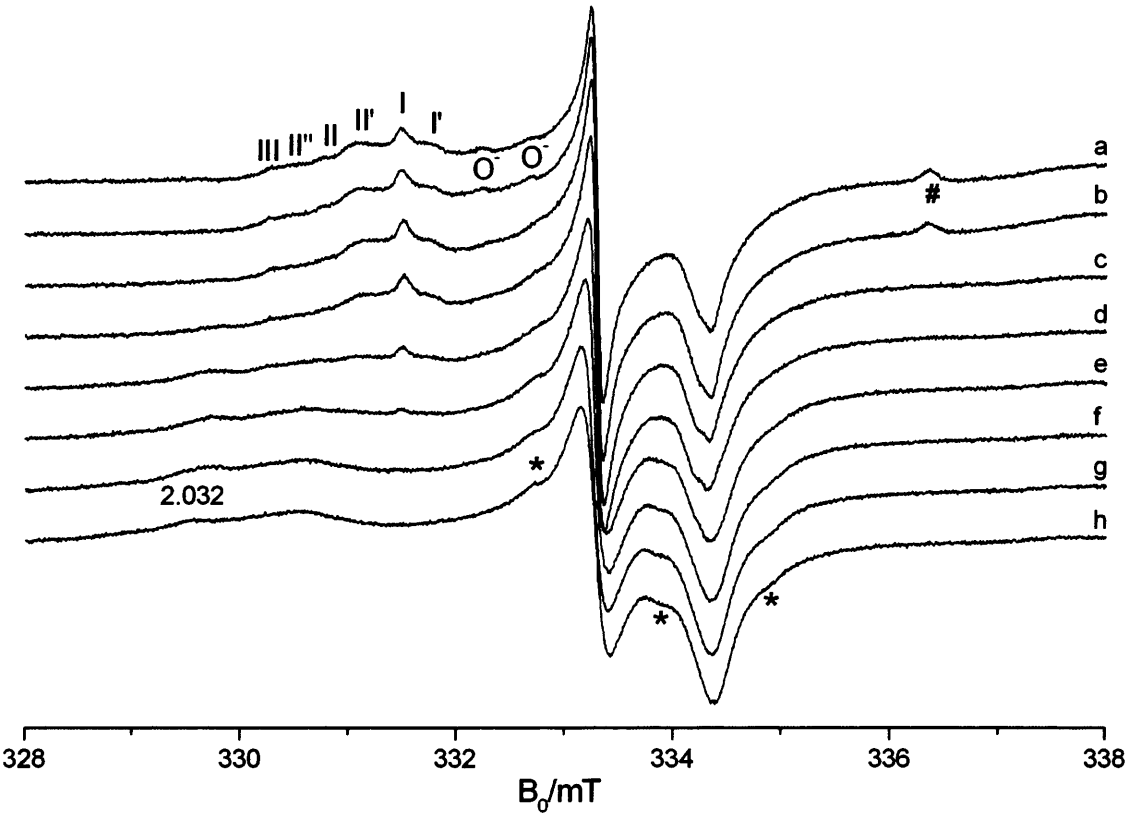

Figure 6.5 *cw*-EPR spectra (130K) of (a) superoxide radicals formed photochemically by irradiation of O_2 over an activated TiO_2 sample. CH_3CN (7.3Torr) was then admitted to the EPR cell at 77K, and the temperature was raised to b) 140, c) 190, d) 200, e) 210, f) 215, g) 220 and h) 230K.

This treatment resulted in the formation of O_2^- with the spin Hamiltonian parameters $g_{xx} \approx 2.004$, $g_{yy} = 2.011$ and at least six observable g_{zz} values = 2.017 (I'), 2.019 (I), 2.020 (II'), 2.023 (II), 2.025 (II'') and 2.026 (III) (Figure 6.5a). The extra sites I' and II' (characterised by $g_{zz} = 2.017$ and $g_{zz} = 2.025$) are due to extra stabilisation

sites on the activated surface compared to the thermally reduced surface as described in Chapter 5. Additional peaks marked # are due to traces of interstitial photo-generated Ti^{3+} centres[39,40], accompanied by traces of photo-generated holes O^-, which are unstable on annealing the sample to T > 190K and which have been studied extensively in the literature[33,34]. Acetonitrile was subsequently added to the sample at 77K. On annealing the sample under the acetonitrile atmosphere, the signal intensity of the superoxide radical dropped, accompanied by the appearance of a new signal at 2.032 (Figure 6.5 b-h) which is first observed at T > 210K but starts to decay irreversibly at T > 250K. As observed for the thermally produced O_2^-, there is site-specific reactivity between the O_2^- and CH_3CN, where the individual O_2^- sites react in the following order (I') ≈ (I) > (II') > (II) > (II'') > (III). Accompanying this new signal are further peaks close to g_e (labelled *) which can be attributed to the hydroperoxy type radical ($HO_2^\bullet$) previously identified in section 6.3.3.

The main difference between the thermally treated and photoirradiated samples is the lower overall intensity of the new radical on the photoirradiated sample. The reason for this is that the initial O_2^- signal on the photochemical sample is lower in intensity. In the photogenerated sample, the O_2^- radicals are formed by electron transfer from the surface, but some are immediately destroyed by UV irradiation.[41] Nevertheless, there is no difference observed in the reactivity of acetonitrile with O_2^-; the formation of radical species B and C is observed, whether the O_2^- has been formed either thermally or photochemically. This is a significant result as it shows that the [$CH_3CN...O_2^-$] radical intermediate can be formed under both thermal and photochemical conditions.

6.3.5 UV irradiation of co-adsorbed acetonitrile/ $^{16}O_2$ over the clean activated surface

In the previous section it has been shown that after addition of acetonitrile to surface adsorbed O_2^-, a thermally unstable intermediate is formed. It is important to understand how the order of substrate adsorption affects the nature of radicals. The UV irradiation of a TiO_2 surface under a co-adsorbed atmosphere of CH_3CN and O_2 was therefore investigated to study the nature of radicals formed under these conditions.

To a clean activated sample a dose of acetonitrile: oxygen was co-adsorbed after being premixed in the vacuum line (ratio 10:1 acetonitrile: oxygen, total pressure 15 Torr) followed by UV irradiation at 77K for 30 minutes. The sample was transferred to

the EPR cavity and evacuated *in-situ* at 130K to remove the excess gas. This treatment results in the spectrum shown in Figure 6.6a and is accompanied by its corresponding computer simulation (Figure 6.6b), which was used to extract the spin Hamiltonian parameters. The spectrum is dominated by an orthorhombic signal with the spin Hamiltonian parameters of $g_1 = 2.034$, $g_2 = 2.010$, and $g_3 = 2.004$; additional EPR signals at $g = 1.989$ and $g \approx 1.972$ (labelled * in Figure 6.6a) are also formed which can be easily assigned to bulk Ti^{3+} cations at substitutional and lattice sites (generated during low temperature irradiation of the TiO_2).[36,39,40]

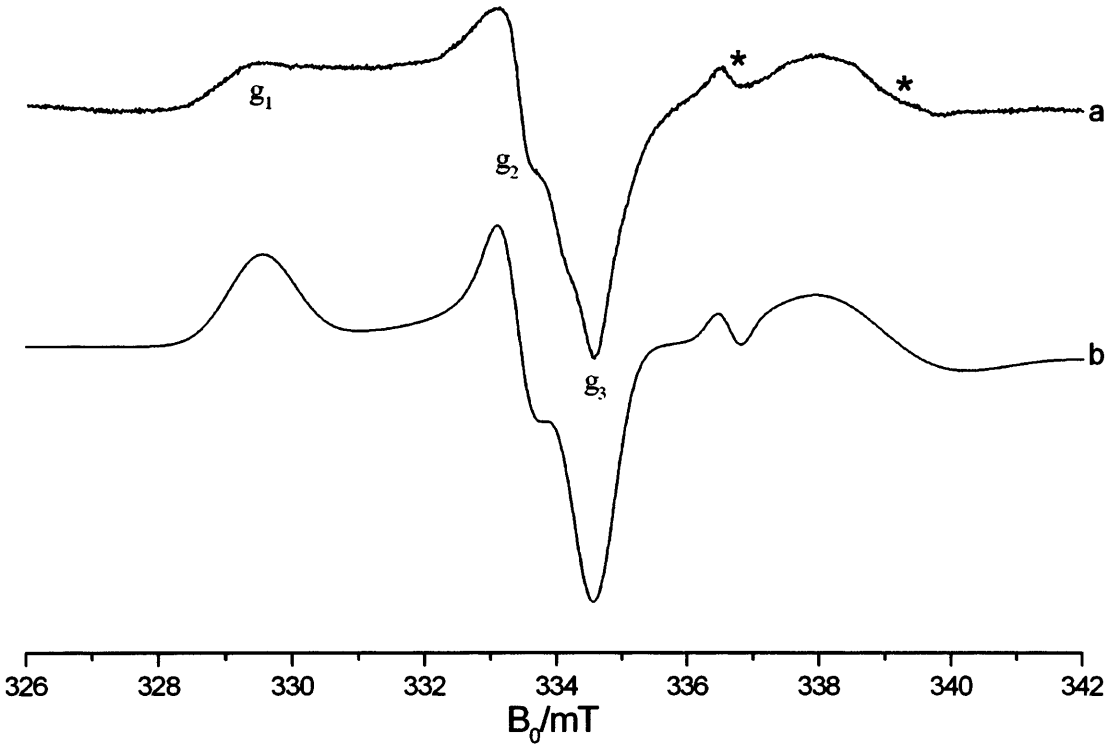

Figure 6.6 Experimental (a) and simulated (b) *cw*-EPR spectrum (130K) of photoirradiated TiO_2 containing co-adsorbed CH_3CN: O_2 in a 10:1 ratio (total pressure 15 Torr). The sample was UV irradiated for 30 minutes before evacuation at 130K.

The orthorhombic signal (hereafter labelled Radical D) is thermally unstable; upon warming to elevated temperatures (T > 180K) the signal intensity decreases significantly (Figure 6.7a-e) until the signal is lost upon warming to 298K (Figure 6.7f). The signal for species D can be regenerated by admission of an addition dose of CH_3CN/O_2 followed be re-irradiation of the sample at 77K. The signal was only observed in conditions where a high acetonitrile: O_2 ratio was used; in acetonitrile-poor conditions a signal corresponding to the photo-generated O_2^- was observed and in the absence of oxygen, no paramagnetic signal was observed. These two observations prove

that the new radical species D formed from the adsorbed acetonitrile/ oxygen contains oxygen but does not arise from an O_2^- radical.

The spin Hamiltonian parameters of species D are not dissimilar to the [O_2^- ...CH_3CN] intermediate. However, the g_1 value of g = 2.034 and spectral profile are similar to that of an organoperoxy species. Organoperoxy type intermediates formed after irradiation of a co-adsorbed mix of organic: O_2 have been identified over both P25 TiO_2[30,42] and rutile TiO_2 samples[36] and are characterised by the spin Hamiltonian parameters of $g_1 = 2.034$, $g_2 = 2.010$ and $g_3 = 2.003$. These values compare favourably with those observed here, therefore taking into consideration the similar thermal behaviour, species D can be readily assigned to an organoperoxy type radical ROO$^\bullet$. The formation and structure of the ROO$^\bullet$ radical produced after UV irradiation of CH_3CN and O_2 will be discussed in detail in section 6.5.2.

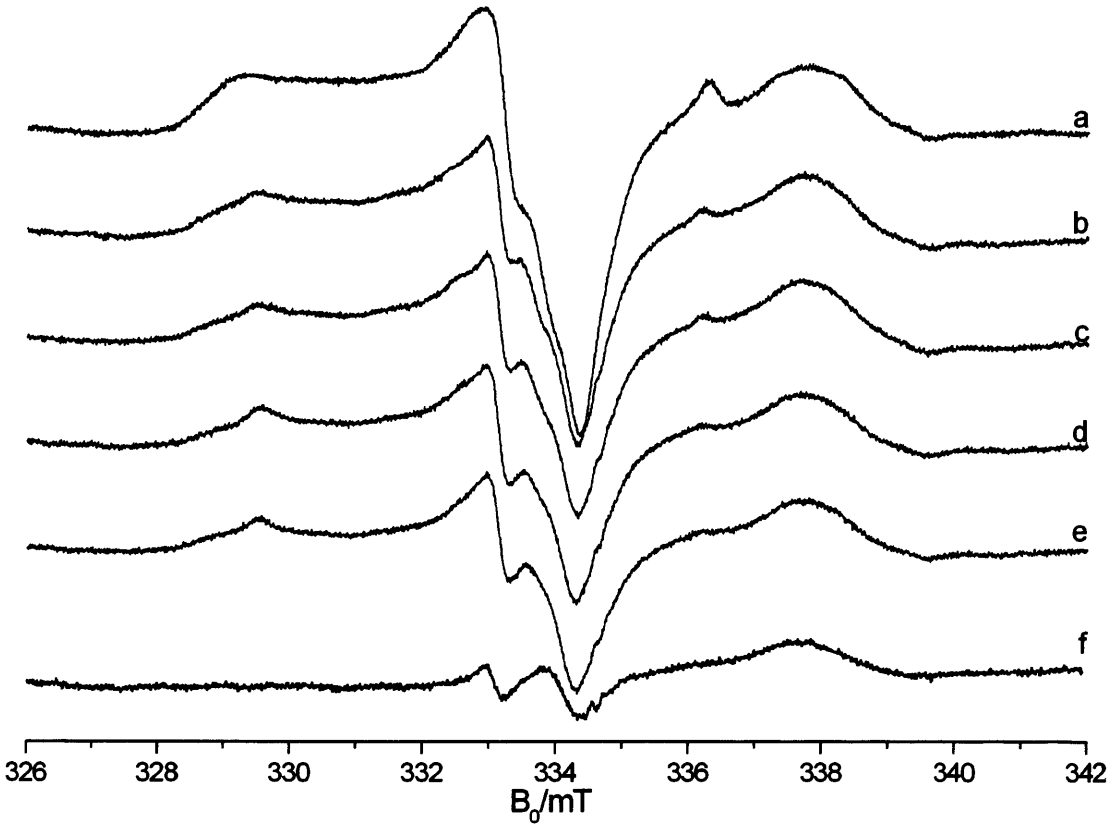

Figure 6.7 *cw*-EPR spectra (130K) of dehydrated TiO_2 after photo irradiation at 77K in the presence of co-adsorbed acetonitrile and oxygen annealed to a) 140, b) 180, c) 200, d) 220, e) 240, and f) 298K.

6.3.6 *Interaction of methanol with $^{16}O_2^-$.*

To probe whether the [O_2^-....Substrate] intermediate observed above with acetonitrile was a common occurrence in the interaction of volatile organic compounds with surface adsorbed O_2^-, it was decided to test the reactivity of O_2^- with methanol. As in the previous study with acetonitrile, exposure of methanol (10 Torr) at room temperature to a sample containing O_2^- radicals (generated on a thermally reduced surface) results in the complete destruction of the EPR signal corresponding to O_2^- radicals. However when the methanol is exposed to the sample at 77K, followed by annealing the sample to elevated temperatures (T = 200-240K), a gradual decrease in the signal intensity of the superoxide radicals is observed, accompanied by a redistribution of the peaks in the g_{zz} region (Figure 6.8b-g).

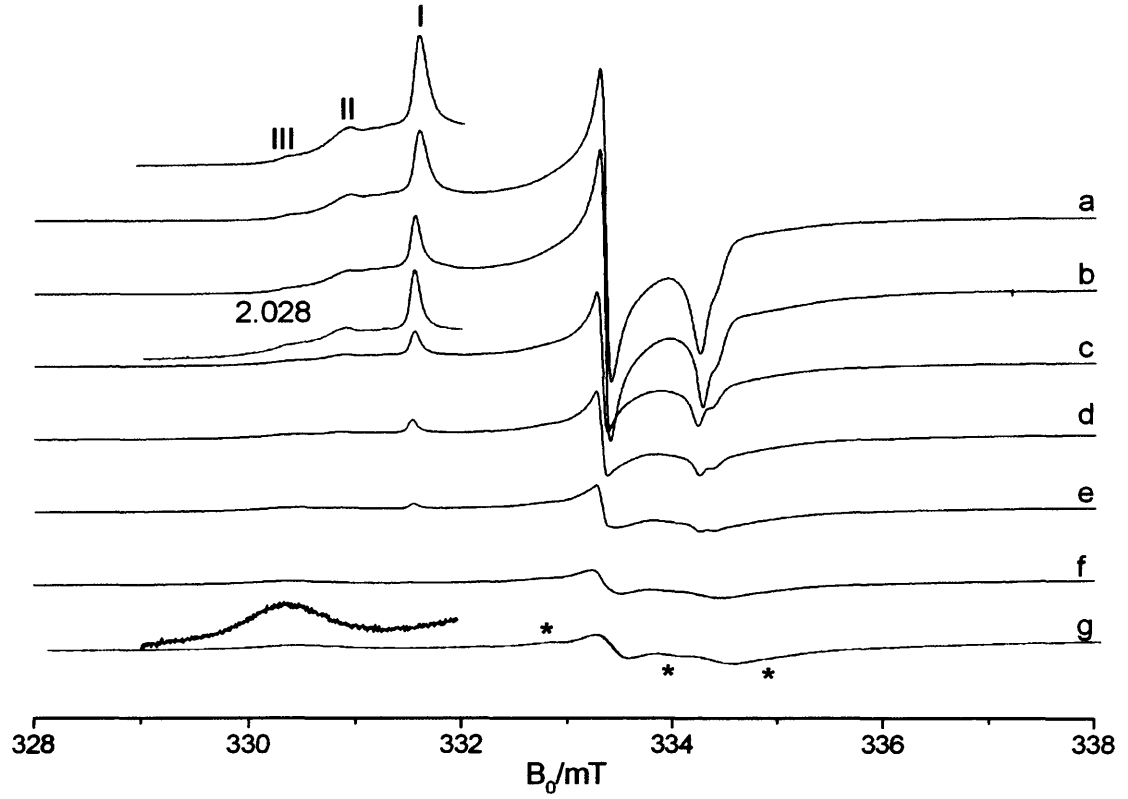

Figure 6.8; *cw*-EPR spectra (130K) of a) superoxide radicals formed by O_2 exposure to a thermally reduced TiO_2 (773K) sample. CH_3OH (10 Torr) was then admitted to the EPR cell at 77K, and the temperature was raised to b) 140, c) 210, d) 215, e) 220, f) 225, and g) 230K.

Simultaneously, upon reaching T ~ 210K the growth of a new signal at g = 2.028 due to a new radical species (E) is observed (see Figure 6.8c). The signal at g = 2.028 increases in intensity as the temperature is increased, before decaying at T > 230K. The reactivity between CH_3OH and O_2^- is not site selective, as observed for the acetonitrile case. Here the intensity of the peaks attributed to sites I-III decrease simultaneously. Additionally a set of peaks close to g_e which can be assigned to species

C ($HO_2^{\bullet}$) are observed at T > 220K. Further confirmation of this assignment was provided by repeating the experiment above with fully deuterated methanol (Figure 6.9) As seen previously in the protic case, annealing the sample to higher temperatures results in a decrease in the superoxide signal intensity which can clearly be seen in Figure 6.9b-g, accompanied by the observation of a new signal at g = 2.028 at T > 210K. However at T > 210K the peaks attributed to the superhyperfine peaks (labelled *) from species C ($HO_2^{\bullet}$) are not seen due to being buried in the intrinsic linewidth of the spectrum.

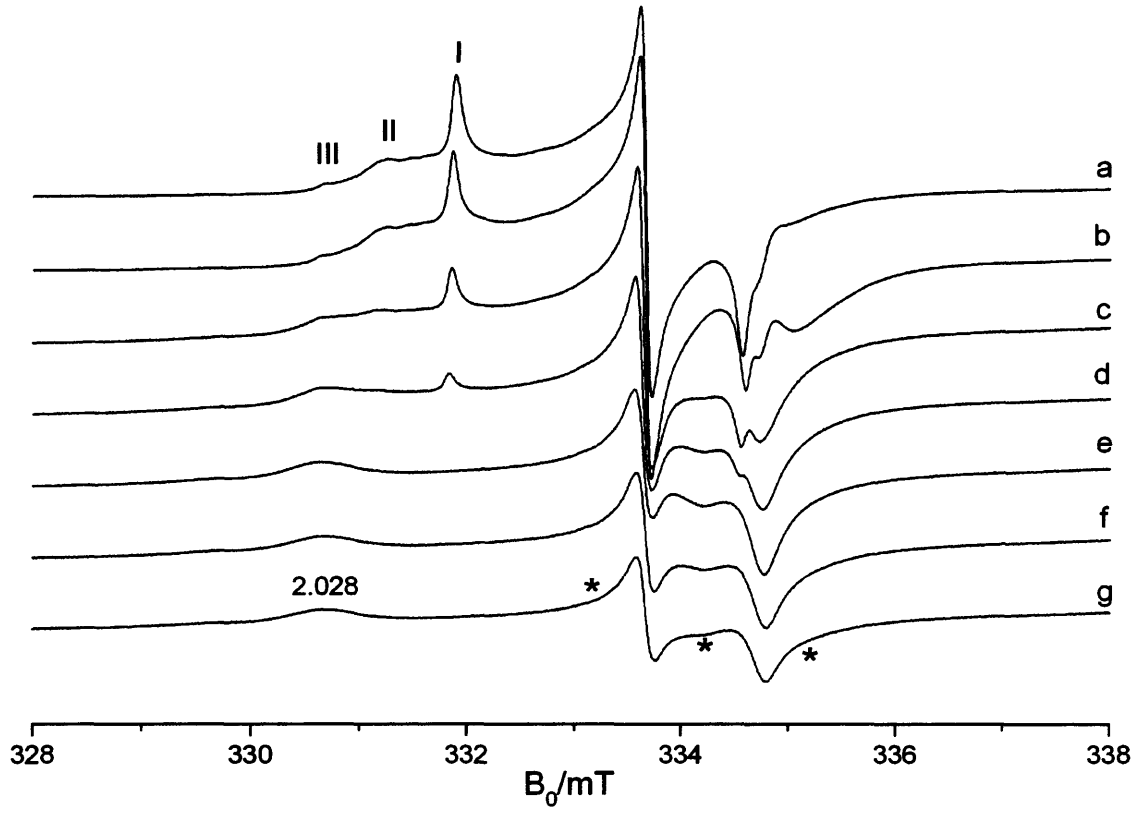

Figure 6.9; *cw*-EPR spectra (130K) of a) superoxide radicals formed by O_2 exposure to a thermally reduced TiO_2 (773K) sample. CD_3OD (10 Torr) was then admitted to the EPR cell at 77K, and the temperature was raised to b) 140, c) 210 , d) 215, e) 220, f) 225 and g) 230K.

Comparison of the experimental spectra (and corresponding computer simulations) for both protic and fully deuterated cases at T = 220K are shown in Figure 6.10. The difference in the spectral profiles between Figure 6.10a,b, where I (^1H) = 1/2 ($HO_2^{\bullet}$) and Figure 6.10c,d where I (^2H) = 1 ($DO_2^{\bullet}$) is easily distinguished. It also provides further information on the identity of the signal arising from species E as the g_1 value of this new radical is very similar to that of $HO_2^{\bullet}$. Upon deuteration however there is no change in the linewidth of the peaks representing the species C.

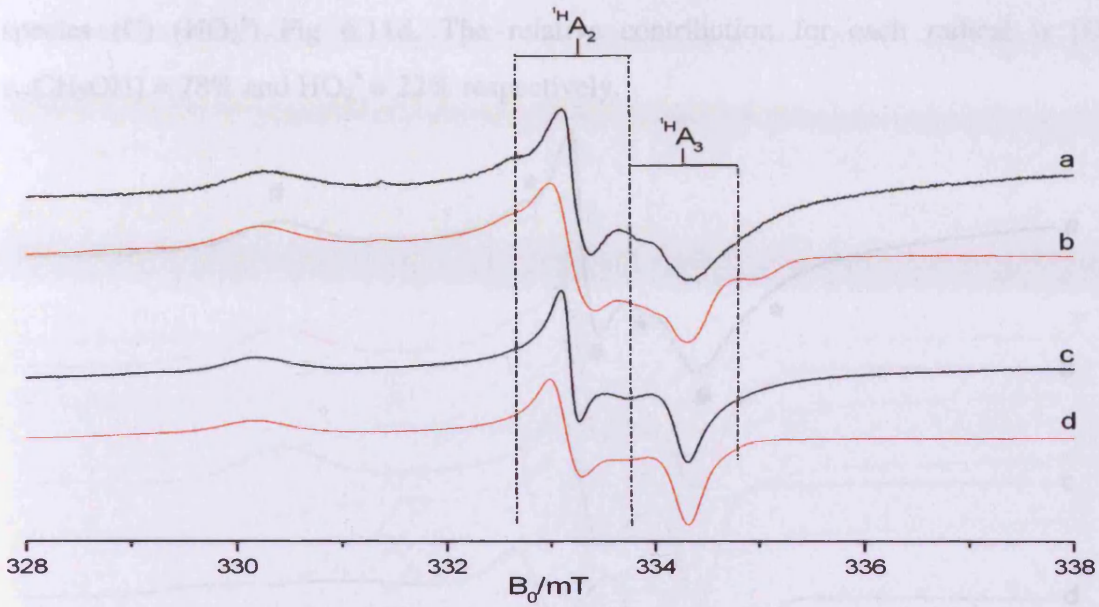

Figure 6.10; (a,c) experimental and (b,d) simulated *cw*-EPR spectra (130K) of CH_3OH adsorption at 77K onto TiO_2 containing O_2^- and following annealing to 220K; (a,b) protic-CH_3OH (c,d) deuterated CH_3OD. The A_2 and A_3 proton superhyperfine couplings are indicated.

The computer simulation enables extraction of the spin Hamiltonian parameters of the transient radical formed on the interaction of O_2^- and methanol at low temperatures (Table 6.2). Deconvolution of the experimental spectrum by simulation, shows that although the spin Hamiltonian parameters of species E and species C are similar, they both give very different spectral profiles, as shown in Figure 6.11a-e.

Table 6.2 Spin Hamiltonian parameters for species C and E, identified after the interaction of methanol with O_2^-.

Radical	g_1	g_2	g_3	A_1/ mT	A_2/ mT	A_3/ mT
Radical E $[O_2^-...CH_3OH]$	2.028	2.01	2.003	No resolved ^1H hfc		
Radical C $(HO_2^{\bullet})$	2.028	2.01	2.004	[(a)] 1.2	1.0	1.0

(a) ^1H

The experimental spectrum resulting from the addition of methanol to O_2^- at 77K, followed by annealing to 220K, is shown in Figure 6.11a. The spectrum is a composite of two signals; the first set is marked with (#) and the second set of signals are marked by (*). The corresponding computer simulation is shown in Figure 6.11b. This complete simulation in Figure 6.11b consists of the summed contributions from the individual simulation of each of the proposed species (E) $[O_2^-...CH_3OH]$ Fig 6.11c and

species (C) ($HO_2^{\bullet}$) Fig 6.11d. The relative contribution for each radical is [O_2^- …CH_3OH] = 78% and $HO_2^{\bullet}$ = 22% respectively.

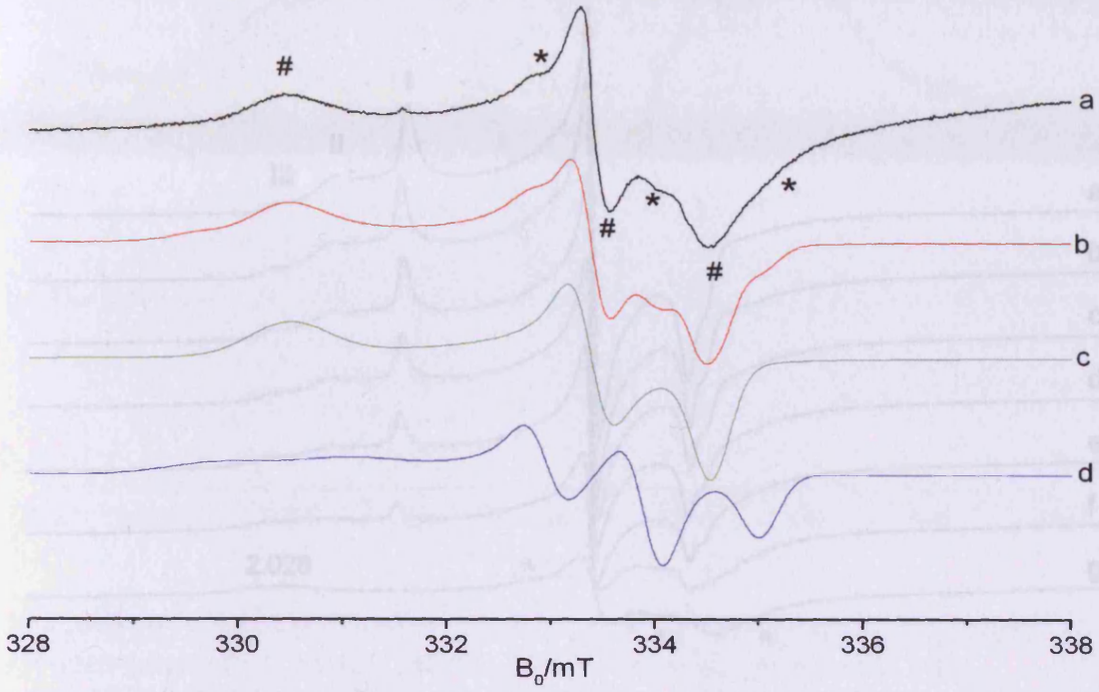

Figure 6.11 a) Experimental and b) simulated *cw*-EPR spectra (130K) of CH_3OH adsorption at 77K onto TiO_2 containing O_2^- and following annealing to 220K. (c,d) are the individual components of b) where the individual contribution of each c) [O_2^-…CH_3OH] = 78% and d) $HO_2^{\bullet}$ = 22% is combined to form the complete simulated spectrum.

The initial step in the formation of the hydroperoxy ($HO_2^{\bullet}$) species is believed to be the abstraction of a proton by the Lewis acid sites on the surface of TiO_2. The use of methanol as a substrate provides a way to confirm the origin of the abstracted proton. In the methanol case there are three possibilities; (1) to abstract the proton from the $-CH_3$ group, (2) from the –OH group of methanol or (3) alternatively from a surface hydroxyl group. It has been shown that full deuteration of the methanol (CD_3OD) results in the loss of the superhyperfine peaks due to $HO_2^{\bullet}$, indicating that the abstracted H^+ comes from the adsorbed substrate and not surface OH groups. In this experiment the –OH group of the methanol is selectively deuterated to give CH_3OD. As in previous experiments the CH_3OD was adsorbed onto a sample of TiO_2 containing the O_2^- radicals at 77K.

As the temperature of the sample was raised the marked decrease in the signal intensity arising from O_2^- (Figure 6.12b-d) is accompanied by a new signal at g = 2.028 at T = 210K as observed previously for methanol with O_2^-. More importantly in this experiment is the presence of the superhyperfine peaks close to g_e, resulting from the $HO_2^{\bullet}$ radical (labelled *) in Figure 6.12g. The presence of these peaks indicates that the

hydrogen for formation of $HO_2^{\bullet}$ has been extracted from the $-CH_3$ group of the methanol.

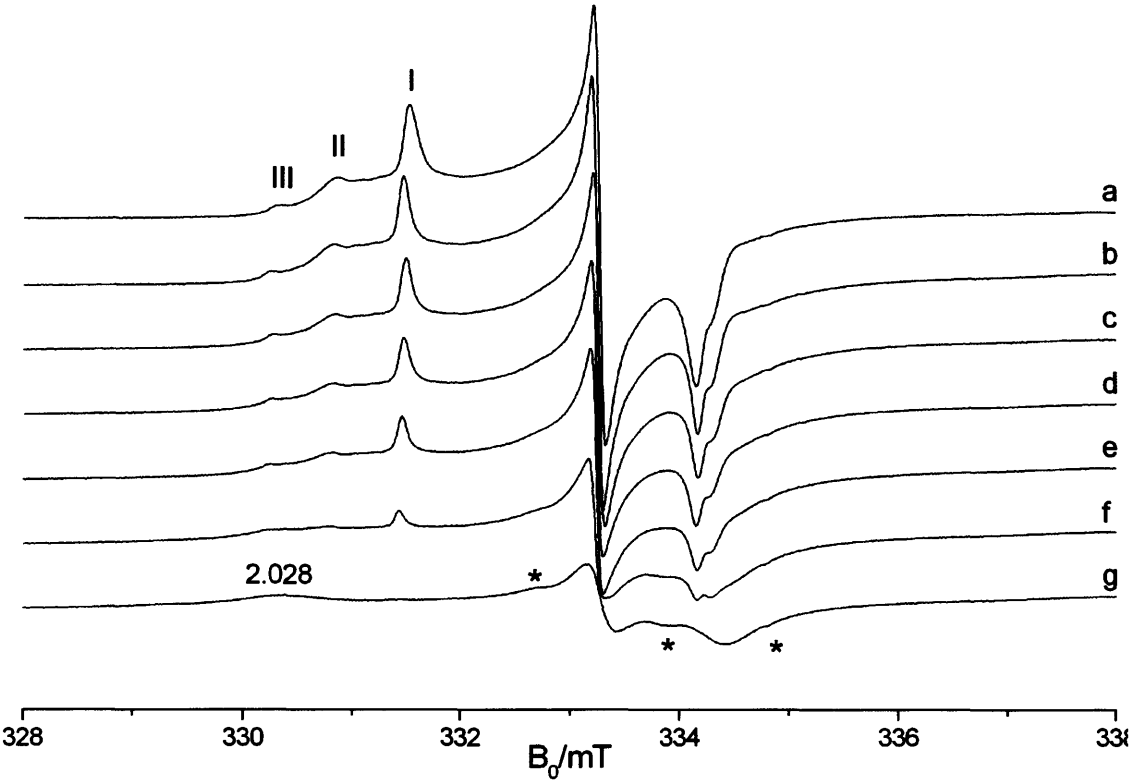

Figure 6.12 *cw*-EPR spectra (130K) of a) superoxide radicals formed by O_2 exposure to a thermally reduced TiO_2 (773K) sample. CH_3OD (10 Torr) was then admitted to the EPR cell at 77K, and the temperature was raised to b) 140, c) 200, d) 205, e) 210, f) 215, g) 220K .

In summary, the addition of methanol to O_2^- results in the formation of two new transient radical species C ($HO_2^{\bullet}$) and E [O_2^-...CH_3OH]. The g-values and thermal behaviour of species E are similar to those observed in the acetonitrile[43] and acetone cases[30]. This assignment for the identity of species E will be discussed further in section 6.4.4

6.3.7 *UV irradiation of co-adsorbed methanol/ $^{16}O_2$ over the clean activated surface*

In order to study how different adsorption conditions affect radical formation, a pre-mixed dose of methanol and oxygen was co-adsorbed onto the TiO_2 surface (ratio 10:1, total pressure 15 Torr). The sample was then UV irradiated at 77K for 30 minutes. The sample was transferred to the precooled EPR cavity (130K). Subsequently the sample was evacuated at 130K *in-situ* to remove the excess gas to give the resulting spectrum shown in Figure 6.13.

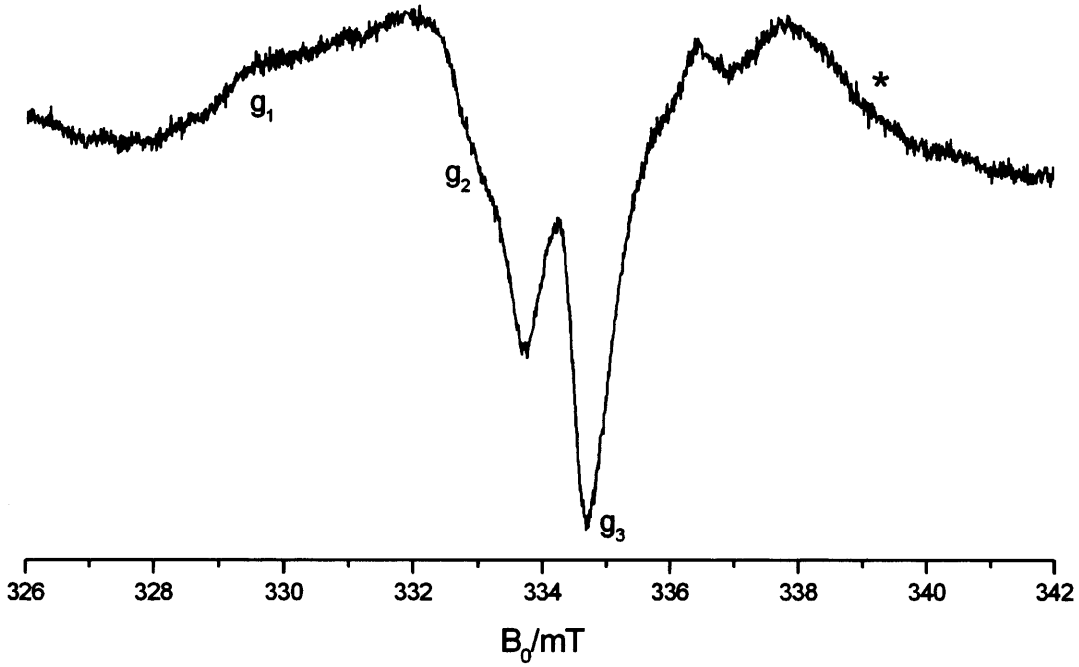

Figure 6.13 Experimental *cw*-EPR spectrum (130K) of photoirradiated TiO_2 containing co-adsorbed methanol: O_2 in a 10:1 ratio. The UV irradiation was performed at 77K.

UV irradiation results in an orthorhombic signal with the spin Hamiltonian parameters of $g_1 = 2.034$, $g_2 = 2.010$ and $g_3 = 2.003$ which can be assigned to a ROO type species ($HOCH_3OO^{\bullet}$). Additionally a second set of signals at g = 1.989 and g = 1.972 (labelled *) are resolved which can be attributed to bulk Ti^{3+} sites formed on low temperature irradiation of TiO_2.[36,39,40] On warming to room temperature both signals are lost; however both can be regenerated *via* low temperature irradiation in the presence of a new dose of CH_3OH:O_2. The signal observed with CH_3OH:O_2 is less intense than that seen under equivalent conditions with CH_3CN (Figure 6.6), which may be due to the reduced stability of the radical formed with CH_3OH compared to that with CH_3CN.

6.3.8 Interaction of toluene with $^{16}O_2^-$

The previous experiments performed for CH_3CN and CH_3OH were repeated with toluene as the chosen substrate. Addition of toluene to a sample of TiO_2 containing superoxide radicals at room temperature resulted in the loss of the O_2^- radicals as evidenced by the complete destruction of the corresponding EPR signal (spectra not shown).

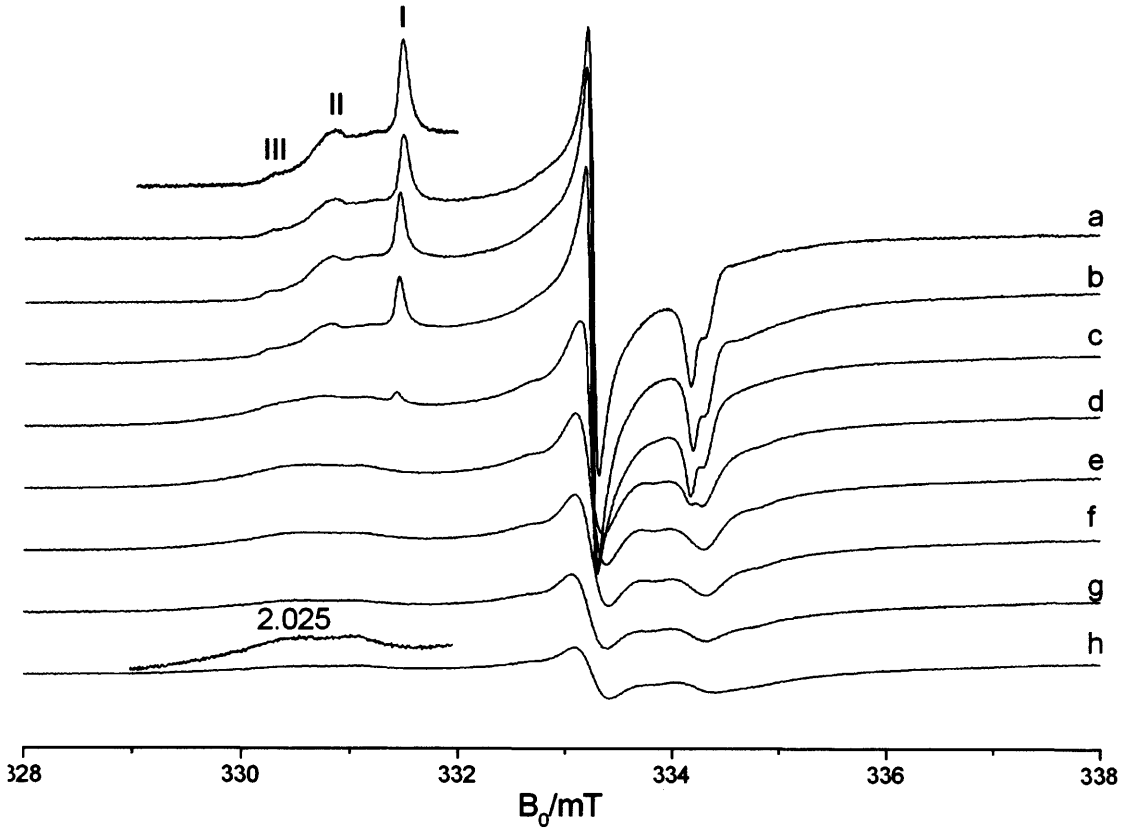

Figure 6.14 *cw*-EPR spectra of a) superoxide radicals formed by O_2 exposure to a thermally reduced TiO_2 (773K) sample. $C_6H_5CH_3$ (10 Torr) was then admitted to the EPR cell at 77K, and the temperature was raised to b) 140, c) 215, d) 230, e) 240, f) 245, g) 255, and h) 265K .

On addition of toluene at 77K, followed by gradual annealing to elevated temperatures (200-265K), there is a gradual decrease in the O_2^- signal intensity on increasing the temperature (Figure 6.14b-h) accompanied by the appearance of a new peak in the g_{zz} region at T > 230K. In this case the reactivity of the O_2^- and toluene is site specific, with site I reacting preferentially compared to sites II-III. This is accompanied by a redistribution of the g_{zz} peaks, signified by the loss in intensity of the g_{zz} peak for site I on increasing temperature. Accompanying the loss in intensity of the superoxide species is the observation of a new signal at T > 230K. Initially it is hard to distinguish the g_1 component of the new radical as it is obscured by the g_{zz} region of the O_2^-, but at T ~ 240K a new peak is clearly resolved at g = 2.025. Additionally, there is a new signal present in the g_{xx} region at g_{xx} = 2.004, which continues to grow in intensity up to T ~ 255 K before decaying at increased temperatures.

By comparison to the results obtained using methanol and acetonitrile the reaction of toluene with the O_2^- occurs at T > 230K with the signal due to the new radical present at these temperatures.

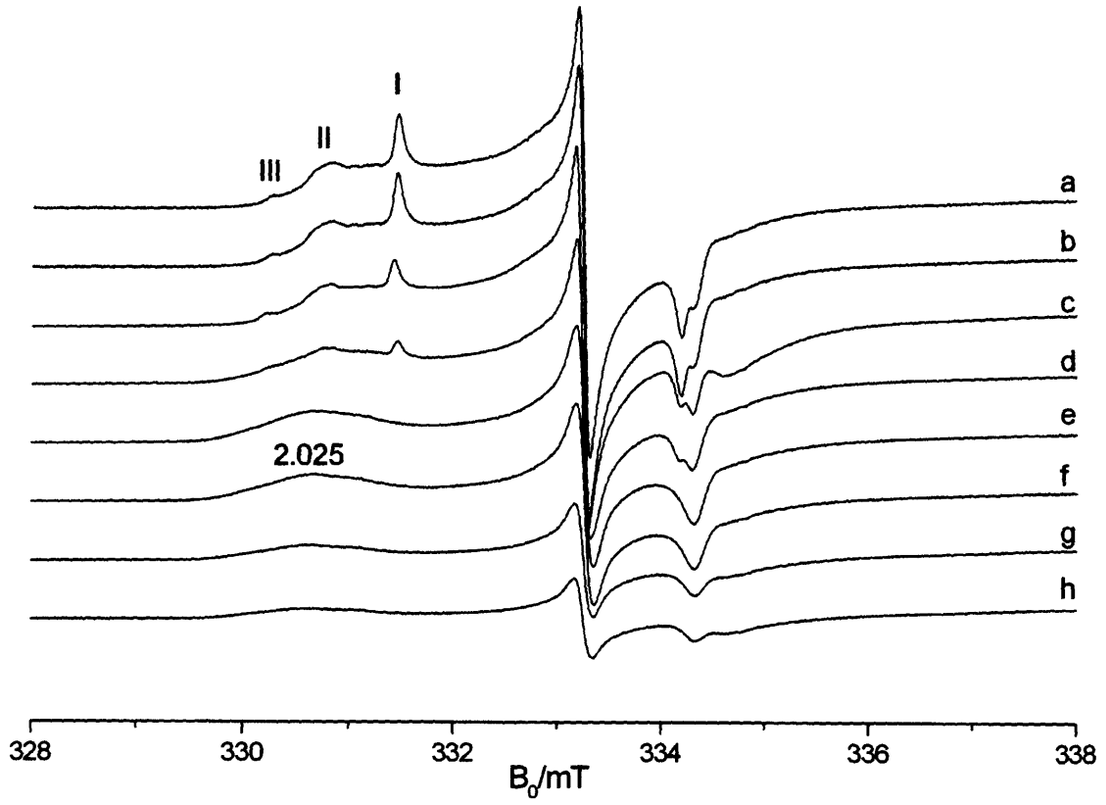

Figure 6.15 *cw*-EPR spectra (130K) of a) superoxide radicals formed by O_2 exposure to a thermally reduced TiO_2 (773K) sample. $C_6D_5CD_3$ (10 Torr) was then admitted to the EPR cell at 77K, and the temperature was raised to b) 140, c) 215, d) 230, e) 240, f) 255, and g) 265K.

The new radical signal was accompanied by peaks close to g_e which appeared at 230K and began to decay on increasing temperature. These can be assigned to species C ($HO_2^{\bullet}$). Confirmation of this assignment was obtained by repeating the experiment using deuterated toluene (Figure 6.15). Once the toluene is added at 77K and annealed to elevated temperatures, the O_2^- signal intensity is seen to decrease in intensity accompanied by the appearance of a new signal at 230K at $g_{zz} = 2.025$ (Species G) and more obviously $g_{xx} = 2.004$. Significantly the peaks associated with the $HO_2^{\bullet}$ are absent due to the fact the linewidth is narrowed on changing from protic (I (^{1}H) = 1/2) to deuterated (I (^{2}D) = 1) toluene and are therefore obscured by the intrinsic line width of the spectrum.

Due to the difficulty in identifying the g_1 value of the radical G, as it is buried among the g_{zz} components of the O_2^-, the experiment was repeated with superoxide generated on a surface thermally reduced to 623K. The lowering of the reduction temperature prevents speciation of the superoxide, resulting in a superoxide with a single site I and the spin Hamiltonian parameters of $g_1 = 2.019$, $g_2 = 2.011$ and $g_3 =$

2.005 significantly simplifying the spectra. Toluene was exposed to the superoxide species and the resulting spectra are shown in Figure 6.16.

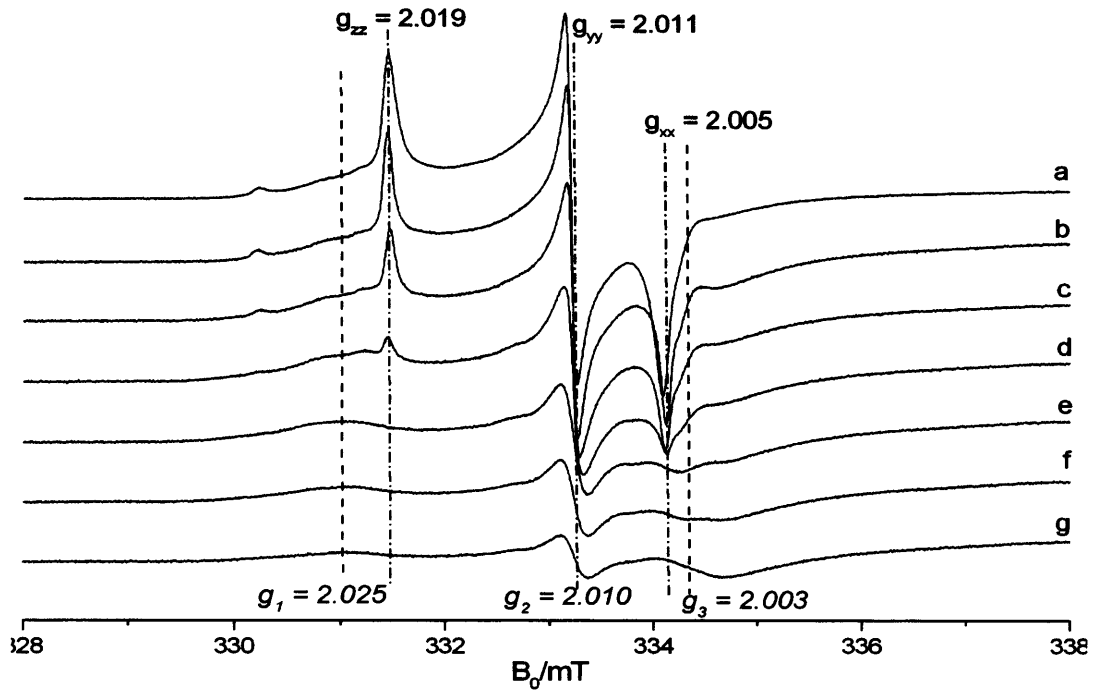

Figure 6.16 *cw*-EPR spectra (130K) of a) superoxide radicals formed by O_2 exposure to a thermally reduced TiO_2 (623K) sample. $C_6H_5CH_3$ (10 Torr) was then admitted to the EPR cell at 77K, and the temperature was raised to b) 130, c) 220, d) 230, e) 240, f) 250, and g) 260K. The g values for radicals A and G are marked in bold and italics, respectively.

Owing to the improved resolution the experimental data was simulated to extract the spin Hamiltonian parameters for species G of g_1= 2.025, g_2 = 2.010 and g_3 = 2.004 (Table 6.3). Once the spin Hamiltonian parameters of the radical species G were extracted the experimental data for both protic and deuterated cases were simulated to check the assignment (Figure 6.17).

Table 6.3 Spin Hamiltonian parameters for the transient radical species G and C identified after the interaction of toluene and O_2^- at low temperature.

Radical	g_1	g_2	g_3	A_1/ mT	A_2/ mT	A_3/ mT
Radical G $[O_2^-...CH_3C_6H_5]$	2.025	2.01	2.004	No resolved ^1H hfc		
Radical C $(HO_2^{\bullet})$	2.028	2.01	2.004	[(a)] 1.2	1.0	1.0

(a) ^1H

The interaction of toluene and O_2^- results in the formation of two radical species C and G. Species C has been indentified as $HO_2^{\bullet}$, by comparison of its spin Hamiltonian parameters to the available literature data and further confirmation was obtained by its

behaviour upon deuteration where the superhyperfine peaks could no longer be resolved (see Figure 6.17). The new radical species G was found to be thermally unstable and is identifiable by the spin Hamiltonian parameters of $g_1 = 2.025$, $g_2 = 2.010$ and $g_3 = 2.004$. Although the g_1 value observed for species G is lower than that of the intermediates identified in the acetone, acetonitrile and methanol cases the radical species shares similar characteristics in its formation and decay. The difference in the g_1 value could be due to the fact that the interaction between the O_2^- and toluene is much stronger due to the stronger electron withdrawing power of the benzene ring. A preliminary assignment for this intermediate is proposed as $[O_2^-...CH_3C_6H_5]$ for reasons which will be discussed in more detail in section 6.4.6.

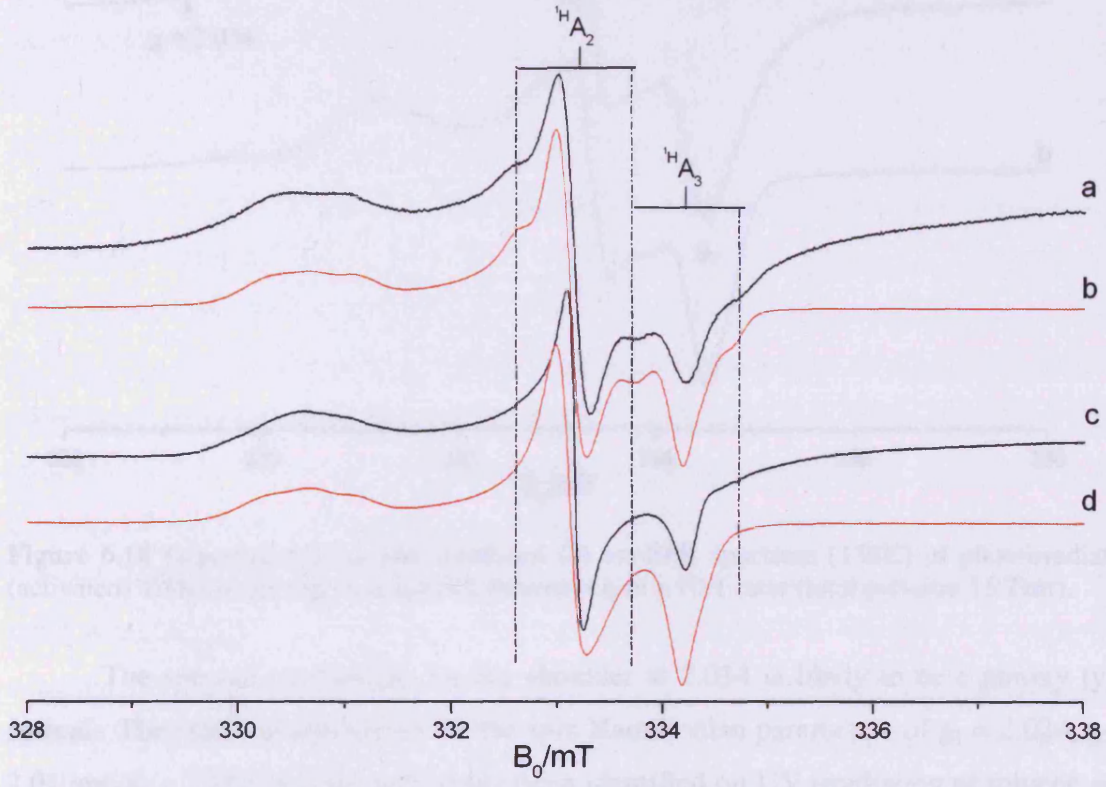

Figure 6.17 (a,c) experimental and (b,d) simulated *cw*-EPR spectra (130K) of $C_6H_5CH_3$ adsorption at 77K onto TiO_2 containing O_2^- and following annealing to 240K; (a,b) Protic-$C_6H_5CH_3$ (c,d) $d^8 - C_6D_5CD_3$. The A_2 and A_3 proton superhyperfine couplings are indicated.

6.3.9 *UV Irradiation of co-adsorbed toluene/ $^{16}O_2$ over the clean activated surface*

To a clean activated sample a dose of toluene: oxygen (10:1 ratio) was co-adsorbed after being premixed in the vacuum line (total pressure 15 Torr). The sample was then UV irradiated at 77K for 30 minutes. The sample was transferred to the EPR cavity precooled to 130K. Subsequently the sample was evacuated at 130K *in situ* to remove the excess gas and the spectra recorded at 130K, shown in Figure 6.18.

The EPR spectrum is dominated by an orthorhombic signal as seen in Figure 6.18a with the spin Hamiltonian parameters $g_1 = 2.024$, $g_2 = 2.01$ and $g_3 = 2.003$. The signal also has an additional shoulder at $g = 2.034$. The signal decays at $T > 190K$ and is lost at room temperature. However, the signal can be regenerated upon subsequent recooling followed by UV irradiation at 77K in the presence of a new dose of $C_6H_5CH_3$:O_2. The signal is only observed under toluene-rich conditions; under O_2-rich conditions the spectra are dominated by superoxide radicals and in a toluene only atmosphere there is no new EPR signal observed after irradiation.

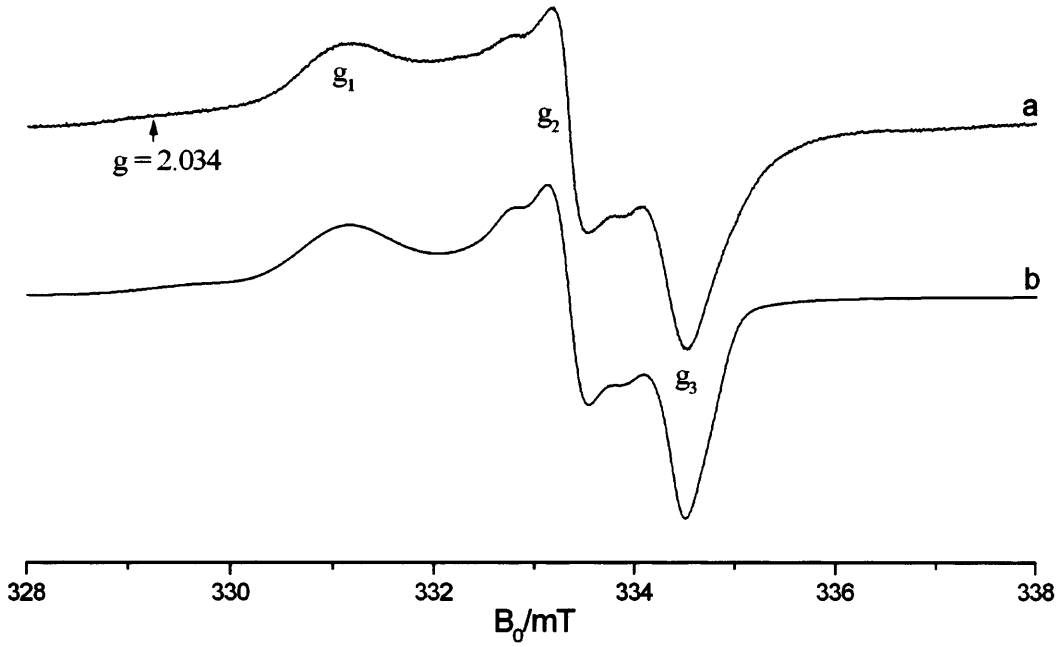

Figure 6.18 Experimental (a) and simulated (b) *cw*-EPR spectrum (130K) of photoirradiated (activated) TiO_2 containing co-adsorbed toluene: O_2 in a 10:1 ratio (total pressure 15 Torr).

The species responsible for the shoulder at 2.034 is likely to be a peroxy type radical. The signal characterised by the spin Hamiltonian parameters of $g_1 = 2.024$, $g_2 = 2.01$ and $g_3 = 2.003$ has not previously been identified on UV irradiation of toluene and oxygen. The signal could be due to O_2^- radicals as the low g_1 value is typical of superoxide, but the signal is lost on warming to room temperature, which would seemingly rule out superoxide which is normally stable at room temperature. The second assignment could be a second peroxy species. Further confirmation of this could be provided by replacing the $^{16}O_2$ in the co-adsorbed mix with $^{17}O_2$ which would result in an EPR signal with a distinctive hyperfine pattern. This would provide a way to distinguish between O_2^- and $ROO^\bullet$ as both species have different hyperfine patterns.

6.4 Discussion

The degradation of VOC's over the surface of TiO_2 is an important area of research. It is believed that oxygen centred radicals are key intermediates in these surface reactions that take place at the surface. However, little is understood about the nature of the transient radical intermediates involved and what role they play in the mechanism. In this chapter a series of transient radical intermediates formed after the reaction of organic substrates (acetonitrile, methanol and toluene) with surface adsorbed O_2^- anions have been identified. For comparison, transient radicals that are formed photochemically after UV irradiation of the TiO_2 in the presence of a co-adsorbed mix of organic/oxygen have also been studied to provide a comparison of how different surface treatments can affect radical formation. The formation and relevance of these radicals will be discussed in detail below.

6.4.1 Interaction of acetonitrile with O_2^- : The [O_2^-...CH_3CN] radical.

The surface adsorbed O_2^- has been postulated as being an important intermediate in heterogeneous catalysis.[31] Here it is shown that surface adsorbed O_2^- can react with acetonitrile to produce a thermally unstable intermediate characterised by the g values, $g_1 = 2.031$, $g_2 = 2.010$ and $g_3 = 2.003$ (labelled species B). Species B is initially observed at 210K and subsequently decays at temperatures T > 250K. It can be formed upon interaction of CH_3CN with superoxide formed photochemically or thermally. The g values of the new species can be compared to those of other known surface oxygen radicals originating from the interaction and reactivity of organic substrates with molecular oxygen over polycrystalline titania.[30,38,42] In the absence of hyperfine coupling, the $HO_2^\bullet$ radical can be eliminated as a possible assignment of species B, while O_2^- can also be discounted on stability grounds (O_2^- is usually stable at room temperature), and the high g_1 component of 2.031 which is not known for O_2^- stabilised on TiO_2. Possible candidates therefore include the surface organoperoxy radical (such as $NCCH_2OO^\bullet$) or a surface adduct formed between acetonitrile and adsorbed superoxide (such as [O_2^-...CH_3CN]). According to previous work by Carter *et al.*,[30] analogous radical adducts were indeed identified on TiO_2 with acetone (i.e. $CH_3COCH_2OO^\bullet$ and [O_2^-...CH_3COCH_3] respectively) which displayed similar g-values and similar thermal stabilities to the radical species observed in this work. The only way to confidently discriminate between the two possible assignments is to use ^{17}O- labelled molecular

oxygen, since the former peroxy radicals produce a characteristic and easily recognisable ^{17}O hyperfine pattern.

The absence of any observable hyperfine patterns, suggestive of inequivalent oxygen atoms (as expected for $NCCH_2O^{17}O^{\bullet}$), thereby rules out any possible assignment based on oxygen atoms with uneven spin densities, such as peroxy ($ROO^{\bullet}$)[42] or peroxyacyl ($RCOOO^{\bullet}$)[36] type species. Furthermore it has previously been shown that both of these families of organoperoxy intermediates are generated *via* hole-mediated processes during photoirradiation,[30,36] and their formation under the current dark conditions would be unexpected and unusual.

Previous studies by Coronado *et al.*,[44] and Henderson *et al.*,[45-47] showed that both thermal and photochemical reactions of acetone on TiO_2 can involve nucleophilic attack by an O_2 species on an acetone molecule, forming an [acetone- oxygen] surface complex. Furthermore, Carter *et al.*,[30] recently identified an analogous paramagnetic intermediate, labelled $[O_2^-...CH_3COCH_3]$, which was formed by the reaction of acetone with adsorbed O_2^- radicals on TiO_2 under dark conditions. The g values of this $[O_2^-....CH_3COCH_3]$ adduct complex were reported as $g_1 = 2.035$, $g_2 = 2.008$, and $g_3 = 2.003$, while the complex was also found to be thermally unstable at temperatures $T > 250K$. Moreover, the ^{17}O hyperfine pattern identified in the complex was also indicative of equivalent oxygen atoms. It is therefore reasonable to assume that the radical formed after reaction of O_2^- and acetonitrile can be assigned to a similar surface complex, labelled $[O_2^-...CH_3CN]$ and formed by the nucleophillic attack of O_2^- on CH_3CN, in which the unpaired spin density in the dioxygen moiety remains equivalent, due to the side-on manner of the interaction between O_2^- and CH_3CN.

6.4.2 Interaction of acetonitrile with O_2^-: the $[HO_2^{\bullet}]$ radical.

The second new species identified in this study is a hydroperoxy type radical (species C), first observed at $T > 220K$ after addition of acetonitrile to O_2^- radicals. Species C has the spin Hamiltonian parameters of $g_1 = 2.028$, $g_2 = 2.010$, and $g_3 = 2.004$, $A_1 = 1.2$ mT, $A_2 = 1.0$ mT and $A_3 = 1.0$ mT, which were extracted *via* computer simulation. By comparison with the literature data, it is reasonable to assign this species C to the hydroperoxy ($HO_2^{\bullet}$) radical. This radical has been identified by EPR on TS-1 and is characterised by analogous spin Hamiltonian parameters ($g_1 = 2.034$, $g_2 = 2.008$, $g_3 = 2.002$, $A_1 = 1.3$ mT, $A_2 = 1.0$ mT and $A_3 = 1.0$ mT).[38,48] The lower g_1 value in this work may be due to the slightly different electrostatic potential of the Ti^{4+} cations in

TS-1 compared to TiO_2. Further confirmation on the identity of this species as the protonated form of O_2^- was confirmed by using deuterated acetonitrile, as the superhyperfine peaks were absent in the deuterated spectrum.

Zhaung *et al.*,[18] showed that, at temperatures below 126K, a layer of (frozen) adsorbed acetonitrile existed on the surface of TiO_2; diffusion of the organic substrate into the porous TiO_2 powder only occurred at higher temperatures.[18] Using IR, the authors confirmed that acetonitrile adsorption occurred both on surface hydroxyl groups and Lewis acid sites at 200K.

$$Ti^{4+}{-}O^{2-} + CH_3CN \rightarrow Ti^{4+}{-}OH + CH_2CN^- \quad (6.1)$$

$$Ti^{4+}{-}OH + O_2^- \rightarrow Ti^{4+}{-}[OH....O_2^-] \quad (6.2)$$

It should be noted that the thermally reduced titania still contains basic surface O^{2-} anions. In the presence of these anions, the adsorbed acetonitrile can act as a Brönsted acid, leading to the formation of the CH_2CN^- anion.[15] The abstracted proton reacts with the basic surface O^{2-} anions forming hydroxyl groups and it is proposed that these can subsequently interact with the O_2^- radical to give the hydroperoxy type radicals (species C).

6.4.3 Interaction of acetonitrile with O^-: The [$NCCH_2OO^\bullet$] radical.

UV irradiation of a co-adsorbed mix of acetonitrile and oxygen over a dehydrated TiO_2 surface resulted in a previously unreported EPR signal. The new species D is characterised by the spin Hamiltonian parameters of $g_1 = 2.034$, $g_2 = 2.007$ and $g_3 = 2.001$. The signal was lost on warming to 298K and could subsequently be regenerated upon further UV irradiation with a fresh dose of CH_3CN/O_2. EPR signals with similar behaviour and spin Hamiltonian parameters have been identified in this chapter, generated after the reaction of superoxide and acetonitrile; however under UV irradiation it is likely that a hole-mediated process is favourable. Further evidence of this is provided as the new species is only observed under organic-rich conditions, where formation of superoxide is blocked by the high surface coverage of CH_3CN. In the literature UV irradiation of a co-adsorbed mix of organic:oxygen, where the organic was a ketone[30,42], an aldehyde[36] or ethylene[49] have been identified as producing organoperoxy type intermediates ($ROO^\bullet$). Irradiation of TiO_2 results in the generation of an electron (e^-)-hole (h^+) pair. These can either recombine in the bulk or migrate to

the surface of the TiO_2, where they can participate in surface reactions with adsorbed species. The electron can migrate to the surface and interact with a Ti^{4+} centre to give a Ti^{3+} centre. The holes are trapped at surface O^{2-} sites to give O^-. The acetonitrile is adsorbed on the titania surface at Lewis acid sites and is quickly deprotonated by H^+ transfer, to produce a hydroxyl group and $NCCH_2^\bullet$ (eq 6.3).

$$CH_3CN + O^- \rightarrow NCCH_2^\bullet + OH^- \qquad (6.3)$$

The resulting radical cation can then react with molecular oxygen forming the peroxy radical as shown in (eq 6.4)

$$CNCH_2^\bullet + O_2 \rightarrow CNCH_2OO^\bullet \qquad (6.4)$$

A similar mechanism for the formation of peroxy ($ROO^\bullet$) type radicals has been identified in the literature.[36,42,49] The resulting thermally unstable organoperoxy intermediates were characterised by the spin Hamiltonian parameters of $g_1 = 2.034$, $g_2 = 2.008$ and $g_3 = 2.001$. The thermal characteristics of these intermediates are identical to that of species D (identified in Figure 6.6). It is reasonable to suggest that species D is an organoperoxy radical, formed upon the UV irradiation of a co-adsorbed mix of oxygen and acetonitrile over TiO_2. Further information on the organoperoxy species could be obtained by using ^{17}O labelled oxygen which would provide further information on the electronic structure of the radical and comprehensive proof that it was a peroxy type intermediate ($ROO^\bullet$). The organoperoxy species when labelled with ^{17}O should give a distinctive hyperfine pattern with two superimposed sextets (due to $^{-17}OO^\bullet$ and $^-O^{17}O^\bullet$) in the EPR spectrum. However, due to the weakness of the signal in Figure 6.6, ^{17}O labelling was not used.

6.4.4 Interaction of CH_3OH with O_2^-: The $[O_2^-...CH_3OH]$ radical.

Thermally unstable intermediates formed at low temperatures after addition of acetonitrile or acetone to O_2^- on the TiO_2 surface have been identified at low temperatures. The radicals are believed to form by the nucleophillic attack of O_2^- on the adsorbed organic substrate, resulting in $[O_2^-...Substrate]$ type intermediates.[30,43]

Methanol was adsorbed to O_2^- radicals at RT and 77 K. At room temperature the methanol reacted with the O_2^- radicals resulting in the loss of the EPR signal. After

addition at 77K and subsequent annealing of the sample to elevated temperatures a new radical (Species E) was observed with the spin Hamiltonian parameters $g_1 = 2.028$, $g_2 = 2.01$ and $g_3 = 2.003$. It is formed at 210K and subsequently decays at elevated temperatures. The behaviour of species E is similar to that of the $[O_2^-...CH_3CN]$ and $[O_2^-....CH_3COCH_3]$ formed on the interaction of O_2^- with acetonitrile and acetone respectively, therefore it is likely that this new radical species is formed by nucleophillic attack of O_2^- on the carbon of the methyl group to give $[O_2^-...CH_3OH]$. The signal intensity of radical E is low; this could be due to competition with other surface processes involving adsorption of methanol, as a number of thermal decomposition routes have been identified.[7,50,51] However, species E is not observed when methanol is adsorbed onto a clean TiO_2 surface (containing no O_2^- species), indicating that the presence of oxygen (in the form of O_2^-) is a requisite in the formation of species E. Definitive proof that species E is an $[O_2^-....Substrate]$ adduct rather than a $ROO^\bullet$ species would be provided by repeating the experiment with $^{17}O_2$, but nevertheless from the available evidence the species is confidently assigned as being an $[O_2^-.....CH_3OH]$ adduct.

This is the first time a transient radical has been identified *via* EPR after the interaction of O_2^- and methanol. The bulk of the literature focuses on the interaction of methanol with the clean TiO_2 surface and the subsequent thermal or photochemical degradation processes. In a detailed study by Hussein *et al.*,[7] a number of decomposition products such as CH_4, CH_2O, $(CH_3)_2O$, CO and H_2O have been identified in the degradation of methanol over the TiO_2 surface. The initial step is the chemisorption of methanol onto the TiO_2 surface *via* the O atom, losing H^+ in the process (eq 6.5).[7,50-52]

$$CH_3OH_{(a)} + O^{2-}_{(a)} \rightarrow CH_3O^-_{(a)} + OH^-_{(a)} \qquad (6.5)$$

However, the results in this work contradict this description. Following the selective deuteration of the methanol, it was found that the hydrogen is extracted from the methyl group of CH_3OH (eq 6.6), confirmed by the fact that no loss in the superhyperfine peaks of $HO_2^\bullet$ was observed when the methanol was selectively deuterated (CH_3OD) and reacted with O_2^- (Figure 6.7).

$$CH_3OH + O^{2-} \rightarrow {}^-CH_2OH + OH^- \qquad (6.6)$$

Alternatively the methanol could be adsorbed as described in (eq 6.5) followed by a further step, where an additional hydrogen atom is abstracted from the adsorbed methoxy by the Lewis acid centres (6.7):

$$CH_3O^- + O^{2-} \rightarrow CH_2O^{2-} + OH^- \qquad (6.7)$$

Either way, the formation of a hydroperoxy type species is observed and the mechanism is the same as described for acetonitrile, where OH^- can subsequently interact with the surface O_2^- to give a hydroperoxy type species as shown below

$$OH^- + O_2^- \rightarrow [OH^- \ldots O_2^-] \qquad (6.8)$$

The identification of this hydroperoxy intermediate is important as it has been postulated to take part in the thermal and photochemical reactions of methanol over TiO_2[51].

The identification of two transient radical species formed after reaction of methanol and O_2^- is important. The first species [O_2^- ...CH_3OH] has not previously been observed in the literature and its structure and role in the decomposition of methanol over TiO_2 needs to be investigated further. The second species $HO_2^\bullet$ has previously been postulated to be involved in the decomposition of methanol[51]. The EPR data presented in this chapter provides comprehensive evidence of its formation.

6.4.5 Interaction of CH_3OH with O^-: the [$HOCH_2OO^\bullet$] radical.

Co-adsorption of methanol and oxygen over the TiO_2 surface followed by UV irradiation results in the formation of a transient radical that is unstable on warming to room temperature. The signal is only observed in a methanol-rich atmosphere and is not observed in a methanol-only or purely O_2 atmosphere. Its spin Hamiltonian parameters are $g_1 = 2.034$, $g_2 = 2.008$ and $g_3 = 2.002$. This suggests that the intermediate is a transient surface species most likely to be the ($ROO^\bullet$) peroxy type. This peroxy type radical is formed *via* hole transfer, with the initial step occurring *via* the reaction of the hole with methanol (eq 6.9) as detailed by Micic *et al.*,[53]

The formation of this methoxy radical has been proposed by many authors[25,51] and it is believed to play an important role in the photooxidation of methanol. Many

reaction routes have been proposed. Wu *et al.*,[51] and Sadegi *et al.*,[54] believe that the photooxdation proceeds *via* a Russel-like mechanism as shown in Figure 6.19.

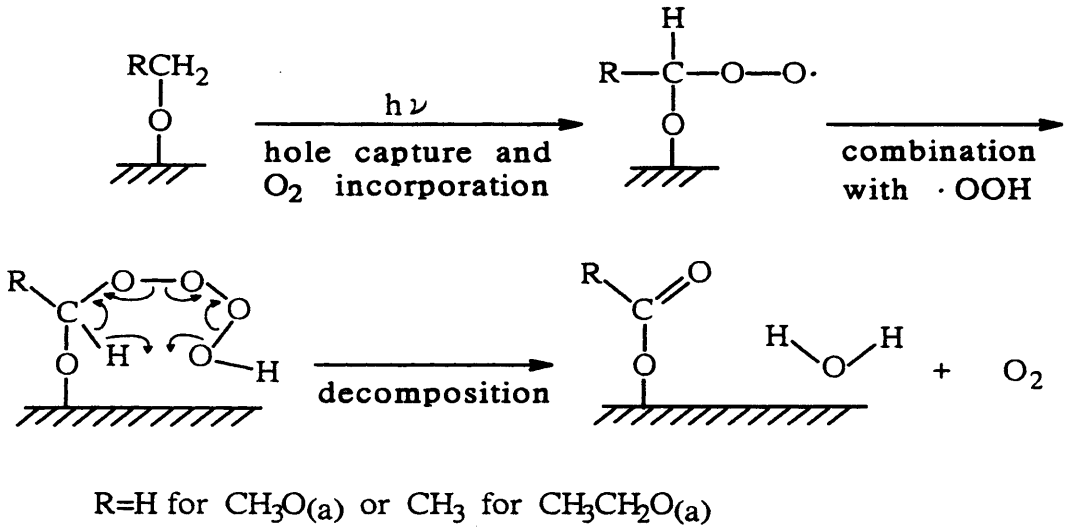

R=H for $CH_3O_{(a)}$ or CH_3 for $CH_3CH_2O_{(a)}$

Figure 6.19 Reaction scheme of the intermediates in the photodegredation of methanol over P25 TiO_2.[51]

The CH_3OH is adsorbed as $CH_3O_{(a)}$ after it captures the photoholes produced after UV irradiation, resulting in $-OCH_2^{\bullet}$ and H^+ (where H^+ is trapped by O^-). (eq 6.9)

$$CH_3OH + Ti^{4+}\text{-}\ O^- \rightarrow Ti^{4+}\text{-}OH^- + HOCH_2^{\bullet} \qquad (6.9)$$

$$HOCH_2^{\bullet} + O_2 \rightarrow HOCH_2OO^{\bullet} \qquad (6.10)$$

The $-OCH_2^{\bullet}$ radical then incorporates the O_2 to produce – $OCH_2OO^{\bullet}$ peroxy radicals. The mechanism has been investigated further; it is proposed that once formed the peroxy radicals can incorporate the $HOO^{\bullet}$ to form a $-OCH_2OOOOH$ tetraoxide, which can then decompose to HCOO(a) and H_2O(a).[51]

The EPR evidence in this chapter shows that a radical ($HOCH_2OO^{\bullet}$) is formed after UV irradiation of CH_3OH and oxygen. Further work is needed to fully characterise this species as it has been proposed to play an important role as an intermediate in the photooxidation of methanol over P25 TiO_2.

6.4.6 Interaction of $C_6H_5CH_3$ with O_2^-: The $[O_2^-...CH_3C_6H_5]$ radical.

The influence of an aromatic group on the interaction of organics with the surface adsorbed O_2^- was investigated by using toluene. It was found that on adsorption of toluene at 77K, followed by annealing to higher temperatures, EPR signals assigned to the following transient radical intermediates were formed. Firstly species (G) was

observed with the spin Hamiltonian parameters of $g_1 = 2.025$, $g_2 = 2.01$ and $g_3 = 2.004$. It formed at 230K before decaying at higher temperatures. The increased temperature of formation compared to the CH_3CN and CH_3OH cases could be due to the reduced mobility of toluene on the surface as the toluene is strongly bound to the TiO_2 surface *via* the aromatic π electrons.[55] Species G behaved in the same way as the other organics upon deuteration, with its signal undergoing no change. Based on these observations it can be assumed that species G is likely to have the structure $[O_2^-....CH_3C_6H_5]$.

The deuteration of the adsorbed toluene confirmed the identity of the accompanying signal (Species C) which was assigned to be the hydroperoxy type ($HO_2^\bullet$) species which has been discussed previously.

The interaction of toluene and TiO_2 has been widely studied in the literature under photochemical conditions. However, there are few studies or indications of its thermal decomposition over TiO_2. Toluene has been shown to decompose over the TiO_2 surface pretreated at high temperature to produce Ti^{3+} centres.[13] These Ti^{3+} centres presumably react with the adsorbed toluene to begin the decomposition process. However in this study no surface Ti^{3+} centres are present as they have previously been reacted with O_2 to produce O_2^-. The radical species G must therefore be a result of the interaction between toluene and O_2^- as it is not observed on addition to the activated or purely reduced surface. Clearly the radical species we have identified has not been observed before in the decomposition of toluene and more work is needed to fully understand its structure and role.

6.4.7 Interaction of toluene with O^-: the $[C_6H_5CH_2OO^\bullet]$ radical.

During the low temperature irradiation of a co-adsorbed mix of toluene and oxygen over TiO_2 a strong EPR signal with the spin Hamiltonian parameters of $g_2 = 2.011$, $g_3 = 2.002$ and two values of 2.024, 2.034 for g_1 was observed. The signal is thermally unstable and is only generated under a toluene-rich atmosphere. Organoperoxy type radicals ($ROO^\bullet$) have previously been identified as a possible intermediate in the photocatalytic oxidation of toluene.[24] The organoperoxy intermediate identified has the spin Hamiltonian parameters of $g_1 = 2.034$, $g_2 = 2.008$ and $g_3 = 2.003$. The intermediate was formed by the addition of toluene to a surface that had undergone a number of treatments; initially the surface was UV irradiated, followed by exposure to oxygen, outgassed at 77K then the surface contacted with toluene at 77K, warmed to RT then UV irradiated with very little oxygen present. In

this chapter, the signal is generated under a co-adsorbed gaseous atmosphere replicating real conditions, consequently the signal displays some different features to the one discussed by Coronado *et al.*,[24]. The EPR signal has two peaks in the g_{zz} region, at g = 2.024 and g = 2.034, indicating a number of species are present and $g_2 = 2.01$, $g_3 = 2.004$. The peak at 2.034 is likely to be due to an organoperoxy type intermediate, with the similar structure and formation to those previously identified. A summary of the formation of the organoperoxy species is described in eqs 6.11 and 6.12.

$$C_6H_5\text{-}CH_3 + Ti^{4+}\text{-}O^- \rightarrow Ti^{4+}\text{-}OH^- + C_6H_5\text{-}CH_2^{\bullet} \qquad (6.11)$$

$$C_6H_5\text{-}CH_2^{\bullet} + O_2 \rightarrow C_6H_5\text{-}CH_2OO^{\bullet} \qquad (6.12)$$

The mechanism of the photocatalytic oxidation of toluene has been discussed in the literature by a number of authors and a number of reactive intermediates have been postulated.[24,26,56] The process is believed to be hole-mediated or initiated by the generation of $OH^{\bullet}$ radicals. In reaction route (1) shown in Figure 6.20, the reaction is initiated *via* electron transfer from toluene to TiO_2 with the formation of an aromatic radical cation and benzyl radical. The benzyl radical can then react with O_2 to form a benzyl peroxy radical which decomposes thermally on the surface to give benzaldehyde and a hydroxyl radical ($^{\bullet}OH$). The aromatic radical cation can also react with oxygen to form an aromatic bridged peroxo intermediate. This structure is unstable and undergoes a fast opening of the aromatic ring and leads to the release of several aliphatic carbonyls.

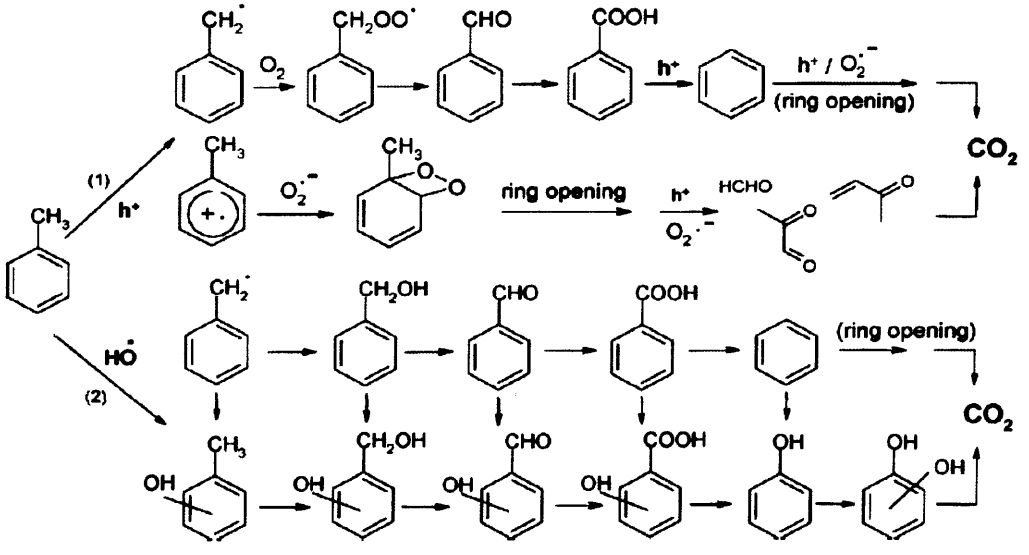

Figure 6.20 Proposed reaction pathways for the photocatalytic oxidation of toluene in the gas phase.[26]

Reaction route (2), is observed under high relative humidity levels, where the population of $^{\bullet}OH$ is enhanced. The $^{\bullet}OH$ radical undergoes addition to the aromatic ring of toluene leading to creosols or it can abstract an H^+ from the toluene methyl group to produce benzyl alcohol. The latter can be oxidised to benzaldehyde and later on to benzoic acid, which undergoes the photoKolbe reaction, to benzene and CO_2. Simultaneously a series of hydroxylations of the aromatic ring can take place and gives rise to several hydroxylated intermediates which are mineralised to CO_2.

The degradation of toluene is complex with many routes proposed; here evidence is provided that under co-adsorption conditions the formation of an organoperoxy intermediate is formed *via* a hole-mediated process.

6.4.8 Transient radical species on the TiO_2 surface

A series of thermally unstable radical intermediates have been identified on addition of a chosen organic substrate (methanol, acetonitrile and toluene) to a TiO_2 surface containing surface adsorbed O_2^-. These transient radical intermediates have been detected by EPR at low temperature (Figure 6.21a-d). The series of radicals all form upon annealing to T > 210K where the substrate and O_2^- react to give an [O_2...Substrate] type species, characterised by the spin Hamiltonian parameters of g_3 = 2.003, g_2 = 2.01 with g_1 values in the range 2.035-2.024 (Table 6.4).

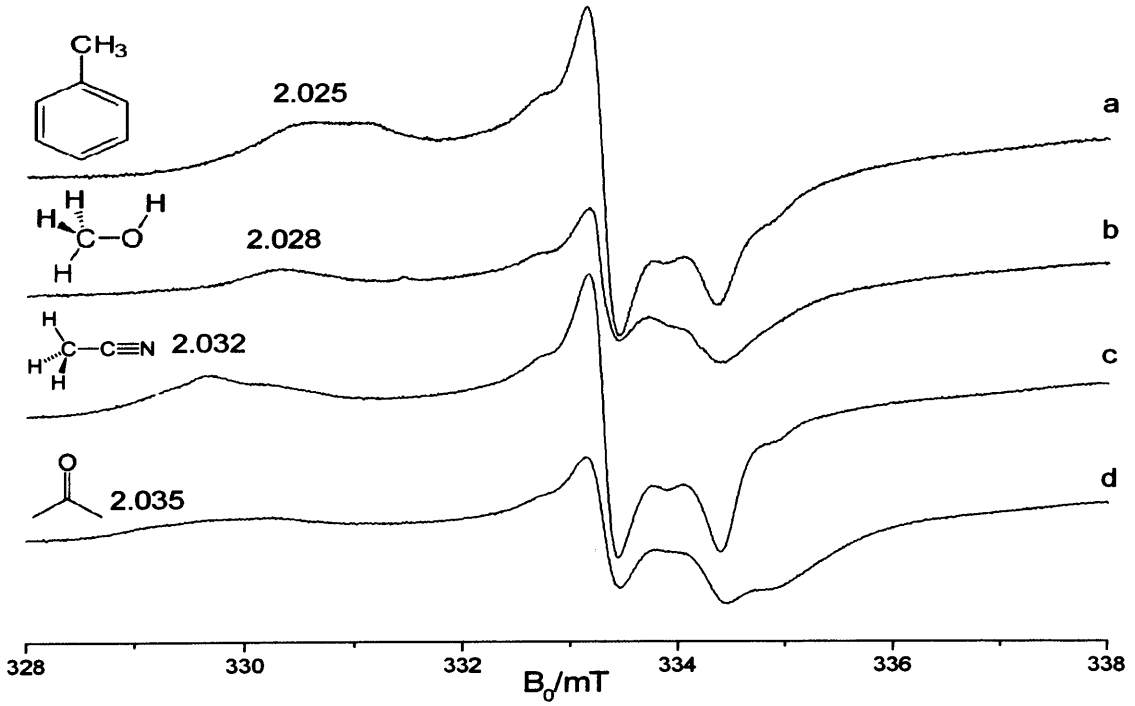

Figure 6.21 *cw*-EPR spectra (130K) of [O_2^-...substrate] species formed on TiO_2 containing O_2^- after addition of the organic at 77K followed by annealing to 220K with the chosen organic a) toluene, b) methanol c) acetonitrile and d) acetone.

The g_1 values increase on moving from the toluene to acetone. Carter *et al.*,[30] tentatively postulated that the formation of the $[O_2^-...CH_3COCH_3]$ was by nucleophillic attack by the weak nucleophile O_2^- on the electrophillic carbon atom of the highly polarised carbonyl group in a 'side on' manner. The authors believe that the interaction with acetone is sufficient enough to perturb the g values away from normal O_2^- values but is unlikely to alter the unpaired electron spin densities of the oxygen nuclei. If the strength of this interaction is dependent on the electrophillic nature of the carbon it is attached to, the series of substrates studied in this chapter provide an insight into how the strength of this interaction is affected. The relative electron withdrawing power of the functional groups to which the CH_3 group is attached for the substrates used is C_6H_5 (toluene) < OH (methanol) < CO (acetone) ~ CN (acetonitrile). The g_1 values for the $[O_2^-...substrate]$ adducts seemingly mirror this trend. In the toluene case, for example, the carbon of the methyl group, i.e. the site of nucleophillic attack by O_2^-, is not as electrophillic as the carbon attacked in the acetonitrile case; this results in a smaller perturbation of the O_2^- g_{zz} values for the toluene case than the acetonitrile case.

Table 6.4 Spin Hamiltonian parameters for the $[O_2^-...Substrate]$ radicals formed after reaction with O_2^-

Substrate	**Melting Point**	**Species**	**g_1**	**g_2**	**g_3**	**Ref**
Acetonitrile	227K	**Radical B** $[O_2^-..CH_3CN]$	2.031	2.01	2.003	This work 42
Methanol	175K	**Radical E** $[O_2^-..CH_3OH]$	2.027	2.01	2.003	This work
Toluene	180K	**Radical G** $[O_2^-...C_6H_5CH_3]$	2.025	2.01	2.004	This work
Acetone	178K	$[O_2^-..CH_3COCH_3]$	I 2.035 II 2.032	2.008	2.003	29

The irreversible reaction of adsorbed superoxide anions with acetone *via* a paramagnetic surface complex under non-radiative conditions was the first time such an intermediate had been identified. Based on the findings presented in this chapter with acetonitrile, methanol and toluene, it appears that these transient surface complexes are not unique to acetone, and in fact, are also formed with CH_3CN, CH_3OH, and $C_6H_5CH_3$,

suggesting that the first step in the oxidation of organic substrates by superoxide radicals over TiO_2 may be a generic [O_2^-...substrate] transient complex.

A series of transient organoperoxy radicals have been identified to form after irradiation of a substrate: O_2 mix (substrate = acetonitrile, methanol and toluene) over TiO_2. The radicals were formed by hole transfer from the TiO_2 to the surface adsorbed organic. This produces a radical anion which then reacts with the oxygen present to form the organoperoxy. The peroxy radicals were found to display similar thermal stabilities to each other, decaying at T > 190K, with no EPR signal visible after warming to room temperature.

Table 6.5 Spin Hamiltonian parameters for peroxy type radical (ROO•) formed over TiO_2.

Substrate	**Species**	g_1	g_2	g_3	**Ref**
Acetonitrile	**Radical D** $NCCH_2OO^•$	2.034	2.007	2.002	This work
Methanol	**Radical G** $HOCH_2OO^•$	2.034	2.007	2.002	This work
Toluene	**Radical F** $C_7H_7OO^•$	2.034 2.026	2.001	2.004	This work
Acetone	$CH_3COCH_2OO^•$	2.0345	2.007	2.001	30
Ethylene	$C_2H_3OO^•$	2.034	2.010	2.001	49
Acetaldehyde	$CH_3CO_3^•$	2.017	2.008	2.003	36

The EPR signal can subsequently be regenerated on re-irradiation. The transient radicals all share common spin Hamiltonian parameters of g_1 = 2.034, g_2 = 2.007 and g_3 = 2.003 (Table 6.5). Unlike the [O_2^-...substrate] species, the g_1 value of 2.034 is constant and independent of the substrate used. Sevilla *et al.*,[35] showed that different substituents (R) have little affect on the reactivity and structure of peroxyl radicals with the g-values for carbon based peroxyl radicals varying only slightly for different substituents. The nature of the R substituent however can affect the stability of the radical and this may explain the different signal strength of the three peroxy radicals

observed. The thermal instability of these intermediates highlights the necessity to study the systems *in-situ* (using EPR spectroscopy) as other spectroscopic techniques are unable to provide this low temperature identification. The identification of these peroxy intermediates is important as it shows how different surface treatments can result in the formation of different species. The organoperoxy radicals have been identified with aldehydes, ketones, alcohols and acetonitrile, indicating that this type of intermediate plays a key role in photooxidation processes using a variety of substrates. The identification of these radicals on the dehydrated surface is an important stepping stone to understanding what happens under real conditions. To understand the process further the role of water must be investigated to understand what role it plays in the photo oxidative process as described in the next chapter.

6.5 Conclusion

A number of oxygen-centred radicals have been proposed to play a key role in the degradation of organics over the TiO_2 surface in dark condition or under UV irradiation. In this chapter it has been shown that the decomposition of acetonitrile, methanol and toluene can occur under dark conditions over polycrystalline TiO_2 containing adsorbed superoxide radicals. The addition of an organic substrate to superoxide radicals resulted in the production of a transient and thermally unstable surface complex labelled [O_2^-...substrate]. These complexes are characterised by the g values of g_1 = 2.031- 2.025, g_2 = 2.010 and g_3 = 2.003. In the acetonitrile case, a ^{17}O hyperfine pattern typical of a diatomic molecular oxygen species possessing equivalent spin densities was observed. The complexes were found to be thermally unstable at temperatures above 240K. Additionally a hydroperoxy ($HO_2^{\bullet}$) radical with the spin Hamiltonian parameters of g_1 = 2.028, g_2 = 2.010, g_3 = 2.004, A_1 = 1.2 mT, A_2 = 1.0 mT and A_3 = 1.0 mT was also formed when the organics were exposed to TiO_2 bearing surface O_2^- radicals.

Secondly a series of thermally unstable surface alkyl organoperoxy type intermediates were identified following UV irradiation of a series of co-adsorbed organic: O_2 mixtures. The transient radicals produced after UV irradiation were characterised by the spin Hamiltonian parameters of g_1 = 2.034, g_2 = 2.007 and g_3 = 2.001. In the acetonitrile case, an intense signal with g values consistent with $NCCH_2OO^{\bullet}$ was produced. This study represents the first identification of such an intermediate with co-adsorbed acetonitrile: oxygen mixtures. The irradiation of

methanol also generated a surface stabilised radical. However the signal recorded was weak which was explained by the low stability of this radical at 140K and also due to the numerous radical pathways that could occur, resulting in the reduced intensity of the species. In the example of toluene: O_2, the organoperoxy signal was intense and was accompanied by an additional peak at g = 2.024 on which additional work is needed to make an assignment of the origin.

The work in this chapter demonstrates that the degradation of organic substrates over the surface of TiO_2 is complex. The organic substrates have been shown to degrade in dark conditions (non-radiative) *via* a reaction with surface O_2^- radicals to form [O_2...substrate] complex or *via* UV irradiation where under co-adsorption conditions an organoperoxy type species is formed *via* a hole- mediated process. While these results go some way to explaining how the degradation of organics proceed on the surface, and in particular the important role played by O_2^-, further studies are needed to understand how the mechanism proceeds under real conditions; In particular, the presence of water may affect the formation of the radicals in both cases or the ratio of organic substrate to oxygen present may affect the reaction mechanism.

6.6 References

(1) Kim, S. B.; Hwang, H. T.; Hong, S. C. *Chemosphere* **2002**, *48*, 437.

(2) Holzinger R, J. A., Hansel. A, Lindinger W. *Journal of Atmospheric Chemistry* **2001**, *38*, 187.

(3) Arana, J.; Dona-Rodriguez, J. M.; Cabo, C. G. I.; Gonzalez-Diaz, O.; Herrera-Melian, J. A.; Perez-Pena, J. *Applied Catalysis B-Environmental* **2004**, *53*, 221.

(4) de Gouw, J. A.; Warneke, C.; Parrish, D. D.; Holloway, J. S.; Trainer, M.; Fehsenfeld, F. C. *Journal of Geophysical Research-Atmospheres* **2003**, *108*.

(5) Holzinger, R.; Warneke, C.; Hansel, A.; Jordan, A.; Lindinger, W.; Scharffe, D. H.; Schade, G.; Crutzen, P. J. *Geophysical Research Letters* **1999**, *26*, 1161.

(6) Schneider, J.; Burger, V.; Arnold, F. *Journal of Geophysical Research-Atmospheres* **1997**, *102*, 25501.

(7) Hussein, G. A. M.; Sheppard, N.; Zaki, M. I.; Fahim, R. B. *Journal of the Chemical Society-Faraday Transactions* **1991**, *87*, 2655.

(8) Nishikawa, H. *Applied Surface Science* **2009**, *255*, 7468.

(9) Addamo, M.; Augugliaro, V.; Coluccia, S.; Di Paola, A.; Garcia-Lopez, E.; Loddo, V.; Marci, G.; Martra, G.; Palmisano, L. *International Journal of Photoenergy* **2006**, *39182*, 1.

(10) Rasko, J.; Kiss, J. *Catalysis Letters* **2006**, *109*, 71.

(11) Lusvardi, V. S.; Barteau, M. A.; Farneth, W. E. *Journal of Catalysis* **1995**, *153*, 41.

(12) Kim, K. S.; Barteau, M. A.; Farneth, W. E. *Langmuir* **1988**, *4*, 533.

(13) Makino, T.; Matsumoto, K.; Ebara, T.; Mine, T.; Ohtsuka, T.; Mizuguchi, J. *Japanese Journal of Applied Physics Part 1-Regular Papers Brief Communications & Review Papers* **2007**, *46*, 6037.

(14) Rasko, J., Kiss, J. *Applied Catalysis A-General* **2006**, *303*, 56.

(15) Davit, P.; Martra, G.; Coluccia, S.; Augugliaro, V.; Lopez, E. G.; Loddo, V.; Marci, G.; Palmisano, L.; Schiavello, M. *Journal of Molecular Catalysis a-Chemical* **2003**, *204*, 693.

(16) Chuang, C. C.; Wu, W. C.; Lee, M. X.; Lin, J. L. *Physical Chemistry Chemical Physics* **2000**, *2*, 3877.

(17) Lichtin, N. N.; Avudaithai, M. *Environmental Science & Technology* **1996**, *30*, 2014.

(18) Zhuang, J.; Rusu, C. N.; Yates, J. T. *Journal of Physical Chemistry B* **1999**, *103*, 6957.

(19) Augugliaro, V.; Coluccia, S.; Garcia-Lopez, E.; Loddo, V.; Marci, G.; Martra, G.; Palmisano, L.; Schiavello, M. *Topics in Catalysis* **2005**, *35*, 237.

(20) Augugliaro, V.; Prevot, A. B.; Vazquez, J. C.; Garcia-Lopez, E.; Irico, A.; Loddo, V.; Rodriguez, S. M.; Marci, G.; Palmisano, L.; Pramauro, E. *Advances in Environmental Research* **2004**, *8*, 329.

(21) Addamo, M.; Augugliaro, V.; Coluccia, S.; Faga, M. G.; Garcia-Lopez, E.; Loddo, V.; Marci, G.; Martra, G.; Palmisano, L. *Journal of Catalysis* **2005**, *235*, 209.

(22) Palmisano, G.; Addamo, M.; Augugliaro, V.; Caronna, T.; Garcia-Lopez, E.; Loddo, V.; Palmisano, L. *Chemical Communications* **2006**, 1012.

(23) Blount, M. C.; Falconer, J. L. *Journal of Catalysis* **2001**, *200*, 21.

(24) Coronado, J. M.; Soria, J. *Catalysis Today* **2007**, *123*, 37.

(25) Balcerski, W.; Ryu, S. Y.; Hoffmann, M. R. *International Journal of Photoenergy* **2008**.

(26) Sleiman, M.; Conchon, P.; Ferronato, C.; Chovelon, J. M. *Applied Catalysis B-Environmental* **2009**, *86*, 159.

(27) Pichat, P.; Disdier, J.; Hoang-Van, C.; Mas, D.; Goutailler, G.; Gaysse, C. *Catalysis Today* **2000**, *63*, 363.

(28) Kamat, P. V. *Chemical Reviews* **1993**, *93*, 267.

(29) Nakamura, R.; Sato, S. *Journal of Physical Chemistry B* **2002**, *106*, 5893.

(30) Carter, E.; Carley, A. F.; Murphy, D. M. *Chemphyschem* **2007**, *8*, 113.

(31) Anpo, M.; Che, M.; Fubini, B.; Garrone, E.; Giamello, E.; Paganini, M. C. *Topics in Catalysis* **1999**, *8*, 189.

(32) Michael A. Henderson, W. S. E., Craig L. Perkins, Charles H. F.Peden ,Ulrike Diebold *Journal of physical Chemistry B* **1999**, *103*, 5328.

(33) Attwood, A. L.; Murphy, D. M.; Edwards, J. L.; Egerton, T. A.; Harrison, R. W. *Research on Chemical Intermediates* **2003**, *29*, 449.

(34) Che, M.; Tench, A. J. *Advances in Catalysis* **1982**, *31*, 77.

(35) Sevilla, M. D.; Becker, D.; Yan, M. Y. *Journal of the Chemical Society-Faraday Transactions* **1990**, *86*, 3279.

(36) Jenkins, C. A.; Murphy, D. M. *Journal of Physical Chemistry B* **1999**, *103*, 1019.

(37) Ito, T.; Wang, J. X.; Lin, C. H.; Lunsford, J. H. *Journal of the American Chemical Society* **1985**, *107*, 5062.

(38) Antcliff, K. L.; Murphy, D. M.; Griffiths, E.; Giamello, E. *Physical Chemistry Chemical Physics* **2003**, *5*, 4306.

(39) Howe, R. F.; Gratzel, M. *Journal of Physical Chemistry* **1985**, *89*, 4495.

(40) Howe, R. F.; Gratzel, M. *Journal of Physical Chemistry* **1987**, *91*, 3906.

(41) Carter, E.; Carley, A. F.; Murphy, D. M. *Journal of Physical Chemistry C* **2007**, *111*, 10630.

(42) Attwood, A. L.; Edwards, J. L.; Rowlands, C. C.; Murphy, D. M. *Journal of Physical Chemistry A* **2003**, *107*, 1779.

(43) Green, J.; Carter, E.; Murphy, D. M. *Research on Chemical Intermediates* **2009**, *35*, 145.

(44) Coronado, J. M.; Kataoka, S.; Tejedor-Tejedor, I.; Anderson, M. A. *Journal of Catalysis* **2003**, *219*, 219.

(45) Henderson, M. A. *Journal of Physical Chemistry B* **2004**, *108*, 18932.

(46) Henderson, M. A. *Journal of Physical Chemistry B* **2005**, *109*, 12062.

(47) Henderson, M. A.; Epling, W. S.; Perkins, C. L.; Peden, C. H. F.; Diebold, U. *Journal of Physical Chemistry B* **1999**, *103*, 5328.

(48) Atkins, P. W., Symons, M. C. R. *Structure of Inorganic Radicals : An Application of Electron Spin Resonance to the study of Molecular Structure*; Elsevier: London, 1967.

(49) Gonzalezelipe, A. R.; Che, M. *Journal De Chimie Physique Et De Physico-Chimie Biologique* **1982**, *79*, 355.

(50) Nuhu, A.; Soares, J.; Gonzalez-Herrera, M.; Watts, A.; Hussein, G.; Bowker, M. *Topics in Catalysis* **2007**, *44*, 293.

(51) Wu, W. C.; Chuang, C. C.; Lin, J. L. *Journal of Physical Chemistry B* **2000**, *104*, 8719.

(52) Hussein, G. A. M.; Sheppard, N.; Zaki, M. I.; Fahim, R. B. *Journal of the Chemical Society-Faraday Transactions* **1991**, *87*, 2661.

(53) Micic, O. I.; Zhang, Y. N.; Cromack, K. R.; Trifunac, A. D.; Thurnauer, M. C. *Journal of Physical Chemistry* **1993**, *97*, 13284.

(54) Sadeghi, M.; Liu, W.; Zhang, T. G.; Stavropoulos, P.; Levy, B. *Journal of Physical Chemistry* **1996**, *100*, 19466.

(55) Nagao, M.; Suda, Y. *Langmuir* **1989**, *5*, 42.

(56) Sun, L.; Li, G. Y.; Wan, S. G.; An, T. C. *Chemosphere* **2010**, *78*, 313.

Chapter 7

The role of water in the formation of transient oxygen radicals on the titanium dioxide surface

7.1 Introduction

Titanium dioxide is used in the photocatalytic remediation of wastewater from industrial, agricultural or civil origin, as well as the decontamination of the atmosphere and soil.[1] The aim is to achieve the complete mineralization of the pollutants to H_2O and CO_2, or at least their transformation into non toxic compounds. An unavoidable factor is the presence of water under 'real' reaction conditions. The titanium dioxide surface can become hydroxylated and covered in adsorbed water, the level of which is dependent on relative humidity and temperature.[2,3] The role which water plays has been a topic of research by many groups. However, it is still unclear whether water acts as a poison[4-8] or a promoter[9,10] in photochemical reactions occurring on the surfaces of TiO_2 photocatalysts.

When water behaves as a poison it inhibits the adsorption of many organic species due to its relatively stronger binding efficiency to the TiO_2 surface. The water is bound strongly particularly as dissociative fragments.[11] For example, the interaction of water on the surface of TiO_2 is stronger than that of alkanes, alkenes and aromatics which are lacking the functional groups needed to form strong electrostatic interactions with the surface cation sites. However, alcohols and carboxylic acids tend to have a greater affinity for the surface compared to water and tend not to be displaced.[12] In contrast, when water acts as a promoter it is thought to provide the catalyst with the means of generating $^{\bullet}OH$ radicals that can participate in oxidation reactions. The two main mechanisms for $^{\bullet}OH$ formation proposed in the literature involve hole mediated oxidation of adsorbed hydroxyl anions, and the reaction of water with O_2^- resulting in $^{\bullet}OH$ through $HO_2^{\bullet}$, which can then participate in photocatalytic oxidation reactions.[13,14]

In this chapter, the formation of O_2^- on dehydrated, partially, and fully hydrated surfaces will be examined to understand the behaviour of the O_2^- radical under these conditions. Secondly, the formation of peroxy type ($NCCH_2OO^{\bullet}$) radicals after the UV irradiation of CH_3CN/O_2 over the partially and fully hydrated TiO_2 surface is investigated. The presence of O_2^- is seen as a key factor in many of the proposed reaction mechanisms. The formation of O_2^- on dehydrated metal oxide surfaces has been widely studied in the literature,[15-19] with the O_2^- species stable on the dehydrated TiO_2

surface. The O_2^- radicals have been shown to display reactivity with gaseous organic substrates, resulting in the formation of an [O_2^-...substrate] type radical adduct.[20,21] The O_2^- can be formed through thermal (addition of O_2 to a reduced surface) or photochemical (UV irradiation of TiO_2 under an oxygen atmosphere) means. In the thermal case it has been shown that the formation of O_2^- at specific surface sites can be blocked in the presence of an additional probe gas (Ar/O_2 and CO_2/O_2).[19] Therefore the investigation of the formation, stability and reactivity of O_2^- radicals on the hydrated surface is important as the surface site could be blocked due to surface hydroxyl groups and physisorbed water.

The photooxidation of CH_3CN over TiO_2 has been studied by a number of groups.[22-27] Lichtin *et al.*,[28] found that a number of products are formed in a dry air stream including CO_2, H_2O and HNO_3; the admission of water vapour was found to result in a reduction of the reaction rate. In the aqueous system, a significant reduction in the reactivity of CH_3CN was observed; this was ascribed to the interaction of adsorbed CH_3CN with liquid water. The authors believed that such an interaction could help dissipate the heat of charge recombination and inhibit the dissociation of CH_3CN. Addamo *et al.*,[24,29] investigated the photocatalytic oxidation of acetonitrile in the gas-solid and liquid-solid regimes. They found that in the gas-solid regime the intermediate products were HCN and CO_2, whereas CN^-, CNO^-, NO_3^-, CO_3^{2-} and $CHOO^-$ ions were found in the liquid-solid regime. It was found that the liquid medium hindered the adsorption and the photo reactivity of dissolved molecules. IR spectroscopy was used to confirm that in the dark, water is the predominant competitor with acetonitrile for TiO_2 surface sites. In the previous chapter, the $^{\bullet}OOCH_2CN$ was found to form on UV irradiation of TiO_2 under a co-adsorbed CH_3CN/O_2 atmosphere. In this chapter the influence of water on the formation of the $^{\bullet}OOCH_2CN$ radical will be investigated.

7.2 Experimental

Full experimental details are given in Chapter 4; however the key steps are briefly summarised below.

7.2.1 Fully dehydrated TiO_2 surface

A fully dehydrated TiO_2 surface was prepared by heating under vacuum overnight at 373K to remove any physisorbed water. The polycrystalline samples were then subsequently slowly heated (over a 5 hour period) to a temperature of 773K and

held at this temperature for 1 hour. The sample was exposed to oxygen (50 Torr, *via* vacuum manifold) at 773K and left under this pressure at the same temperature for 1 hour. Subsequently the sample was cooled to room temperature under the oxygen atmosphere, before evacuation of the excess oxygen at 298K. The fully dehydrated (*activated*) TiO_2 surface was then hydrated to varying degrees by the following methods. (*cf* 7.2.2 and 7.2.3)

7.2.2 Partially hydrated TiO_2 surface

Following the activation of the TiO_2 surface (as described above in 7.2.1), a premixed dose of water and oxygen in selected ratios was co-adsorbed onto the activated sample at 298K. These samples hereafter will be referred to as the *partially hydrated* surface. Subsequently the sample was UV irradiated at 77K, before evacuation at 140K to remove the excess H_2O/O_2 mixture.

7.2.3 Fully hydrated TiO_2 surface

Following activation of the TiO_2 (as described in 7.2.1), the vapours of triply distilled water vapour (10 Torr) were added to an activated sample, and left at 673K for 1 hour. The sample was subsequently cooled to 298K before evacuation for 30 minutes to remove the excess physisorbed water molecules. This sample hereafter will be referred to as a *fully hydrated* surface.

7.3 Results

7.3.1 Formation of O_2^- on the dehydrated TiO_2 surface by photolysis

In previous chapters it has been shown that O_2^- can be formed by; (1) addition of molecular oxygen (O_2) to a thermally reduced surface, or (2) UV irradiation of the TiO_2 surface under an oxygen atmosphere at 77K. In both cases, the sample is warmed to room temperature before evacuation of the excess oxygen. Once evacuated at room temperature a typical O_2^- signal is present as shown in Figure 7.1a (along with its corresponding computer simulation, Figure 7.1b). The superoxide generated under photolysis conditions is essentially the same as that generated thermally, with similar g_{yy} and g_{xx} values. Differences are apparent in the g_{zz} region. The g_{zz} region of the O_2^- generated *via* photolysis case shows a greater complexity than the thermally generated O_2^- case, with two extra sites present at g_{zz} (I') = 2.017 and g_{zz} (II'') = 2.025. The extra sites are representative of extra Ti^{4+}stabilisation sites on the TiO_2 surface.

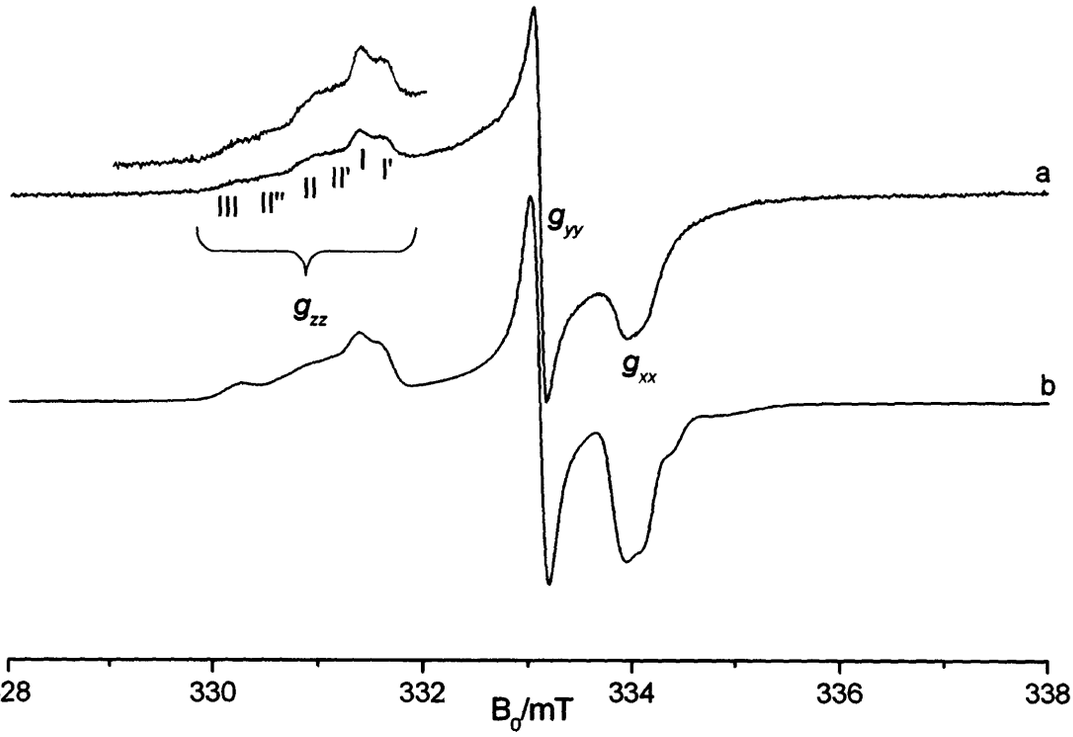

Figure 7.1 *cw*-EPR spectrum (130K) of O_2^- formed after oxygen exposure to fully dehydrated P25 TiO_2 surface (773K) followed by UV irradiation at 77K. Oxygen was admitted at 298K a) Experimental and b) Simulated.

The formation of O_2^- under photolysis conditions occurs *via* transfer of the photogenerated electron (e^-) to the surface adsorbed oxygen to give O_2^- radicals. On irradiation of TiO_2, photogenerated holes (h^+) are created but any subsequent species that they form are lost upon warming to room temperature. To detect these species, the sample needs to be studied at low temperatures (T < 298K). This provides information on transient radical species otherwise lost at room temperature. Therefore, in the following after UV irradiation for 30 minutes at 77K, the excess oxygen is evacuated at low temperature (130K). The EPR signal is subsequently recorded at 130K to detect any transient oxygen species present.

Addition of oxygen at room temperature to the TiO_2 surface, followed by UV irradiation at 77K for 30 minutes then evacuation at 130K (to remove the excess molecular oxygen) resulted in the formation of a number of distinct EPR signals as shown in Figure 7.2a. The removal of the excess oxygen is vital, as its presence causes line broadening and subsequent loss of resolution in the EPR spectra. The EPR spectrum shown in Figure 7.2a is complex and consists of a series of different signals corresponding to a number of radicals. The g_{zz} values fall in the range of g = 2.014 – 2.026, with a number of oxygen based radicals (O_2^-, O^- and O_3^-) as possible candidates.

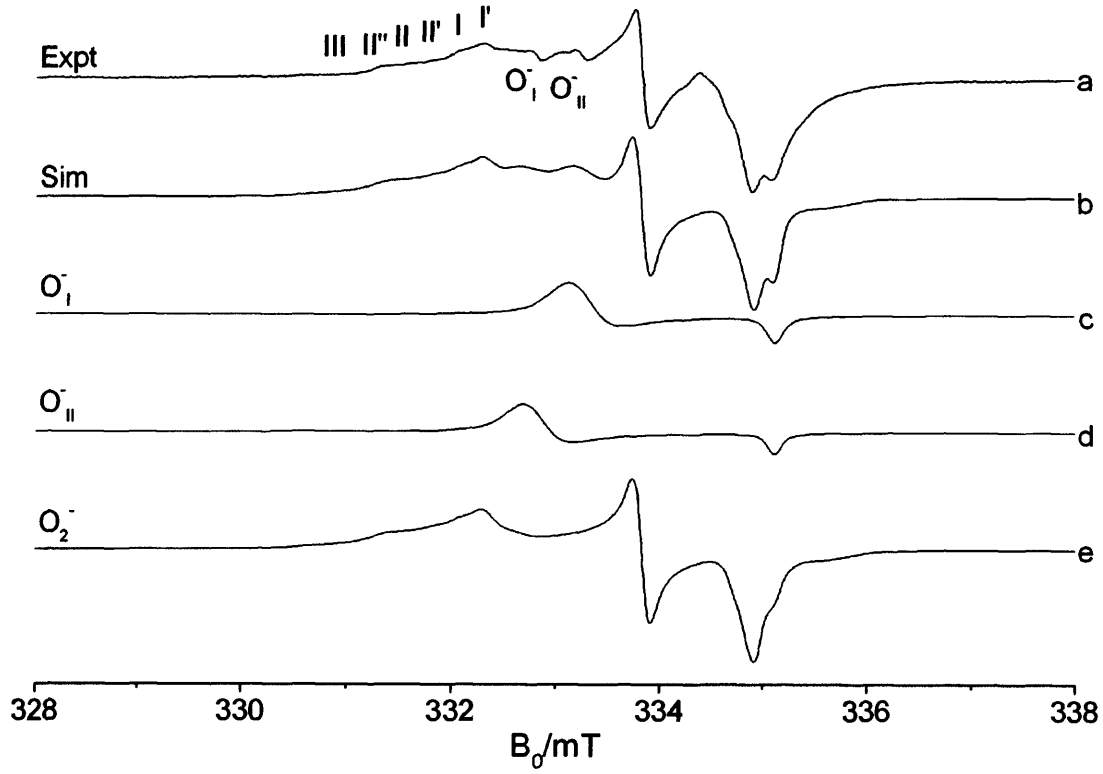

Figure 7.2 *cw* - EPR spectra (130K) of P25 TiO_2 after a) UV irradiation under an oxygen atmosphere (10 Torr) followed by evacuation at 130K b) complete computer simulation c) - e) Simulated single component spectra of O^-_I, O^-_{II} and O_2^-, respectively.

To help gain additional information, the experimental spectrum was deconvoluted into its individual spectral components using a computer simulation program (Sim32) (Figure 7.2 c-e).[30] Two sets of spin Hamiltonian parameters were extracted for distinct O^- species; where O^-_I $g_\perp = 2.014$ and $g_\parallel = 2.02$ (Figure 7.2c) and O^-_{II} $g_\perp = 2.016$ and $g_\parallel = 2.02$ (Figure 7.2d). The two O^- species represent 28% of the overall EPR signal intensity. The second species present in Figure 7.2a is identified as the O_2^- species with the following spin Hamiltonian parameters: g_{zz} = I' (2.017), I (2.019), II (2.023), II' (2.021), II'' (2.025) and III (2.026) with $g_{yy} = 2.011$ and $g_{xx} = 2.005$ with the relative signal contributions for each species shown in Table 7.1. The O_2^- species represents 72% of the overall signal intensity. The relative distribution of the g_{zz} peaks labelled in Figure 7.2a is I' > I > II > II' > II'' > III, where site I' is most prevalent at 140K.

To gain further confirmation on the identity and stability of the oxygen species observed, a variable temperature study was performed. The sample was annealed to a series of different temperatures (T = 140-250K) before recooling to 130K for EPR measurements (Figure 7.3a-h).

Table 7.1 Spin Hamiltonian parameters for O_2^- radicals adsorbed on the photoactivated TiO_2 (P25).

Site	g_{xx}	g_{yy}	g_{zz}	% Cont.
I	2.005	2.011	2.019	25
I'	2.005	2.011	2.017	19
II'	2.004	2.011	2.020	19
II	2.004	2.011	2.023	22
II''	2.004	2.011	2.025	11
III	2.001	2.011	2.026	4

The peaks at $g_\perp = 2.014$ and $g_\perp = 2.016$, corresponding to the O^-_I and O^-_{II} species respectively, decay on increasing the temperature and are subsequently lost at RT (Figure 7.3a-h). The decrease in these peak intensities is accompanied by a shift in the g_{xx} value of the EPR signal; the peaks at $g_\perp = 2.014$ and $g_\perp = 2.016$ can be regenerated on subsequent re-irradiation of the sample.

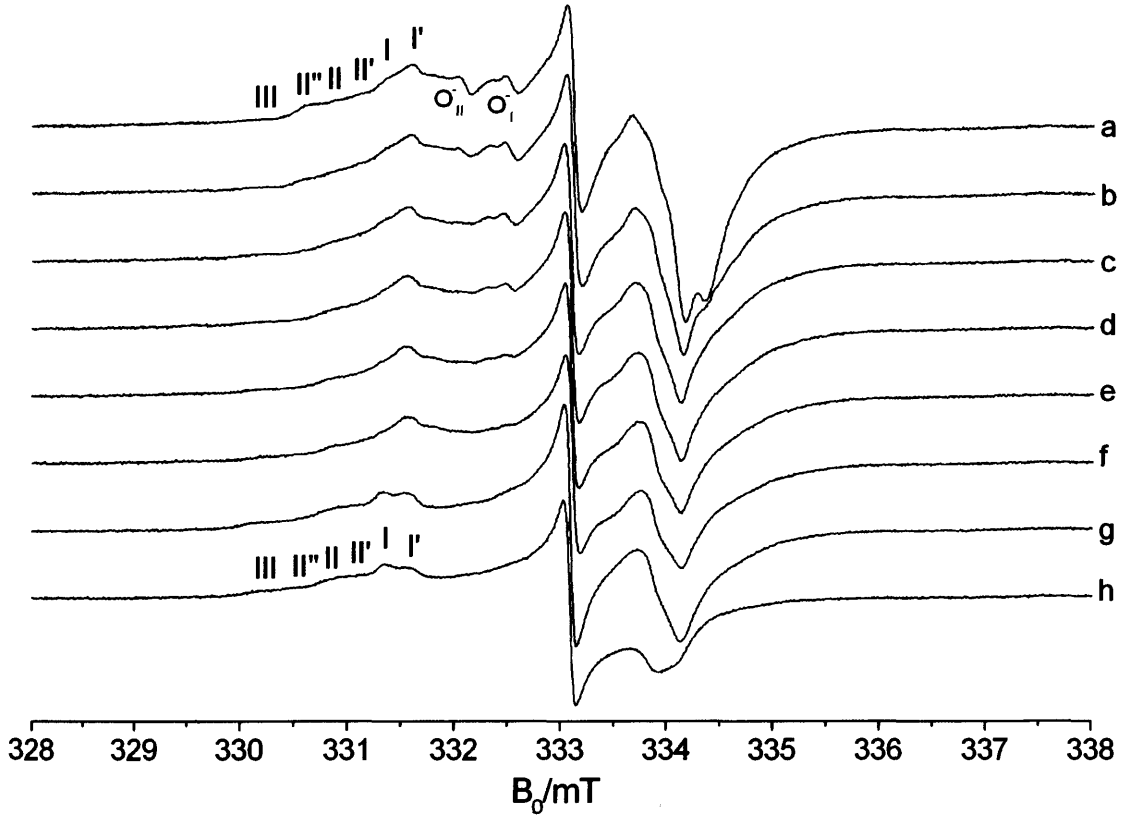

Figure 7.3 *cw* - EPR spectra (130K) of P25 TiO_2 after exposure to oxygen (10 Torr), followed by UV irradiation at 77K. The excess gas was evacuated at 130K and the sample subsequently annealed to a) 140, b) 170, c) 190, d) 200, e) 210, f) 220, g) 250, and h) 298K.

The loss of the O^- species is accompanied by a redistribution of the peaks in the g_{zz} region of O_2- between $g_{zz} = 2.017$ - 2.026 (Figure 7.3a-h). The relative peak intensity

for the O_2^- at 140K is I' > I > II > II' > II'' > III (Figure 7.3a). Seemingly the O_2^- species at site I' is thermally unstable and decays on annealing to higher temperatures; at 298K (Figure 7.3h) the EPR spectrum has changed and the relative peak intensities are in the order of I > I' > II > II' > II'' > III. At 298K, the profile is characteristic of the EPR spectrum of photogenerated surface adsorbed O_2^- (Figure 7.1a) with spin Hamiltonian parameters of $g_1 = 2.017\text{-}2.026$, $g_2 = 2.011$ and $g_3 = 2.005$ as described and discussed above, see also (Table 7.1).

The loss in O_2^- (site I') and O^- species is responsible for the reduction in overall signal intensity. This is better illustrated in Figure 7.4. Several spectra from the VT study have been simulated to confirm the spin Hamiltonian parameters of each species and to calculate the relative signal intensities of O_2^- and O^- (*via* deconvolution of the experimental data). The experimental spectra and corresponding computer simulations are shown on the top line of Figure 7.4.

The relative signal intensities of the oxygen species O_2^- and O^- are plotted as a function of temperature. Figure 7.4 clearly shows that on increasing the temperature, the thermally unstable O^- species decay until at T > 240K they are lost. The superoxide species is stable at low temperature but loses some intensity on warming to room temperature, with the loss in intensity primarily due to the loss of the thermally unstable site I'.

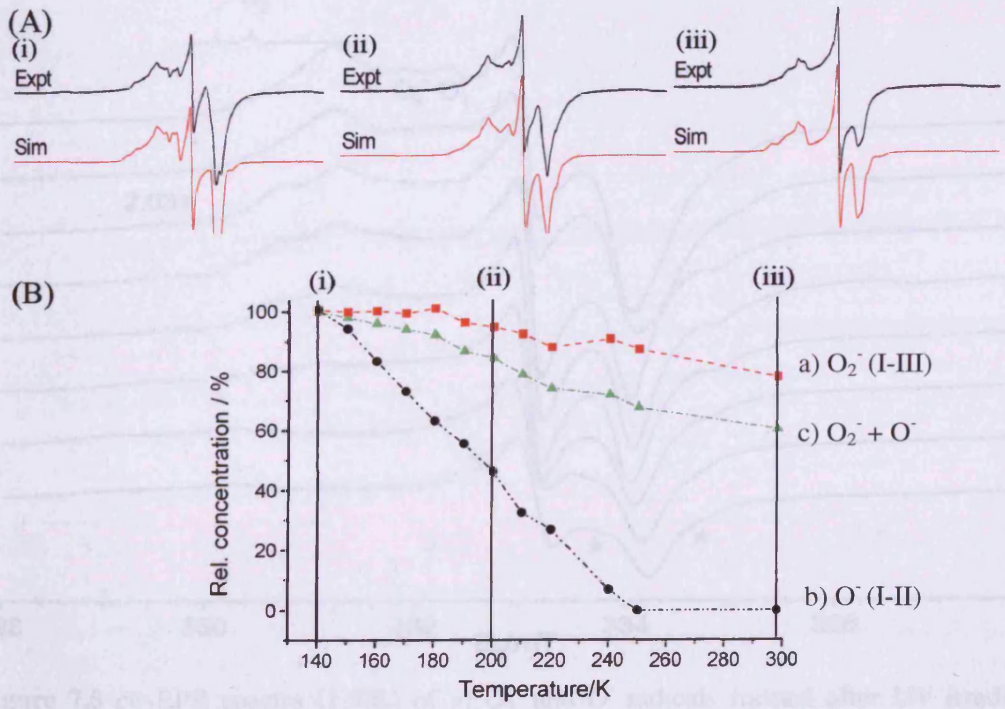

Figure 7.4 (A) Experimental and simulated EPR spectra for the O_2^- and O^- radicals after annealing to (i) 140, (ii) 200, and (iii) 298K. (B) Concentration plotted as a function of temperature for a) superoxide O_2^-, b) O^- ions and c) The overall signal intensity ($O_2^- + O^-$).

The identification of the O^- species highlights the need to study the systems, both at low temperatures and room temperature, so that important information is not lost. The O^- species is believed to play an important role in catalysis and has previously been shown to display reactivity with organic substrates.[31-33]

To test the reactivity of the O^- species observed at 140K, a sample pre-treated to produce the O^- was exposed to acetonitrile (7.3 Torr) at 77K. The sample was then transferred to the EPR cavity and subsequently annealed to temperatures in the range 140-240K. Upon addition of acetonitrile, followed by annealing to 140K, there is a loss in intensity of the O^- peaks but no new paramagnetic signals are observed, see Figure 7.5a-b. The signal intensity due to O^- continues to decrease on increasing the temperature, until all O^- peaks are lost at T > 200K. At T > 205K, the O_2^- signal intensity begins to decline accompanied by the appearance of a new signal at g = 2.031 (Figure 7.5c). On reaching T ~ 225K (Figure 7.5g), the profile and spin Hamiltonian parameters of the EPR spectrum is identical to that of the $[O_2^-...CH_3CN]$ radical in Chapter 6, identified after addition of CH_3CN to surface adsorbed O_2^- radicals. The spectrum arising from the $[O_2^-...CH_3CN]$ radical has the spin Hamiltonian parameters of $g_1 = 2.031$, $g_2 = 2.01$ and $g_3 = 2.003$, and is accompanied by the hydroperoxy type radical with the spin Hamiltonian parameters of $g_1 = 2.028$, $g_2 = 2.01$, $g_3 = 2.004$, $A_1 = 1.2$ mT, $A_2 = 1.0$ mT and $A_3 = 1.0$ mT.

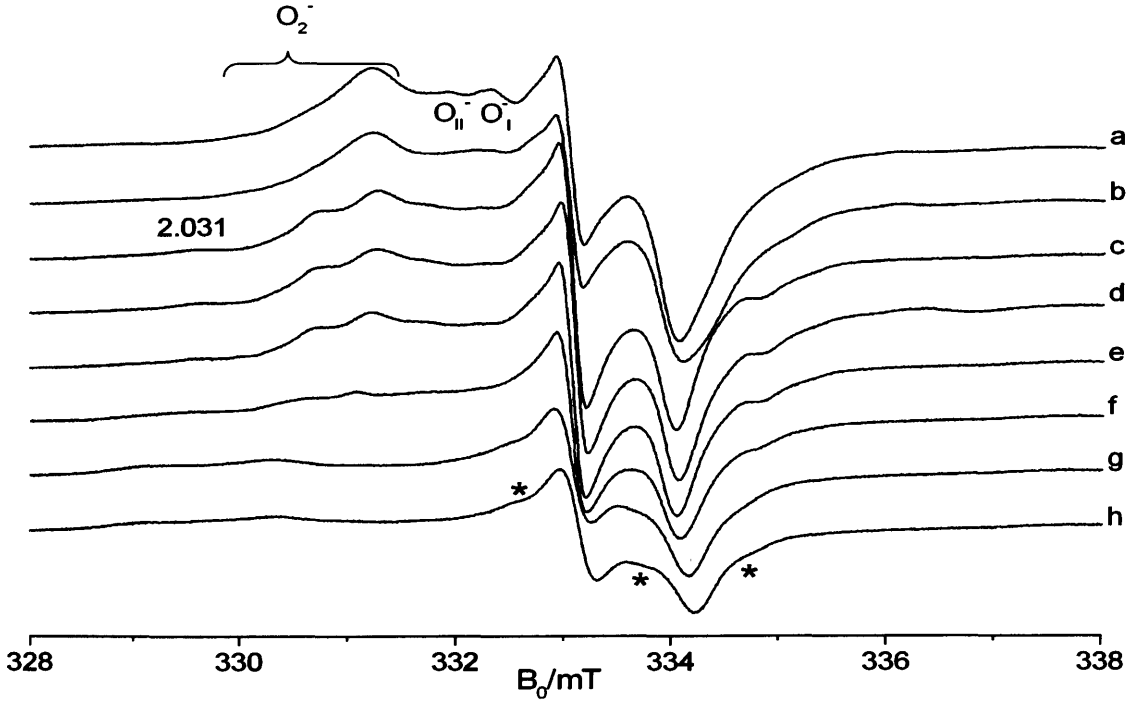

Figure 7.5 *cw*-EPR spectra (130K) of a) O_2^- and O^- radicals formed after UV irradiation of activated P25 TiO_2 sample under an oxygen atmosphere (10 Torr) at 77K, followed by evacuation at 130K. CH_3CN (7.3 Torr) was then added at to the EPR cell at 77K and the sample subsequently annealed to b) 140, c) 205, d) 210, e) 215, f) 220, g) 225, and h) 230K.

In summary, the UV irradiation of O_2 and TiO_2 at low temperature resulted in the formation of O^- and O_2^- radicals; on warming to room temperature the O^- species decays leaving the stable O_2^- radicals. The reactivity of both species was tested by addition of CH_3CN. The O^- signal disappeared at 140K but no new EPR signals were observed indicating the decay or reaction of this species. The reactivity between the O_2^- radical and CH_3CN was the same as that described previously in Chapter 6 i.e. at T > 210K a new signal attributed to $[O_2^-...CH_3CN]$ was observed.

7.3.2 Formation of O_2^- on the partially hydrated TiO_2 surface.

To create a partially hydrated TiO_2 surface, a co-adsorbed mixture of H_2O/O_2 (total pressure 15 Torr) was adsorbed onto a fully dehydrated surface at RT. The co-adsorbed mixture should ensure that the oxygen remains in excess, while the 1 Torr of water delivered in the experiment should ensure good coverage of the surface. The sample was then irradiated at 77K for 30 minutes, before evacuation of the excess gas at 130K.

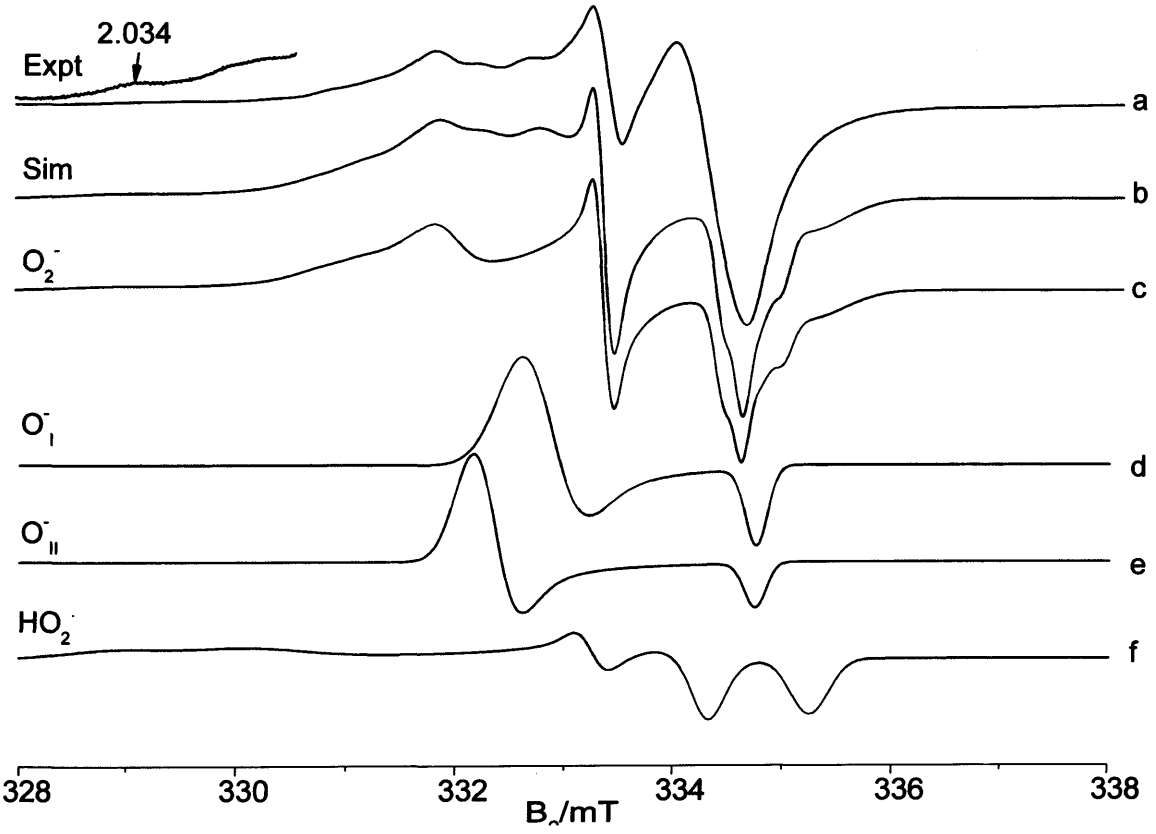

Figure 7.6 *cw*-EPR spectrum (130K) of P25 TiO_2 after exposure to co-adsorbed mix of H_2O: O_2 (1:10 ratio, total pressure 15 Torr). The sample was UV irradiated at 77K then evacuated at 130K.a) Experimental b) simulated EPR spectrum and c-f) individual simulated spectral components of O_2^-, O^-_I, O^-_{II} and $HO_2^\bullet$.

The resulting EPR spectrum consists of multiple signals resulting from a number of paramagnetic species which have previously been observed on the TiO_2 surface (Figure 7.6). The signals in the g_{zz} region at g_{zz} = 2.017-2.026 are due to O_2^- radicals (confirmed by computer simulation). The spin Hamiltonian parameters are g_{zz} = I' (2.017), I (2.019), II (2.023), II' (2.021), II'' (2.025), III (2.026), g_{yy} = 2.011 and g_{xx} = 2.005. The individual spectral simulation of O_2^- is shown in Figure 7.6c. The peaks at $g_\perp$ = 2.014 and $g_\perp$ = 2.016 can be assigned to the species O^-_I and O^-_{II} respectively (the $g_\parallel$ values are obscured by the stronger O_2^- g_{xx} components). The individual spectral profiles for the $O^-_{I\text{-}II}$ which have previously been identified over the fully dehydrated surface are shown in Figure 7.6 d-e. These species have all previously been observed following the UV irradiation of oxygen over the dehydrated surface. However, over the partially hydrated surface, there is an additional peak observed at g = 2.034. It is hard to identify purely on the basis of the g value alone, but g = 2.034 is usually used as a 'fingerprint' of the hydroperoxy ($HO_2^\bullet$) radical. This radical has been shown to form on the TiO_2 surface after UV irradiation of TiO_2 under a partially hydrated atmosphere.[15] The spin Hamiltonian parameters extracted by computer simulation are g_1 = 2.034, g_2 = 2.008, g_3 = 2.002, A_1 = 1.2 mT, A_2 = 1.0 mT and A_3 = 1.0 mT. However, in Figure 7.6a the g_2 and g_3 components are overlapped by the more abundant O_2^- and O^- signals and are therefore unresolved. The individual spectral component of $HO_2^\bullet$ was simulated and is shown in Figure 7.6f.

The effect of water on the stability of these O_2^- and O^- radicals is an important factor. Therefore, to investigate the stability of these radicals, a variable temperature study was performed. At 140K, the spectra are comprised of a mixture of signals from O_2^-, O^- and $HO_2^\bullet$ (Figure 7.7a). The sample was subsequently annealed to a series of elevated temperatures (T ~ 140-298K) and then recooled to 130K before recording the EPR spectra shown in Figure 7.7a-h. Upon raising the temperature a decrease in the peaks associated with the $O^-_{I\text{-}II}$ sites is observed, with both species $O^-_{I\text{-}II}$ lost at T ≥ 200K. The signal intensity of O_2^- also decreased as the annealing temperature increased, with a loss of 40% of the initial integrated signal intensity. The relative distribution of the g_{zz} peaks representing O_2^- changed with the increased temperature, with an obvious decrease in the intensity of the peak representing site I' on annealing to room temperature.

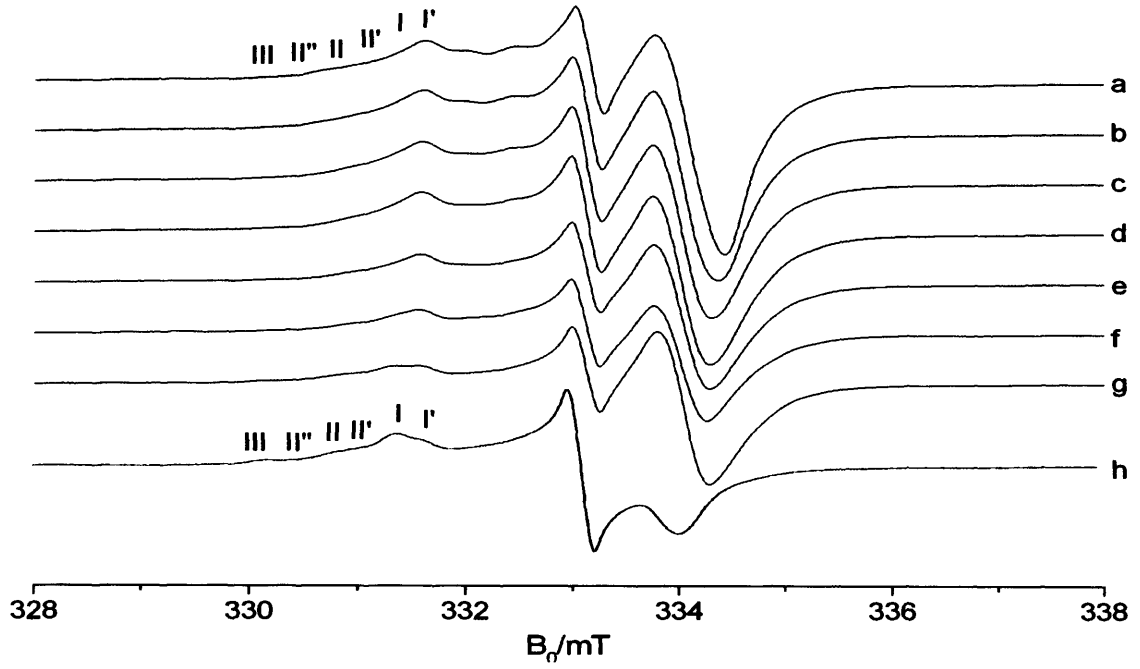

Figure 7.7 *cw*-EPR spectra (130K) of P25 TiO_2 after exposure to a co-adsorbed dose of H_2O:O_2 followed by UV irradiated at 77K. The excess gas was evacuated at 130K and the sample subsequently was annealed to a) 140K, b) 150, c) 170, d) 180, e) 190, f) 210, g) 298, and h) after evacuation at 298K.

On evacuation at room temperature, an EPR signal corresponding to the O_2^- radical is observed with parameters characteristic of a normal photogenerated O_2^-. The fact that O_2^- is stable under these partially hydrated conditions is surprising; work by Attwood *et al.*,[15] using similar experimental conditions has shown that irradiation of TiO_2 under a co-adsorbed H_2O/O_2 atmosphere resulted in the formation of O^- and HO_2• species with no O_2^- species present.

Table 7.2 Spin Hamiltonian parameters of oxygen radicals formed after low temperature UV irradiation under an H_2O/O_2 atmosphere.

Species	Relative Populations		
	140K	200K	298K
O^-	14%	5%	0
O_2^-	82%	91%	100%
HO_2•	4%	4%	0

Subsequent warming of the sample to room temperature, followed by evacuation of the excess H_2O/O_2 mixture, resulted in the loss of the EPR signals attributed to O^- and $HO_2^•$. This was attributed to the fact that on warming to room temperature, the O_2^- radical will react with the H_2O resulting in the destruction of the EPR signal, similar to

the behaviour between organic substrates and O_2^- (Chapter 6). In the case above, the excess H_2O/O_2 (Figure 7.7) is evacuated at 130K. On annealing to room temperature, the O_2^- signal is still present; this is because no gaseous water is present to react with the O_2^-. Clearly the O_2^- can be formed under a partially hydrated atmosphere. The O_2^- is stable once water is removed, but in the presence of water the O_2^- reacts to give products unseen in the EPR spectra (spectra not shown).

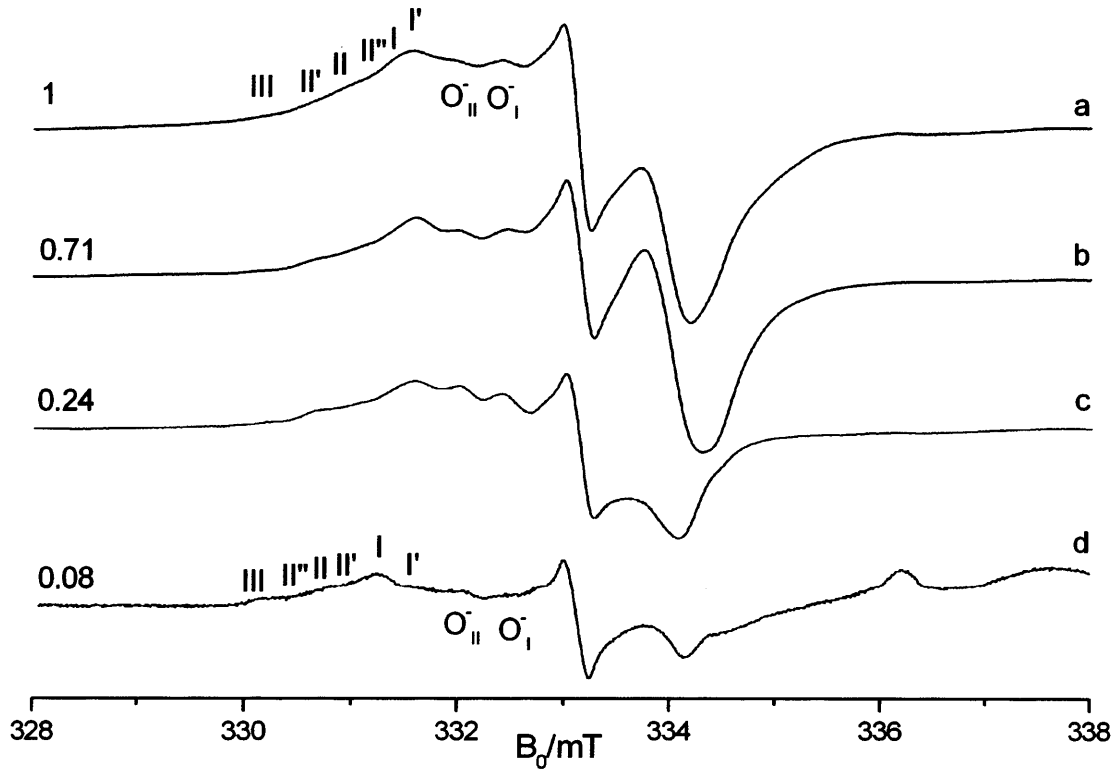

Figure 7.8 *cw*-EPR spectra (130K) of dehydrated P25 TiO_2 after exposure to a co-adsorbed mixture of H_2O:O_2 followed by UV irradiation at 77K. The following ratios were used a) 1:10, b) 1:4, c) 1:1 and d) 20:1. The total pressure in each case was 15 Torr.

In the first part of the investigation on partially hydrated TiO_2, the ratio of H_2O/O_2 was kept constant. In the following the ratio of H_2O/O_2 adsorbed prior to irradiation was varied to investigate the effect this has on the formation of O_2^- and O^- radicals. As in previous experiments the H_2O/O_2 was premixed in the vacuum line prior to adsorption onto the TiO_2 surface at 298K. The ratio of water to oxygen was varied in each experiment, ranging from 1:10 to 10:1 (total pressure 15 Torr). Following irradiation at 77K for 30 minutes, the excess H_2O/O_2 gas mixture was evacuated at 130K. The resultant EPR spectra are shown in Figure 7.8a-d. At low water pressures (Figure 7.8a (O_2 rich)), the spectrum is dominated by a strong O_2^- signal accompanied by signals from the O^- species. In Figure 7.8a, the overall signal intensity of the oxygen species (O_2^- and O^-) is increased by a factor 1.5 compared to the double integrated

intensity of the oxygen species over the dehydrated surface. As the ratio of water vapour to oxygen is increased, there is a clear decrease in the signal intensity of the O_2^- and O^- signals this is illustrated by the decrease in the overall integrated signal intensity in each case as displayed on the left of Figure 7.8a-d. When the ratio of H_2O: O_2 is 1:1 (Figure 7.8c), the EPR signal intensity dropped by a factor of 5. Under an H_2O rich atmosphere (Figure 7.8 d) the O^- signal is greatly reduced and the O_2^- signal intensity has reduced by a factor of 10. The drop in signal intensity of O_2^- could be due to a number of factors; on increasing the pressure of H_2O in the gas mixture the surface sites for O_2^- stabilisation are blocked by H_2O or –OH groups on the TiO_2 surface, or the O_2^- are unstable on the hydrated surface and are lost on warming to room temperature.

7.3.3 Formation of O_2^- on the fully hydrated TiO_2 surface

The fully hydrated surface was prepared by addition of H_2O (10 Torr) at 673K to an activated TiO_2 sample and held at this temperature for one hour (described in 7.2.3). A background EPR spectrum was recorded (but no EPR signal was observed). Oxygen (10 Torr) was added to the sample at RT and subsequently UV irradiated at 77K for 30 minutes. The sample is then warmed to 298K and the excess oxygen was removed before recooling to 130K to record the EPR spectrum (Figure 7.9a).

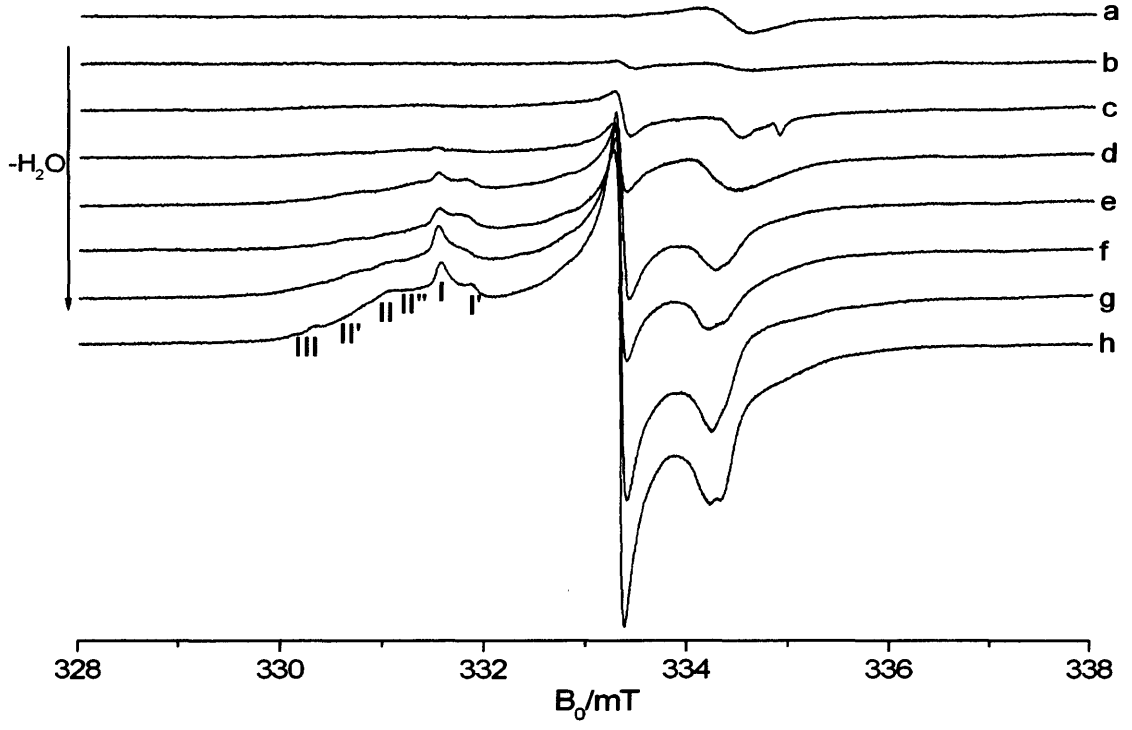

Figure 7.9 *cw*-EPR spectra (130K) of fully hydrated P25 TiO_2 evacuated under dynamic vacuum at a) RT, b) 373, c) 473, d) 498, e) 523, f) 548, g) 573, and h) 673K followed by UV irradiation under an oxygen atmosphere (10 Torr) at 77K for 25 minutes. Samples were evacuated at RT.

Following this treatment, no EPR signals due to O_2^- were observed in the EPR spectrum, suggesting the O_2^- radicals are unstable on the hydrated surface. The sample was then returned to the vacuum line and heated under dynamic vacuum to elevated temperatures. Irradiation under an oxygen atmosphere was the repeated (as described above). This method was repeated for a number of temperatures (298K-540K), to give the series of spectra shown in Figure 7.9 a-h. On the fully hydrated TiO_2, no O_2^- is observed as the Ti^{4+} sites are blocked, as these sites are progressively un-blocked at elevated temperatures, more O_2^- is observed (Figure 7.9a-h).

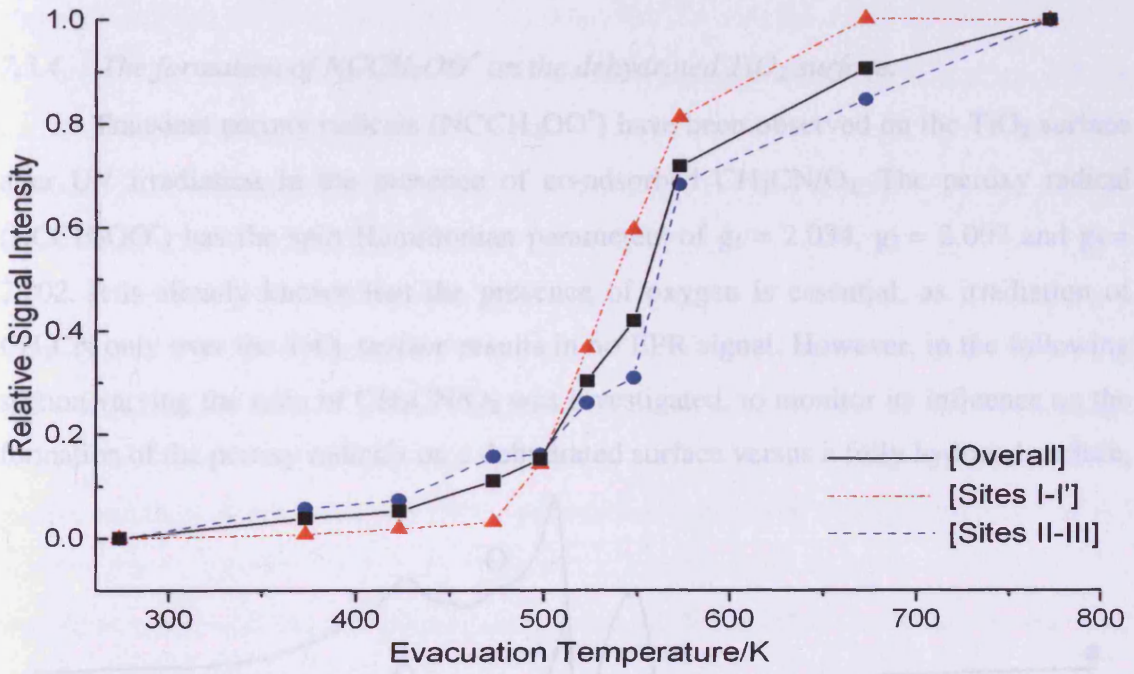

Figure 7.10 Variation in the relative signal intensities of adsorbed O_2 versus evacuation temperature. The relative intensities of sites I - I', and II-III were determined by simulation. The relative integrated intensity of the entire superoxide spectrum (including all three contributing sites) is labelled [Overall].

On closer inspection there appears to be selective un-blocking of the O_2^- stabilisation sites, evidenced by the reappearance of selected peaks. This is illustrated clearly in Figure 7.10; which shows the individual spectral contribution of sites I-I' and sites II-III to the overall O_2^- integrated signal intensity plotted against evacuation temperature.

The relative increase in signal intensity of sites II-III compared to site I is clearly illustrated in Figure 7.10. As the evacuation temperature is increased the overall superoxide intensity increased. Initially, this signal intensity increase is more pronounced for sites II-III at low temperature (0-500K). However, at T >450 K the signal intensity increase is more pronounced for sites I-I'. On reaching 575K the

increase in signal intensity is global i.e. all sites are increasing in intensity at the same rate. Heating the sample under dynamic vacuum causes not only the chemisorbed and physisorbed water but also the surface bound hydroxyl groups to be removed. As the evacuation temperature is increased, more hydroxyls are removed freeing up surface stabilisation sites. Upon subsequent irradiation more surface sites are available and as a result there is an increase in O_2^- signal intensity (Figure 7.9b-h). In Figure 7.9h (540K) the EPR signal intensity and profile is the same as the typical superoxide formed *via* photolysis on a fully dehydrated surface.

7.3.4 The formation of $NCCH_2OO^\bullet$ on the dehydrated TiO_2 surface.

Transient peroxy radicals ($NCCH_2OO^\bullet$) have been observed on the TiO_2 surface after UV irradiation in the presence of co-adsorbed CH_3CN/O_2. The peroxy radical ($NCCH_2OO^\bullet$) has the spin Hamiltonian parameters of $g_1 = 2.034$, $g_2 = 2.007$ and $g_3 = 2.002$. It is already known that the presence of oxygen is essential, as irradiation of CH_3CN only over the TiO_2 surface results in no EPR signal. However, in the following section varying the ratio of CH_3CN/O_2 was investigated, to monitor its influence on the formation of the peroxy radicals on a dehydrated surface versus a fully hydrated surface.

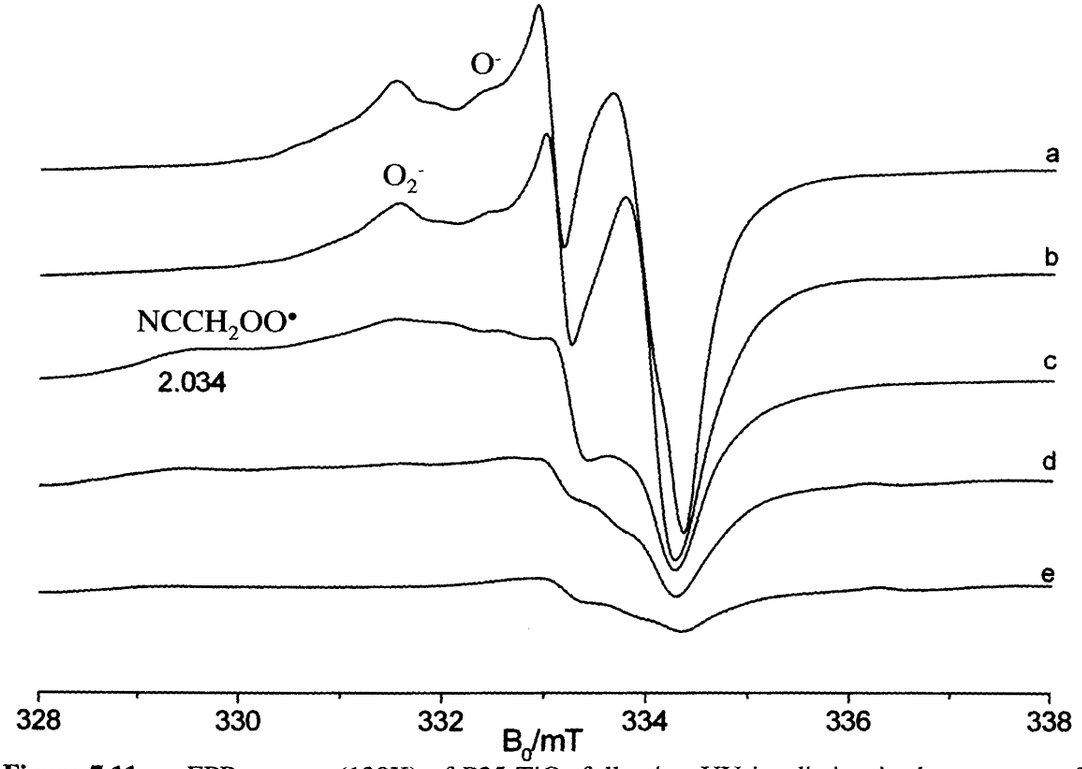

Figure 7.11 *cw*-EPR spectra (130K) of P25 TiO_2 following UV irradiation in the presence of co-adsorbed $CH_3CN:O_2$ in the following ratios a) 1:1, b) 3:1, c) 5:1, d) 10:1 and e) 20:1.

The premixed ratios of CH_3CN/O_2 were exposed to the activated TiO_2 sample at 298K before cooling to 77K. The sample was then UV irradiated under the co-adsorbed atmosphere for 30 minutes at 77K. Following irradiation the excess gas mixture was evacuated at 130K. The resultant EPR spectra are shown in Figure 7.11.

In Figure 7.11, the ratio of CH_3CN is increased on moving from 7.11a-e (the total pressure was kept constant at 15 Torr in each experiment). In Figure 7.11a, the UV irradiation of TiO_2 under a co-adsorbed atmosphere of O_2 and CH_3CN, results in the formation of O_2^-, O^- and $NCCH_2OO^\bullet$ radicals on the TiO_2 surface, with the relative signal intensities 80% (O_2^-): 17% (O^-): 3% ($ROO^\bullet$). As the ratio of CH_3CN to O_2 (Figure 7.11 a-e) is increased, there are obvious changes in the EPR spectra. As the mixture becomes CH_3CN rich, fewer O_2^- and O^- radicals are formed. In Figure 7.11e, the spectrum is dominated by the signal from the ($NCCH_2OO^\bullet$) species with the relative signal intensities of 25% (O_2^-): 0% (O^-): 75% ($NCCH_2OO^\bullet$).

This is clearly demonstrated graphically in Figure 7.12. The individual spectra from Figure 7.11a-e have been deconvoluted *via* computer simulation to extract the individual relative spectral contribution for each species which are plotted against CH_3CN pressure. When oxygen is in excess (far left of the graph), the population of the peroxy radicals is low, and the EPR spectrum is dominated by signals from the O_2^- species and O^- species. On the far right of the graph, representing an acetonitrile-rich atmosphere, the spectrum is predominately that of $NCCH_2OO^\bullet$ as shown by the high relative concentration (~80%).

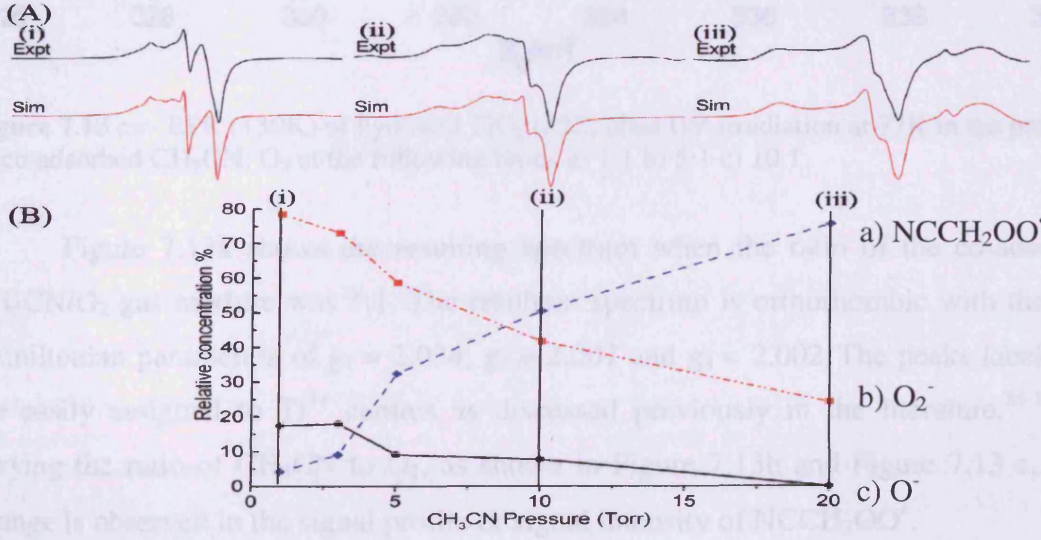

Figure 7.12 (A) Experimental and simulated EPR spectra after UV irradiation of co-adsorbed CH_3CN/O_2 over the TiO_2 surface at the following ratios: (i) 1:1 (ii) 5:1 (iii) 20:1 surface.(B) Concentration plotted as a function of acetonitrile pressure for a) peroxy radical $NCCH_2OO^\bullet$ b) superoxide radical O_2^- and c) O^- ions are plotted

7.3.5 Formation of transient oxygen radicals on the fully hydrated TiO_2 surface

The fully hydrated surface is completely saturated with –OH groups (and possibly physisorbed water). This provides the chance to probe whether the presence of –OH groups and water has an effect on the formation of transient peroxy type radicals ($NCCH_2OO^{\bullet}$). The hydrated surface was prepared as discussed in section 7.2.3 and then exposed to a dose of premixed CH_3CN/O_2 at 298K. The sample was cooled to 77K and irradiated for 30 minutes. The excess gas mixture was evacuated at 130K before recording the EPR spectrum. This was repeated for a number of different ratios of CH_3CN/O_2. The resulting EPR spectra are shown in Figure 7.13a-b.

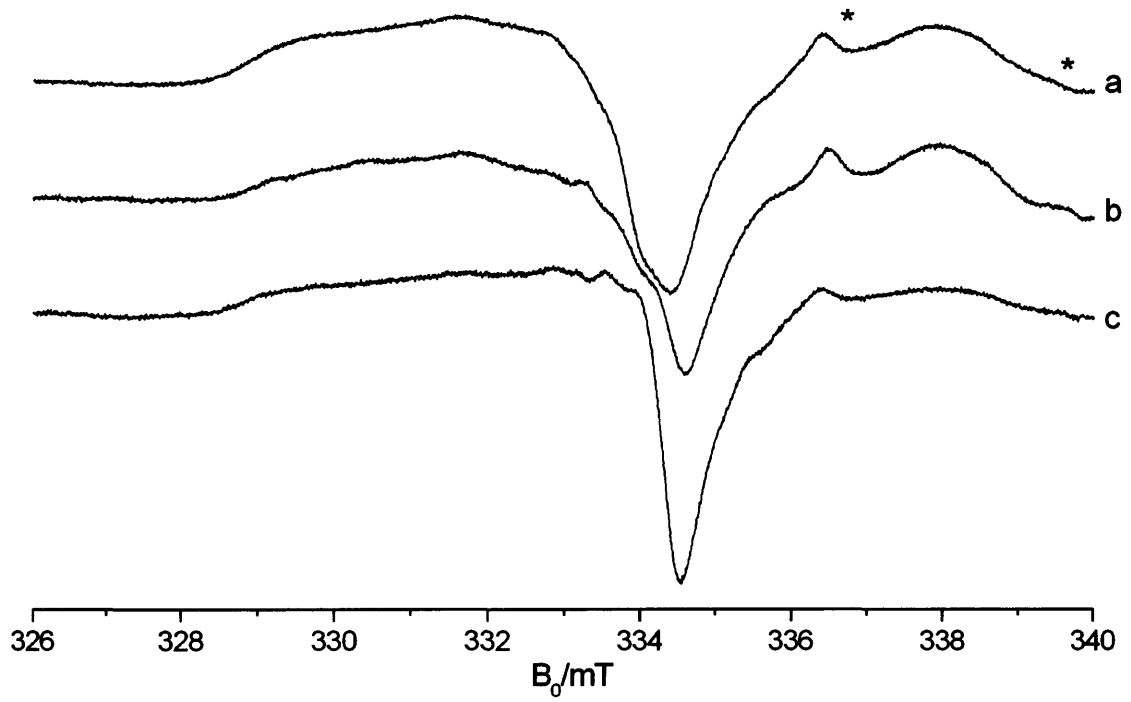

Figure 7.13 *cw*- EPR (130K) of hydrated TiO_2 (P25) after UV irradiation at 77K in the presence of co-adsorbed CH_3CN: O_2 at the following ratios a) 1:1 b) 5:1 c) 10:1.

Figure 7.13a shows the resulting spectrum when the ratio of the co-adsorbed CH_3CN/O_2 gas mixture was 1:1. The resultant spectrum is orthorhombic with the spin Hamiltonian parameters of $g_1 = 2.034$, $g_2 = 2.007$ and $g_3 = 2.002$. The peaks labelled * are easily assigned to Ti^{3+} centres as discussed previously in the literature.[34-36] On varying the ratio of CH_3CN to O_2, as shown in Figure 7.13b and Figure 7.13 c, little change is observed in the signal profile or signal intensity of $NCCH_2OO^{\bullet}$.

It was previously observed on a fully dehydrated surface, that irradiation of the co-adsorbed mixture with a co-adsorbed ratio of 1:1 (CH_3CN/O_2) resulted in the formation of O_2^- and O^- species. In contrast, on the fully hydrated surface the EPR

spectrum is dominated by the $NCCH_2OO^{\bullet}$ species with little or no sign of signals due to O_2^- radicals and O^- radicals. Seemingly the hydrated surface inhibits the formation of superoxide on the surface of TiO_2 as observed in 7.3.3.

Although formed on the hydrated surface the integrated signal intensity of the $NCCH_2OO^{\bullet}$ species is reduced by a factor of 3.5 indicating that the signal intensity of the $NCCH_2OO^{\bullet}$ is affected by the presence of water on the TiO_2 surface.

Further confirmation of the blocking of the surface sites for O_2^- and $NCCH_2OO^{\bullet}$ formation was obtained by the following experiment. The sample with the $NCCH_2OO^{\bullet}$ species was annealed to 298K to ensure destruction of the $NCCH_2OO^{\bullet}$ signal. The sample was then evacuated at 298K to remove any surface adsorbed CH_3CN, before being heated under dynamic vacuum at 540K. This treatment should result in the removal of surface adsorbed hydroxyl as discussed in section 7.3.3. The sample was then exposed to an additional dose of $CH_3CN:O_2$ (1:1) at 298K. The sample was irradiated at 77K for 30 minutes followed by evacuation at 130K to remove the excess gas. The resulting EPR spectrum is shown in Figure 7.14b.

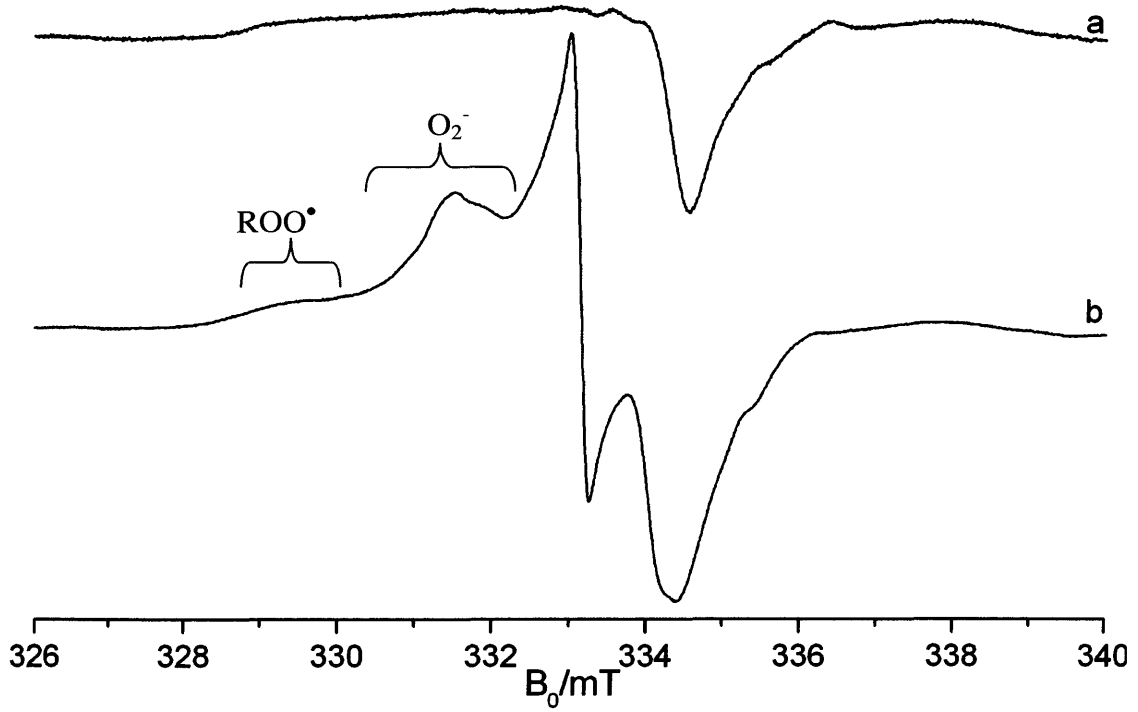

Figure 7.14 *cw*-EPR spectra (130K) of fully hydrated P25 TiO_2 after UV irradiation at 77K in the presence of a co-adsorbed mix of CH_3CN/O_2 followed by evacuation at a) 130K. The sample was annealed to 298K, before evacuation under dynamic vacuum at 673K, followed by b) UV irradiation at 77K under an atmosphere of $CH_3CN:O_2$ 1:1 (15 Torr). Once irradiated the sample was evacuated at 130 K

Clearly the surface heating under vacuum has resulted in the removal of physisorbed water and the surface –OH groups which were blocking the stabilisation

sites for the O_2^- radicals. The overall integrated signal intensity has increased by a factor of 7, with the population of both O_2^- and $ROO^\bullet$ increasing. The EPR spectrum clearly shows the difference with signals corresponding to O_2^- in Figure 7.14.

This result is important as it shows how the formation of superoxide is hindered on the fully hydrated surface, yet the $NCCH_2OO^\bullet$ radical is still formed, albeit in lower concentration. It has been shown in previous chapters that the presence of superoxide is vital to decompose organics *via* a thermal decomposition route. So on a fully hydrated surface the decomposition of acetonitrile is limited to only a hole mediated process producing ($NCCH_2OO^\bullet$) as an intermediate.

7.3.5 *Formation of transient oxygen radicals over the partially hydrated TiO_2 surface.*

Under photocatalytic conditions, water, oxygen, and organic substrates will all be present in different concentrations on the TiO_2 surface. It is therefore important to understand what role each individual component plays. For instance, the presence of oxygen has been shown to be vital in the formation of the $NCCH_2OO^\bullet$ radical. In the following section, the type of radicals formed and their behaviour when different ratios of $H_2O/O_2/CH_3CN$ are co-adsorbed on the TiO_2 surface will be investigated.

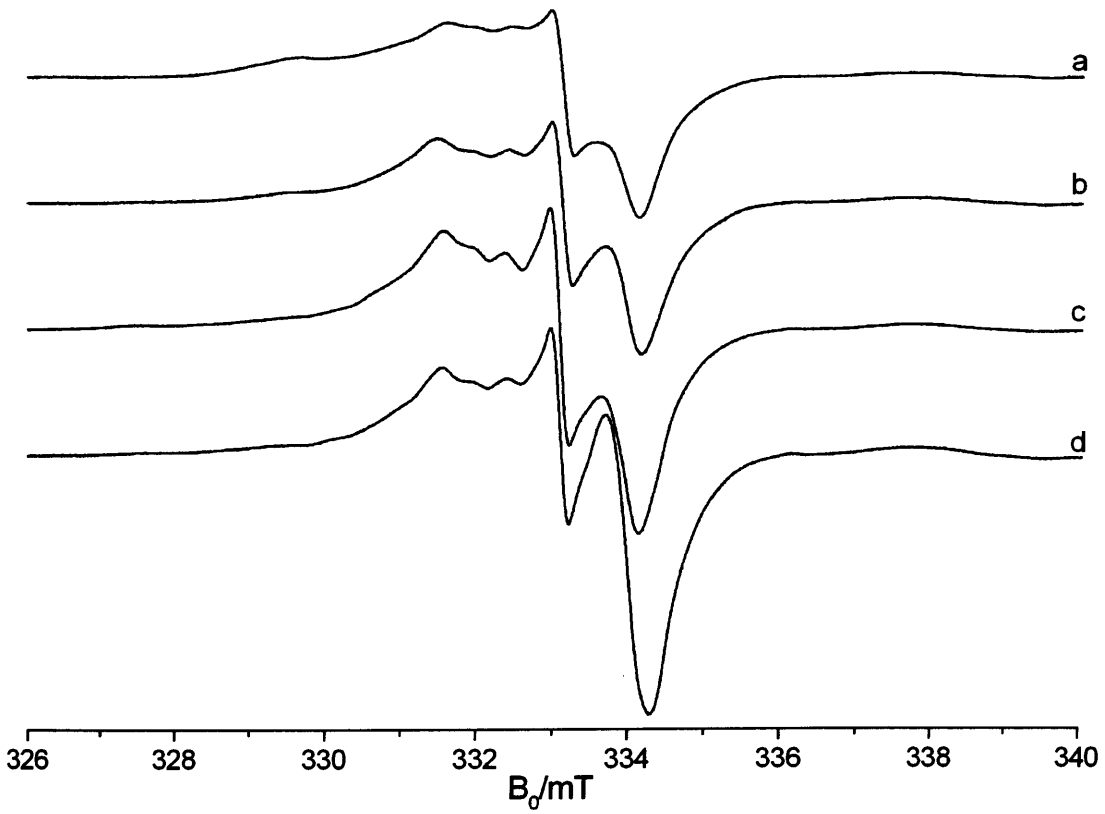

Figure 7.15 *cw*-EPR spectra (130K) of P25 TiO_2 after UV irradiation in the presence of co-adsorbed H_2O: CH_3CN: O_2 (total pressure 15 Torr) in the following ratios a) 1:4:1, b) 1:1:1, c) 4:1:1 and d) 10:1:1.

To a dehydrated surface, a co-adsorbed mixture of $H_2O/CH_3CN/O_2$ was admitted (total pressure: 15 Torr). The sample was UV irradiated for 30 minutes at 77K before transfer to the EPR cavity, followed by evacuation at 130K. This process was repeated for a number of different ratios of $H_2O/CH_3CN/O_2$ with the resultant EPR spectra shown in Figure 7.15a-d. It must be noted that the key component of the gaseous mixture is oxygen; when the TiO_2 surface was irradiated under a co-adsorbed CH_3CN/H_2O atmosphere, no EPR signal was observed.

As the pressure of H_2O is increased in the co-adsorbed mixture, there is a change in the EPR spectra observed. In Figure 7.15a, (where the water pressure = 2.5 Torr) the spectrum is a composite of signals arising from O_2^-, O^- and $NCCH_2OO^\bullet$. As the pressure of water is increased in the co-adsorbed mix the population of the $NCCH_2OO^\bullet$ species decreases as the water pressure increases accompanied by the increase in relative signal intensities of the O_2^- and O^- species. This is illustrated graphically in Figure 7.16. Each individual spectrum in Figure 7.15a-d has been deconvoluted into its individual spectral components of O_2^-, O^- and $NCCH_2OO^\bullet$. The relative signal intensities of each species were plotted against pressure of water in the co-adsorbed ratio.

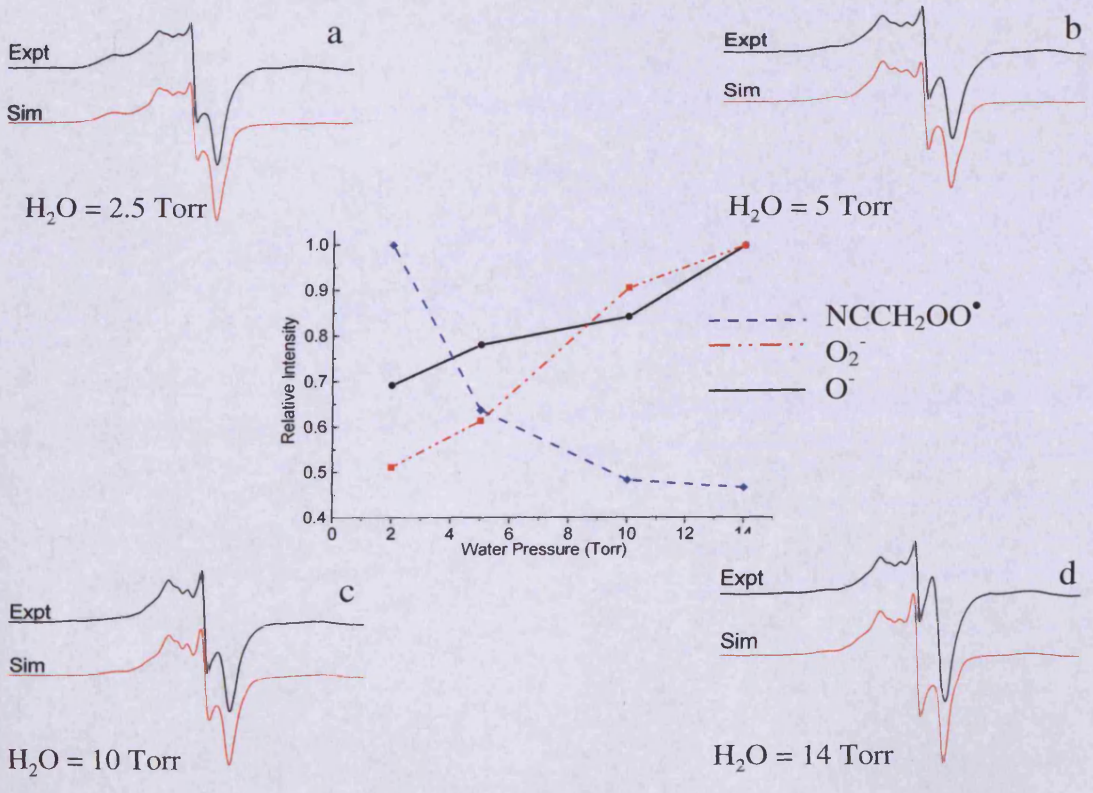

Figure 7.16 Influence of water on the formation of oxygen centred radicals on the TiO_2 surface. The concentration of peroxy radicals ($NCCH_2OO^\bullet$), superoxide radicals O_2^- and O^- ions are plotted as a function of water pressure. Representative experimental and simulated EPR spectra from Figure 7.15 are presented for the following co-adsorbed ratios of $H_2O/CH_3CN/O_2$ a) 1:4:1, b) 1:1:1, c) 4:1:1 and d) 10:1:1.

In Figure 7.16, the trend is shown clearly that on increasing the water pressure the relative intensity of the $NCCH_2OO^{\bullet}$ decreases, whereas the O_2^- and O^- signal intensity increases.

This behaviour is seemingly contradictory to that of the $NCCH_2OO^{\bullet}$, O_2^- and O^- on the fully hydrated surface, where no O_2^- or O^- species were observed and the $NCCH_2OO^{\bullet}$ was observed in reduced concentrations. In this experiment however the three gases are co-adsorbed, which leads to differing surface coverages of each gas. For example, in Figure 7.16d the ratio of gases is 10:1:1 ($H_2O/CH_3CN/O_2$). In previous work (Figure 7.11c) it was shown that when CH_3CN/O_2 is adsorbed in a (1:1) ratio the EPR signal is dominated by the O_2^- and O^- species with a small amount of the $NCCH_2OO^{\bullet}$ species for which Figure 7.16d agrees. When H_2O/O_2 is adsorbed in (10:1) ratio the population of O_2^- and O^- was shown to be reduced slightly. However, in Figure 7.16d the population of the O_2^- and O^- radicals is increased with the increase in water vapour. The most important result from Figure 7.16 is it shows that under these co-adsorption conditions, all three species O_2^-, O^- and $NCCH_2OO^{\bullet}$ can be formed.

The stability of the O_2^-, O^- and $NCCH_2OO^{\bullet}$ radicals is an important characteristic and has bee shown to be dependant on the co-adsorption conditions in each case. When the CH_3CN is in excess (e.g $H_2O/CH_3CN/O_2$ 1:4:1) in the co-adsorbed mix, the EPR signal has the highest relative signal intensity of $NCCH_2OO^{\bullet}$ radicals (Figure 7.17a-h), with the lowest abundance of O_2^- and O^- radicals. The sample was annealed to elevated temperatures (140K- 250K) and held at the selected temperature for 10 minutes. Subsequently the sample was then recooled to 130K prior to recording the EPR spectra.

On increasing the temperature a number of changes occur in the EPR spectra in the range 170 – 250K (Figure 7.17b-h). Initially the most prominent feature is the loss in intensity of the peaks due to the $O^-_{(I\text{-}II)}$ species in the range of 130-200K which is in agreement with the behaviour observed on the dehydrated and partially hydrated surfaces. The second important feature is that the peak at g = 2.034 seemingly does not decrease significantly on increasing the annealing temperature. This is surprising as it has been shown to decrease at increased temperatures in section 6.3.4 and also in the literature.[37] This can be explained by taking into account the behaviour of the O_2^- signal intensity in Figure 7.17b-i. On increasing the temperature the O_2^- signal intensity diminishes. At T = 250K the spectrum is similar to that observed in Chapter 6 when O_2^- radicals reacted with CH_3CN. The signal at T = 250 K has the spin Hamiltonian

parameters of g_1 = 2.031, g_2 = 2.010 and g_3 = 2.003 which can be attributed to a [$CH_3CN....O_2^-$] type adduct. This is accompanied by signals due to the $HO_2^\bullet$ species, with both sets of EPR signals are lost on reaching room temperature.

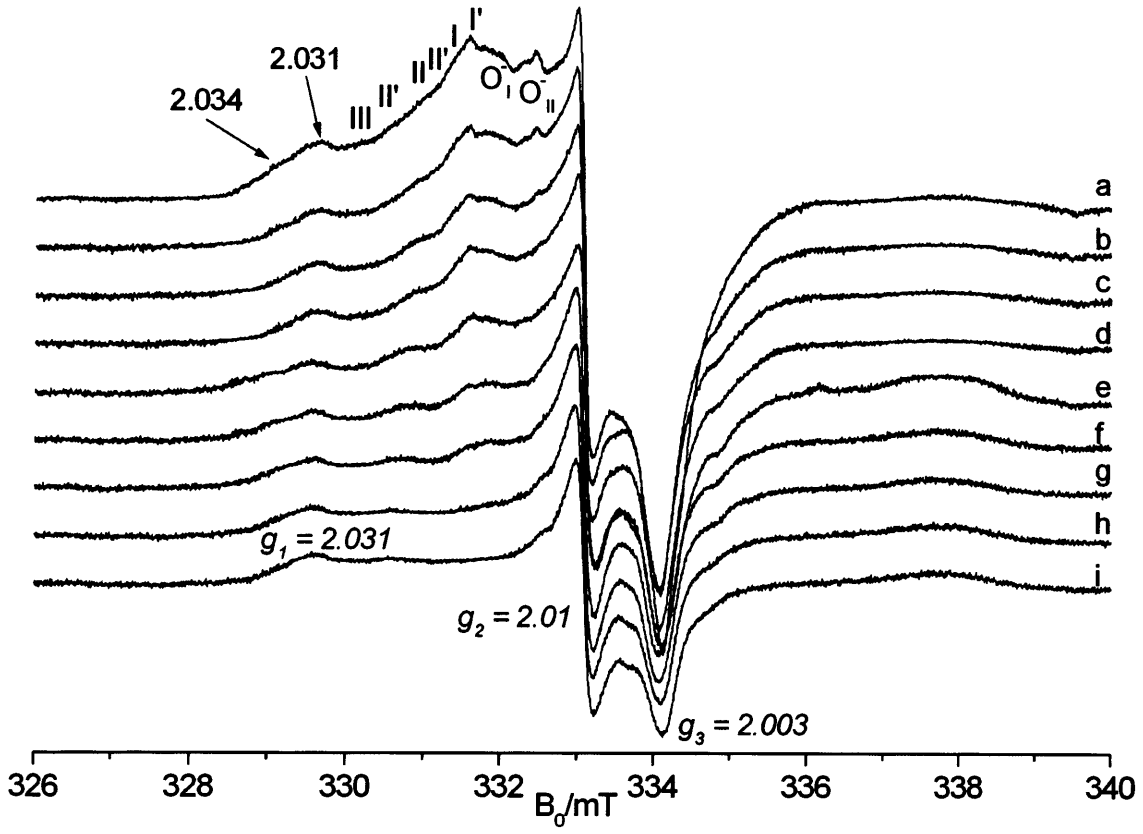

Figure 7.17 *cw*-EPR spectra (130K) of activated P25 TiO_2 after exposure to a co-adsorbed mix of H_2O: CH_3CN: O_2 (1:4:1, total pressure 15 Torr). The sample was UV irradiated at 77K. The sample was annealed to a) 130K before evacuation at this temperature. The sample was subsequently annealed to b) 170, c) 190, d) 200, e) 210, f) 220, g) 230, h) 240, i) 250K.

The initial signal at g = 2.034 at 130K is due to $NCCH_2OO^\bullet$ radicals, which begins to decay at T > 190K. At T > 190K, the O_2^- radicals begin to react with CH_3CN left on the surface after evacuation to give the [$O_2^-....CH_3CN$] adduct with g_1 = 2.031, which explains why the peak at 2.034 does not decrease as expected.

The behaviour of the O_2^-, O^- and $NCCH_2OO^\bullet$ species are different when the water is in excess in the co-adsorbed mixture ($H_2O/CH_3CN/O_2$ = 4:1:1 Figure 7.18a-j). The EPR signal is dominated by the O_2^- and O^- species with a small amount of $NCCH_2OO^\bullet$. The $O^-_{(I\text{-}II)}$ signal loses intensity at T > 150K and is lost altogether on reaching 200K (Figure 7.18d). The O_2^- signal intensity remains constant between 140-200K (Figure 7.18a-d); above 200K there is a decrease in the signal intensity of sites I', I and II. At room temperature, the O_2^- signal is stable but has a slightly different relative signal distribution. The major difference here is that no loss in the superoxide signal is

seen unlike the previous cases - this is due to the CH_3CN being in low concentration and being removed on evacuation. Hence unlike the CH_3CN excess case the peak at g = 2.034 loses intensity in the temperature range of 140-250K and is completely lost on reaching room temperature.

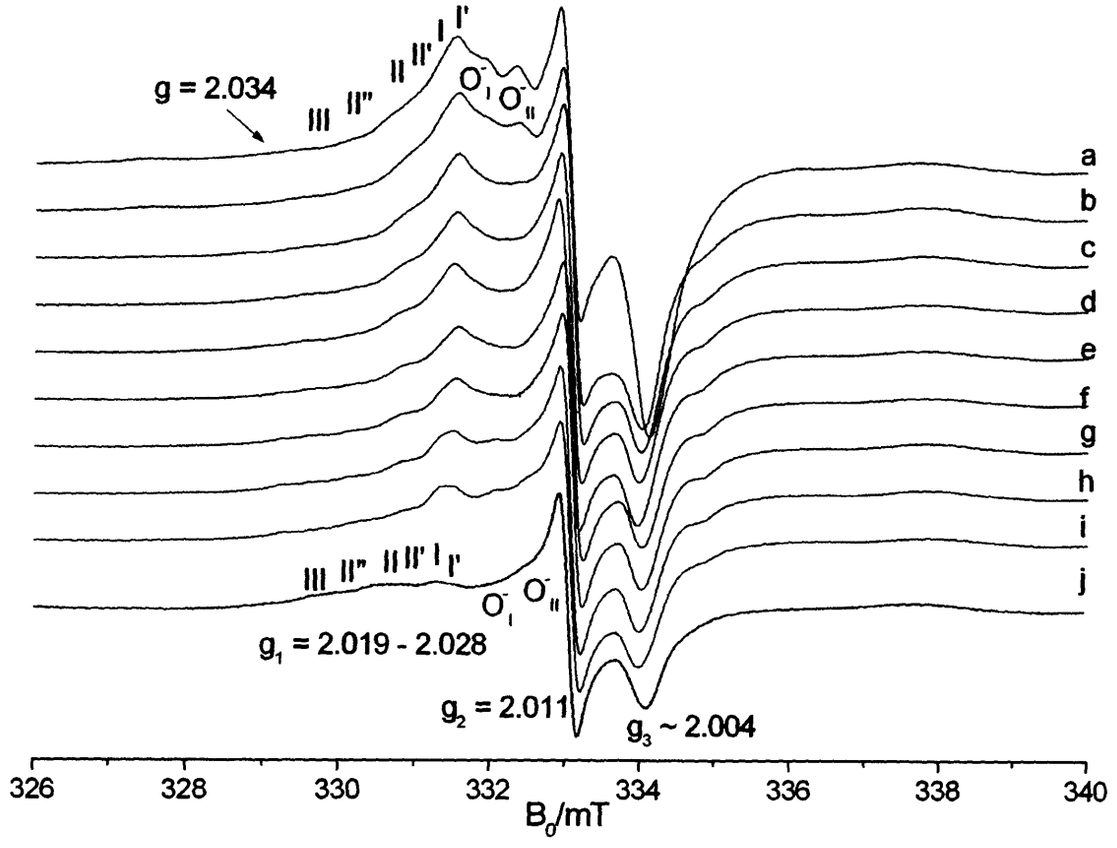

Figure 7.18 *cw*-EPR spectra (130K) of activated P25 TiO_2 after exposure to a co-adsorbed mix of H_2O: CH_3CN: O_2 (4:1:1, total pressure 15 Torr). The sample was UV irradiated at 77K. The sample was annealed to a) 130K before evacuation at this temperature. The sample was subsequently annealed to b) 170, c) 190, d) 200, e) 210, f) 220, g) 230, h) 240, i) 250, and j) 298K .

7.4 Discussion

Irradiation of TiO_2 results in the generation of an electron-hole (e^-/h^+) pair which can subsequently migrate to the surface. Once at the surface the photogenerated charge carriers can participate in a number of redox reactions, either with electron donors or acceptors, to produce a number of transient reaction intermediates. In the presence of molecular oxygen it has been shown that oxygen based radicals, such as O_2^-, O_3^-, O_2^{2-} and O^-, can be generated when the photogenerated species are captured. These oxygen based species have been shown to play a crucial role in TiO_2 photocatalysis.[18,38] Under photocatalytic conditions these species must be generated in the presence of water and organic substrates which can hinder the formation of these radicals and affect their stability. The effect of these co-adsorbates has been investigated in this chapter.

7.4.1 The O_2^- and O^- species on the dehydrated TiO_2 surface

After irradiation of TiO_2 under an oxygen atmosphere at 77K, followed by evacuation at 298K, an EPR signal due to the formation of a stable O_2^- species is observed. The O_2^- species is characterised by the spin Hamiltonian parameters of an O_2^- generated *via* photochemical means. The g_{zz} region is characterised by a number of extra sites along with a different relative distribution of the g_{zz} peaks compared to the O_2^- species formed on the thermally reduced surface (Chapter 5). The difference is due to extra stabilisation sites and fewer surface defects due to reoxidation being present on the activated sample compared to a thermally reduced sample. The formation of O_2^- on a clean activated surface is different as on the activated surface no thermally produced surface Ti^{3+} centres exist. The O_2^- is formed *via* the following processes (eq 7.1-7.4). After UV irradiation of the TiO_2 sample electron-hole (e^-/h^+) pairs are created. These migrate to the surface where the photogenerated e^- can be trapped by surface Ti^{4+} centres (eq 7.2) to form Ti^{3+} species. In the presence of gas phase oxygen however the electron is scavenged to form O_2^- as shown in (eq 7.3)

$$TiO_2 \rightarrow (e^- + h^+)\ TiO_2 \qquad (7.1)$$

$$Ti^{4+} + e^-_{cb} \rightarrow Ti^{3+} \qquad (7.2)$$

$$Ti^{3+} + O_2 \rightarrow Ti^{4+} \ldots O_2^- \qquad (7.3)$$

$$O^{2-} + h^+ \rightarrow O^- \qquad (7.4)$$

At room temperature, the O_2^- species is clearly observed and can be detected by EPR spectroscopy (Figure 7.1). However the transient species formed by the interaction of the photogenerated hole (h^+) with lattice oxygen (O^{2-}) is unseen at room temperature as it is thermally unstable. Clearly vital information has been lost by annealing the sample to room temperature, as the transient O^- species that may be present at low temperature are lost on reaching room temperature, T > 298K. This highlights the necessity to perform low temperature experiments

The irradiation of dehydrated TiO_2 in the presence of O_2 followed by evacuation at low temperature (130K) resulted in evidence of both the O_2^- and O^- species (Figure 7.1a). Some debate has existed as to whether the trapped hole O^- species and the O_2^- species can both be stabilised on the same dehydrated surface. In a study by Gratzel *et al.*, [35] they found that this could only occur on the hydrated anatase surface. On the

dehydrated P25 surface (80% anatase, 20% rutile), both the O_2^- and O^- species were detected.

The O^- species are distinguished by the spin Hamiltonian parameters of O^-_I $g_{\|}$ = 2.002 and $g_{\perp}$ = 2.014 and O^-_{II} $g_{\|}$ = 2.002 and $g_{\perp}$ = 2.016 (Table 7.1) Both O^- species in this study were found to be thermally unstable and are annihilated at T > 190K. The spin Hamiltonian parameters and the thermal behaviour displayed agree with the literature values, which all state that the O^- species is lost on reaching 300K due to recombination or annihilation. The O^- species can be regenerated by further low temperature irradiation.[34,38-40] Similar species have been identified by Che *et al.*,[38] and are discussed in their excellent review. The O^- is believed to form when a photogenerated hole h^+ (eq 7.1) is trapped at a surface O^{2-} site (eq 7.4).[41]

The hole trapping sites are important as they have been identified and generally accepted as active species in photocatalytic oxidation reactions.[42] The O^- can have either axial or orthorhombic symmetry. In this case the O^- species appears to have axial symmetry. This is confirmed by computer simulation where the use of axial parameters gives the best fit to the experimental spectrum. For the O^- species with axial symmetry, the p_x and p_y orbitals are symmetrical and energetically degenerate. The first order expressions for the g-tensor components of the O^- anion in an axial symmetry field are:

$$g_{\|} = g_{zz} = g_e \qquad (7.5)$$

$$g_{\perp} = g_{xx} = g_{yy} = g_e + 2\,(\lambda / \Delta E) \qquad (7.6)$$

where λ is the spin orbit coupling constant (0.014 eV) and ΔE is the energy separation between the p_z orbital containing the unpaired electron and the degenerate p_x and p_y orbitals.[38] Larger splitting of the p orbitals and consequently lower $g_{\perp}$ values, are expected for the O^- centres stabilised close to more positively charged ions, as the value for the $g_{\perp}$ is dependent upon the energy splitting ΔE, which is governed by the local cationic charge in much the same way as for O_2^- (Chapter 5). The two values of $g_{\perp}$ = 2.014 and $g_{\perp}$ = 2.016 can be attributed to two different O^- species present at two different surface sites. The $g_{\perp}$ components for the two O^- species can be fitted to eq 7.6 to calculate values of ΔE for O^-_I = 2.40 eV and O^-_{II} = 2.044 eV. The values obtained can then be used to allocate the nature of the stabilisation site. The values calculated fit more closely to values of an O^- species stabilised at a site on the anatase phase, with the structure Ti^{4+}- O^- - Ti^{4+}.[35]

The structure and location of the O^- has been studied by many groups. For example, Nakaoka and Nosake,[43] assigned the trapped hole to a photo produced hole trapped at the lattice oxygen atom located in the subsurface layer of TiO_2. Further information on the location of the trapped hole was provided by Micic *et al.*,[39,40] who reported that the holes produced are trapped directly on oxygen atoms bound to the Ti^{4+} atoms. The use of ^{17}O enriched water provided further identification of trapped holes as an oxygen anion radical covalently bound to titanium atoms, Ti^{4+}-O^{2-} Ti^{4+}- O^-.[39,40] In a study of light induced charge separation on anatase nanoparticles, Berger *et al.*,[41] found that the O^- species was formed after irradiation of the nanoparticles at 90K and 140K. At 90K the signal was accompanied by Ti^{3+} signals. However, at 140K the O^- signal was not accompanied by Ti^{3+} centres due to recombination at higher temperatures. This explains why the UV irradiation of purely dehydrated P25 resulted in no sign of the O^- species or Ti^{3+}, as efficient recombination of the e^-/h^+ pairs in the absence of electron/hole scavengers occurs at this temperature. Berger *et al.*,[41] repeated the UV irradiation of the anatase nanoparticles in the presence of oxygen. It was found that a ten fold increase in the number of trapped charges was observed. This mirrors the behaviour observed in our experiments where the O^- species are observed in the presence of oxygen which stops recombination, but not on the pure P25 in the absence of electron/hole scavengers.

Berger *et al,.*[41,44] found that after addition of oxygen to the surface after irradiation both O^- and O_2^- species exist on the surface in comparable intensities of ~1.1:1. Raising the temperature resulted in the annihilation of the O^- signal but the O_2^- signal remained. The behaviour observed is similar to that observed on the dehydrated P25 TiO_2 surface in this chapter, although the population of O^- to O_2^- is different with comparable intensities of 1: 2.6. Additionally on the P25 TiO_2 surface, two species of $O^-_{I\text{-}II}$ and six O_2^- species were identified, highlighting the heterogeneity of the P25 surface.

In the Berger *et al.*,[41] study the authors observed the formation of O_3^- species *via* reaction of O^- with O_2. The ozonide O_3^- ion is formed on reaction of O^- with molecular oxygen to form a 17 electron triatomic radical, as discussed in Chapter 2. The ozonide radical has been observed in accompaniment with the O^- and O_2^- over anatase nanoparticles.[41] O_3^- however is thermally unstable and decays to O^- and O_2^- at T > 110K. So while it may have been present initially in our study after irradiation at 77K, due to the spectra being recorded at 130K, it was not observed in the EPR spectra in this investigation.

The O_2^- and O^- species are believed to play a role in the photocatalytic oxidation of organic species. The O_2^- species has been shown to react with CH_3CN to give a thermally unstable [O_2^-...CH_3CN] adduct (Chapter 6).[21] The experiment was repeated to probe the reaction of the O^- species and CH_3CN. The O^- species decayed on addition to the CH_3CN but no new signals were observed, which indicates that there was reactivity with the likelihood that the new species formed is diamagnetic and undetectable by EPR spectroscopy.

After UV irradiation under an oxygen atmosphere, the O_2^- and O^- species are formed on the TiO_2 surface. The O^- species is thermally unstable and decays at T > 190K, whereas the O_2^- is thermally stable and is present at room temperature for a number of days. The formation of these species agrees with EPR studies performed on other TiO_2 powders reported in the literature. Analogous experiments were performed on the partially hydrated and fully hydrated surfaces to understand the role of water on the formation of these species.

7.4.2 The O_2^- and O^- species on the partially hydrated TiO_2 surface

After the investigation of photogenerated species on the dehydrated surface, the experiments were repeated on the partially hydrated surface. UV irradiation of TiO_2 under a co-adsorbed atmosphere of water and oxygen produced an intense EPR signal. The EPR signal contained contributions from both the O^- species and O_2^- as observed previously on the dehydrated case, accompanied by a weak signal that was attributed to the $HO_2^\bullet$ species. The stability of these oxygen species was studied by performing a Variable Temperature study. On increasing the temperature it was found that the O^- and $HO_2^\bullet$ signals decayed leaving the stable O_2^- species.

The stability and presence of O_2^- was surprising as previous studies have shown the O_2^- species generated *via* low temperature irradiation in a H_2O/O_2 atmosphere are unstable at all temperatures.[15] In this study two main differences from the literature arise. In the Attwood study[15] the excess gas mix was still present at 130K. However, in this study the excess H_2O/O_2 had been evacuated at this temperature, eliminating any line broadening effects due to O_2 and thereby allowing the observation of the O_2^- species. Secondly, the VT study described in this chapter was performed without excess water present, hence the stability of O_2^- at room temperature. If a second dose of H_2O is admitted to the evacuated sample at 298K the O_2^- EPR signal is lost indicating reactivity

of the O_2^- species with H_2O. No new EPR signals were observed following this treatment indicating the species formed is either diamagnetic or thermally unstable.

In the metal oxide-water system after the generation of the electron-hole (e^-/h^+) pair, the following proposed reactions can take place:

$$h^+ + OH^- \rightarrow {}^\bullet OH \qquad (7.7)$$

$$h^+ + H_2O \rightarrow H^+ + {}^\bullet OH \qquad (7.8)$$

The oxygen present acts as an electron scavenger and O_2^- is formed; this can then react with H^+ to form the $HO_2^\bullet$.

$$O_2^- + H^+ \rightarrow HO_2^\bullet \qquad (7.9)$$

This reaction sequence explains the presence of both O_2^- and $HO_2^\bullet$ on the partially hydrated surface. Interestingly only small amounts of $HO_2^\bullet$ are present at 130K - presumably the reaction between O_2^- and H^+ (eq 7.9) proceeds at elevated temperature, but due to the reactive nature of $HO_2^\bullet$ in the hydrated environment it is immediately lost *via* a series of disproportionation reactions (eq 7.10 to 7.12).

$$HO_2^\bullet + O_2^- + H^+ \rightarrow H_2O_2 + O_2 \qquad (7.10)$$

$$HO_2^\bullet + HO_2^\bullet \rightarrow H_2O_2 + O_2 \qquad (7.11)$$

$$O_2^- + O_2^- + 2H^+ \rightarrow H_2O_2 + O_2 \qquad (7.12)$$

The ${}^\bullet OH$ radicals are extremely short lived and reactive intermediates which cannot be directly observed by EPR on the TiO_2 surface even at low temperature (10K). The ${}^\bullet OH$ radicals can be indirectly observed by spin trapping experiments or through analysis of the secondary radicals formed by the reactions of ${}^\bullet OH$.[45] The spin Hamiltonian parameters of bulk ${}^\bullet OH$ and ${}^\bullet OH$ irradiated in ice are well known in the literature.[46,47]

The ratio of water to oxygen in the co-adsorbed gas mixture was investigated in order to probe the competition for surface stabilisation sites between water and O_2 to form ${}^\bullet OH$ radicals and O_2^- respectively. Initially small amounts of water lead to an increase in population of the O^- and O_2^- radicals; however increasing the pressure of

water vapour further resulted in a decrease in the population of both the O_2^- and O^- species on the TiO_2 surface. The presence of water clearly has an effect on the formation of the various oxygen species indicating that the presence of physisorbed water on the surface and the formation of hydroxyl groups can block the surface Ti^{4+} sites that act as conduits for ET to O_2 to form and stabilise O_2^- at Ti^{4+} sites. The effect of water on the formation of oxygen centred radicals has been discussed by Park *et al.*,[48] in a study on anatase and rutile based photocatalysts used in the photocatalytic oxidation of C_2H_4. Park *et al.*,[48] found that addition of a small amount of water vapour (< 5 Torr) to the photocatalyst led to an enhancement of the photoinduced uptake of oxygen on the surface of the catalyst and subsequently an increase in oxidation reactivity. However on increasing the amount of water (> 5 Torr) the uptake of oxygen decreased ad was accompanied by a decrease in photocatalytic activity. This behaviour was attributed to the fact that when small amounts of water vapour were adsorbed at the surface of the catalyst, subsequent UV irradiation produced reactive $^{\bullet}OH$ radicals which increased the photooxidation rate. When the water vapour was introduced in excess, the effective adsorption sites were occupied completely by water molecules. This was found to decrease the photo induced uptake of oxygen and the $^{\bullet}OH$ radicals produced decreased.

7.4.3 The O_2^- species on the fully hydrated surface

Since the stability and formation of O_2^- radicals was studied on the fully dehydrated and partially hydrated surfaces it was decided to perform the analogous experiments over a fully hydrated surface to further explore the effect of surface hydration on the nature of the radicals formed. The fully hydrated P25 TiO_2 was UV irradiated in the presence of oxygen and no O_2^- species were detected. Attwood *et al.*,[15] have studied the fully hydrated surface of P25 and found that no O_2^- was present; they believed this was due to either the fact that the hydroxyl groups present may block the surface sites for O_2^- adsorption or that the O_2^- species displayed increased mobility on the hydrated surface and there was no evidence for any radical existing within the lifetime of the EPR measurement at low temperatures.

The mobility and reactivity of O_2^- has been studied in aqueous systems. The O_2^- radicals can readily interact with H^+ to form the hydroperoxy radicals (eq 7.9). It has also been reported that O_2^- deactivation on TiO_2 proceeds *via* first-order kinetics, suggesting a reaction with species present in large excess[49]. The presence of hydroxyl groups on the hydrated surface will remove any adsorption sites for O_2^- anions, as shown on the partially hydrated surface. The O_2^- anions have been shown to be stable on

the dehydrated surface and stabilised at the site of initial electron transfer; on the fully hydrated surface they can be mobile such that diffusion occurs and the disproportionation reactions detailed in eq 7.10-7.12 may take place.

If the hydroxyl groups are blocking the site they should be removable *via* surface heating under vacuum. Nosaka *et al.*,[43] have shown that an increase is observed in the EPR signal intensity of surface O^- radicals, which was attributed to the recovery and removal of surface hydroxyl groups by heat treatment. After evacuation of the fully hydrated surface at selected elevated temperatures, to remove surface adsorbed water and hydroxyls, an increase in signal intensity was observed following UV irradiation of the TiO_2 surface under an oxygen atmosphere. As the temperature of evacuation prior to irradiation under O_2 was increased, the growth of an EPR signal assigned to O_2^- was observed. Seemingly specific peaks in the g_{zz} region return at different rates to each other.

These results are supported by the work by Nosaka *et al.*,[43] who studied the removal of surface OH groups and water by thermogravimetry. They found that physisorbed water was removed at T > 423K with a second significant decrease in weight between 423 and 837K which was due to surface hydroxyl groups. Two types of surface OH groups were believed to be present i.e. terminal Ti-OH and bridging Ti-OH-Ti. Dissociation temperatures of these surface OH were found to differ from each other due to the chemical structure of the surroundings.[50] The different thermal behaviour of the surface hydroxyl groups gives an indication of the heterogeneity of the TiO_2 surface. Further proof of the heterogeneity of the surface sites at which hydroxyl groups were formed at has been postulated before in a number of literature studies. Davit *et al.*,[51] stated that OH groups formed by dissociation of water molecules on Ti^{4+}-O^{2-} pairs at the P25 TiO_2 surface. The authors identified a number of OH groups present on the TiO_2 surface by studying the surface with IR spectroscopy. A series of peaks in the 3800-3600cm^{-1} region of the IR spectra were identified as belonging to hydroxyl groups, the presence of the series of peaks was thought to be due to hydroxyl groups situated at different surface plane and to OH groups at sites in defect positions (steps, edges and corners), and they believe reflect the heterogeneous character of the system.[52,53]

In summary, the behaviour of O_2^- radicals on the TiO_2 surface is well understood on the dehydrated surface. The presence of water either in the form of surface hydroxyl groups or physisorbed water can have differing effects. The dehydrated, fully and partially hydrated surfaces have been studied. On the dehydrated surface adsorption of

oxygen followed by UV irradiation results in the formation of thermally unstable O^- and thermally stable O_2^- radicals. On the partially hydrated surface, an increased population of O^- and O_2^- species was observed at low water pressures. However, on increasing the ratio of water present the population of oxygen species decreased, which was attributed to blocking of the surface Ti^{4+} sites responsible for ET to O_2 to form O_2^-. On the fully hydrated surface, formation of O^- or O_2^- was not observed at low temperature or room temperature. Once the surface was heated under dynamic vacuum to remove the physisorbed water and hydroxyl groups, with subsequent readmission of oxygen followed by irradiation O_2^- species were observed. Clearly this has important implications for catalysis as both O_2^- and O^- have been shown to be important in oxidation reactions. Here it has been shown that their formation can be inhibited by the presence of water.

7.4.4 The $NCCH_2OO^\bullet$ species on the dehydrated TiO_2 surface

As discussed earlier, UV irradiation of TiO_2 results in the generation of an electron-hole (e^-/h^+) pair, which can migrate to the surface and participate in reactions with surface adsorbates. It has been shown earlier that the electron can be trapped at the surface by electron scavengers such as oxygen, forming O_2^-. In the presence of an organic substrate, the h^+ is trapped at surface O^{2-} sites to form O^- which can subsequently react with the adsorbed organic substrate, (in this case CH_3CN) to form an $NCCH_2^\bullet$ type species. The $NCCH_2^\bullet$ species can then react with molecular oxygen to form the peroxy radical, $NCCH_2OO^\bullet$.

The effect of varying the ratio of acetonitrile to oxygen in the co-adsorbed mixture prior to irradiation was investigated. If the ratio is oxygen rich, the spectrum is dominated by the O_2^- and O^- species with only a small population of $NCCH_2OO^\bullet$ present. This indicates that under oxygen rich conditions the favoured reaction is the transfer of an electron to O_2 to form O_2^- and the h^+ are trapped at the surface O^{2-} sites. However, this leaves a surface rich in O_2^- radicals which can subsequently react with the organic substrate to form an [O_2^-...organic] adduct (Chapter 5). On the other hand, UV irradiation in the presence of the organic rich atmosphere results in an EPR spectrum typical of the $NCCH_2OO^\bullet$ species previously identified in Chapter 6.3.5. Under these conditions, the hole h^+ based mechanism is favoured, where O^- is trapped by the CH_3CN to form a $CH_2CN^\bullet$ radical which then reacts with molecular oxygen to give the peroxy radical ($NCCH_2OO^\bullet$), as described in 6.4.3.

This dependency on surface adsorption conditions has been investigated by Jenkins *et al.*,[36] who studied the reactivity of aldehydes over the rutile surface. They found that the pre-adsorption of oxygen, followed by the adsorption of an aldehyde, resulted in the formation of purely O_2^- species. They also observed that the concentration of surface radicals obtained in the co-adsorption studies varied in direct proportion to the aldehyde vapour pressure when the O_2 pressure is held constant.

Clearly consideration has to be taken in the co-adsorption conditions as this affects how the photogenerated charge carriers are trapped. This has important implications for catalysis as it means that, depending on the reaction conditions a number of different reaction routes are available to the charge carrier and adsorbed species.

7.4.5 Formation of $NCCH_2OO^\bullet$ on the fully hydrated TiO_2 surface

The fully hydrated surface is of special interest as it is representative of the real system found in catalytic applications. Earlier work has shown that the formation of O_2^- radicals on the fully hydrated TiO_2 surface is blocked due to the presence of surface OH groups and physisorbed water. Peroxy radicals ($NCCH_2OO^\bullet$) have been shown to form *via* h^+ transfer from the dehydrated TiO_2 surface. It is believed that the surface hydroxyl groups and water can act as hole trapping sites (eq 7.7 -7.8). Therefore the formation of $NCCH_2OO^\bullet$ could be affected by the presence of hydroxyl groups on the hydrated TiO_2 surface.

In Figure 7.13, UV irradiation of O_2/CH_3CN on the hydrated surface resulted in an EPR spectrum due to peroxy radicals $NCCH_2OO^\bullet$ ($g_1 = 2.034$, $g_2 = 2.007$ and $g_3 = 2.002$) as observed in the dehydrated case. It was found that for all ratios tested ranging from O_2 in excess to CH_3CN in excess the surface species observed after UV irradiation was the $NCCH_2OO^\bullet$ peroxy type species, but always in lower concentrations than observed on the dehydrated surface.

This indicates that peroxy radicals are still formed on the fully hydrated surface which, compared to the dehydrated surface, raises an interesting point. In Figure 7.11a when the ratio of CH_3CN to O_2 is low (i.e. oxygen rich) on the dehydrated surface the spectrum was dominated by O_2^- radicals with only a trace of $NCCH_2OO^\bullet$ radicals. When the experiment was repeated on the fully hydrated surface the EPR spectrum was completely different: no O_2^- radicals are observed and the resulting spectrum is typical of that of a $NCCH_2OO^\bullet$ species.

The absence of oxygen based radicals in the form of O_2^- seemingly rules out the Russell type mechanism for photooxidation of CH_3CN, whereby the superoxide can react with H^+ to give a hydroperoxy radical which can then go on to form thermally unstable tetraoxides. Alternatively the photooxidation reaction could take place *via* the following series of reactions with or without oxygen as an electron sink providing there was a trap for electrons to keep them from recombining.[54]

$$h^+ + RCH_2R' \rightarrow R^{\bullet}CHR' + H^+ \quad (7.13)$$

$$R^{\bullet}CHR' + {}^{\bullet}OH \rightarrow RCOHR' \quad (7.14)$$

$$RCH_2R' + {}^{\bullet}OH \rightarrow R^{\bullet}CHR' + H_2O \quad (7.15)$$

However, the only radicals observed on the fully hydrated surface by EPR are the $NCCH_2OO^{\bullet}$ radicals. The reduced population could be explained by the possibility of competing reactions occurring on the TiO_2 surface producing intermediates that are unseen in EPR. However, evidence of competition between water and CH_3CN has also been presented as a reason for lower photooxidation rates.

The study of CH_3CN photocatalytic oxidation using P25 TiO_2 in a aqueous suspensions was performed by Addamo *et al.*,[22,24] They found for high H_2O/CH_3CN ratios, as is typical for the liquid-solid regime, acetonitrile molecules were not able to provide specific interaction with surface sites of TiO_2, remaining dissolved in interface water molecular layers. This helps to explain the reduction in intensity for the $NCCH_2OO^{\bullet}$ radicals observed on the hydrated surface compared to the dehydrated surface. Further evidence for a reduction in photooxidation due to the presence of water was presented by Lichtin *et al*,[28] who found that in aqueous systems there is a strong interaction between adsorbed CH_3CN and liquid water. They believed that this interaction could lead to the dissipation of the heat of charge recombination and inhibit the dissociation of CH_3CN.

7.4.6 Formation of $NCCH_2OO^{\bullet}/O_2^-/O^-$ under partially hydrated conditions

The co-adsorption of the ternary system ($H_2O/O_2/CH_3CN$) has yet to be investigated by EPR spectroscopy in the literature. This system represents the type of conditions that are present in industrial catalytic processes, where the three substrates can be simultaneously found in differing amounts and ratios.

Experiments were conducted with a number of different ratios tested. It was found that the O_2^-, O^- and $NCCH_2OO^\bullet$ were formed on the TiO_2 surface. The population and relative signal contribution of each species was found to vary depending on the ratio of gases in the co-adsorbed mixture. When the ratio was dominated by CH_3CN with O_2 and H_2O in equal amounts (4:1:1), the spectrum contained the largest observed concentration of $NCCH_2OO^\bullet$ radicals and with the lowest concentration of the O_2 and O^- species. However, the O_2^- species was still the dominant species in the EPR spectrum. This is due to the fact that oxygen and water have a higher affinity for the TiO_2 surface. A VT study provided information on the stability of the radicals in this system. The O^- was found to decay as previously observed on the dehydrated and partially hydrated surfaces and was lost at T = 200K. The O_2^- species decayed at T > 210K, and on reaching 220K the spectrum was similar to that observed on reaction of O_2^- + CH_3CN. The signal at $g_1 = 2.034$ did not significantly decrease but shifted in value slightly to g = 2.032. This behaviour was explained as being due to the decay of $NCCH_2OO^\bullet$ at T > 140K. At T > 200K O_2^- reacts with CH_3CN to form the [O_2^- ....CH_3CN] adduct with the g_1= 2.032.[21]

The concentration of water was varied and the general trend was found to be that as the concentration of water increased, this resulted in the decrease in population of $NCCH_2OO^\bullet$ radicals and an increase in the population of O_2^- and O^- species. This trend is very general. The lowering in concentration of $NCCH_2OO^\bullet$ may be explained by the fact that at higher pressures of water, adsorption of CH_3CN at the TiO_2 surface is blocked. In an IR study of CH_3CN of the TiO_2 surface Zhaung *et al.*,[55] they assigned the 2318cm^{-1} band to CH_3CN bonded to a Lewis acid site, and found that on increasing OH coverages this band was lost. This was accompanied by an increase in the band at 2274cm^{-1} which was due to CH_3CN bonded to surface OH groups. They also found that water is not needed for the onset of the photooxidation of CH_3CN on the TiO_2. The presence of O_2 was found to be indispensable as a reactant and they believed this implied the function of O_2 is not just that of an electron scavenger. This would fit with the theory that $NCCH_2OO^\bullet$ is a key intermediate in the photooxidation of CH_3CN as well as the reaction of O_2^- and CH_3CN.

The role of water in the gas-solid regime was studied by a number of groups. Lichtin *et al.*,[28] found that the completed oxidation of CH_3CN in the presence of oxygen is represented by (eq 7.16);

$$CH_3CN + 4\ O_2 \rightarrow 2\ CO_2 + H_2O + HNO_3 \qquad (7.16)$$

The increasing presence of water was found to decrease the photooxidation rate of the CH_3CN vapour by a small amount. The gas-solid regime was investigated by Addamo *et al*,[24,29] who found that for low H_2O/CH_3CN ratios, typical of the gas-solid regime (partially hydrated surface), acetonitrile would win the surface competition with water for surface hydroxyls but as the ratio of water increased, a decrease in acetonitrile at the surface was observed. They found that this was important as photodegradation was likely to occur faster for molecules adsorbed on Ti^{4+} ions than those adsorbed on surface hydroxyls.

7.5 Conclusion

The role of water in heterogeneous catalysis is important; however its exact role as either a promoter or poison of reactions at the TiO_2 surface remains under debate. In this chapter the formation of surface adsorbed radicals on TiO_2 surfaces of differing levels of hydration was probed to try and shed further light on the role of water.

On the dehydrated surface it was found that when the TiO_2 surface is UV irradiated under an oxygen atmosphere and subsequently warmed to room temperature, stable O_2 species were formed. On investigating the formation at low temperature it was found that accompanying the O_2^- species were the trapped hole species O^- which were found to disappear on warming to room temperature. When the O^- and O_2^- were exposed to CH_3CN at 77K, the O^- species was lost, but no additional EPR signals were observed, indicating the species formed is likely to be diamagnetic. The O_2^- species reacted with the CH_3CN at T > 190K which resulted in an EPR spectrum of the $[O_2^-...CH_3CN]$ adduct identified in Chapter 6.

Once identified, the formation and stability of these oxygen species was investigated on the partially hydrated surface. Both species were found to be present on the partially hydrated surface at 140K but both were lost on warming to room temperature in the presence of water. When the water was evacuated at low temperature, followed by annealing at room temperature, the O_2^- species were stable, indicating that the instability of O_2^- is due to reaction between H_2O and O_2^-. The addition of water has a second effect, namely that at high levels of water vapour the population of oxygen radicals decreases as the water begins to block the surface sites for ET and stabilisation.

The formation of O_2^- on the fully hydrated surface was investigated. No O_2^- species were observed under these conditions - this was attributed to the surface sites being blocked by surface hydroxyl groups and physisorbed water. When the fully hydrated sample was heated under dynamic vacuum, the water and hydroxyl groups were removed and readmission of oxygen, followed by re-irradiation, resulted in the formation of superoxide radicals. The formation is selective with sites II-III formed first followed by sites I-I'.

Hole mediated processes result in the formation of transient peroxy type species $NCCH_2OO^\bullet$ on the TiO_2 surface. These processes have been shown to be dominant under organic rich conditions, where the organic substrate is in excess and saturates the TiO_2 surface. Under organic poor (oxygen rich) conditions the EPR spectrum is dominated by the O_2^- and O^- species. Clearly the formation of each radical is dependent on the adsorption conditions present at the TiO_2 surface.

On the fully hydrated surface it was found that the ratio of CH_3CN/O_2 had no significant effect on the type of radicals formed. Under both organic rich and poor conditions no O_2^- radicals were found to form on the surface of TiO_2. The spectra were purely that of the $NCCH_2OO^\bullet$ radical. This however was formed on the hydrated surface in lower concentrations, due to the competition for surface sites between acetonitrile and water molecules. This result again indicates that on the fully hydrated surface the superoxide radical is not observed at 140K, which could mean that O_2^- is not formed in the hydrated surface. This indicates that under fully hydrated conditions the degradation of CH_3CN proceeds with $NCCH_2OO^\bullet$ as an intermediate.

The partially hydrated surfaces provide a way of probing the gas-solid interface and the results differ from that of the hydrated surface. After UV irradiation of the different ratios of the co-adsorbed gas ($H_2O/CH_3CN/O_2$) it was found that O_2^-, O^- and $NCCH_2OO^\bullet$ were all formed. The population and relative signal intensities of each species varied dependant on the ratio of co-adsorbed gases. The fact that both peroxy type radicals are present, which are formed *via* hole mediated processes and then O_2^- (which could subsequently react with CH_3CN to give $[O_2^-....CH_3CN]$) seems to indicate that a number of processes could occur leading to the degradation of CH_3CN.

The initial question poised was whether water acts as a promoter or poison. Within the limits of this study the radicals identified are the same as those formed on the dehydrated surface, so the presence of water does not result in any new paramagnetic species. However there could be diamagnetic species unseen by EPR. The

presence of water or hydroxyl groups seems to create competition for the surface stabilisation sites where ET and hole transfer events take place which lead to reduced populations of the reactive surface radicals (O_2^-, O^- and $NCCH_2OO^\bullet$)

7.6 References

(1) Abdullah, U. I. G. A. H. *Journal of photochemistry and Photobiology C - Photochemistry Reviews* **2008**, *9*, 12.

(2) Grassian, V. H. *International Reviews in Physical Chemistry* **2001**, *20*, 467.

(3) Morterra, C. *Journal of the Chemical Society-Faraday Transactions I* **1988**, *84*, 1617.

(4) Vorontsov, A. V.; Stoyanova, I. V.; Kozlov, D. V.; Simagina, V. I.; Savinov, E. N. *Journal of Catalysis* **2000**, *189*, 360.

(5) Vorontsov, A. V.; Kurkin, E. N.; Savinov, E. N. *Journal of Catalysis* **1999**, *186*, 318.

(6) Sauer, M. L.; Ollis, D. F. *Journal of Catalysis* **1994**, *149*, 81.

(7) Peral, J.; Ollis, D. F. *Journal of Catalysis* **1992**, *136*, 554.

(8) Kim, S. B.; Hong, S. C. *Applied Catalysis B-Environmental* **2002**, *35*, 305.

(9) El-Maazawi, M.; Finken, A. N.; Nair, A. B.; Grassian, V. H. *Journal of Catalysis* **2000**, *191*, 138.

(10) Coronado, J. M.; Zorn, M. E.; Tejedor-Tejedor, I.; Anderson, M. A. *Applied Catalysis B-Environmental* **2003**, *43*, 329.

(11) Henderson, M. A. *Surface Science Reports* **2002**, *46*, 5.

(12) Henderson, M. A. *Journal of Catalysis* **2008**, *256*, 287.

(13) Kubo, W.; Tatsuma, T. *Journal of the American Chemical Society* **2006**, *128*, 16034.

(14) Tatsuma, T.; Tachibana, S.; Fujishima, A. *Journal of Physical Chemistry B* **2001**, *105*, 6987.

(15) Attwood, A. L.; Murphy, D. M.; Edwards, J. L.; Egerton, T. A.; Harrison, R. W. *Research on Chemical Intermediates* **2003**, *29*, 449.

(16) Anpo, M.; Che, M.; Fubini, B.; Garrone, E.; Giamello, E.; Paganini, M. C. *Topics in Catalysis* **1999**, *8*, 189.

(17) Carter, E.; Carley, A. F.; Murphy, D. M. *Journal of Physical Chemistry C* **2007**, *111*, 10630.

(18) Che, M. T., A.J. *Advances in Catalysis* **1983**, *32*, 1.

(19) Green, J.; Carter, E.; Murphy, D. M. *Chemical Physics Letters* **2009**, *477*, 340.

(20) Carter, E.; Carley, A. F.; Murphy, D. M. *Chemphyschem* **2007**, *8*, 113.

(21) Green, J.; Carter, E.; Murphy, D. M. *Research on Chemical Intermediates* **2009**, *35*, 145.

(22) Addamo, M.; Augugliaro, V.; Coluccia, S.; Di Paola, A.; Garcia-Lopez, E.; Loddo, V.; Marci, G.; Martra, G.; Palmisano, L. *International Journal of Photoenergy* **2006**.

(23) Augugliaro, V.; Coluccia, S.; Garcia-Lopez, E.; Loddo, V.; Marci, G.; Martra, G.; Palmisano, L.; Schiavello, M. *Topics in Catalysis* **2005**, *35*, 237.

(24) Addamo, M.; Augugliaro, V.; Coluccia, S.; Faga, M. G.; Garcia-Lopez, E.; Loddo, V.; Marci, G.; Martra, G.; Palmisano, L. *Journal of Catalysis* **2005**, *235*, 209.

(25) Augugliaro, V.; Prevot, A. B.; Vazquez, J. C.; Garcia-Lopez, E.; Irico, A.; Loddo, V.; Rodriguez, S. M.; Marci, G.; Palmisano, L.; Pramauro, E. *Advances in Environmental Research* **2004**, *8*, 329.

(26) Davit, P.; Martra, G.; Coluccia, S.; Augugliaro, V.; Lopez, E. G.; Loddo, V.; Marci, G.; Palmisano, L.; Schiavello, M. *Journal of Molecular Catalysis A-Chemical* **2003**, *204*, 693.

(27) Chuang, C. C.; Wu, W. C.; Lee, M. X.; Lin, J. L. *Physical Chemistry Chemical Physics* **2000**, *2*, 3877.

(28) Lichtin, N. N.; Avudaithai, M. *Environmental Science & Technology* **1996**, *30*, 2014.

(29) Addamo, M.; Augugliaro, V.; Coluccia, S.; Di Paola, A.; Garcia-Lopez, E.; Loddo, V.; Marci, G.; Martra, G.; Palmisano, L. *International Journal of Photoenergy* **2006**, *39182*, 1.

(30) Spalek, T.; Pietrzyk, P.; Sojka, Z. *Journal of Chemical Information and Modeling* **2005**, *45*, 18.

(31) Kamat, P. V. *Chemical Reviews* **1993**, *93*, 267.

(32) Nakamura, R.; Sato, S. *Journal of Physical Chemistry B* **2002**, *106*, 5893.

(33) Kim, S. B.; Hwang, H. T.; Hong, S. C. *Chemosphere* **2002**, *48*, 437.

(34) Howe, R. F.; Gratzel, M. *Journal of Physical Chemistry* **1985**, *89*, 4495.

(35) Howe, R. F.; Gratzel, M. *Journal of Physical Chemistry* **1987**, *91*, 3906.

(36) Jenkins, C. A.; Murphy, D. M. *Journal of Physical Chemistry B* **1999**, *103*, 1019.

(37) Attwood, A. L.; Edwards, J. L.; Rowlands, C. C.; Murphy, D. M. *Journal of Physical Chemistry A* **2003**, *107*, 1779.

(38) Che, M.; Tench, A. J. *Advances in Catalysis* **1982**, *31*, 77.

(39) Micic, O. I.; Zhang, Y. N.; Cromack, K. R.; Trifunac, A. D.; Thurnauer, M. C. *Journal of Physical Chemistry* **1993**, *97*, 13284.

(40) Micic, O. I.; Zhang, Y. N.; Cromack, K. R.; Trifunac, A. D.; Thurnauer, M. C. *Journal of Physical Chemistry* **1993**, *97*, 7277.

(41) Berger, T.; Sterrer, M.; Diwald, O.; Knozinger, E. *Chemphyschem* **2005**, *6*, 2104.

(42) Turchi, C. S.; Ollis, D. F. *Journal of Catalysis* **1990**, *122*, 178.

(43) Nakaoka, Y.; Nosaka, Y. *Journal of Photochemistry and Photobiology a-Chemistry* **1997**, *110*, 299.

(44) Berger, T.; Sterrer, M.; Diwald, O.; Knozinger, E.; Panayotov, D.; Thompson, T. L.; Yates, J. T. *Journal of Physical Chemistry B* **2005**, *109*, 6061.

(45) Jenkins, C. A.; Murphy, D. M.; Rowlands, C. C.; Egerton, T. A. *Journal of the Chemical Society-Perkin Transactions 2* **1997**, 2479.

(46) Brivati, J. A.; Symons, M. C. R.; Tinling, D. J. A.; Williams, D. O. *Journal of the Chemical Society a -Inorganic Physical Theoretical* **1969**, 719.

(47) Brivati, J. A.; Symons, M. C. R.; Tinling, D. J. A.; Wardale, H. W.; Williams, D. O. *Transactions of the Faraday Society* **1967**, *63*, 2112.

(48) Park, D. R.; Zhang, J. L.; Ikeue, K.; Yamashita, H.; Anpo, M. *Journal of Catalysis* **1999**, *185*, 114.

(49) Ihibashi. K. , N. Y., Hasihmoto, K. Fujishima, A. . *Journal of physical Chemistry B* **1998**, *102*, 2117.

(50) Nosaka, Y.; Kishimoto, M.; Nishino, J. *Journal of Physical Chemistry B* **1998**, *102*, 10279.

(51) Davit, P.; Martra, G.; Coluccia, S. *Journal of the Japan Petroleum Institute* **2004**, *47*, 359.

(52) Cerrato, G.; Marchese, L.; Morterra, C. *Applied Surface Science* **1993**, *70-1*, 200.

(53) Tanaka, K.; White, J. M. *Journal of Physical Chemistry* **1982**, *86*, 4708.

(54) Perkins, C. L.; Henderson, M. A. *Journal of Physical Chemistry B* **2001**, *105*, 3856.

(55) Zhuang, J.; Rusu, C. N.; Yates, J. T. *Journal of Physical Chemistry B* **1999**, *103*, 6957.

Chapter 8

General Conclusions

During the course of this Thesis, continuous wave (CW)-EPR spectroscopy has been used to study a number of defects and transient oxygen radicals formed over the surface of polycrystalline TiO_2 (P25). This technique offers the advantage of exceptionally high sensitivity compared to other spectroscopic techniques, coupled with the ability to easily study systems *in-situ* at low temperatures. The detection and identification of thermally unstable radicals, which may not be detected by higher temperatures, is therefore possible.

The work discussed in Chapter 5, has shown that specific surface stabilisation sites for the superoxide radicals (O_2^-) can be selectively blocked by the addition of probe molecules. The reduced TiO_2 surface is highly heterogeneous with many different Ti^{3+} centres located at different facets. These surface Ti^{3+} centres are believed to play an important part in (electron transfer) catalysis. Upon addition of O_2 to the Ti^{3+} centres, surface O_2^- radicals are formed. These O_2^- radicals have been classified into two groups; those stabilised at Ti^{4+}_{vac} centres (labelled Site I) and those at $Ti^{4+}_{non\text{-}vac}$ centres (labelled Sites II-III). In the latter case selective blocking of the Ti^{3+} centres by CO_2 was achieved; this prevents ET to molecular oxygen both under sequential and co-adsorption conditions. By comparison, sequential adsorption of Ar and O_2 was found to have the opposite effect to that of CO_2/O_2. Ar was found to preferentially adsorb at the Ti^{3+}_{vac} surface sites, preventing ET transfer from these lower co-ordinate Ti^{3+} sites which are associated with oxygen vacancies. These findings reveal the importance of understanding the structure/location of the surface defect sites (Ti^{3+}) responsible for ET reactions, since specific substrates may inadvertently block these sites and prevent oxidation of the defects (possibly leading to deactivation of the catalyst).

Superoxide radicals (O_2^-) are often presumed to be involved in non-selective heterogeneous oxidation reactions; although widely implicated, direct evidence for their role in heterogeneous photo-oxidation remains sparse. In this Thesis, it has been shown that this radical does indeed participate in the decomposition of organic substrates under dark conditions over the TiO_2 surface. Upon exposure of acetonitrile, methanol and toluene to adsorbed O_2^-, a series of thermally unstable intermediates, labelled [O_2^- ...substrate], were identified. These intermediates all displayed similar thermal characteristics and possessed similar spin Hamiltonian parameters. When acetonitrile and O_2 enriched with ^{17}O was used, it was found that the oxygen atoms in the [O_2^-

...CH_3CN] complex were equivalent, indicating that the interaction between the O_2^- and acetonitrile in the complex occurred in a 'side-on' manner. The identification of this surface intermediate, produced during the decomposition of acetonitrile, methanol and toluene, is important since it may be a common intermediate in the degradation of a variety of organic substrates over TiO_2.

UV irradiation of a co-adsorbed mixture of organic substrates (methanol, acetonitrile and toluene) and molecular oxygen over TiO_2 was also investigated. After irradiation at low temperatures, a series of organoperoxy type species were formed (labelled $ROO^{\bullet}$) which displayed similar thermal stabilities and spin Hamiltonian parameters. These species were found to be unstable at elevated temperatures (190-250K) and were completely destroyed upon annealing to 298K. The $ROO^{\bullet}$ radicals were suggested to form *via* a hole mediated process. The population of the $ROO^{\bullet}$ species was found to depend on the level of surface hydration, as significantly reduced signal intensities were observed on both partially and fully hydrated surfaces compared to a fully dehydrated surface.

Under standard photocatalytic conditions, the TiO_2 surface is exposed to water vapour. The water can be chemisorbed, physisorbed or dissociated on the surface of TiO_2. The role of water in the photocatalytic processes is a hotly debated topic with some contrasting indications suggesting that water can act as a poison or alternatively a promoter of photocatalytic reactions. Therefore the nature and stability of oxygen based radicals (O^- and O_2^-) as a function of surface hydration was studied. On the dehydrated surface, the O^- and O_2^- species were observed at low temperatures. The O^- species were found to be thermally unstable and decayed at room temperature. At low relative water pressures, both O^- and O_2^- species were observed. However, as the surface hydration increased, the populations of the O_2^- and O^- species were found to decrease as the surface sites for ET and stabilisation were progressively blocked by the pre-adsorbed water.

On the fully hydrated surface, no O_2^- species were observed. It is proposed that the surface sites for stabilisation were blocked by surface water and surface hydroxyl groups. It was found that the surface sites could be 'un-blocked' by heating under dynamic vacuum, which removes the physisorbed water and hydroxyl groups. As the evacuation temperature was increased, leading to the removal of the surface hydroxyl groups, the superoxide radical was found to be stabilised in increasing intensity.

The work performed in this Thesis highlights the importance of surface adsorbates on the reactivity of the TiO_2 surface. In the presence of co-adsorbates, potential stabilisation sites for surface radicals can be perturbed or blocked by the presence of other gases/adsorbates, which in turn leads to a reduction in the reactivity of the surface.

The reactivity of surface radicals at the TiO_2 is an important feature of heterogeneous photocatalysis. Adsorbed organic substrates were shown to react with surface oxygen radicals producing a series of thermally unstable intermediates (both in the dark and under UV irradiation). The thermally unstable intermediates were observed to form for a variety of organic substrates. The thermally unstable nature of these species highlights the need to study photocatalytic reactions at low temperatures. Possessing a greater understanding of the processes which occur at the TiO_2 surface will hopefully lead to the design of catalysts with high photo-activities by being able to tune surface properties to enhance the concentration of stabilisation sites for surface radicals.

J. Green.

Cardiff. September 2010.